A PRACTICAL NUMERICAL ANALYSIS OF A THREE-DIMENSIONAL TRENCH SLURRY WALL DURING CONSTRUCTION USING FLAC3D

By

OMAR ALI M. MOUDABEL

Bachelor of Civil Engineering
Tripoli University
Tripoli, Libya
1997

Master of Civil Engineering
Oklahoma State University
Stillwater, OK
2013

Submitted to the Faculty of the
Graduate College of the
Oklahoma State University
in partial fulfillment of
the requirements for
the Degree of
DOCTOR OF PHILOSOPHY
May, 2019

A PRACTICAL NUMERICAL ANALYSIS OF A

THREE-DIMENSIONAL TRENCH SLURRY WALL

DURING CONSTRUCTION USING FLAC3D

Dissertation Approved:

Dr. Rifat Bulut

Dissertation Adviser

Dr. Mohamed Samir Ahmed

Dr. Mohamed Soliman

Dr. Omer San

ACKNOWLEDGEMENTS

My graduated and Praise be to Almighty Allah (God) for blessing me for what I get in this life and hopping his mercy and forgiveness in the hereafter. Graduated are to my family and great people around me who have had great support throughout my doctoral journey.

I would like to thank Dr. Xiaoming Yang and Dr. Garry Gregory for mentoring and helping me throughout my graduate studies both at M.S. and Ph.D. levels from spring 2011 to summer 2018 at Oklahoma State University.

I'm grateful to my previous advisor, Dr. Xiaoming Yang for helping me through my FLAC software coding journey. I appreciate his guidance and support in the four years of my Ph.D. studies. I extend my gratefulness to Dr. Garry Gregory for his great support and for providing data for this study.

My appreciation goes to Dr. Rifat Bulut, for accepting me for completing this degree under his supervision in this great school OSU and guiding me through all the difficulty I have had.

My appreciation also goes to my all previous and new committee members for their support and advice. Special thanks to Dr. Samir Ahmed, Dr. Mohamed Soliman, and Dr. Omer San for supporting me academically and emotionally.

Name: OMAR ALI M. MOUDABEL

Date of Degree: MAY, 2019

Title of Study: A PRACTICAL NUMERICAL ANALYSIS OF A THREE-DIMENSIONAL TRENCH SLURRY WALL DURING CONSTRUCTION USING FLAC3D

Major Field: CIVIL ENGINEERING

Abstract: A soil-bentonite cutoff wall is constructed by excavating a trench with a backfill mix of soil, bentonite, and water. The trench will be a vertical barrier to support the ground movement during construction and permanent barrier. It is constructed panel by panel causing changes on stresses of the soil. These considerable changes in stress cause substantial ground movement. Despite the fact that soil-bentonite cutoff slurry walls are common, their mechanical behavior is not always well understood. There is a greater need to understand the behavior of the soil during the construction to avoid damages to near structures. Current studies do not consider the final stress state of the soil-bentonite backfill or deformations in the adjacent ground for multiple soil layers. A three-dimensional Lagrangian base numerical method was used to model the mechanical responses of the ground for Lake Tyler Dam. The ground response including horizontal normal stresses, shear stresses, lateral ground displacement, and vertical ground surface settlement was analyzed during the slurry excavation for each diaphragm wall panels. Numerical results show that slurry trenching leads to horizontal stress relief of ground and shear stresses in the panel elements. However, there are some magnitude differences of these reliefs caused by each layer. The large magnitude of lateral ground displacement and vertical ground surface settlement were found in the excavation of some panels at the upper part of the trench. The backfill of the wall should consider the need to compensate partially the horizontal stress loss and reduces the lateral displacement as well as the vertical settlement of ground. This finding implies the necessity of protecting the upper part of the trench in a certain stage of excavating individual wall panels. There is a non-uniform horizontal stress distribution behind the panel, the stress being the smallest at the center but increasing in magnitude toward the corner and decreasing beyond the panel. This needs more attention during the excavation of each panel with the consideration of each layer of material properties.

TABLE OF CONTENTS

Chapter Page

Chapter Page

LIST OF TABLES

Table Page

LIST OF FIGURES

Figure Page

Figure Page

Figure Page

Figure Page

Figure Page

Figure Page

CHAPTER I

INTRODUCTION

1.1 Background

Slurry trenching is frequently used in civil and environmental engineering projects when a long, narrow, and deep excavation is needed especially in high-groundwater conditions. The construction begins with excavating vertical trenches that are of several different styles in engineering practice. The trench is temporarily supported by a suspension of bentonite which is then replaced with concrete, soil-bentonite (SB), or soil-cement-bentonite (SCB) backfills. After the backfill slurry hardens, a continuous underground wall is formed, which is commonly called a slurry trench wall. Slurry trench walls are often used as cutoff walls against seepage or ground motion. The most critical stage during the construction process is at the time when the trench is just excavated and backfilled and before the slurry hardens. At this stage, the trench may collapse if the hydraulic thrust of the slurry cannot support active earth pressure from the soil.

Since slurry trench walls are constructed panel by panel or at a certain speed in feet per day, there is only a finite length of the slurry trench wall, at a certain time, which is filled with the backfill slurry while the rest of the slurry wall is either hardened or not excavated yet.

The length of such a liquid slurry-filled trench (L) is needed to be carefully controlled by regulating the construction speed so that the trench failure is avoided. Engineering experience shows that most failures occur when the length of the liquid slurry-filled trench exceeds about one to two times the depth of the trench (Barrier 1995). In practice, the stability of the slurry trench wall and the maximum allowable speed of construction need to be assessed by a slope stability analysis.

Slope stability analysis is an important and delicate problem in civil engineering. It is also one of the most conventional research areas in the field of soil mechanics (Duncan and Wright 2005). The main interest in the slope stability analysis is typically to determine a factor of safety value (FS) against the slope failure and the location of the critical failure surface. To simplify the analysis, slope stability is often assessed with a two-dimensional (2-D) slope stability analysis based on the critical cross-section of the project. The assumption is that the same cross-section extends significantly longer in the perpendicular direction than its width and depths so that a plane-strain condition is approximately satisfied (Duncan and Wright 2005). However, in fact, the behavior of soil is not two-dimensional. It is rather a three-dimensional (3-D) stress-strain behavior act on that dimension. This assessment is needed for more accurate, practical, and economical design.

The stability failure of a slurry trench wall often occurs when the length of the liquid slurry-filled trench is about one to two times the depth of the trench (Duncan and Wright 2005). Therefore, the slope stability problem is essentially three-dimensional (3-D) rather than (2-D) (infinitely long slope). Although running a (3-D) slope stability analysis on a slurry trench wall is technically not difficult today, there are limited researches for stress-strain behaviors during the construction.

1.2 Slurry Trench Wall Usages

Integrating hydrogen dioxide to bentonite (montmorillonite) forms the bentonite slurry or drilling mud clays which has the consistency of very soft mud. The slurry exerts hydraulic pressure against the trench wall during trench excavation which acts as shoring to avert collapse and forms a filter cake to reduce groundwater flow. Soil-Bentonite backfill material is then placed into the trench (displacing the slurry) to engender the cutoff wall which provides a barrier to low permeability and chemical resistance at low cost (Filz and Davidson 2004).

The most use of slurry trench wall is to create impermeable groundwater barriers. It has also other usages like economic cutoff walls, positive cutoff walls in the core foundation soils beneath dams, contain or divert contaminated groundwater, and provide a barrier for the groundwater treatment system.

1.3 Construction Process

Soil-bentonite cutoff walls are constructed by using the slurry trench technique. In this technique, a slim trench (usually three to five feet wide) is excavated with a slurry that is used to hold the trench. For a soil-bentonite cutoff wall, the trench is packed with bentonite-water slurry and is typically four percent to six percent of bentonite by weight (Barrier 1995).

Usually, the slurry level is higher than the water table in the adjacent soil. That will help the slurry particles to move to the adjacent soil forming the “filter cake” which is a thin layer of bentonite at the trench wall. The filter cake will provide a semi-non permeable face, depending on the trench soil

permeability. When the slurry in the trench acts against the filter cake, it provides a hydrostatic stabilizing force to support the trench soil (Filz et al. 1997).

Excavation of the trench can be conducted by excavation crane or modified boom backhoe. The excavation is proceeding on one side of the trench and on the other side is backfilled with soil-bentonite. The bulldozer pushes the soil-bentonite mixed on the field until backfill reaches the ground surface and create a ram, as shown in Figure 1.1. Subsequently, the soil-bentonite replaces the bentonite slurry and become the final form of the slurry wall.

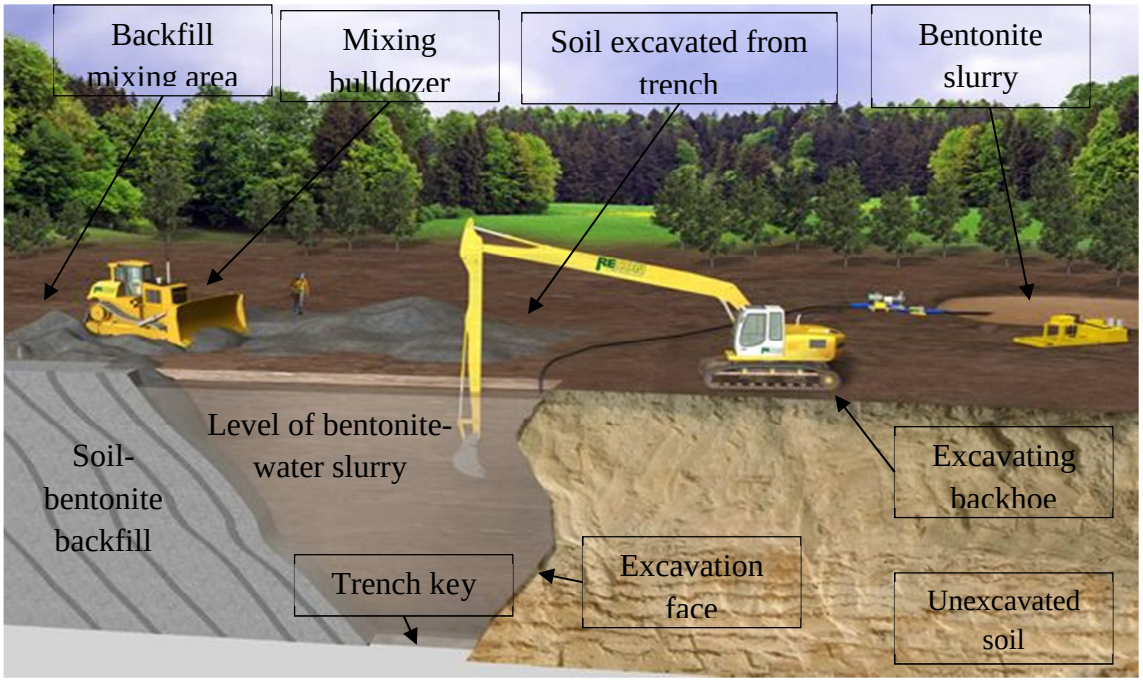

Figure 1.1 Slurry wall construction process (Barrier 1995).

1.4 The Factor of Safety (FS)

The factor of safety (FS) is the primary design criteria utilized in the slope stability analysis. The fundamental aim of slope stability analysis is to determine a factor of safety against a potential failure, landslide or cut. If this factor of safety is greater than 1.0, the slope is judged to be stable (safe). If it is 1.0 or less, it is unsafe. However, in the three-dimensional analysis, the factor of safety tends to be greater than this value. To calculate the factor of safety by conventional (traditional) slope stability analysis the single value of each input variable is used to produce a single-value of a factor of safety output (Duncan and Wright 2005).

To have a boundary between stability and instability of the slope or cut, a value of FS equal 1.0 indicates that stable which means the shear strength of soil (resistance forces or moments) equals the shear stress (driving forces or moments). The value of 1.01 would be acceptable if all the factors are computed absolutely precisely. However, due to uncertainties involved in computing factor of safety, the result is never absolutely precise.

$$FS=\frac{\text{Resistance forces or Moments}}{\text{Driving forces or Moments}}$$

Because the quantities involved in computed values of the FS are not precise, due to the uncertainty of variables, the factor of safety should be larger to ensure the safety of the slope from failure (Duncan and Wright 2005). Therefore, the stress-strain analysis studies are very important to reveal the validity of the calculated factor of safety.

Table 1.1 presents some recommended values of a two-dimensional factor of safety (Bowles 1992).

Table 1.1 Typical values of customary (2-D) safety factors, FS, as presented by Bowles (1992)

Failure Mode	Structure Type	FS
Shear	Earthwork for Dams, Fills, etc.	1.2 - 1.6
Shear	Retaining Walls	1.5 - 2.0
Shear	Sheet piling, Cofferdams	1.2 - 1.6
Shear	Braced Excavations (Temporary)	1.2 - 1.5
Shear	Spread Footings	2 - 3
Shear	Mat Footings	1.7 - 2.5
Shear	Uplift for Footings	1.7 - 2.5
Seepage	Uplift, heaving	1.5 - 2.5
Seepage	Piping	3 - 5

1.5 Problem Statement and Objectives

Deep excavation is very common in construction fields. Full understanding of the factors that cause trenches to collapse will minimize construction failure accidents and damages. Trench failure occurs because of the instability of the soil mass due to excavation and displacement. One common technique to support the trench during the construction is adding bentonite slurry to the trench which is called slurry trench wall (Barrier 1995).

Due to the high efficiency of the new excavation equipment, the rate of excavation becomes high. That is urging the need for understanding the behavior of the soil information about the stress-strain behavior and deformations of the soil supported by the slurry wall on a certain length/depth ratio. In fact, in a certain length/depth ratio the side restrains effect is largely contributed to the stability of the trench which is more (3-D) effect than a (2-D) effect. Unfortunately, many unrealistic geometrical simplifications are involved in both (2-D) and (3-D) analysis methods in order to design the depth and length of the slurry wall which led to a too conservative approach (Ding and Wang 2008). However, most of the recent researches are done on simplified models that try to represent the effect of the actual failure mode and factor of safety. This simplification is adapted due to the complexity and uncertainty of the soil.

The objectives of this research are to provide information in the area of the mechanical behavior of slurry walls, including the following:

1. Add to the current body of knowledge of design slurry walls in the construction stage. This objective was accomplished by first summarizing the current body of knowledge that exists in the literature and then executing a solution to a current cut off example.

2. Model a slurry wall using a three-dimensional Lagrangian formulation based finite difference approach. This objective was accomplished using the computer program FLAC. FLAC, Fast Lagrangian Analysis of Continua, is numerical modeling software package for advanced geotechnical analysis of soil, rock, and groundwater. FLAC is used for analysis, testing, and design by geotechnical, civil, and mining engineers. The model was implemented into the finite difference and used to represent the slurry wall trench. The following construction sequences were simulated numerically: trench excavation under bentonite-water slurry, and under interval of construction length. The model was constructed based on Lake Tyler Dam geometry.

3. Investigate the influence of several factors on the deformations and failure surface. This objective was accomplished by performing a numerical study using the finite difference assuming different excavation length, excavation width, and multiple layers of the model. Deformations in the adjacent ground were calculated for various soil conditions, and trench configurations. Conclusions are drawn regarding the importance of these factors on the stability of the trench during excavation.

1.6 Significance of Research

Even though soil-bentonite cutoff walls are common construction techniques, their mechanical behavior is not always well understood or predicted. Current researches and design procedures are primarily based on simplified shape or past experience. Currently, it is difficult to predict the final state of stress in the soil-bentonite due to the construction of the wall. Therefore, this model will build more knowledge to study the stress-strain behavior due to multiple layers effects and on realistic model geometry.

Despite the fact that deformations are not typically primary design criteria for a cutoff wall, they do impact the cutoff wall's effectiveness. Deformations close to the cutoff wall may be substantial and might cause damage to adjacent structures. There is a great need to understand the three-dimensional mechanical behaviors of soil-bentonite cutoff walls in order to enhance analysis methods and design practices. The results of this research could help understand the behavior of deformation of the soil due to the construction of the slurry wall.

1.7 Overview of Dissertation

This dissertation describes the research performed on the three-dimensional molding of mechanical behavior of soil-bentonite cutoff walls for actual properties from a selected project. Chapter 2 describes the literature review of soil-bentonite cutoff walls with respect to the method of calculation of the factor of safety and the mechanical behavior of the cutoff. Chapter 3 describes the modeling sequence of the selected project. Chapter 3 also describes the development of the FLAC model used to simulate construction all stages of a soil-bentonite cutoff wall. Chapter 4 presents the numerical results including a total of 60 different simulations performed for 12 excavated panels. Chapter 5 summarizes the results and conclusions of the research and presents recommendations for further studies.

The FLAC input data codes for the model are given in Appendix A. The model construction stages results from FLAC^{3D} are described in Appendix B.

CHAPTER II

LITERATURE REVIEW

2.1 Introduction

This chapter presents background information about slurry walls and information gathered from the literature concerning the stability of the slurry walls. Background information includes the design models, geometry and soil properties. Current researches are based primarily on simplification of the shape and layers of the structure. Most researches to date have not focused on the stability of the trench during an excavation on a complex structure.

The literature review indicates a lack of information on how the stress state in the ground is changed by the construction of the slurry wall and what deformations will result in the adjacent ground. In order to better understand the mechanical behavior of the slurry walls, there is a need for more analyses and investigations of the stability of the slurry backfill and deformations of adjacent ground (Li and Lin 2018). This section will present the state of the art knowledge on the stability of the slurry walls and calculation of the factor of safety techniques.

2.2 Calculation of the Factor of Safety

Many studies have been done in the past regarding the determination of the factor of safety against the stability failure for slurry walls. Three categories of design/analysis methods are reviewed in this study: (1) analytical (close-form) solution, (2) limit equilibrium method, and (3) shear reduction technique for the numerical method.

2.2.1 Analytical (Close form) Solution

Fox (2004) presents his work on the analytical solutions for a slurry-supported trench as obtained from two- and three-dimensional analysis which mainly determines factor of safety and critical failure plane angle under Coulomb-type force equilibrium analyses. His work is based on the assumptions that the sliding surface is planar and the failure wedge is a rigid block. The solutions can accommodate drained effective stress analysis and undrained total stress analysis for two- and three-dimensional cases.

2.2.1.1 Three-Dimensional Solution for Drained and Undrained Analysis

Case-1 in the work performed by Fox (2004) is concerned with drained effective stress analyses and the variable of groundwater table elevation below tension crack zone, trench depth, trench length, slurry depth, surcharge loading, and tension crack depth. Figure 2.1 and Figure 2.2 have shown drained effective stress stability analysis for Case-1 geometry, forces on failure wedge, possible tension crack, and boundary pore pressure configurations.

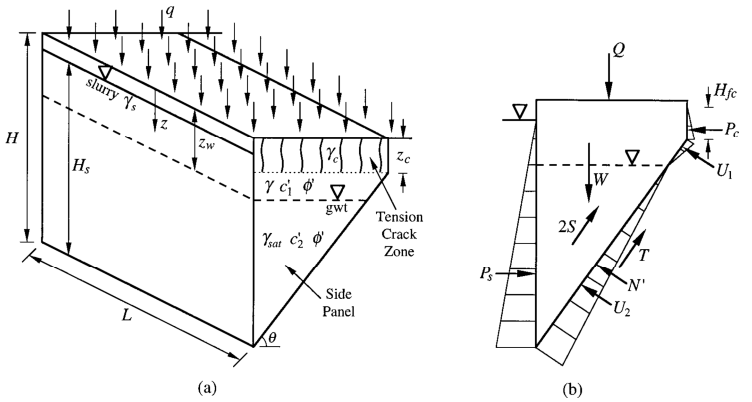

Figure 2.1 Drained effective stress stability analysis for Case-1: (a) geometry and (b) forces on failure wedge (Fox 2004).

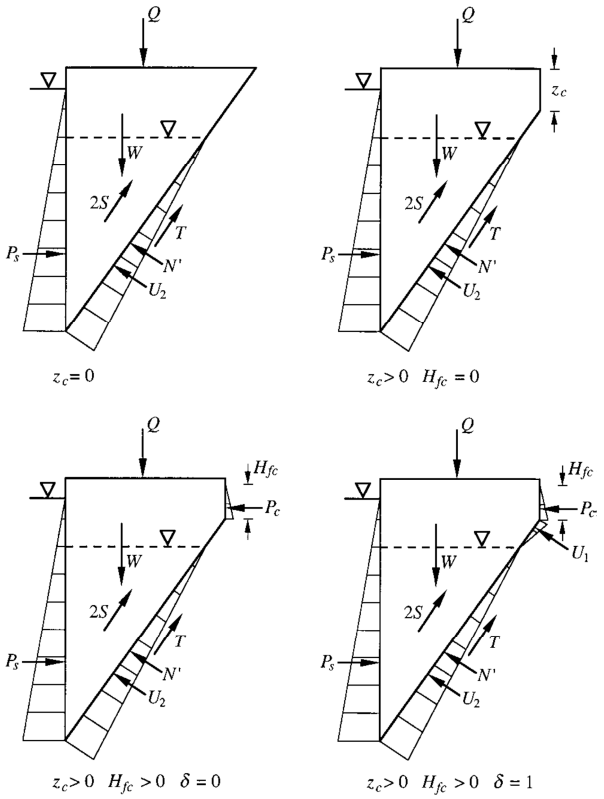

Figure 2.2 Possible tension crack and boundary pore pressure configurations for Case-1 For three-dimensional stability (Fox 2004).

Where:

a = undrained shear strength at z = 0;

b = rate of change of undrained shear strength with depth;

c' = effective stress cohesion intercept;

c'_c = effective stress cohesion intercept in tension crack zone;

c'_1 = effective stress cohesion intercept above groundwater table;

c'_2 = effective stress cohesion intercept below groundwater table;

F = factor of safety with respect to shear failure;

F_N = force component normal to bottom failure plane (N);

F_S = minimum factor of safety (corresponding to θ_{cr});

F_T = force component tangential to bottom failure plane (N);

H = depth of trench;

H_{fc} = height of fluid in tension cracks;

H_s = depth of slurry;

K = average lateral earth pressure coefficient for side panels of failure wedge;

L = length of trench;

N = total normal force on bottom failure plane;

N' = effective normal force on bottom failure plane;

P_c = fluid force from tension cracks on failure wedge;

P_s = slurry force on failure wedge;

Q = surcharge force on failure wedge;

q = vertical surcharge pressure;

q_r = vertical surcharge pressure that contributes to shear resistance of side panels;

S = shear resistance force on each side panel of failure wedge;

s_u = undrained shear strength;

$s_{u,c}$ = average undrained shear strength in tension crack zone;

T = shear force on bottom failure plane;

U = pore water force on bottom failure plane;

U_1 = pore water force on bottom failure plane between tension crack zone and groundwater table;

U_2 = pore water force on bottom failure plane below groundwater table;

W = weight of failure wedge;

z = depth below ground surface;

z_c = depth of tension crack zone;

z_w = depth of groundwater table;

γ = unit weight of soil between groundwater table and tension crack zone;

γ_c = unit weight of soil in tension crack zone;

$\gamma_{c,sat}$ = unit weight of saturated soil in tension crack zone;

γ_{fc} = unit weight of fluid in tension cracks;

γ_s = unit weight of slurry;

γ_{sat} = unit weight of saturated soil below groundwater table;

γ_w = unit weight of water;

γ' = buoyant unit weight of soil below groundwater table;

γ'_c = buoyant unit weight of soil in tension crack zone;

δ = operator to allow inclusion or exclusion of force U_1;

θ = angle of bottom failure plane from horizontal;

θ_{cr} = critical angle of bottom failure plane from horizontal (corresponding to F_S);

ϕ = angle of internal friction;

ϕ' = effective stress angle of internal friction;

The shear resistance of each panel is calculated under the assumption of failure wedge. The failure wedge, which uniformly and proportionally is acting parallel to bottom failure plane mobilized along the failure surface. When the shear failure of each side panel is equal to the bottom failure plane the factor of safety is defined. This is calculated by summation of all forces component for the failure wedge in directions normal and tangential to the bottom failure plane as of equations (2.1) and (2.2).

$$\sum F_N = N' + U_1 + U_2 - (W + Q)\cos\theta - (P_s - P_c)\sin\theta = 0 \quad (2.1)$$

$$\sum F_T = 2S + T - (W + Q)\sin\theta - (P_s - P_c)\cos\theta = 0 \quad (2.2)$$

Where S is the shear resistance force for each panel of the failure wedge as shown below:

$$S = \frac{\cot\theta}{2F}\Phi_1$$

The factor of safety then is solved for the failure wedge as of the equation (2.3) .

$$FS = A_1 \sec\theta_{cr} \csc\theta_{cr} + B_1 \cot\theta_{cr} + C_1 \tan\theta_{cr} + D_1 \csc\theta_{cr} \quad (2.3)$$

The corresponding critical angle of the bottom failure θ_{cr} to the minimum factor of safety Fs for the failure wedge is calculated from the derivative of $dF/d\theta = 0$ which result in this following equation (2.4).

$$\cos^3\theta_{cr} + \frac{2A_1 + B_1 + C_1}{D_1} + \cos^2\theta_{cr} - \frac{A_1 + C_1}{D_1} = 0 \quad (2.4)$$

Where A_1, B_1, C_1, D_1, Ψ_1, Λ_1, Γ_1, Φ_1, and Ω are the calculated variables as shown below:

$$A_1 = \frac{\Psi_1 - \Lambda_1 \tan\phi'}{\Gamma_1 - \Omega}$$

$$B_1 = \frac{\Gamma_1 \tan\phi'}{\Gamma_1 - \Omega}$$

$$C_1 = \frac{\Omega \tan\phi'}{\Gamma_1 - \Omega}$$

$$D_1 = \frac{\Phi_1}{L(\Gamma_1 - \Omega)}$$

$$\begin{aligned}\Phi_1 = c_1'[2H(z_w - z_c) + z_c^2 - z_w^2] + c_2'(H - z_w)^2 \\ + K\tan\phi'\left(q_r + \gamma_c z_c + \delta\frac{\gamma_{fc}H_{fc}(H - z_w)}{z_w - z_c}\right)(H - z_c)^2 \\ + \frac{K}{3}\tan\phi'\left(\gamma' + \gamma + \delta\frac{\gamma_{fc}H_{fc}}{z_w - z_c}\right)(H - z_w)^3 \\ + \frac{K}{3}\tan\phi'\left(\gamma - 2\delta\frac{\gamma_{fc}H_{fc}}{z_w - z_c}\right)(H - z_c)^3\end{aligned}$$

$$W + Q = \Gamma_1 L\cot\theta$$

$$\Gamma_1 = (q + \gamma_c z_c)(H - z_c) + \frac{\gamma}{2}[2H(z_w - z_c) + z_c^2 - z_w^2] + \frac{\gamma_{sat}}{2}(H - z_w)^2$$

$$U_1 + U_2 = \Lambda_1 L\csc\theta$$

$$\Lambda_1 = \tfrac{1}{2}\left[\delta\gamma_{fc}H_{fc}(z_w - z_c) + \gamma_w(H - z_w)^2\right]$$

$$P_s - P_c = \Omega L$$

$$\Omega = \tfrac{1}{2}\left(\gamma_s H_s^2 - \gamma_{fc}H_{fc}^2\right)$$

$$T = \frac{\Psi_1 L\csc\theta - N'\tan\phi'}{F}$$

$$\Psi_1 = c_1'(z_w - z_c) + c_2'(H - z_w)$$

Case-2 in the work performed by Fox (2004) is concerned with undrained total stress analyses and the variable of trench depth, trench length, slurry depth, surcharge loading, and tension crack depth. Figure 2.3 has shown undrained total stress stability analysis case- 2 geometry and forces on failure wedge.

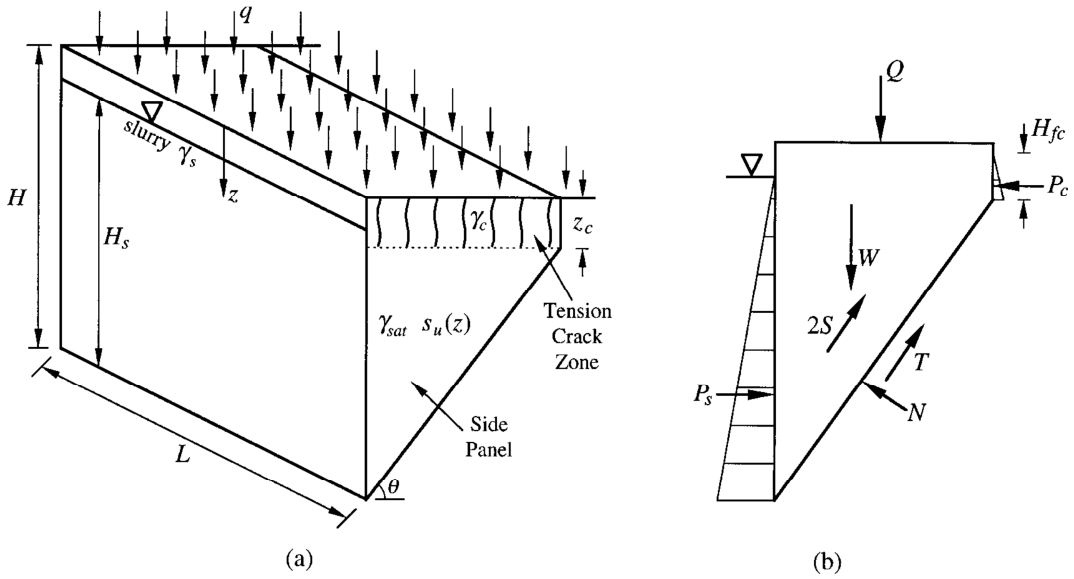

Figure 2.3 Case-2 undrained total stress stability analysis: (a) geometry and (b) forces on failure wedge. (Fox 2004).

It is mostly the same as the effective stress analyses except that the soil assumed to be saturated and fail in isotopic undrained shear strength. The factor of safety and the critical angle of bottom failure plane are then solved for the failure wedge, as shown in equations (2.5) and (2.6).

$$\cos^3\theta_{cr} + \frac{2A_3}{D_3}\cos^2\theta_{cr} - \frac{A_3}{D_3} = 0 \quad (2.5)$$

$$FS = A_3 \sec\theta_{cr} \csc\theta_{cr} + D_3 \csc\theta_{cr} \quad (2.6)$$

Where A_3, D_3, Ψ_3, Λ_3, Γ_3, Φ_3, and Ω are the calculated variables as shown below:

$$A_3 = \frac{\Psi_3}{\Gamma_3 - \Omega}$$

$$D_3 = \frac{\Phi_3}{L(\Gamma_3 - \Omega)}$$

$$W + Q = \Gamma_3 L \cot\theta$$

$$\Gamma_3 = (H - z_c) + \left(q + \gamma_c z_c + \frac{\gamma_{sat}}{2}(H - z_c)\right)$$

$$P_s - P_c = \Omega L$$

$$T = \frac{\Psi_3 L \csc\theta}{F}$$

$$\Psi_3 = a(H - z_c) + \frac{b}{2}(H^2 - z_c^2)$$

2.2.1.2 Two-Dimensional Solution for Drained and Undrained Analysis

The two-dimensional stability for case-1 in the work by Fox (2004) is calculated by neglecting the contribution of side panel shear resistance forces by letting L→∞. This can be represented by equations (2.7) and (2.8).

$$\tan\theta_{cr} = \sqrt{\frac{A_1+B_1}{A_1+C_1}} = \sqrt{\frac{\psi_1 + \Gamma_1 - \Lambda_1)\tan\phi'}{\psi_1 + (\Omega-\Lambda_1)\tan\phi'}} \tag{2.7}$$

$$\begin{aligned} FS &= A_1 \sec\theta_{cr} \csc\theta_{cr} + B_1 \cot\theta_{cr} + C_1 \tan\theta_{cr} \\ &= 2\sqrt{(A_1 + B_1)(A_1 + C_1)} \end{aligned} \tag{2.8}$$

The two-dimensional stability for case-2 in the work by Fox (2004) is calculated by neglecting the contribution of side panel shear resistance forces by letting L→∞. The critical angle of bottom failure plane and a factor of safety are calculated from previous equations (2.5) and (2.6) which gives $\theta_{cr} = 45^{\circ}$ and factor of safety as of equation (2.9).

$$FS = 2A_3 \tag{2.9}$$

The three-dimensional method has been used as a simplified solution to preliminary evaluate the effect of soil properties and external factors for three-dimensional analysis which results in focusing on some influential soil properties to be selected in this research. However, this research will be considering more parameter and layers affecting the stability of the slurry wall which is not considered in the above research.

2.2.2 Limit Equilibrium Analysis

In spite of the recent development of numerical techniques, limit equilibrium method (LEM) still in use to assess slope stability and vertical cuts. The minimum global safety factor of slopes or vertical cuts is calculated based on assumptions on interslice forces by locating the critical slip surface.

These slice methods solve force and moment equilibrium equations with gravity stability on the relationship between normal and tangential forces and their positions acting along failure planes and inner forces (Bishop 1955, Spencer 1967, Aydan et al. 1992, Kumsar 1993).

Previous types of research and a number of methods have been developed and suggested the LEM for the stability of the slurry trench wall. These developed trench stability theories are introduced in this research based on two groups. The first group is two-dimensional (2-D) and the second is a three-dimensional (3-D) assumption.

In the (3-D) solution, Piaskowski and Kowalewski (1965) introduced a vertical elliptic cylinder cut by a critical plane shape. This idealized shape was the first solution for the (3-D) sliding wedge of slurry trench wall stability under (3-D) conditions. The approach has a profound justification in term of arching effect. In this analysis, the lateral earth pressure acting along the trench face computed from (3-D) sliding wedge was compared with the horizontal pressure developed in the slurry filling. See Figure 2.4 for shape assumption.

Washbourne (1984) his assumption was modifying the shape of rigid block assuming the angle α between slide surface and face of the trench. And then analyzing the stability of the wedge as the Coulomb wedge was analyzed in the (2-D) retaining wall. The safety factor was calculated as the ratio of horizontal force due to slurry pressure to the active thrust of the (3-D) wedge. See Figure 2.4 for shape assumption.

Tsai and Chang (1996) proposed sophisticated (3-D) LEM method solutions for slurry trench wall analysis in a cohesionless soil which presents more realistic shear surface from the shell-shape sliding surface. The sliding surface is found using the Mohr-Coulomb criterion. The method is determined, the effective weight, the vertical stress acting on the soil vertical columns as a generalization of (3-D) slices which calculated by Huder's formula that takes into account the horizontal arching effect introduced by Terzaghi. To check force equilibrium on the slip surface all external forces acting on each discrete column are summed up. The safety factor was calculated as the ratio of the hydrostatic slurry stabilizing force to the required stability of sliding wedge horizontal driving force. Figure 2.4 has shown the shape assumption.

However, these techniques do not consider the impact of the slurry pressure while looking for the critical sliding surface or while ascertaining the pressure acting on the base of the soil column. The in-situ stress in the soil is partly replaced by slurry pressure causing the redistribution of the stress behind the trench face. It can be normal that the slurry pressure would influence the vertical stresses acting on the critical sliding surface and horizontal arching in the soil. Therefore, the slurry pressure will impact the stress redistribution behind the trench face, on both failure and shape of the critical sliding surface.

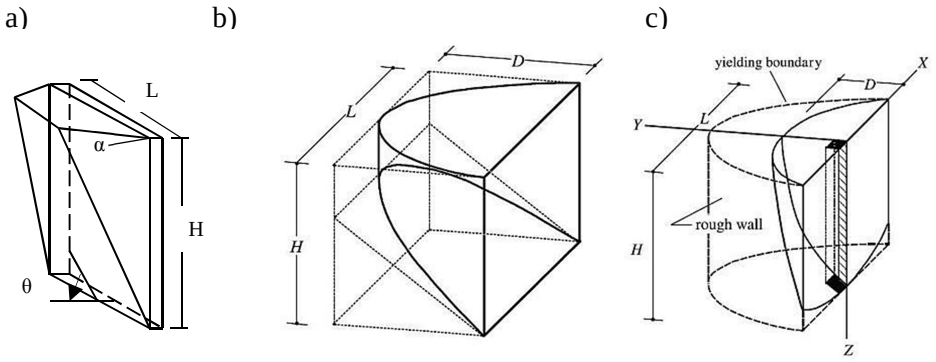

Figure 2.4 Shapes of the sliding wedges studied by a) Washbourne (1984); b) Piaskowski and Kowalewski (1965); c) Tsai and Chang (1996).

Recently, Yu and Ugai (1997) presented an equivalent approach from limit equilibrium to calculate the three-dimensional effect of slurry-wall trenches constructed in the sandy ground. This improved (3-D) LEM method based on Tsai and Chang assumptions. The different assumptions were the sliding surface is assumed as two ellipse caps attached smoothly to a cylindrical surface. Moreover, the effect of confining forces acting on the bottom of the soil column is included. This method agreed well with ones by the centrifuge tests (Yu and Ugai 1997).

In this method, equations developed to find the effect of the confining force acting on the trench which affects the safety factor of the slurry-wall trenches. All results explained and compared with (3-D) elastoplastic finite element method (FEM) and experimental centrifuge tests (Yu and Ugai 1997).

The slurry resultant pressure force is calculated and the water pressure acts on the wall of the trench calculated for assumed schematic slurry trench wall as shown in Figure 2.5.

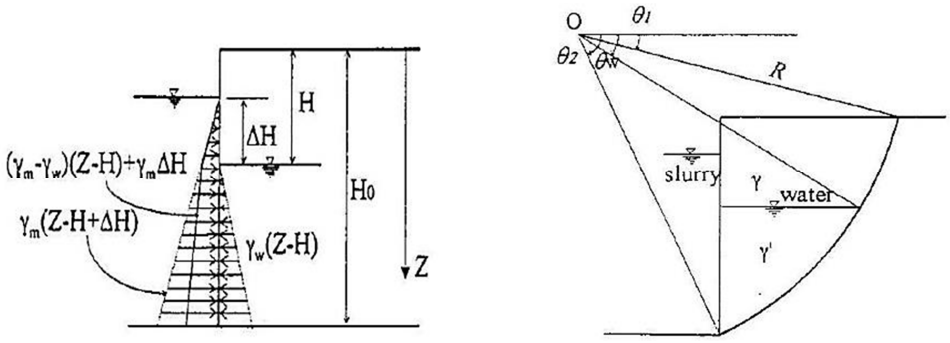

Figure 2.5 Schematic of the slurry trench wall. (Yu and Ugai 1997).

Two ellipse caps attached smoothly to the cylindrical surface are assumed for the sliding surface, as shown in Figure 2.6.

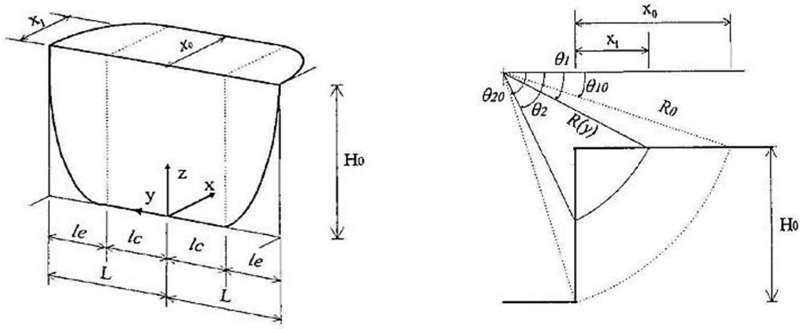

Figure 2.6 Shape of the (3-D) sliding body. (Yu and Ugai 1997).

To determine the critical sliding surface the area above the critical sliding surface is divided by numbers of columns. Then the determination of vertical stress acting on the bottom and vertical

stress acting at the bottom of each column should be calculated with regard to the horizontal arching in the soil, as shown in Figure 2.7.

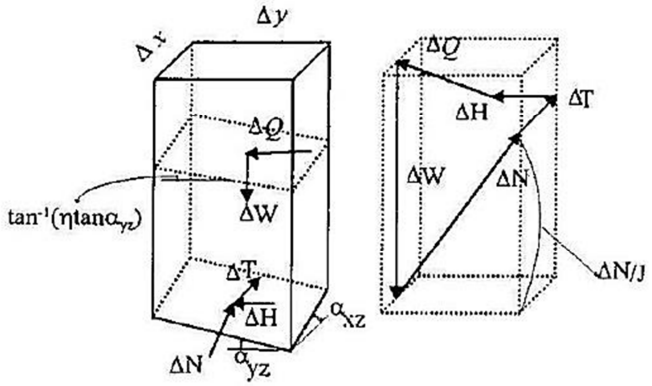

Figure 2.7 Forces acting on the column of the (3-D) sliding body. (Yu and Ugai 1997).

The factor of safety calculated under failure condition is defined by the simultaneous equations of vertical and horizontal force equilibrium for sliding body and also by searching for its minimum value in the range of $0 \leq \theta_1 \leq \theta_2 < \pi/2$ and $0 \leq Le \leq L$ from the equation (2.10), whereas the vertical stresses are decomposed into normal and tangential components.

$$\Delta T = (cJ\ \Delta x\ \Delta y + \Delta N\ \tan\phi)/FS \qquad (2.10)$$

The simultaneous equations of vertical and horizontal force equilibrium for the sliding body are shown in equations (2.11), (2.12), and (2.13).

$$F_v = \sum (N_v/D_e) \Big/ \sum (\Delta W) \qquad (2.11)$$

$$F_h = \sum (N_h / D_e) / \left(\sum (\Delta W \tan \alpha_{yz}) - U \right) \quad (2.12)$$

$$F_v = F_h = FS \quad (2.13)$$

Where:

ΔT = total shear forces acting on the base.

ΔN = total normal forces acting on the base.

U = the total difference pressure.

c = the cohesion.

J = the plane composed of ΔQ_1 and ΔQ_2.

ΔQ_1 = the resultant of the intercolumn forces acting on the sides at the x-z plane and parallel to the x-axis.

ΔQ_2 = the resultant of the intercolumn forces acting on the sides with inclined to the x-y plane by $\tan^{-1} (\eta \alpha_{yz})$.

η = constant.

ϕ = angle of internal friction.

Where:

$D_e = (1 + \eta \tan^2 \alpha_{yz}) / J + \sin \alpha_{xz} \tan \phi / FS$

$$N_v = \left(F_v/J + \tan\phi \sin\alpha_{xz}\right)\left(1+\kappa\eta \tan^2\alpha_{yz}\right)+c\eta \sin\alpha_{xz} \tan^2\alpha_{yz}\, \Delta x\Delta y$$

$$N_h = F_h \Delta W \eta \tan^2\alpha_{yz} \tan\alpha_{xz} (1-\kappa)/J + [\Delta W \tan\phi \left(1+\kappa\eta \tan^2\alpha_{yz} \cos^2\alpha_{xz}\right) + c\Delta x\Delta y(1 + \eta \tan^2\alpha_{yz} \cos^2\alpha_{xz})]/\cos\alpha_{xz}$$

$$k = K_o\,(L/H_o)^{0.138/ko}$$

$$K_o = 1 - \sin\phi'$$

ϕ' = the angle of internal friction which is determined from conventional triaxial tests.

One of the disadvantages of LEM massive iterations developed to satisfy the displacement if not, the system has to be defined as failed.

2.2.3 Shear Strength Reduction Technique for the Numerical Method

Shear strength reduction technique (SSR) has developed and become the base technique to evaluate the factor of safety for the finite element method (FEM) and finite difference method (FDM). It was first introduced by Zienkiewicz in early 1975 to evaluate the factor of safety (Oblozinsky et al. 2001). Then the validity of SSR was discussed and demonstrated by others using desktop computers (Oblozinsky et al. 2001).

The SSR technique is based on reducing the soil strength parameters until the soil fails. If we use the variables of the soil strength parameters c and ϕ the equation will be presented as below:

$$c_F = \frac{c}{F} \; ; \phi_F = \tan^{-1}\left(\frac{\tan\phi}{F}\right) \qquad (2.14)$$

The F is a parameter which reduces the soil strengths.

To analyze the slurry trench stability, the pressure of the soil strength is applied as a small incremental pressure in the elastic condition. The first step is to calculate the stability by a small value of F which equal to 0.01. The strength value of soil parameter will be high due to a small value of the reduction parameter F which causes the domain to be in the elastic condition. Then the soil strength is correspondingly reduced when F is incrementally increased. This incremental pressure repeats until failure occurs. When the failure occurs, the value of F becomes the global minimal safety factor (FS). This technique is used in software programs like finite element software PLAXIS and three-dimensional Lagrangian formulation based finite difference approach software FLAC (Oblozinsky et al. 2001).

Oblozinsky et al. (2001) discussed a design method for slurry trench wall stability in sandy ground bases on elasto-plastic FEM. The soil was modeled as elasto-perfectly-plastic material with Mohr-Coulomb failure criteria. This was based on the calculating of a factor of safety to evaluate the slurry trench stability by using the shear strength reduction technique (SSR). The mesh geometry in Figure 2.8 shows that the soil beyond the ends of the trench was ignored for simplicity which has a minor influence on the value of the factor of safety by using the SSR-FEM. This method is verified by comparing it with centrifuge lab tests (Oblozinsky et al. 2001).

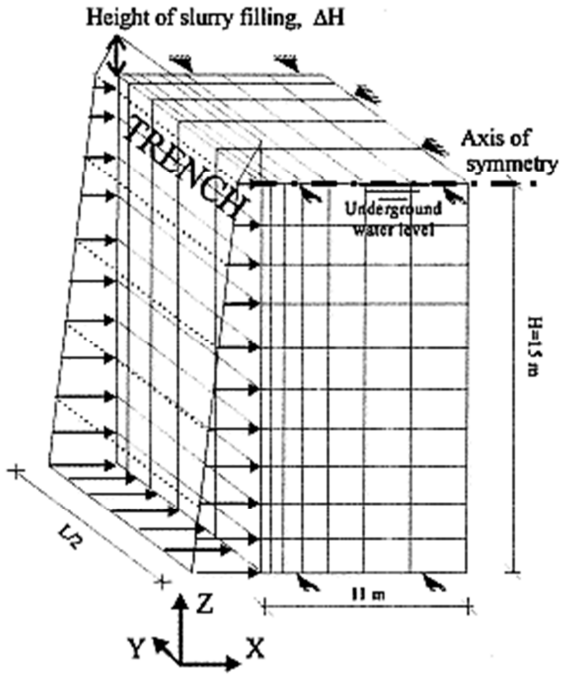

Figure 2.8 Mesh geometry for trench supported by slurry in FEM idealization (Oblozinsky et al. 2001).

One of the advantages of the numerical method SSR-FEM and SSR-FDM is to capture the redistribution of the stresses behind the trench face caused by slurry pressures. These pressures are replacing the in-situ pressure soil behavior (soil arching effect), while in LEM needs complicated assumption to account the (3-D) effect. Moreover, the critical sliding surface is automatically found.

2.3 Stability

Instability due to deformations and or overstresses can be important design considerations for soil-bentonite slurry walls for various reasons. Several damage reports have been reported of a

nearby building due to the construction of soil-bentonite slurry walls. For example, cracking of large dams due to the inability to withstand the significant deformation accrue on the construction of the cutoff wall. Therefore, the stability of slurry trenches during excavation is a major concern in design and construction. Although some papers have been addressing this issue from a different perspective, this issue is more complex due to the uncertainty of the soil.

Stability of slurry trench excavation in cohesive soil was experimentally discussed by Tamano et al. (1996). The displacement caused by the lateral pressure of the slurry wall is extremely difficult to measure. However, based on the mechanical behavior measured by the trench wall stability is examined via the horizontal stress before and after trench excavation. The horizontal stresses before trench excavation are presented by K= $\sum_{i=1}^{n} \gamma_i H_i$ where K is the coefficient of lateral pressure, γ_i is the unit weight of each layer's soil, and H_i is each layer's thickness. The horizontal stresses produced by slurry pressure are $\gamma_f h$ where h is the depth of slurry level. The difference between the two stresses will produce the stresses that will make the trench wall displaced $\Delta\sigma_R$, which is expressed in the equation (2.15) (Tamano et al. 1996).

$$\Delta\sigma_R = K \sum_{i=1}^{n} \gamma_i H_i - \gamma_f h \qquad (2.15)$$

The slurry wall stability during the trench excavation in cohesive soil at different ground level is presented in Figure 2.9. This figure presents the trench wall stability at ground level -0.3 m the lateral pressure decreases below the value of lateral pressure at rest and maintains a balance with the slurry pressure which keeps the trench stabile. However, at ground level -3.5 m the lateral pressure did not decrease below the slurry pressure despite the large trench wall displacement.

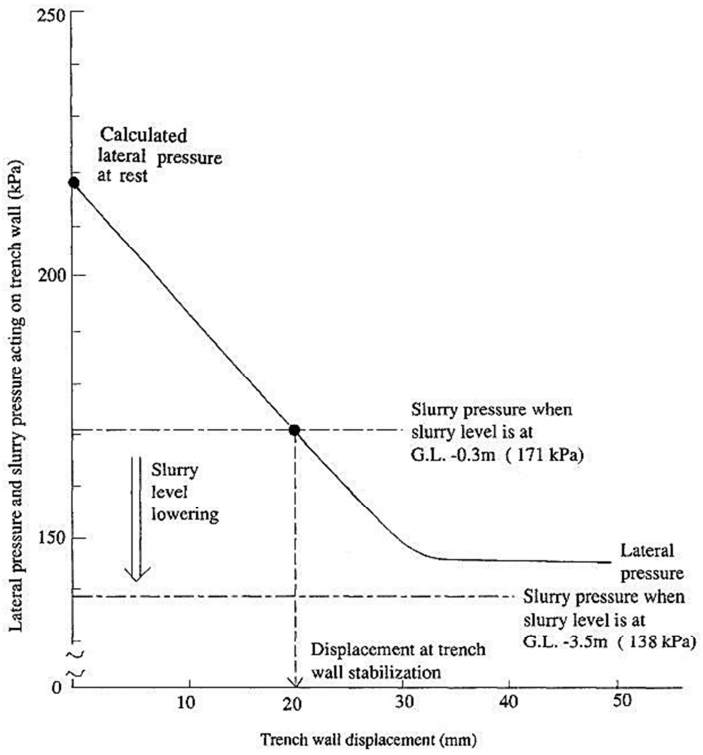

Figure 2.9 Trench wall stabilization at level -16 m (Tamano et al. 1996).

The work by Tamano et al. (1996) describes the stabilizing mechanism in term of displacement of slurry trench excavation in soft clay under normal consolidation. However, they did not represent the displacement due to the effect of several layers and length depth ratio which give the third dimension to the problem.

The stability of a long slurry wall of cohesionless soil is described by Filz et al. (2004). This study used a parametric study with a closed-form solution which was implemented on a homogenous soil. The most important stabilizing mechanism for long, slurry supported trenches

in the sand is the lateral hydrostatic pressure from the slurry wall. Without the filter cake, however, the stability of the trench significantly decreased. If the filter cake formation criteria are satisfied, the global trench stability is still a challenge. The possible factors for instability contributions are a lower level of the slurry, a decreasing the unit weight, an increasing the water level or external surcharge pressure to the ground surface near the trench wall. Figure 2.10 has shown the impacts of the slurry level and elevation of the sliding surface on the factor of safety. However, the base assumption is that the soil is cohesionless homogenous soil.

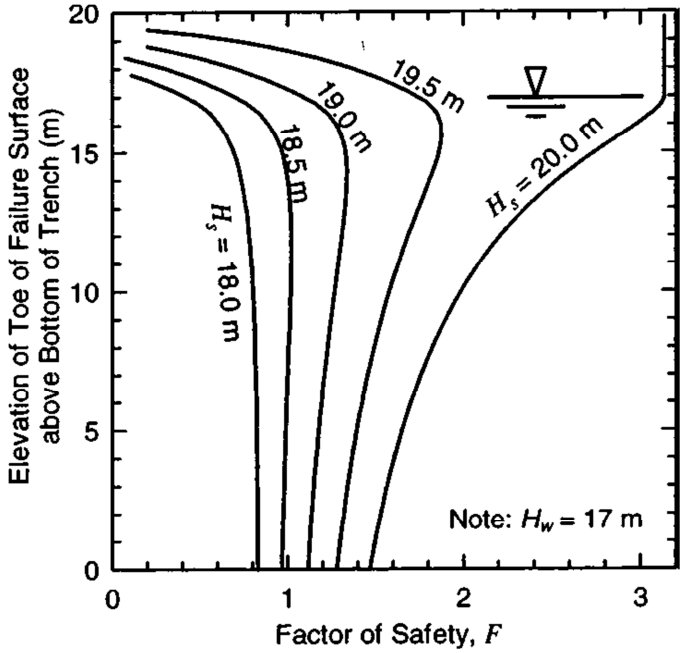

Figure 2.10 Impact of the slurry level and elevation of the sliding surface on the factor of safety (Filz et al. 2004).

Where: Hs is the slurry level.

Regarding the safety of slurry trench wall simulation, there is a numerical simulation of ground movements and stability evaluation during trench excavation processes done by Brzakala and Gorska (2007). The soil model was modeled to correspond to macro-homogeneous sand, and an elastoplastic material with the Mohr-Coulomb yield criteria. The results show that the factor of safety depends on the depth of the excavation. However, the model did not consider such variables as the movement of the bucket of the trenching machine, trench length, and soil layers inhomogeneity. The relationship between the factor of safety and the depth of excavation is presented in Figure 2.11 and the displacements of the sliding wedge, as shown in Figure 2.12.

The stability of the trench is investigated by SSR for three parameters, Sand friction angle, unit weight of the bentonite slurry, and unit weight of surrounding sand. The calculations of the factor of safety are executed for every increased trench depth by one meter.

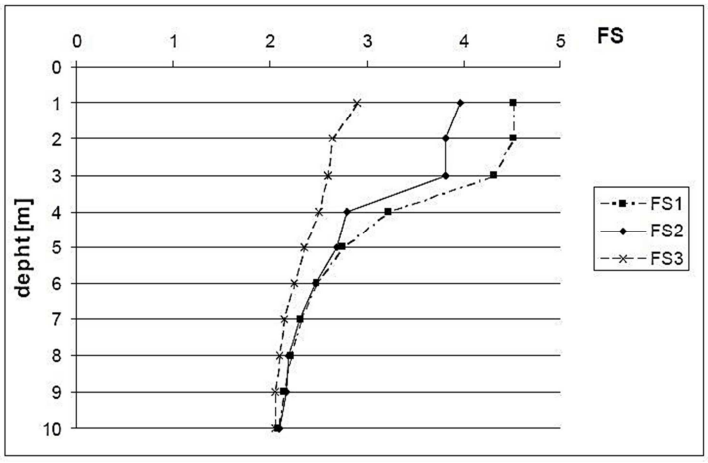

Figure 2.11 The dependence of the safety factors FS_i on the depth of excavation [m] (Brzakala and Gorska 2007).

Where

FS_1 = reduction of the ground strength parameter (cohesion=0) = $\frac{tg\ \phi}{tg\ \phi_{zred}}$

FS_2 = reduction of unit weight of the bentonite slurry = $\frac{\gamma_z}{\gamma_{zred}}$

FS_3 = increase of unit weight of the surrounding sand = $\frac{\gamma_{zgw}}{\gamma_g}$

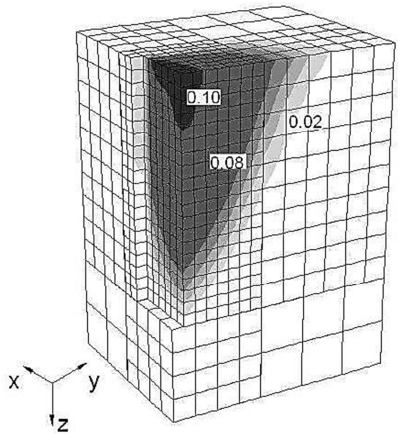

Figure 2.12 The displacements of the continuum within the sliding wedge near the trench, [m] (Brzakala and Gorska 2007).

Ding and Wang (2008) performed a numerical study. Their model was to represent ground response during slurry wall construction. The results show that during the construction of the slurry wall a substantial ground movement could happen. This displacement due to the mechanical response of the ground is reduced by the hydraulic pressure from the slurry wall. However, the soil has been modeled as one linear elastic, perfectly plastic isotropic material with

a Mohr-Coulomb yield surface to reduce the complexity of the soil interaction with the slurry wall. During the modeling, the change of stresses and strain for deferent depth and the length of the slurry were analyzed. The model mesh and the settlement of soil in both directions are shown in Figure 2.13 andFigure 2.14.

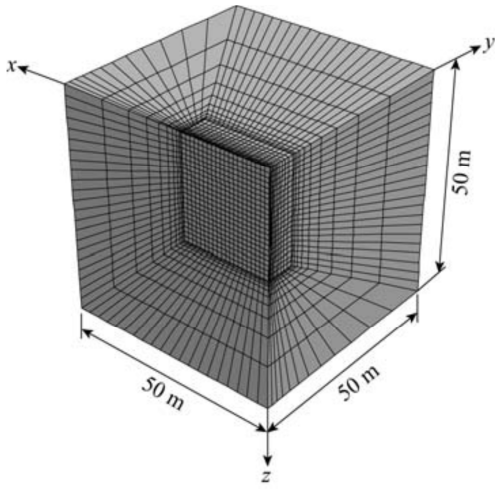

Figure 2.13 The Mesh of the model (Ding and Wang 2008).

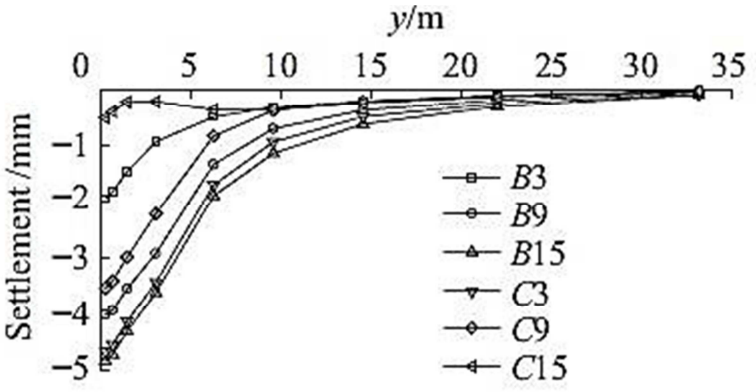

Figure 2.14 The Settlement perpendicular to panel $x = 0$ (Ding and Wang 2008).

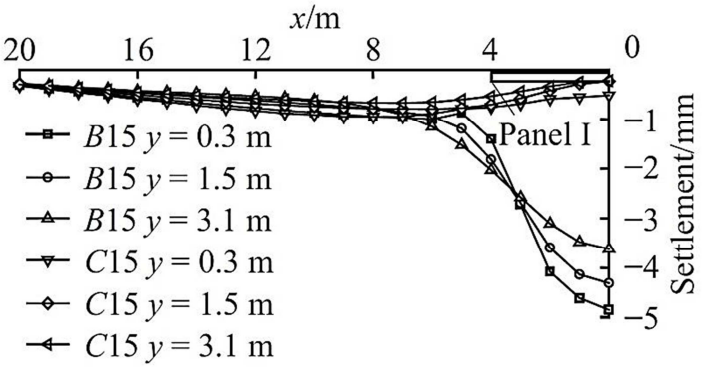

Figure 2.15 The Settlement along longitudinal direction $y = 0$ (Ding and Wang 2008).

The stages from B-3 to B-15 are the different stages of construction excavation depth that will apply hydrostatic bentonite pressure on the trench face. The stages from C-3 to C-15 are the steps of construction depth by concrete pressure applying the lateral pressure inside the panel, as shown in Figure 2.16.

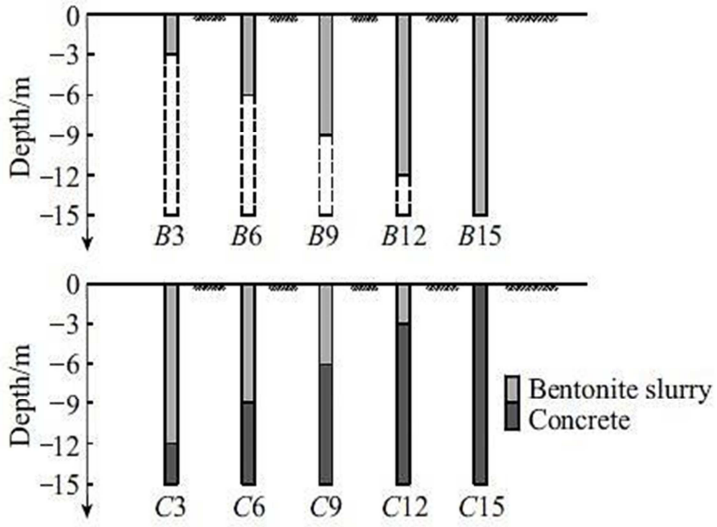

Figure 2.16 Modeling steps of constructing diaphragm wall panels (Ding and Wang 2008).

Zhang et al. (2013) studied the stability of the over-length trench wall by a numerical simulation analysis and developed a model of slurry-filled trench wall in the actual excavation. The stability is analyzed based on the elasto-plastic finite-element method. Several factors were considered for the analysis including the influence of dewatering condition, excavation depth and length, and slurry unit weight. The deformation amplitude of the wall is increased gradually with the increase of excavation depth and length, as shown in Figure 2.17 and Figure 2.18. However, the model does not study the influence of multiple layers on a slope surface model that influences the deformation, stresses, and factor of safety.

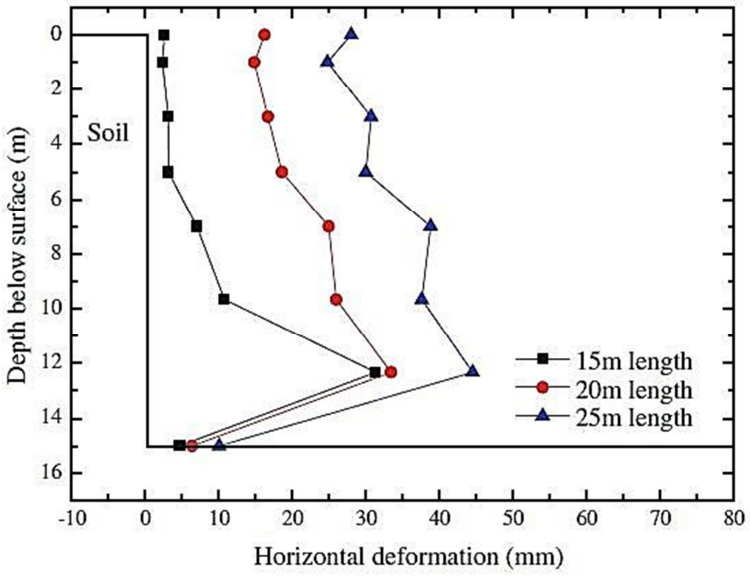

Figure 2.17 The wall deformation in different excavation lengths (Zhang et al. 2013).

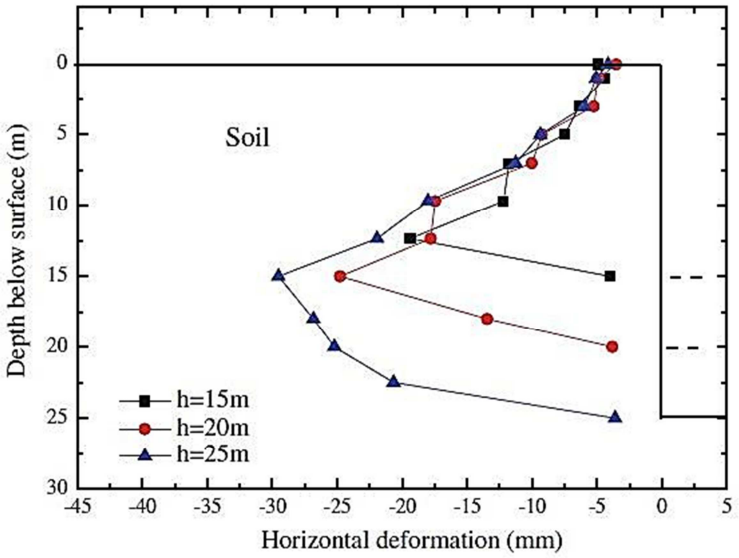

Figure 2.18 The Wall deformation in different excavation depths (Zhang et al. 2013).

The stability of a slurry trench with an inclined ground surface was calculated by Li et al (2013) using the Coulomb-type force equilibrium method. The trench stability and the angle of failure for the inclined surface were investigated via a parametric study. This kind of inclination is expected on the excavated cutoff wall near an earth dam or landfill in downstream location.

The model assumption and dimensions are given as following: The depth of the trench is h; the ground surface slopes at angle β to the horizontal, with the counterclockwise direction as positive; the groundwater surface has a depth z_w; the slurry in the trench has a depth z_s with a unit weight γ_s; the unit weight and effective stress cohesion intercept of the soil above the groundwater table are γ_1 and c'_1, and for the soil below the groundwater surface are γ_2 and c'_2, respectively; the

effective stress friction angle of the entire soil profile is ϕ′; and the uniform vertical surcharge pressure on the inclined ground surface is q, as shown in Figure 2.19.

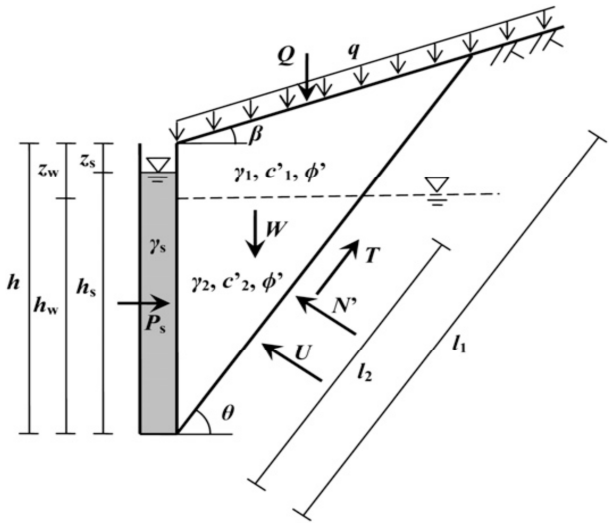

Figure 2.19 Configuration and forces on the sliding wedge of a slurry trench with an inclined ground surface (Li et al. 2013).

The failure surface is assumed planar, sloping at angle θ to the horizontal. The forces, that is, soil weight W, slurry force P_s, hydrostatic groundwater force U, effective normal force N′, shear force T, and surcharge force Q, acting on the wedge are illustrated in Figure 2.19.

Force equilibrium in the directions normal and tangential to the failure surface for the wedge yields is presented by the equations (2.16) and (2.17):

$$\sum F_N = 0, \qquad N' + U - (W + Q)\cos\theta - P_s \sin\theta = 0 \tag{2.16}$$

$$\sum F_T = 0, \qquad T - (W + Q)\sin\theta + P_s \cos\theta = 0 \tag{2.17}$$

The minimum value of F_s, $F_{s,min}$, corresponding to the angle of critical slip surface θ_{cr} , can be found by taking $\partial F_s/\partial\theta=0$ For cohesionless soils ($c'_1= c'_2= 0$), as shown in the equations (2.18):

$$F_s = f(\theta)\tan\phi' \tag{2.18}$$

Where:

$$f(\theta) = \frac{-U + (W + Q)\cos\theta + P_s \sin\theta}{(W + Q)\sin\theta - P_s \cos\theta}$$

$$U = \frac{h_w l_2}{2}\gamma_w$$

$$W = \left(\frac{h l_1 \cos\theta}{2} - \frac{h_w l_2 \cos\theta}{2}\right)\gamma_1 + \frac{h_w l_2 \cos\theta}{2}\gamma_2$$

$$Q = \frac{h\cos\theta}{\sin(\theta - \beta)}q$$

$$P_s = \frac{h_s^2}{2}\gamma_s$$

$$l_1 = \frac{\cos\beta}{\sin(\theta - \beta)}h$$

$$l_2 = \frac{h_w}{\sin\theta}$$

As the ground surface inclination increases, the slurry trench stability factor of safety decreases considerably, as shown in Figure 2.20.

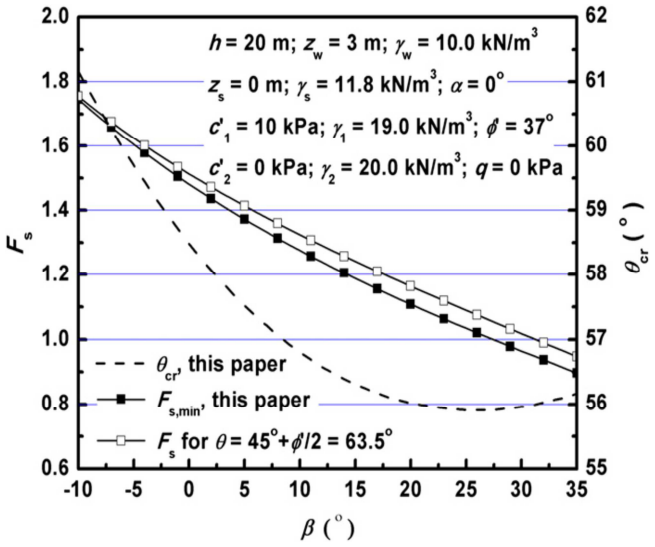

Figure 2.20 $F_{s,min}$ and θ_{cr} for varied b for an example slurry trench (Li et al. 2013).

Therefore, considering ground surface inclination is a conservative approach to assess trench stability. This study is showing the importance of including an inclined surface. This method, however, does not include the shear forces on the sides of the sliding wedge, which is the real case on the three-dimensional analyses.

This result is extended with the work done in 2015 by Jin et al. (2015) who used a model of the three-dimensional slurry trench with an inclined ground surface. A three-dimensional model of failure wedge with length L and force analysis of the model is shown in Figure 2.21.

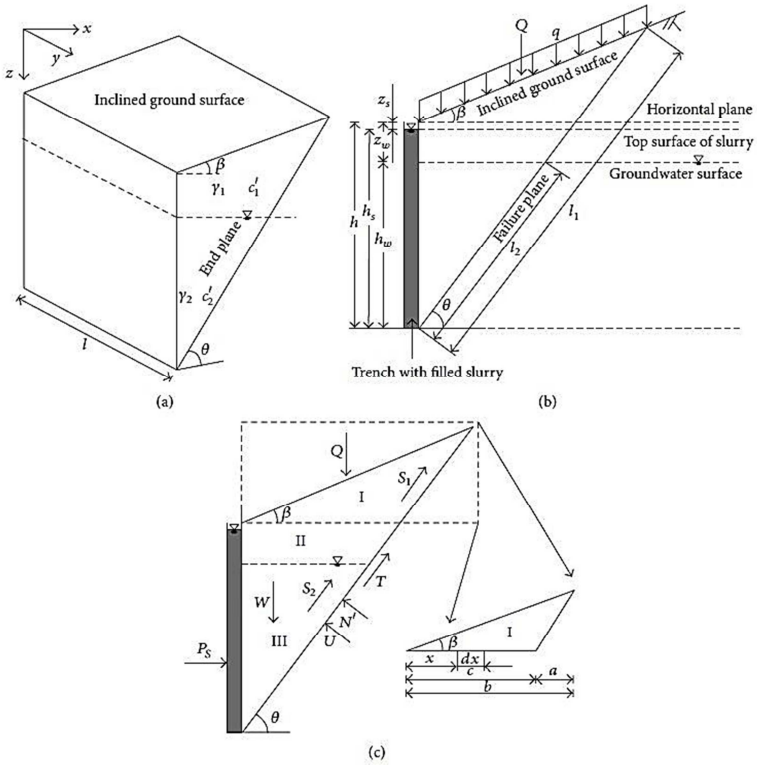

Figure 2.21 The three-dimensional failure wedge. (a) Schematic model of failure wedge, (b) definitions of geometric parameters, and (c) force analysis (Jin et al. 2015).

The factor of safety and the critical angle θ_{cr} of the failure plane which correspond to the minimum safety factor F_s for the failure wedge is found by taking $dF/d\theta = 0$. The equation can be solved by an iterative method.

The analysis result showed that increasing inclined angle β and trench length L results in decreasing the safety factor, as shown in Figure 2.22 and Figure 2.23. However, this work presents an analytical solution (close-form solution) to solve the factor of safety and the critical angle of failure, but it is not designed to study the deformation and stresses for the inclined surface. Moreover, the study is based on one homogenous soil parameter.

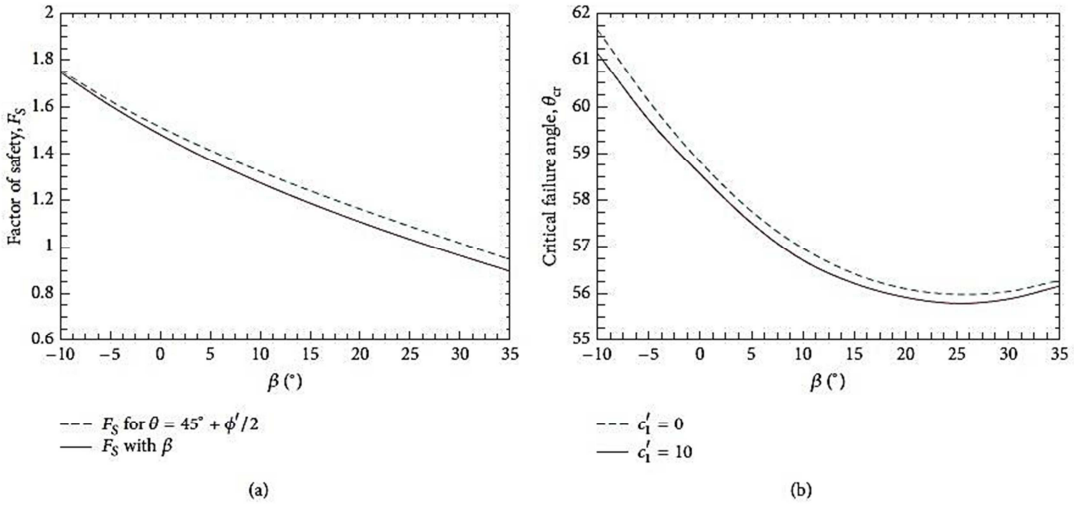

Figure 2.22 Influences of the inclined angle β on (a) F_s and (b) θ_{cr} (Jin et al. 2015).

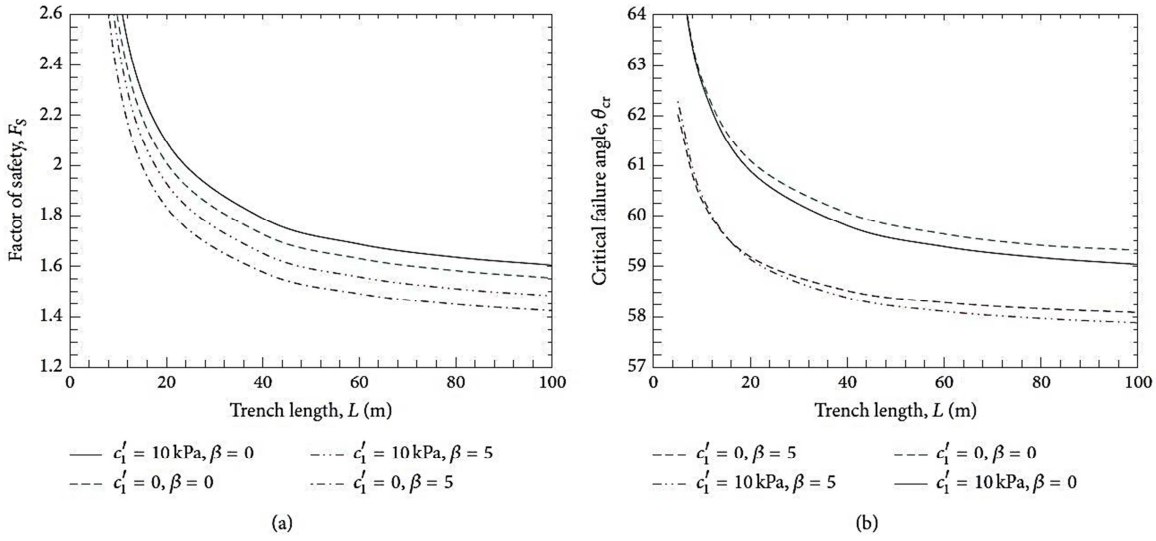

Figure 2.23 Influences of the length L on (a) F_s and (b) θ_{cr} (Jin et al. 2015).

Stability analysis of slurry trench in similarly layered soil is discussed by Li et al. (2013) to calculate the stability of the trench during excavation and prior to backfill which is a major concern in design. The failure surface is assumed to consist of a series of polygon prism surfaces and the shear forces acting on the side planes are included to consider the three-dimensional effect. Force equilibrium in terms of vertical direction for each slice and horizontal direction for whole sliding mass are established on the basis of limit equilibrium. The factor of safety is obtained by the Newton–Raphson method and the critical slip surface corresponding to the minimum factor of safety is located by the pattern search method (Li et al. 2013). Figure 2.24 has shown the model configuration.

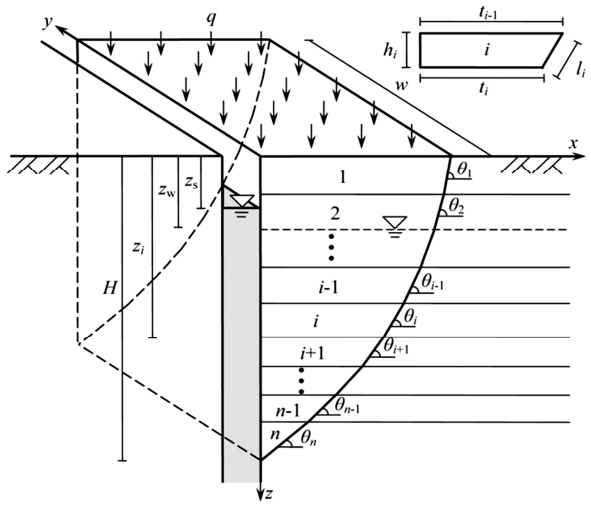

Figure 2.24 Configuration of a slurry trench in layered soils (Li et al. 2013).

Where:

The total number of soil layers is n with layer numbering starting from the ground surface; the depth of the lower boundary and thickness for i^{th} layer are z_i and h_i.

The i_{th} layer's soil unit weight, effective stress cohesion intercept, and effective stress friction angle are γ_i, c'_i, and ϕ'_i.

The slurry in the trench has a depth z_s with a unit weight γ_s; a uniform vertical effective surcharge pressure, q, is applied at the surface.

The groundwater surface is assumed to be horizontal with a depth of z_w.

However, the calculated minimum factor of safety for variable depths of the slurry surface is shown a nearly linear decrease in the factor of safety with increasing depth of the slurry surface,

as shown in Figure 2.25. This result is not considering the effect of the trench length of excavation.

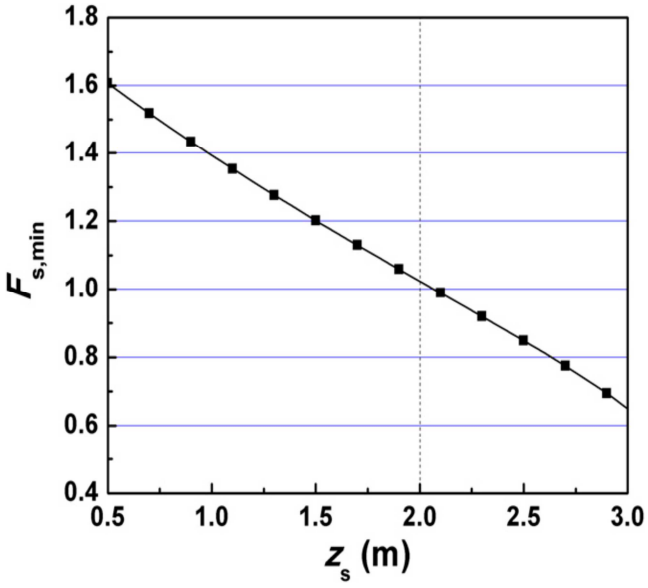

Figure 2.25 Minimum factor of safety for the varied depth of slurry surface (Li et al. 2013).

An analytical and numerical (FEM) approach of the arching dual effect describing the stability of slurry wall trenches in cohesionless soil is studied by Saadi et al. (2017). The analytical solution was proposed using the effective stress analysis method for the description of the phenomenon of deep trench stability of slurry walls. Trench stability was governed by the contribution of the interaction between horizontal and vertical arching, creating a length f of the soil disturbance zone behind the sidewall and causing the formation of an inclined sliding surface from the horizontal axis in this area, as shown in Figure 2.26.

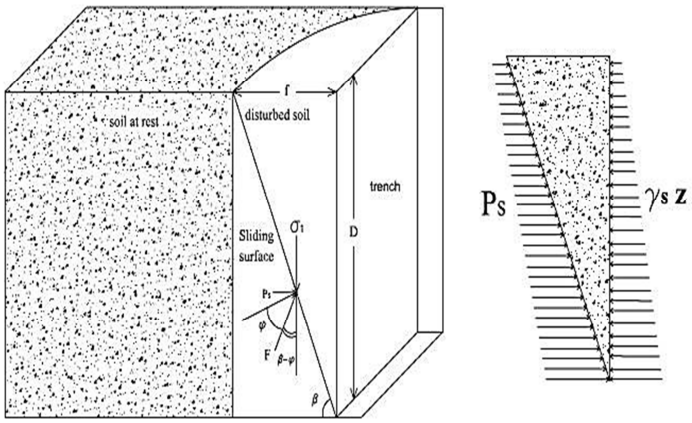

Figure 2.26 Downward load interaction with horizontal arching through the sliding surface (Saadi et al. 2017).

Reasonable data was obtained between the results from the proposed solution and the FE analyses by adopting an appropriate set of material parameters. The result of the earth pressure on the interface and horizontal stress behind the wall was some equivalent relationship between the analytical and the numerical solution, as shown in Figure 2.27 and Figure 2.28.

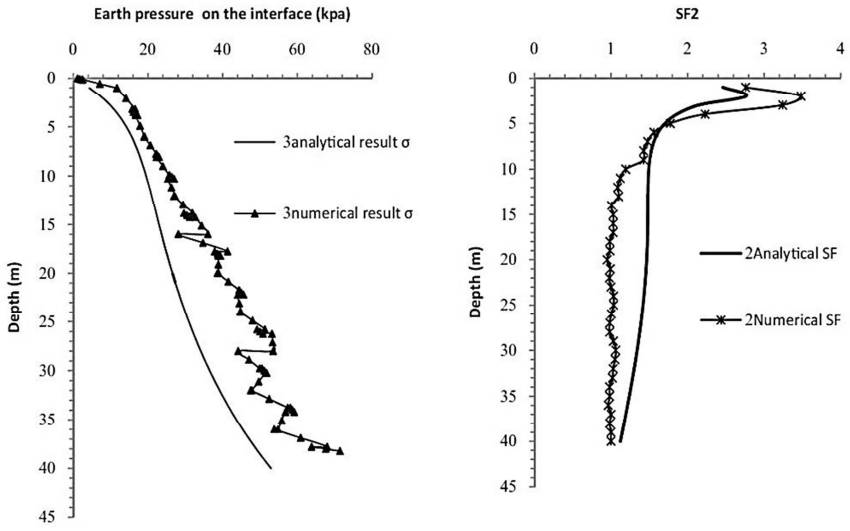

Figure 2.27 Numerical and analytical results of earth pressure on the interface (Saadi et al. 2017)

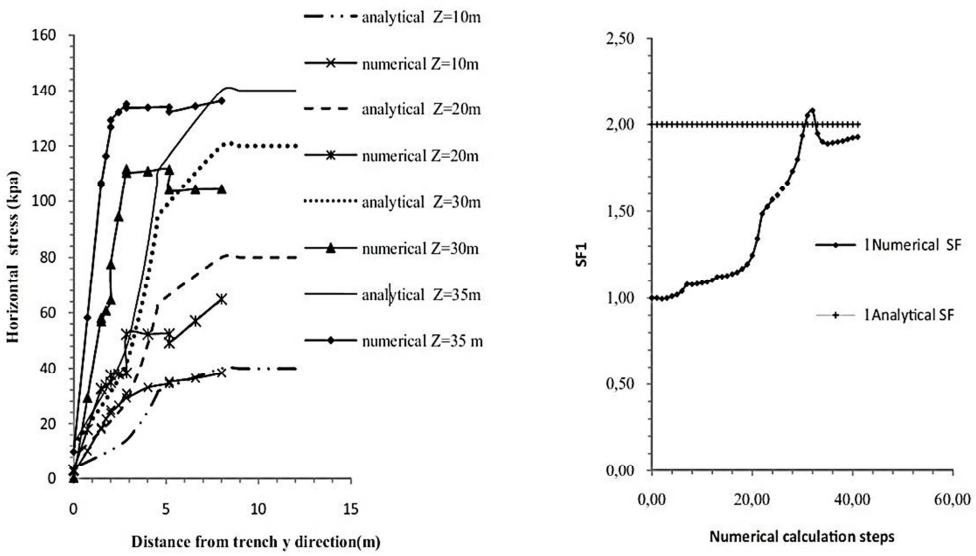

Figure 2.28 Variation of horizontal stress behind the wall (Saadi et al. 2017).

The analytical approach developed in this research gave results comparable to those found by measurements for slurry-supported trenches in the case history, as shown in Figure 2.29.

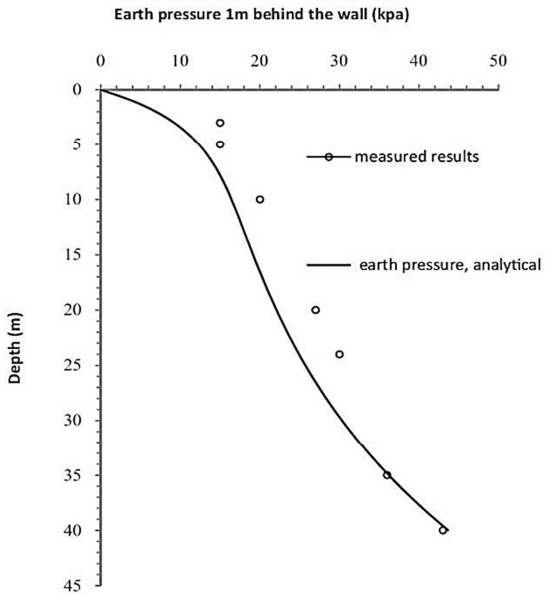

Figure 2.29 Comparisons between calculated and field measurements; σ'_3 (Saadi et al. 2017).

However, the Saadi et al. (2017) expect to improve the analytical solution by taking into account buildings near excavation sites and the cohesion effect on trench stability. Moreover, the model is involved in the simplified assumption of the soil parameter to be homogenized, of the water level at the ground level, and of a constant fragment from excavation length.

An analysis of ground response induced by diaphragm wall installation is introduced by Li and Lin (2018). The three-dimensional numerical modeling based on a simple geometry was investigated to analyze and depict the ground response due to slurry wall construction in a consequence of excavation panels. The commercial three-dimensional Lagrangian based numerical software, FLAC^{3D}, is used to simulate the slurry wall construction with a model of failure of the Mohr-Coulomb criterion with the elastic-perfectly plastic. The mesh configuration used in the numerical analysis is shown in Figure 2.30.

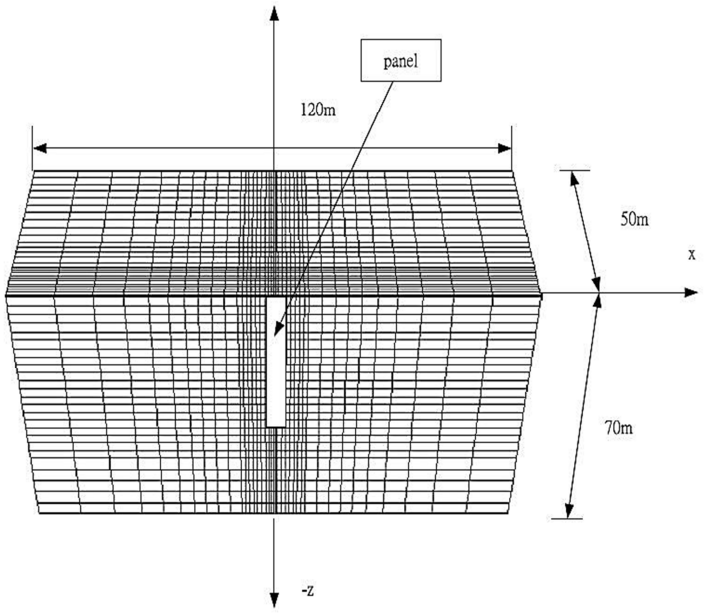

Figure 2.30 The mesh configuration (Li and Lin 2018).

Seven diaphragm wall panels construction is simulated and the diaphragm installation induced settlement increases with increasing wall dimensions, as shown in Figure 2.31.

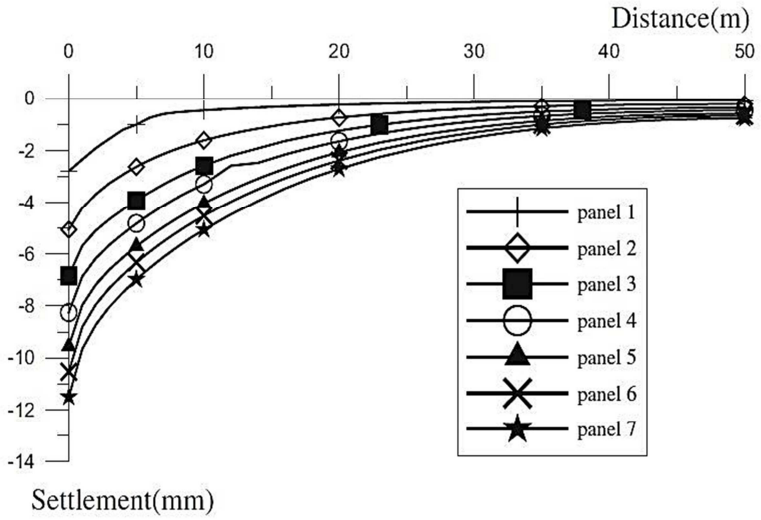

Figure 2.31 surface settlement at the center of a panel on the y-axis for various panel depths (Li and Lin 2018).

The numerical analysis shows that the surrounding panel installation will cause surface displacement. However, the amount of influence of distance is not clear. The author is proposing that more detailed investigations are needed in the future. Also, involving more soil parameters will give a broad view of the displacement when constructed panel by panel. Moreover, this study addresses only the displacement factor.

Review of the literature indicates that current researches are based on oversimplified geometry and do not consider the final state of stress in the slurry or deformations in the adjacent ground. In order to achieve a soil-bentonite slurry wall that is stable and easily constructible more complex modeling is vital. In general, the issue of stresses changes caused by continues excavation is critical. This critical state is due to greatest unbalanced forces between the trench and the soil mass. Thus, one of the objectives of this study is to investigate the stability of the trench under bentonite pressure for different length depth ratio and more realistic geometry.

CHAPTER III

NUMERICAL MODEL OF THE BENTONITE SLURRY WALL

3.1 Introduction

A model of a bentonite slurry wall was developed based on the soil information obtained at a site in Texas from the geotechnical firm in this research study (Gregory 2015). The model simulates excavation of the trench under bentonite-slurry wall stages of wall construction.

The three-dimensional discretization Lagrangian formulation, built in the FLAC^{3D} program which was developed at Itasca Consulting Group Inc., is an explicit finite difference algorithm to study the mechanical behavior of continuous systems. The equilibrium response is derived from a specific numerical implementation and a particular mathematical model (FLAC^{3D} Theory and Background, Itasca 2012).

The mathematical expression is a set of partial differential equations derived from general principles strain and laws of motion. Those equations are solved for kinematic strain rates and mechanical stresses for particular geometries and properties at given specific boundary and initial conditions (FLAC^{3D} Theory and Background, Itasca 2012).

The three-dimensional Lagrangian method (FLAC^{3D} Theory and Background, Itasca 2012) is used to study the mechanical behavior of the ground around the excavated trench simulating the construction responses behavior by using the panel's steps. Moreover, it is used to investigate changes in the ground stress state of each panel as well as the ground movement patterns during the period of slurry trenching construction.

Soil model and soil parameters used to represent the Lake Dam (Lake Tyler) site are described next. A description of the model is then given below, and the procedures used to model the construction sequence are described. The calculated stress-strains and deformations from the model are presented at the end of this chapter.

3.2 Previous Studies of Numerical Modeling of Soil-Bentonite Cutoff Walls

Two studies of numerical modeling of soil-bentonite cutoff walls were found in the literature.

A model of a three-dimensional Lagrangian formulation based finite difference approach study described in Li and Lin (2018) was performed to model the stresses in soil-bentonite backfill in a completed soil-bentonite cutoff wall. This study has the following drawbacks: 1) the model could not simulate the excavation process, backfill process, or settlement of the soil-bentonite backfill on a sloped area; 2) soil parameters for the soils were all assumed similar materials which were modeled with an elastic-plastic Mohr-Coulomb model, and 3) the level of influence distance of the surrounding panel installation is not clear. Despite these drawbacks, the study indicates that when the wall dimensions are increased the settlement increased.

The research of Li and Lin (2018) did not simulate the complexities of soil-bentonite cutoff wall construction. Since details of the modeling procedures are not provided, they cannot be evaluated for usefulness or accuracy.

A second model of a three-dimensional Lagrangian formulation based finite difference approach of a soil-bentonite cutoff wall has been described by Ding and Wang (2008). A soil-bentonite cutoff wall was constructed to simulate a simple geometry shape. The model was to study stress transfer during bentonite slurry hydrostatic pressure and the potential for placing concrete pressure of the soil-bentonite cutoff wall.

The previous study indicates that construction of the trench should result in a significant settlement or lateral deformations of the adjacent soil. Moreover, the horizontal stress distributions and horizontal shear stress distributions behind panels at excavating and concreting stages were significantly large. The author concludes the following, 1) the lateral displacement and the vertical settlement of the ground is reduced due to pacing concrete that compensates some of the soil horizontal stresses that lost during the excavation, 2) due to the redistribution of horizontal shear stress component of each panel, the stress being the smallest at the center while increasing toward the corner and decreasing beyond the panel, 3) the maximum settlement occurs at the face of the panel.

The Ding and Wang (2008) study have the following limitations: 1) multiples layers of the soil were not considered on the analyses of the deformations and horizontal stresses, 2) an unrealistic shape was assumed to present the settlement caused by the slurry and soil-bentonite.

To sum up, the two previous studies of modeling of soil-bentonite cutoff walls described in this section show that it is difficult to accurately model the complex of soil-bentonite cutoff wall construction. It is important to accurately model excavation and backfilling of the trench and the corresponding changes in stress in the ground adjacent to the trench. These phases of construction cannot be accurately modeled by simplifying the case shape or material properties. A realistic model condition of the trench must be assumed. In addition, it is important to model soil layers that interact with the soil-bentonite after were placed in the trench.

3.3 Soil Model and Parameters

For modeling of the soil-bentonite cutoff wall similar to Lake Dam (Lake Tyler) in Tyler Taxes, material parameter values were collected from the native soil, soil-bentonite, and bentonite-water slurry from the geotechnical firm (Gregory 2015). As described in the previous chapter, soil conditions at Lake Tyler consist of multiple layers of coarse and fine-grained soils. A representative soil profile, shown in Figure 3.1and Figure 3.2, was modeled to represent the conditions of an actual model of the cutoff wall. The profile consists of an upper clay layer and clay embankment with lower layers of sand and basal clay base. The average depth of groundwater was estimated to be 22.5 ft at the side of the dam. This depth of water was used in modeling to represent the initial groundwater condition.

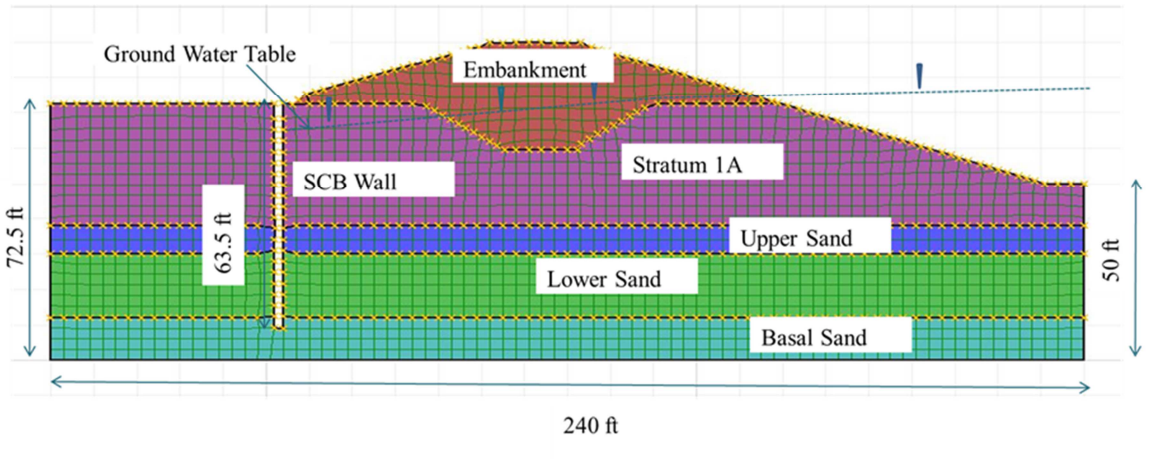

Figure 3.1 Cross section of the slurry trench wall of Lake Dam (Lake Tyler).

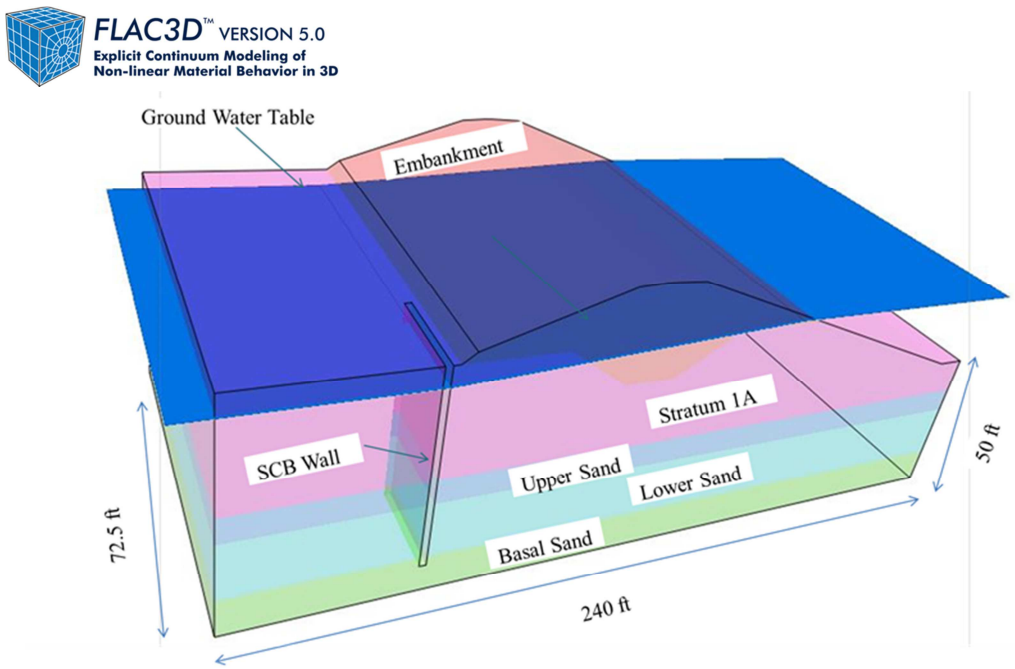

Figure 3.2 Geometry of the (3-D) FLAC model.

Considering the symmetry of the model half of the width of the trench was modeled, and the three-dimensional section of soil-bentonite was used to represent the half-width, with the embankment next to the trench wall.

The parameter values for all materials used in the model are listed in Table 3.1.

Table 3.1 Soil Properties

Material	**γ (pcf)**	**γ_{sat} (pcf)**	**c (psf)**	**ϕ (degree°)**
Embankment	125	130	180	22
SCB Wall	100	100	0	0
Stratum A1	125	130	180	22
Upper Sand	125	130	0	32
Lower Sand	125	130	0	32
Basal Clay	125	130	180	22

3.4 Finite Difference Mesh and Boundary Conditions

The three-dimensional Lagrangian formulation based finite difference approach program FLAC^{3D} was used to model the construction process of the soil-bentonite cutoff wall at the Lake Tyler site. This case geometry and material properties are given in this chapter. A discretization of the volume under study was done using hexahedra elements. The numerical model is divided into a

medium course mesh that consists of 8,352,000 quadrilateral elements. The vertical boundary planes (y = 0 ft and y = 120 ft) are allowed to move freely in the y-direction and z-direction, but not in the x-direction. Similarly, the vertical boundary planes (x = 0 ft and y = 240 ft) are allowed to move freely in the x-direction and z-direction, but not in the y-direction. The horizontal bottom boundary plane (z = 0) movements in all directions are restrained. The horizontal top plane is the free surface. The half native ground inside the cutoff wall and the half width of the cutoff wall at y-direction were modeled.

The mesh used in all the analyses of the Lake Tyler site is shown in Figure 3.3, together with the boundary conditions used.

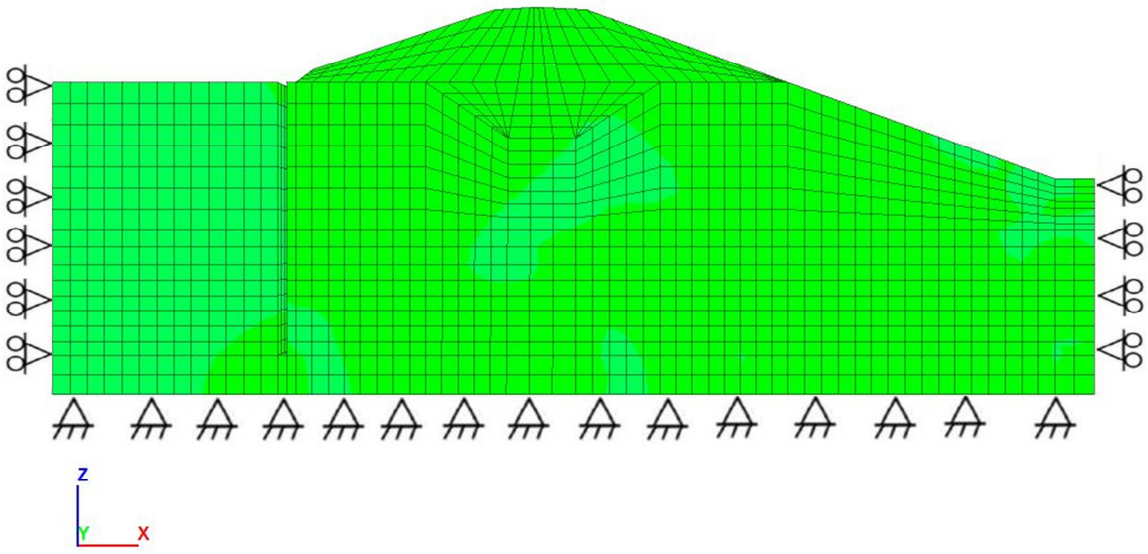

Figure 3.3 The mesh configuration and boundary conditions constructed with FLAC^{3D}.

All stresses and nodal velocity are initially set to zero. Then, initial stresses are specified. Concentrated and distributed loads from the slurry and soil-bentonite pressure are applied and specified at given surface nodes.

FLAC^{3D} program uses an explicit "time-marching" finite difference solution scheme; for every timestep, the calculation sequence can be summarized as follows: first, new strain rates are derived from element nodal velocities. Then, constitutive equations are used to calculate new stresses from the strain rates and stresses at the previous time. Finally, the equations of motion are invoked to derive new nodal velocities and displacements from stresses and forces (FLAC^{3D} Theory and Background, Itasca 2012).

The sequence is repeated at every timestep, and the maximum out-of-balance force in the model is monitored. This force will either approach zero, indicating that the system is reaching an equilibrium state, or it will approach a constant, non-zero value, indicating that a portion (or all) of the system is at a steady-state (plastic) flow of material (FLAC^{3D} Theory and Background, Itasca 2012).

The mesh represents a section of soil simulating the case of the Lake Tyler with 240 ft wide by 72.5 ft depth. The first assumption is to model the section with a model that extends to a length that duple the excavation depth of the slurry wall which is assumed to be 120 ft simulate the half-width of the soil-bentonite trench.

The size of the mesh was chosen by a large number of elements available with FLAC^{3D}, and the desire to limit computational time. The average computational time on a personal computer with

a 3.4 GHz Pentium Processor with 8.0 GB RAM was 1.5 hours for each run. A close up of the model mesh in the region of the soil-bentonite cutoff wall is shown in Figure 3.3.

Roller boundary conditions were assumed at the sides of the mesh, i.e. the nodes were constrained in the x-direction. The nodes were pinned along the bottom of the mesh, constraining the nodes in the x and z directions. On the third dimension, the nodes were constrained in the y-direction. A constant head boundary condition was maintained as normal stress along the upper boundary of the mesh. This head condition was varied according to the water elevation measured inside the area contained by the cutoff wall. The water elevations shown in three points are point 1 x-direction 504 ft and z-direction 366 ft, point 2 x-direction 611.5 and z-direction 374 ft, and point 3 x-direction 690 ft and z-direction 374 ft.

3.5 Procedures for Modeling Construction Sequence

Initial vertical effective stresses were assigned at each node assuming geostatic stresses with the pore pressures. The model then runs for the initial condition of all applied forces to simulate the over-consolidation of the clay layers. Then the model forces reset to be ready for the next step which is the excavation of trench under the bentonite-water slurry.

The excavation of the trench under bentonite-water slurry was modeled in 12 steps by excavating the elements of sand and clay in the trench and applying stress distributions to represent the fluid pressure. Each step represents a panel width excavation that increased by 5 ft each time. Since considering the symmetry of the model, the only half of the whole model has been taken into account that 5 ft are presenting actual 10 ft of excavation. Each panel excavation depth is

modeled by 12.7 ft incremental depth until the desired excavation depth is satisfied. Stress distributions were applied along with the side of the trench and along the bottom of the trench equal to the unit weight of the slurry times the depth of the slurry. Since the shear strength of bentonite-water slurry is very small all bentonite slurry has been modeled only with fluid pressure.

The model thickness dimension of the all diaphragm slurry wall panels from panel 1 to panel 12 is constructed with 2 ft thick, which simulates the actual excavation bucket. The third dimension is the panel width in the y-direction of the model which starts from 5 ft “half-width” on panel 1 till 60 ft “half-width” on panel 12. However, due to the symmetry, the actual excavation width is equal to duple that value. During the modeling of each panel the excavation depth “second dimension” varies from 12.7 ft to 63.5 ft representing five excavation phases. For each panel, the construction is carried out by excavating 12.7 ft deep trench for every step and applying normal hydrostatic bentonite pressure on the trench faces as mention above simultaneously, as shown in Figure 3.4 and Figure 3.5 for the sequences of the modeling. The applied pressure magnitude bulk unit weight is 100 pcf. During excavation, a filter cake is assumed not to form along the trench wall which is usually formed due to the chemical reaction between the bentonite and the adjacent soil which could result in a conservative output.

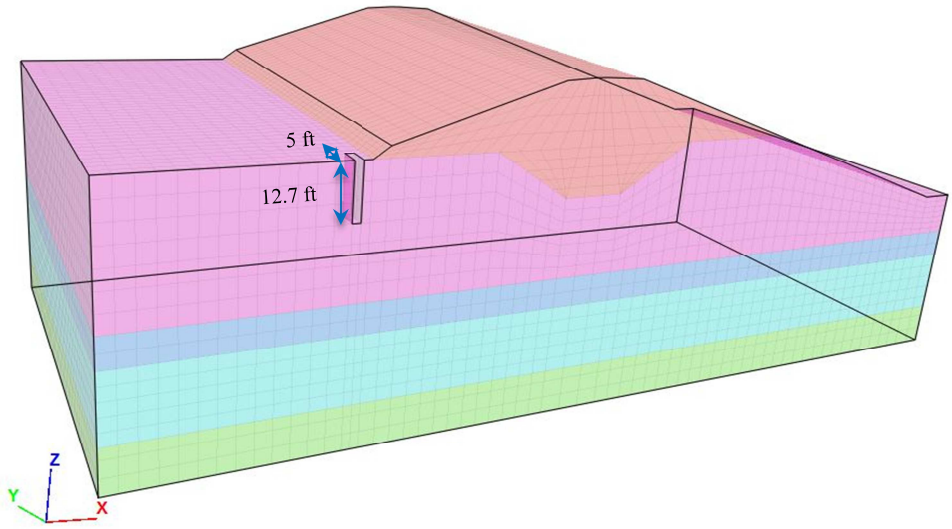

(a) Panel 1 (5 ft) first step of constructing 12.7 ft depth.

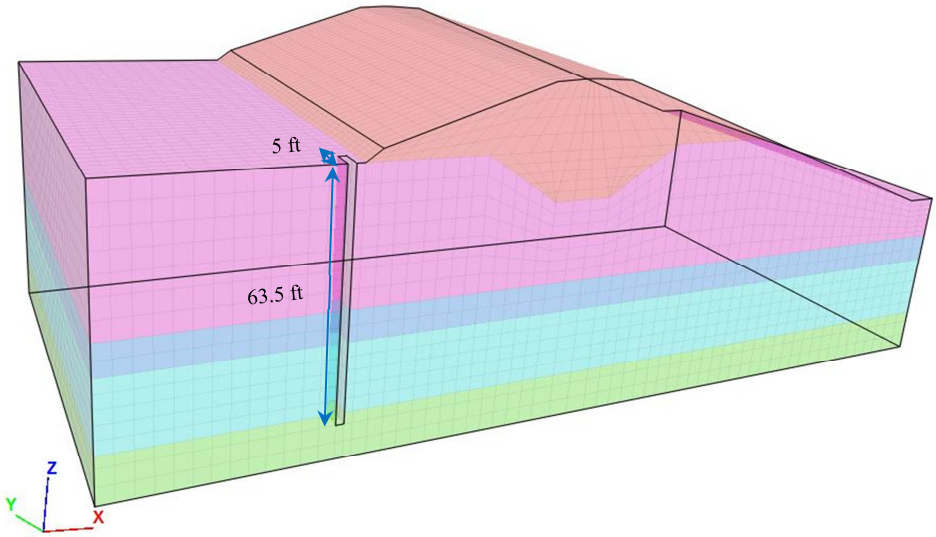

(b) Panel 1 (5 ft) last step of constructing 63.5 ft depth.

Figure 3.4 The model first step of constructing diaphragm wall panels.

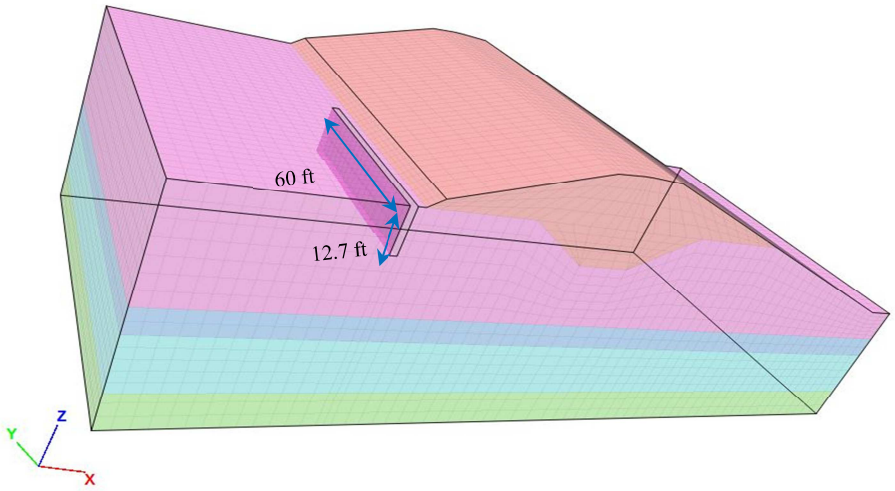

(a) Panel 12 (60 ft) first step of constructing 12.7 ft depth.

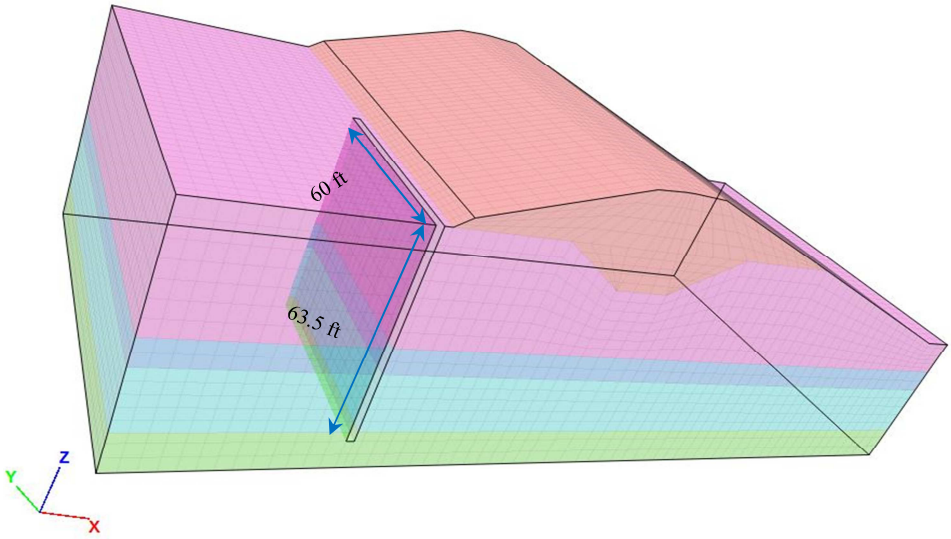

(b) Panel 12 (60 ft) first step of constructing 63.5 ft depth.

Figure 3.5 The model last step of constructing diaphragm wall panels.

CHAPTER IV

NUMERICAL RESULTS

4.1 Introduction

This chapter presents the (3-D) Lagrangian numerical results and discussion of the model to reveal the mechanical behavior of the excavated ground around the panels. This includes the changes in the ground stress state and as well as the ground movement patterns during the period of slurry wall construction. The result presents the stability of the model and the ground response including horizontal normal stress, shear stress, lateral ground displacement, and vertical ground surface settlement during the slurry wall excavation for all diaphragm wall panels.

4.2 Stability Analyses (Factor of Safety)

Table 4.1 The global factor of safety for all construction panels of the model

Panel No.	Modeled excavation width (Y) in ft	Actual excavation width (Y) in ft	Excavation depth (z) in ft	FOS
Panel 1	5	10	12.7	1.602
			25.4	1.600
			38.1	1.598
			50.8	1.596
			63.5	1.594
Panel 2	10	20	12.7	1.598
			25.4	1.598
			38.1	1.609
			50.8	1.607
			63.5	1.602
Panel 3	15	30	12.7	1.608
			25.4	1.604
			38.1	1.598

Panel No.	Modeled excavation width (Y) in ft	Actual excavation width (Y) in ft	Excavation depth (z) in ft	FOS
			50.8	1.596
			63.5	1.595
Panel 4	20	40	12.7	1.601
			25.4	1.590
			38.1	1.590
			50.8	1.582
			63.5	1.582
Panel 5	25	50	12.7	1.598
			25.4	1.590
			38.1	1.574
			50.8	1.570
			63.5	1.568
Panel 6	30	60	12.7	1.598
			25.4	1.571
			38.1	1.463
			50.8	1.461

Panel No.	Modeled excavation width (Y) in ft	Actual excavation width (Y) in ft	Excavation depth (z) in ft	FOS
			63.5	1.458
Panel 7	35	70	12.7	1.602
			25.4	1.540
			38.1	1.387
			50.8	1.381
			63.5	1.379
Panel 8	40	80	12.7	1.604
			25.4	1.508
			38.1	1.360
			50.8	1.344
			63.5	1.340
Panel 9	45	90	12.7	1.578
			25.4	1.470
			38.1	1.305
			50.8	1.303
			63.5	1.290

Panel No.	Modeled excavation width (Y) in ft	Actual excavation width (Y) in ft	Excavation depth (z) in ft	FOS
Panel 10	50	100	12.7	1.586
			25.4	1.44
			38.1	1.276
			50.8	1.258
			63.5	1.260
Panel 11	55	110	12.7	1.586
			25.4	1.431
			38.1	1.258
			50.8	1.254
			63.5	1.251
Panel 12	60	120	12.7	1.586
			25.4	1.398
			38.1	1.251
			50.8	1.227
			63.5	1.222

Results show that with the elastic soil model utilized by FLAC^{3D}, the placed soil-bentonite panels have an overall stable state. There is no clear evidence of stability, however, until the stress analysis is conducted. The global factor of safety was decreasing with the panel increasing excavation depth. Additionally, the most critical excavation parts were accounted at the panels which have high width and depth ratio, as shown in Table 4.1.

4.3 Horizontal Normal Stress Distribution

As can be expected, the construction of the slurry wall panels causes ground stresses to be altered. Stresses would also be different for each panel across the width of soil-bentonite, and would also be different for each width. From the results of the trench analyses, it was found that the maximum stresses were achieved on the excavation of panel 12. However, the comparison between panels calculated stresses obtained from that analysis was relatively small.

The computed distributions of horizontal normal stresses σ_{xx} behind panel 12 at the final slurry trenching excavation stage are shown in Figure 4.1.

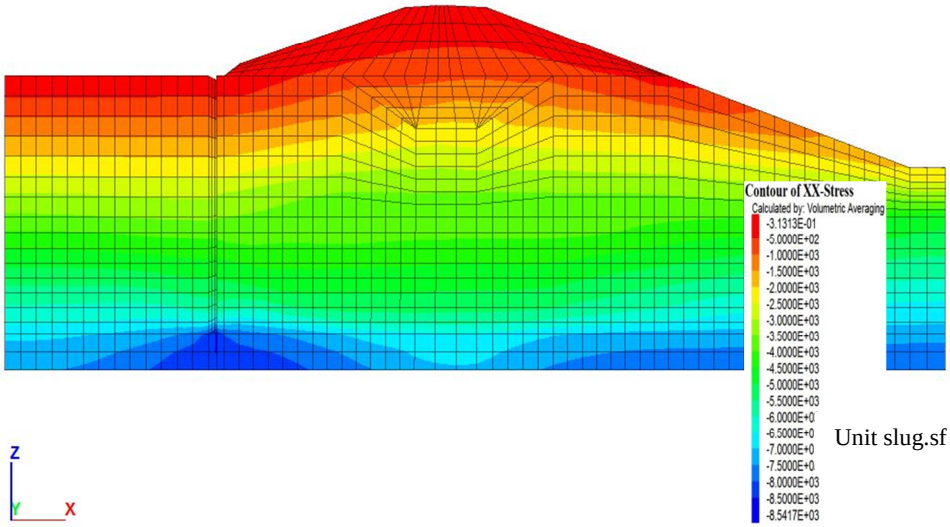

Figure 4.1 Horizontal stresses σ_{xx} distribution contour behind panel 12 at slurry trenching of the last stage.

The unit shown in the figure is slug square feet. The one slug force unit is an equal 32.174 pound-force. The result shows that there is a slight increase of the horizontal stress at each stage of excavation. That was expected due to the lateral forces from the bentonite slurry pressure replacing the initial stress of the soil. The critical stage was found at the points near the corner of the panels and around the toe. The horizontal and vertical stresses of the surrounding soil increase significantly at those locations of the construction, as shown in Figure 4.2.

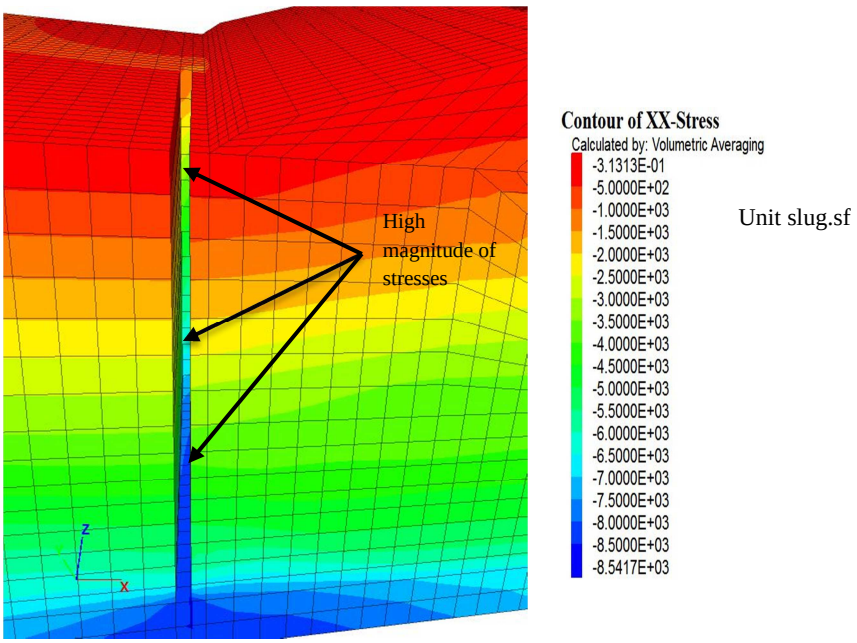

Figure 4.2 High magnitude of horizontal stresses σ_{xx} contour around the edges and toe of panel 12 at slurry trenching of the last stage.

Results indicate that the stresses at the bottom and edges of excavation of soil-bentonite were high. This was due to the pressure of soil-bentonite were replacing the soil initial stresses, the initial effective stresses would be low, as shown in Figure 4.3. Stresses would also be different across the width of soil-bentonite, and would also be different for each width. From the results of trench analyses, it was found that the fill should be placed with precaution to achieve the desired stresses with consistency across the width and for each subsequently placed excavated width.

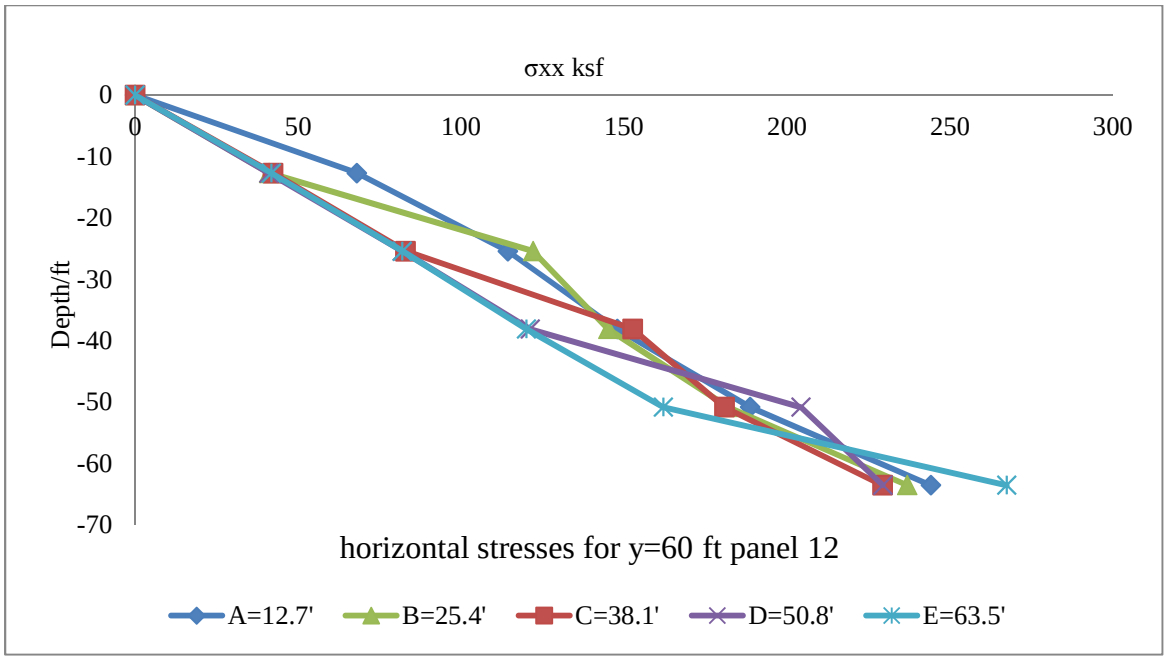

Figure 4.3 Horizontal stresses σ_{xx} distribution along deep direction behind panel 12 at slurry trenching.

Although the process described above was successful for placement of soil-bentonite elements, the process did not consider the placement of interface elements (filter cake). This could be achieved in a future study if the stiffness of interface was changed. The computed distributions of horizontal normal stress σ_{xx} for all panels are shown in Appendix B.

4.4 Horizontal Shear Stress Distribution

The distributions of computed horizontal shear stress τ_{xy} for all panels are shown in Appendix B. Result of the horizontal shear stress magnitude increases from the top of the excavation to the toe gradually. Panel 1 shows the maximum value of the shear stresses is obtained at the lower layer of the sand, as shown in Figure 4.4. As the construction sequence continued, the value of the

shear stresses change from each stage of excavation but the maximum value will be maintained on the sandy layer. The maximum value of the shear stresses of all stages is obtained on the last stage of the excavation on panel 12, as shown in Figure 4.5. From the results of trench analyses, it was found that the shape of the distributions is consistent with that of the horizontal normal stress distributions from each segmentally placed stage. The effect of the layers, however, was significantly changed the magnitude of the shear stresses, as shown in Figure 4.6 and Figure 4.7.

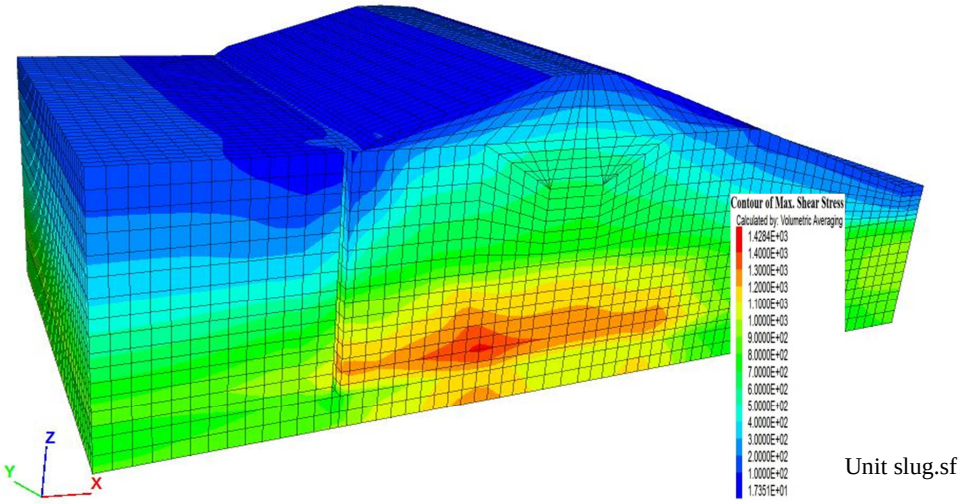

(a) Horizontal shear stresses τ_{xy} distribution contour behind panel 1 at slurry trenching of the last stage.

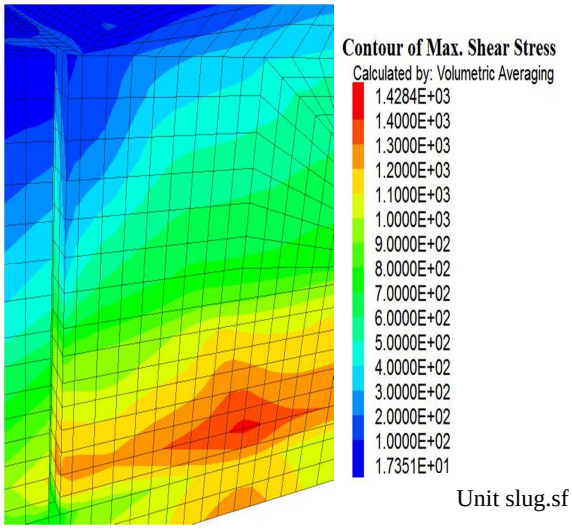

(b) The high magnitude of horizontal shear stresses τ_{xy} distribution contour behind panel 1 at slurry trenching of the last stage.

Figure 4.4 Horizontal shear stresses τ_{xy} distribution contour of panel 1.

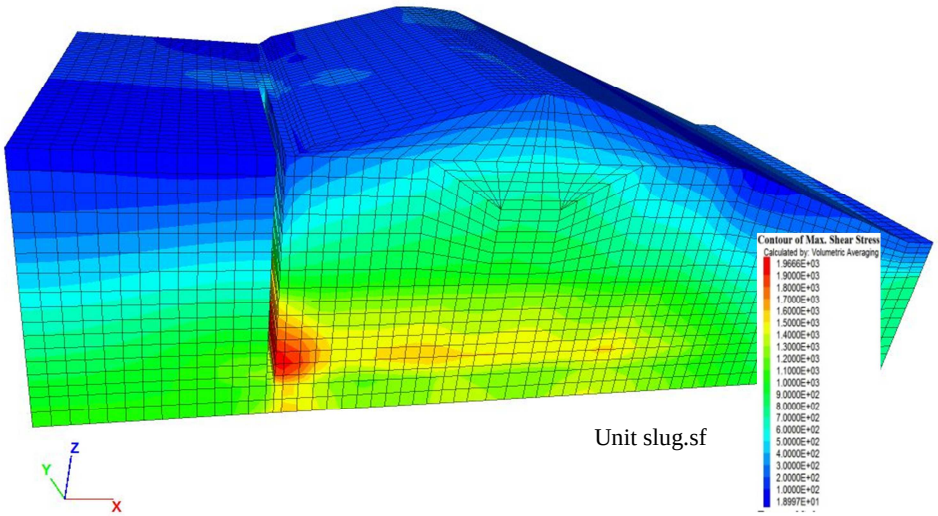

(a) Horizontal shear stresses τ_{xy} distribution contour behind panel 12 at slurry trenching of

the last stage.

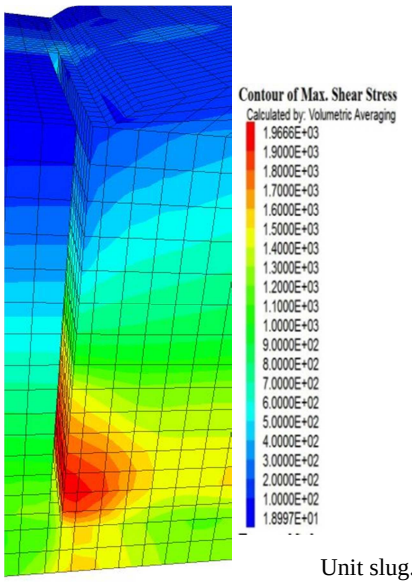

(b) The high magnitude of horizontal shear stresses τ_{xy} distribution contour behind panel 12 at slurry trenching of the last stage.

Figure 4.5 Horizontal shear stresses τ_{xy} distribution contour of panel 12.

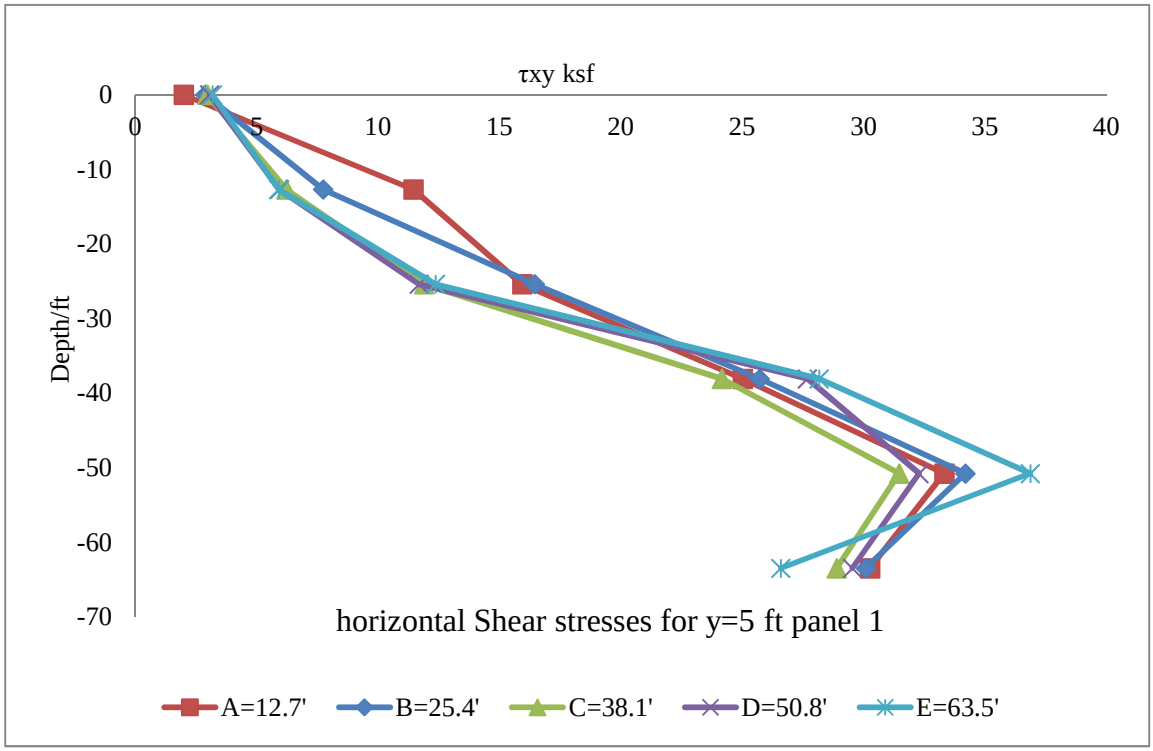

Figure 4.6 Horizontal shear stresses τ_{xy} distribution along deep direction behind panel 1 at slurry trenching.

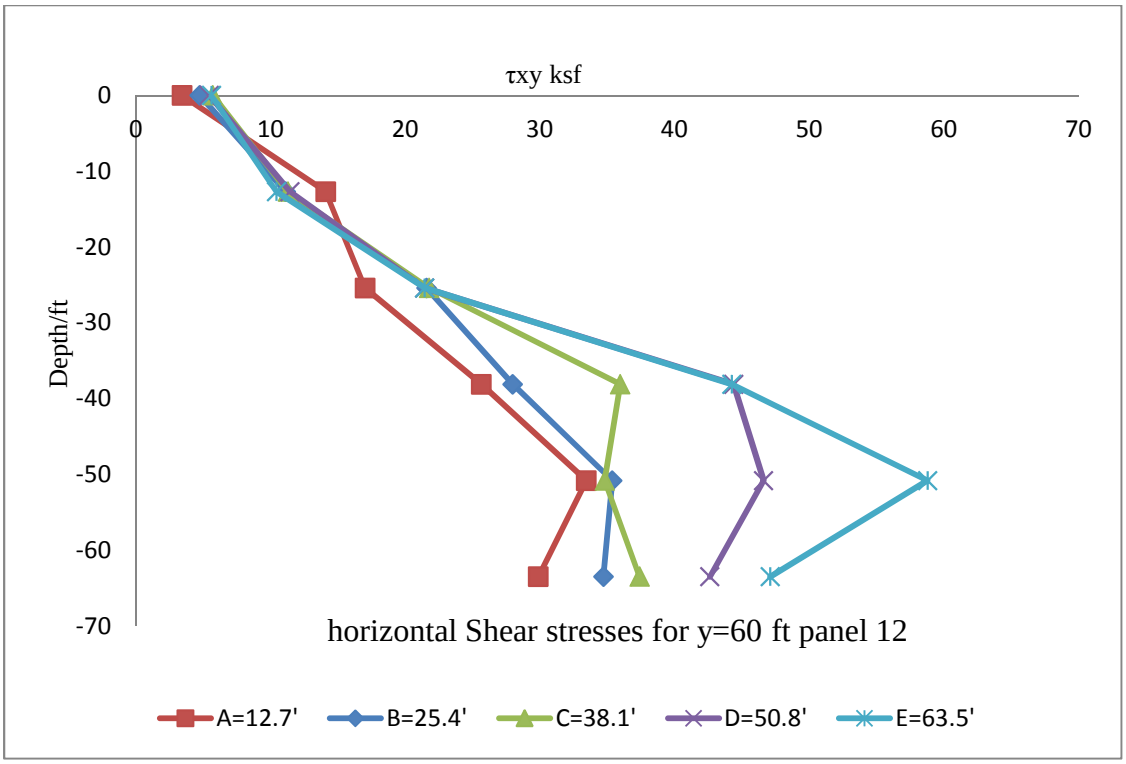

Figure 4.7 Horizontal shear stresses τ_{xy} distribution along deep direction behind panel 12 at slurry trenching.

4.5 Lateral Ground Displacement

The proposed model simulates all phases of construction that occurred near excavation of the cutoff slurry wall. Lateral deformations or ground movement happened due to the changes of stresses during diaphragm wall panel construction. The lateral displacement from the numerical analyses of the model creates predictions as follows:

The first prediction of the lateral displacement behind the panel in the first stage of the excavation was clearly not uniform. The value of the displacement relatively small behind the slurry wall and the large movement was at the top surface of the model as predicted, as shown in Figure 4.8 and Figure 4.9. Due to the stiffness of ground around the top of the panel is relatively lower than the

under layers the deformation is relatively high and the ground tends to move. This result shows the importance of the guide wall on the top of the cutoff wall. This guide walls need to be installed first to prevent ground surface being disturbed by construction machines and to locate panels at the right position.

In addition, first-panel excavation shows the little movement of the ground for each step of excavation, as shown in Figure 4.10. The deformations at the surface indicate an abrupt displacement at a depth of 10 to 30 feet for further panels' construction phases, as shown in Figure 4.11. That sharp deformation is depicted on the xx-strain curve was shown in Figure 4.12. The maximum value of the lateral displacement was predicted at panel 5 at the value of about 14 inches toward the inside trench.

One thing to note about Figure 4.11 is that the shape of the predicted lateral deformations shows that maximum lateral deformations occur at or near the ground surface and deformations gradually decrease with depth. The predicted deformations show that very little incremental deformation (less than 1/2 inch) occurs below the cutoff wall at the depth below 40 ft. Also, the trend of movement is the relatively same for predicted deformations for each phase of panels construction. Specifically, they all show inward deformation during excavation.

The model shows the correct trend of movement for each phase of construction; however, the model could be overestimating the magnitude of lateral movement for each phase due to the assumption of fully saturated soil material parameters. The incremental lateral deformations for the case analysis are shown for each construction phase in Appendix B.

After excavation, the lateral deformations in the adjacent ground for the case analysis indicate the less inward movement at a depth below of about 50 ft and greatest inward movement near the ground surface. This trend is explained by the net horizontal pressure at the trench wall due to excavation. From modeling result of the Lake Tyler case, an inward lateral movement was predicted with the largest magnitude at the ground surface. Little deformation occurs below the bottom of the trench.

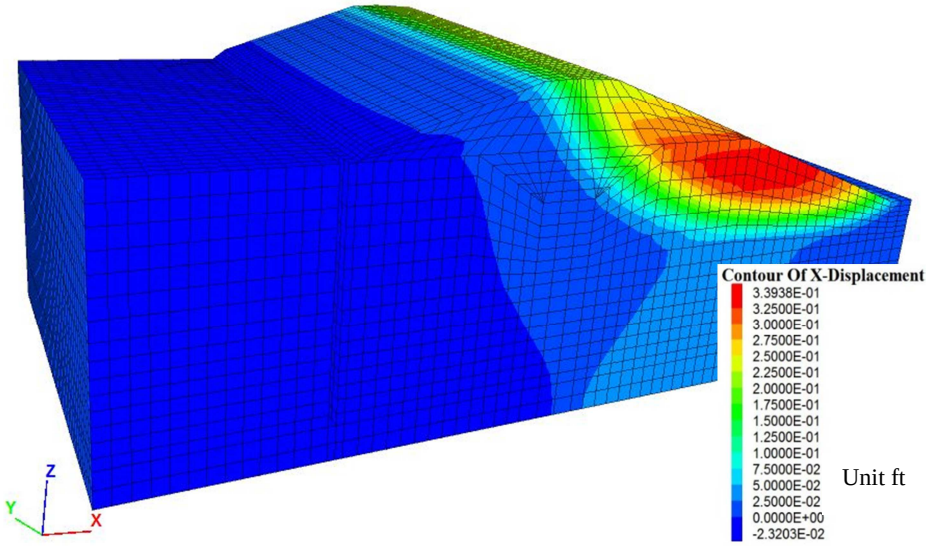

(a) Lateral ground displacement contour for panel 1 last stage.

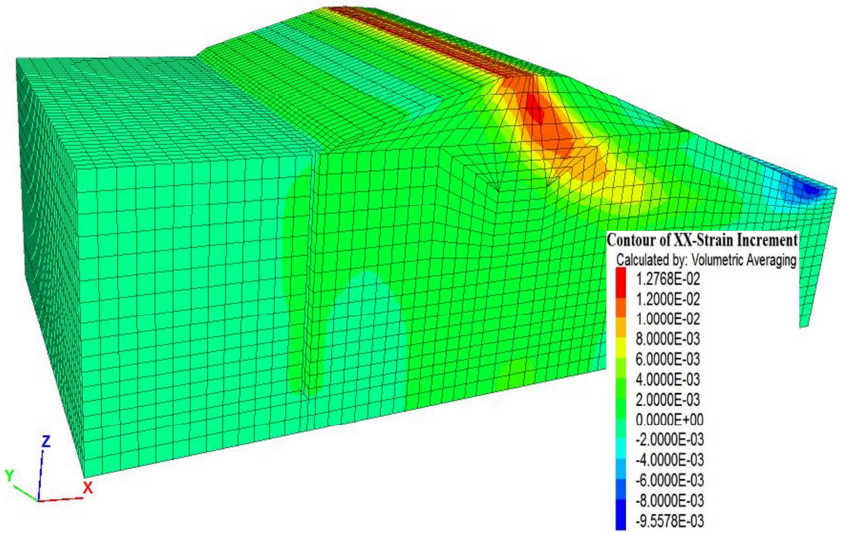

(b) Lateral ground strain increment contour for panel 1 last stage.

Figure 4.8 Lateral displacement of the ground around panel 1.

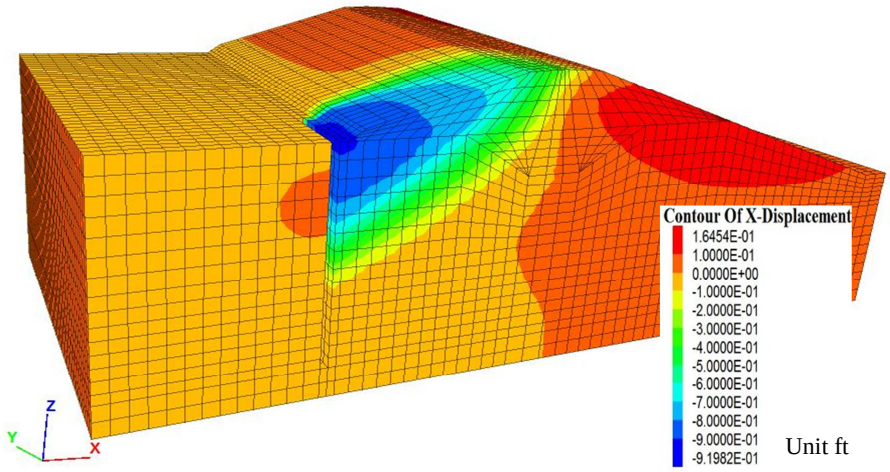

(a) Lateral ground displacement contour for panel 5 last stage.

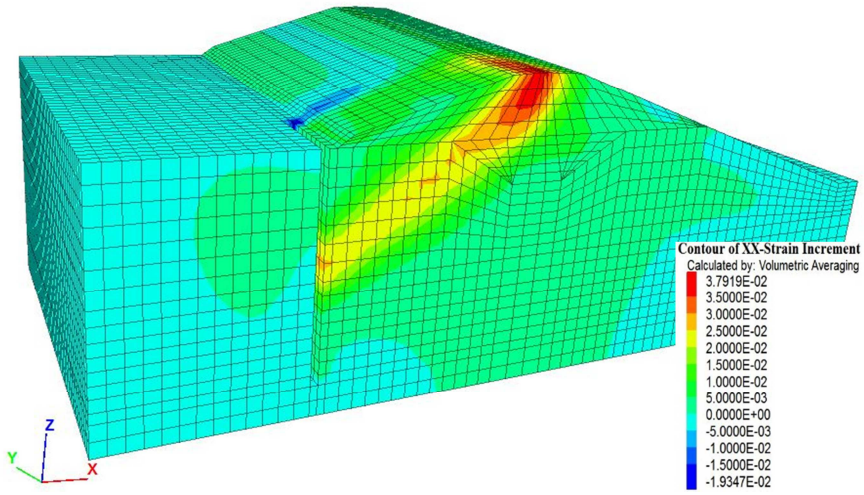

(b) Lateral ground strain increment contour for panel 5 last stage.

Figure 4.9 Lateral displacement of the ground around panel 5.

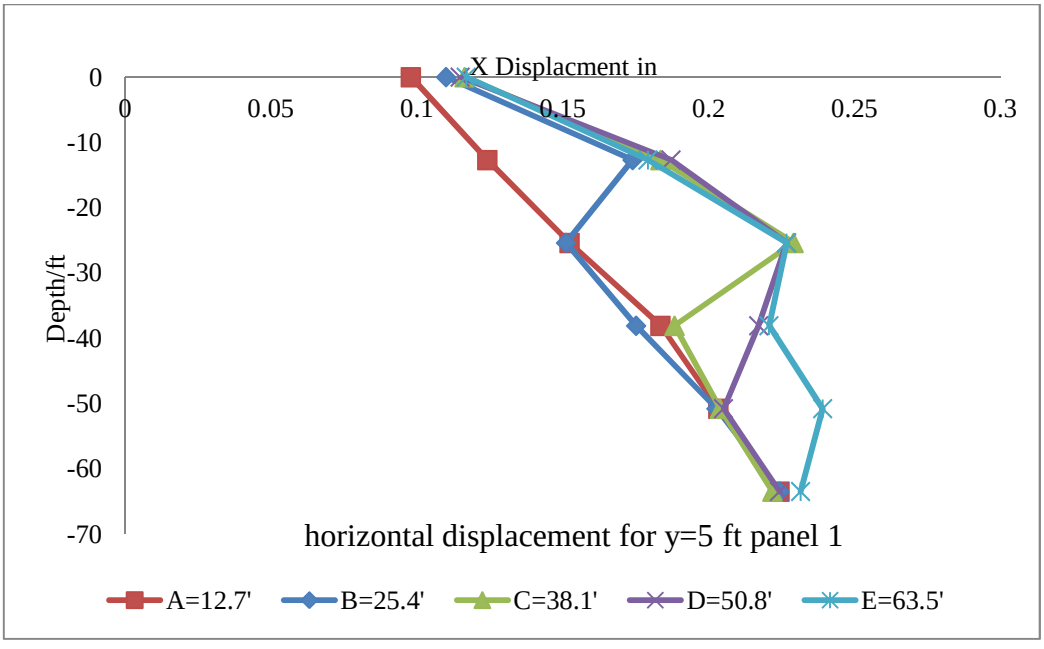

Figure 4.10 Lateral ground displacement of panel 1 in inches.

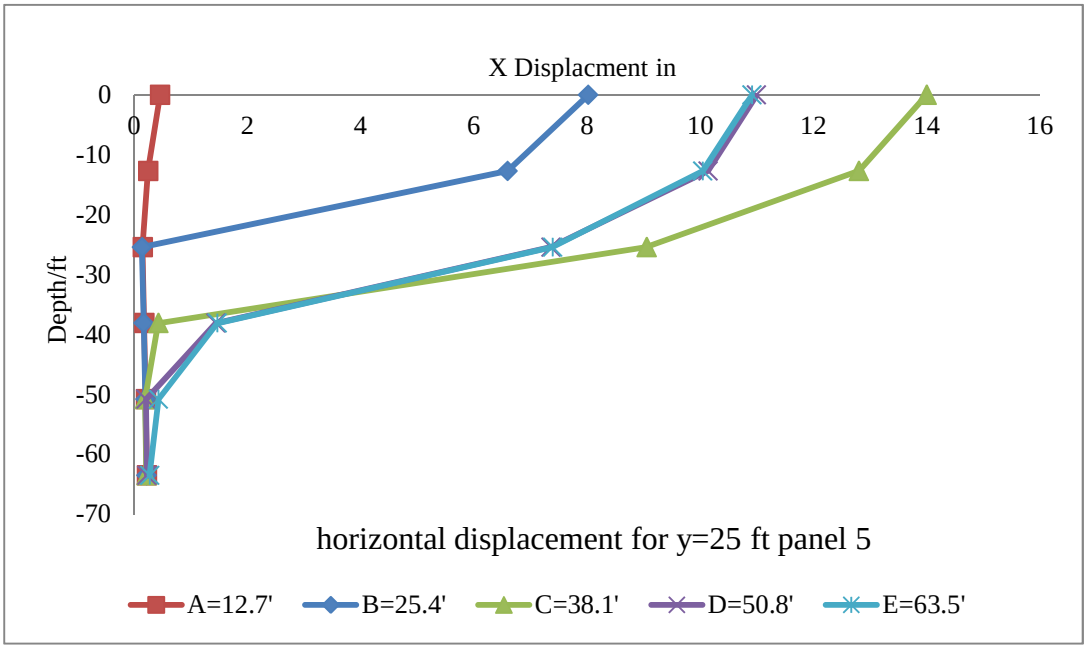

Figure 4.11 Lateral ground displacement of panel 5 in inches.

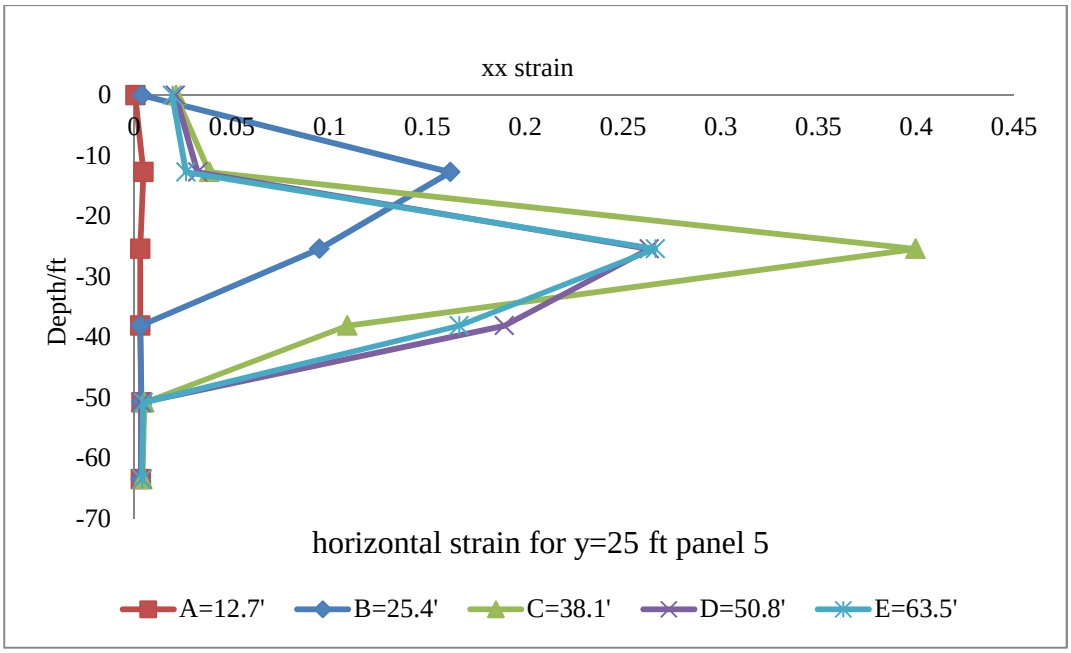

Figure 4.12 Lateral strain increment for panel 5 in inches.

4.6 Ground Surface Settlement

The total settlements at the ground surface at the end of each construction phase for panel one and panel five are shown in Figure 4.13 and Figure 4.14. The settlement plot shows that settlement increases with each phase of construction, as a similar trend was predicted previously for the lateral deformation. Very little deformation is predicted during the excavation phases of the three first panels, as shown in Figure 4.15 for panel 1. Those deformations are not uniform due to the effect of each layer. This indicates a wide range of values, which could be caused by differences in backfill properties, along with the depth of the trench. The most ground settlement occurs nearest the surface of the trench and decreases with distance from the top of the trench. The predicted settlement becomes less than 1 inch at a distance of about 30 ft below the trench surface.

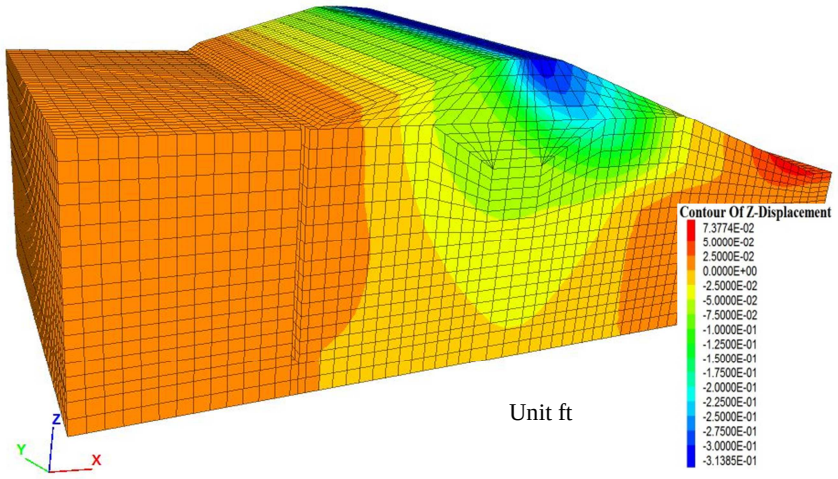

Figure 4.13 Vertical surface settlement contours during panel 1 construction.

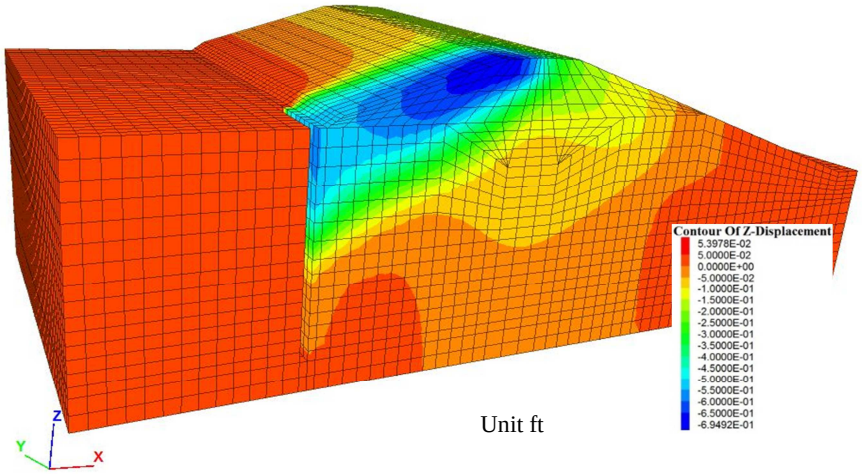

Figure 4.14 Vertical surface settlement contours during panel 5 construction.

The calculated settlement in the trench at panel 5 is shown in Figure 4.16. About 8.5 in of the settlement was predicted to occur near the surface of the trench, while less than an inch is predicted in the sand at the trench depth below about 50 ft. However, the model predicts a significant amount of incremental heave during excavation at the top of the dam slope. Also, it should be noted that the settlement points outside the area contained by the cutoff wall experience higher settlement on high groundwater levels than the settlement points inside the area contained by the cutoff wall.

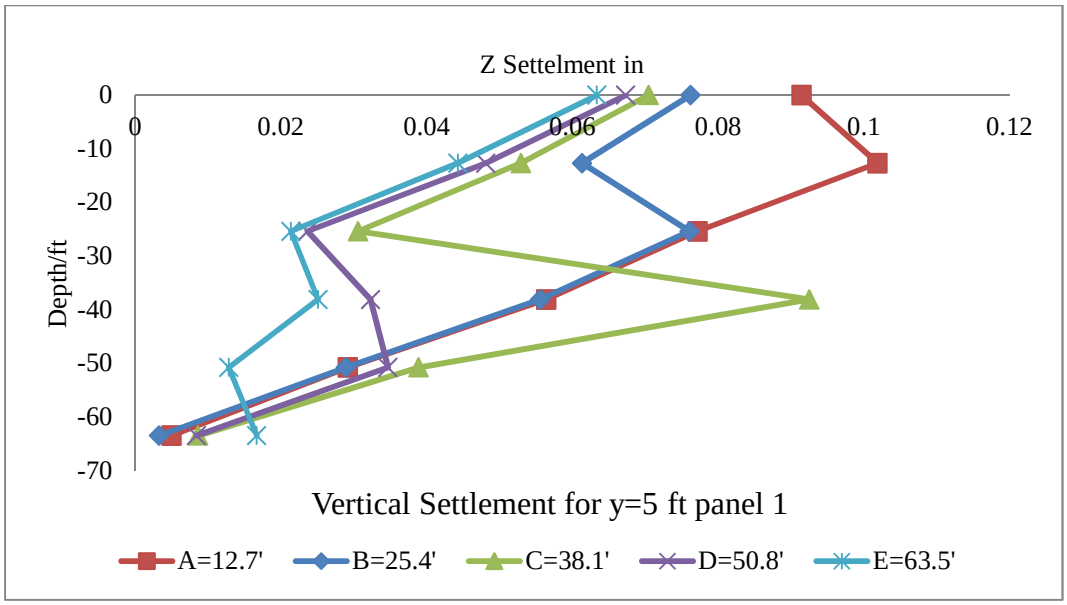

Figure 4.15 Vertical surface settlement during panel 1 construction.

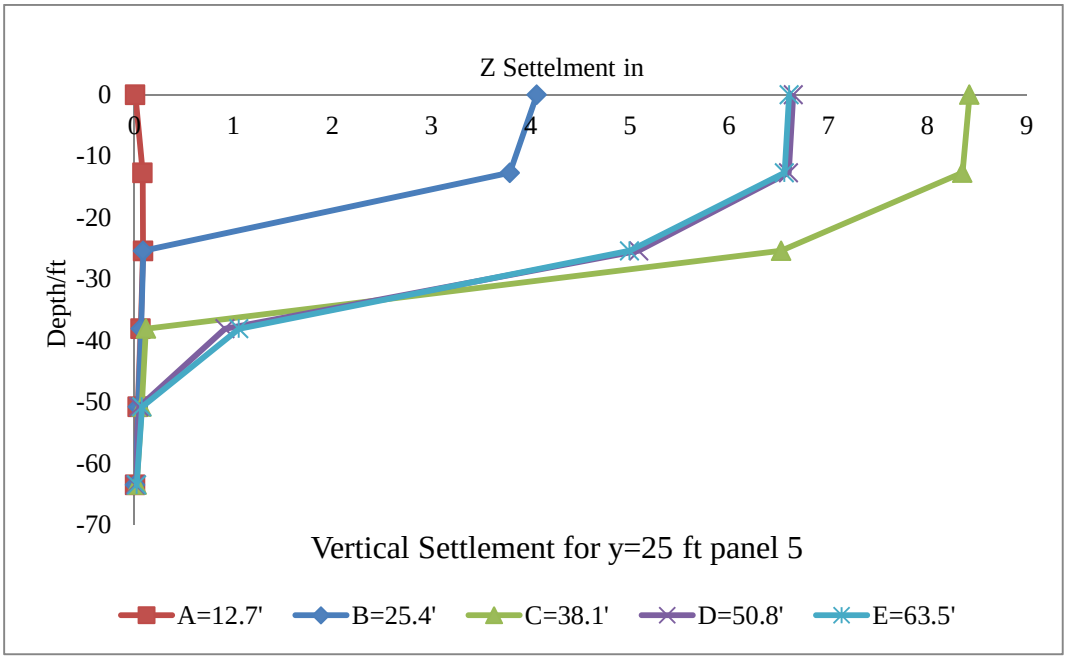

Figure 4.16 Vertical surface settlement during panel 5 construction.

CHAPTER V

SUMMARY AND CONCLUSIONS

5.1 Summary

A soil-bentonite slurry cutoff wall is a type of subsurface vertical barrier constructed by backfilling a trench with a mixture of soil, bentonite, and water. It is typically constructed using the slurry trench method, in which the trench is stabilized with bentonite-water slurry. The purpose of a soil-bentonite cutoff wall is to create economical temporary support for the trench excavation and to create a low permeability structure in the ground to contain or direct groundwater flow. Despite the fact that soil-bentonite cutoff slurry wall is common their mechanical behavior is not always well understood. Current design procedures do not consider the final state of stress in the soil-bentonite backfill or deformations in the adjacent ground. The final stress state in the completed wall is important because it influences the magnitude of deformations adjacent to the cutoff wall. Deformations adjacent to the cutoff wall can be significant and can cause damage to adjacent structures.

The objectives of this research are to provide information about the mechanical behavior of soil-bentonite cutoff walls. Specific objectives are to 1) add to the current body of knowledge of soil-bentonite behaviors, 2) select a real case (Lake Tyler Dam) to represent soil-bentonite model, 3) model a soil-bentonite cutoff wall using a three-dimensional Lagrangian formulation based finite difference approach and investigate the influence of several factors on the stability and deformations in the adjacent ground.

Objective 1 was met by first summarizing information in the literature on soil-bentonite slurry cutoff wall behaviors from simple models. Objective 2 was met by the proposed model that best represents the behavior of soil-bentonite. Objective 3 was met by developing a Lagrangian-based FLAC model to simulate the behavior of the soil-bentonite cutoff wall using Lake Tyler Dam data.

The rest of this chapter provides summary and conclusions from numerical results of modeling the soil-bentonite cutoff wall. Also included in this chapter are a discussion of the finding and recommendations for future research.

5.2 Conclusions from Numerical Modeling of a Soil-Bentonite Cutoff Wall

Previous researches on the modeling of soil-bentonite cutoff walls were presented and evaluated. The examples are limited in layers and much simpler than the model developed for this research.

Previous examples of a three-dimensional Lagrangian formulation based finite difference approach modeling of soil-bentonite cutoff walls also do not consider changing material properties which do not model the excavation phases accurately. The changes in stresses that result due to excavation must be modeled considering the changes of properties of each layer.

A model of a soil-bentonite cutoff wall was developed in this research to simulate the excavation stages of the construction of the trench under the bentonite-water slurry.

The Taylor lake dam case that is described in Chapter 3 was simulated. The three-dimensional Lagrangian formulation based finite difference approach program FLAC^{3D} was used for the analyses. The Mohr-Coulomb constitutive model was implemented into FLAC^{3D} and was used to represent soil.

The FLAC^{3D} can handle any constitutive model with no adjustment to the solution algorithm as many finite element codes need different solution techniques for different constitutive models (FLAC^{3D} User's Guide, 2012). The soil-bentonite was modeled as fluid pressure acting on the soil surface on all directions. Half of the soil-bentonite trench and the area contained by the cutoff wall were modeled with the three-dimensional Lagrangian formulation based finite difference approach mesh. The depth of the trench was 63.5 ft deep, and the width was 2 ft.

To model the site conditions, geotechnical data was compiled from laboratory tests, field tests, and in situ tests performed by the geotechnical firm (Gregory 2015). From this data, a soil profile and material parameter values were used. A soil profile consisting of layers of clay and sand was developed.

The excavation phase was modeled by removing the elements in the trench and applying stress distributions to the trench wall and trench bottom to represent the bentonite-water slurry pressure. The initial stress state was applied by running the analyses of the model without excavation and reset the model.

The predicted lateral deformations were within 6 inches to 14 inches for all phases of construction. The predicted settlements were within 3 inches to 8 inches of the observed settlements during excavation. The predicted settlements were within 4 inches of most of the settlement points below excavation depth of 25 ft.

It was found that slurry trenching leads to horizontal stress relief of ground and shear stresses in the elements that were high. However, there are some differences in magnitude caused by each layer. The largest magnitude of lateral ground displacement and vertical ground surface settlement were found in the excavation of panel 5 at the upper part of the trench. In this stage, the backfill of the wall should consider the needs to compensate partially the horizontal stress loss and reduces the lateral displacement as well as the vertical settlement of ground. This finding implies the necessity of protecting the upper part of the trench in the shallow stage of the excavation individual wall panels with consideration of the material properties layers.

It was found that the horizontal stress distribution behind the panel is not uniform, the stress being the smallest at the center but increasing in magnitude toward the corner of the panel and decreasing beyond the panel. This needs more attention during the excavation of deep excavation of each panel with the consideration of each layer material properties. Also, a settlement trench appears behind each panel, while the maximum settlement occurs at the face of the panel.

5.3 Recommendations for Further Research

Recommendations to increase the understanding of the mechanical behavior of soil-bentonite cutoff walls are suggested below:

The formation of the bentonite filter cake is not taken into account in the analysis. The permeability of the filter cake can be modeled by the hydraulic conductivity of the filter cake into the element of soil adjacent to the trench wall. The hydraulic conductivity of the adjacent element can be modeled by reduced to reflect the lower hydraulic conductivity of the filter cake. This factor may result in the computed displacement of the ground being greater than the measured value.

Case history data are very limited. It is recommended that more soil-bentonite cutoff walls are instrumented for lateral deformations and settlement in the adjacent ground as well as the settlement of the soil-bentonite in the trench. It is recommended that soil-bentonite cutoff walls should be instrumented for stresses in the soil-bentonite backfill.

This study can be expanded to include the influence of all stages of the construction including the backfill and placing concrete in the trench, different unit weight of the bentonite-water slurry, height of bentonite-water slurry in the trench, the drawdown of water table, and influence of surcharges and buildings adjacent to the trench on the deformations in adjacent ground.

REFERENCES

Barrier (1995). *Containment Technologies for Environmental Remedial Applications*, John Wiley & Sons, Inc., New York, USA.

Bowles, J. E. (1992). *Engineering Properties of Soils and Their Measurement*, McGraw-Hill, Inc, New York, USA.

Brzakala, W., and Gorska, K. (2007). "On Safety of Slurry–Wall Trenches." , *18 Congrès Français de Mécanique Grenoble*, 27(3), 1-6.

Ding, Y.-c., and Wang, J.-h. (2008). "Numerical Modeling of Ground Response During Diaphragm Wall Construction." *Journal of Shanghai Jiaotong University (Science)*, 13(4), 385-390.

Duncan, J. M., and Wright, S. G. (2005). *Soil Strength and Slope Stability*, John Wiley & Sons, Inc., Hoboken, NJ, USA

El-Ramly, H., Morgenstern, N. R., and Cruden, D. M. (2002). "Probabilistic Slope Stability Analysis for Practice." *Canadian Geotechnical Journal*, 39(3), 665-683.

Filz, G. M., Adams, T., and Davidson, R. R. (2004). "Stability of Long Trenches in Sand Supported by Bentonite-Water Slurry." *Journal of Geotechnical and Geoenvironmental Engineering*, 130(9), 915-921.

Fox, P. J. (2004). "Analytical Solution for Stability of Slurry Trench." *Journal of Geotechnical and Geoenvironmental Engineering*, 130(7), 749-758.

Fox, P. J. (2006). "Discussion of “Stability of Long Trenches in Sand Supported By Bentonite-Water Slurry" by M. Filz, Tiffany Adams, and Richard R. Davidson." *Journal of Geotechnical and Geoenvironmental Engineering*, 132(5), 666-666.

Gorska, K. (2015). "Trench Stability in Cohesive Soil." *Wroclaw University of Technology, ul. Wybrzeze Wyspianskiego*, 27, 1-6

Grandas-Tavera, C. E., and Triantafyllidis, T. (2012). "Simulation of a Corner Slurry Trench Failure in Clay." *Computers and Geotechnics*, 45, 107-117.

Gregory, H. G. (2015), personal communication.

Han, C. Y., Chen, J. J., Wang, J. H., and Xia, X. H. (2013). "2D and 3D Stability Analysis of Slurry Trench in Frictional/Cohesive Soil." *Journal of Zhejiang University SCIENCE A*, 14(2), 94-100.

Han, C. Y., Wang, J. H., Xia, X. H., and Chen, J. J. (2015). "Limit Analysis for Local and Overall Stability of a Slurry Trench in Cohesive Soil." *International Journal of Geomechanics*, 15(5), 1-8.

Itasca Consulting Group, Inc. (2012). Fast Lagrangian Analysis of Continua in 3 Dimensions, User manual, Version 5.0, Minneapolis, Minnesota, USA (2012).

Jin, X.-F., Liang, S.-T., and Zhu, X.-J. (2015). "Stability of Three-Dimensional Slurry Trenches with Inclined Ground Surface: A Theoretical Study." *Advances in Materials Science and Engineering*, 2015, 1-7.

Koch, D. (2002). "Bentonites as A Basic Material for Technical Base Liners and Encapsulation Cut-Off Walls." *Applied Clay Science*, 21, 1-11.

L'Amante, D., and Flora, A. (2012). "Effects of the Excavation Procedure on the Stability of Diaphragm Wall Panels." *Geotechnical Aspects of Underground Construction in Soft Ground*,415, 417-423.

Li, A. J., and Lin, H. D. (2018). "Analyses of Ground Response Induced by Diaphragm Wall Installation." *Springer Nature Singapore Pte Ltd. and Zhejiang University Press*, 10, 583-591.

Li, A. J., Merifield, R. S., Lin, H. D., and Lyamin, A. V. (2014). "Trench Stability under Bentonite Pressure in Purely Cohesive Clay." *International Journal of Geomechanics*, 14(1), 151-157.

Li, Y.-C., Cleall, P. J., Wen, Y.-D., Chen, Y., -M, and Pan, Q. (2015). "Stresses in Soil–Bentonite Slurry Trench Cut-Off Walls." *Géotechnique*, 65(10), 843-850.

Li, Y.-C., Pan, Q., and Chen, Y.-M. (2013). "Stability of Slurry Trenches with Inclined Ground Surface." *Journal of Geotechnical and Geoenvironmental Engineering*, 139(9), 1617-1619.

Li, Y.-C., Pan, Q., Cleall, P. J., Chen, Y.-M., and Ke, H. (2013). "Stability Analysis of Slurry Trenches in Similar Layered Soils." *Journal of Geotechnical and Geoenvironmental Engineering*, 139(12), 2104-2109.

Li, Y.-C., Wei, L., John Cleall, P., and Lan, J.-W. (2018). "Rankine Theory-Based Approach for Stability Analysis of Slurry Trenches." *International Journal of Geomechanics*, 18(11), 1-6.

Lim, K., Li, A. J., and Lyamin, A. V. (2015). "Three-Dimensional Slope Stability Assessment of Two-Layered Undrained Clay." *Computers and Geotechnics*, 70, 1-17.

Liu, G., Li, L., Yang, X., and Guo, L. (2016). "A Numerical Analysis of the Stress Distribution in Backfilled Stopes Considering Nonplanar Interfaces between the Backfill and Rock Walls." *International Journal of Geotechnical Engineering*, 10(3), 271-282.

Mingfeng, L., Yao, L., and Chengyong, C. (2017). "Design Method of Slurry Volume–Weight in Trenching Construction of Underground Diaphragm Wall in Soft Stratum." *Geotechnical and Geological Engineering*, 35(6), 2697-2704.

Mohamed, A. (2015). "Effect of Groundwater Table Rising and Slurry Reduction during Diaphragm Wall Trenching on Stability of Adjacent Piles." *IOP Conference Series: Earth and Environmental Science*, 26, 1-12.

Oblozinsky, P., Ugai, K., Katagiri, M., Saitoh, K., Ishii, T., Masuda, T., and Kuwabara, K. (2001). "A Design Method for Slurry Trench Wall Stability in Stability in Sandy Ground Based on the Elasto-Plastic FEM." *Computers & Geosciences*, 28, 145-159.

Park, B.-S., Lee, J., Kim, S. C., and Lee, S. D. (2018). "Investigation of Three-Dimensional Active Earth Pressure and Load Transfer According to Aspect Ratio." *Marine Georesources & Geotechnology*, 10, 1-9.

Park, B.-S., Lee, J., and Lee, S. D. (2017). "Experimental Investigation of Three-Dimensional Earth Pressure According to Aspect Ratio of Retaining Wall." *Marine Georesources & Geotechnology*, 36(2), 181-189.

Piaskowski, A., and Kowalewski, Z. (1965). "Application of Thixotropic Clay Suspension for Stability of Vertical Sides of Deep Trenches without Strutting." *6th Int. Conf. SMFE* Montreal, 526-529.

Saadi, R., Baheddi, M., and Ferhoune, N. (2017). "Analytical Approach of the Arching Dual Effect Describing the Stability of Slurry-Wall Trenches in Cohesionless Soil." *International Journal of Geomechanics*, 17(10), 1-13.

Tamano, T., Fukui, S., Suzuki, H., and Ueshita, K. (1996). "Stability of Slurry Trench Excavation in Soft Clay." *Japanese Geotechnical Society*, 36(2), 101-110.

Tsai, J.-S., Jou, L.-D., and Hsieh, H.-S. (1996). "Three-Dimensional Stability Analysis for Slurry-Filled Wall in Cohesionless Soil." *Canadian Geotechnical Journal*, 33, 798-808.

Tsai, J.-S., Jou, L.-D., and Hsieh, H.-S. (2000). "A Full-Scale Stability Experiment on a Diaphragm Wall Trench." *Canadian Geotechnical Journal*, 37, 379-392.

Wang, G. C. Y. (1984). "Stability Analysis of Slurry Trenches." *Journal of Geotechnical Engineering"*, 110(11), 1577-1590.

Wang, J., Liu, J., Fu, L., Ye, W., and Xu, G. (2018). "On Trench Construction of Diaphragm Wall in Medium-Coarse Sand: Slurry Composition and Construction Optimization." *Proceedings of China-Europe Conference on Geotechnical Engineering*,34, 1041-1045.

Wörden, t. F., and Achmus, M. (2013). "Numerical Modeling of Three-Dimensional Active Earth Pressure Acting on Rigid Walls." *Computers and Geotechnics*, 51, 83-90.

Xiao, H., and Sun, Y. (2016). "Global and Local Stability Analysis of Slurry Trenches under Surcharge in Soft Soils." *International Journal of Geotechnical Engineering*, 10(2), 205-211.

Yang, Y.-L., Reddy, K. R., Du, Y.-J., and Fan, R.-D. (2018). "Sodium Hexametaphosphate (SHMP)-Amended Calcium Bentonite for Slurry Trench Cutoff Walls: Workability and Microstructure Characteristics." *Canadian Geotechnical Journal*, 55(4), 528-537.

Yu, Y., and Ugai, K. (1997). "A new 3D limit Equilibrium Method Evaluating Stability of Slurry Trenches in Sandy Ground." *Computer Methods Advances in Geomechanics*, 3, 1659-1662.

Zhang, F., Dai, G., Gao, Y., and Bian, J. (2018). "Effects of Tension Crack on Stability of Bentonite-Water Slurry Trenches in Clay." *European Journal of Environmental and Civil Engineering*, 10, 1-14.

Zhang, F., Gao, Y., Leshchinsky, D., Yongxin, W., and Zhang, N. (2017). "Closed-Form Solution for Stability of Slurry Trenches." *International Journal of Geomechanics*, 17(1), 1-13.

Zhang, F., Gao, Y. F., Leshchinsky, D., Zhu, D. S., and Lei, G. H. (2016). "Three-Dimensional Stability of Slurry-Supported Trenches: End Effects." *Computers and Geotechnics*, 74, 174-187.

Zhang, Z. X., Pan, C. H., and Duan, C. F. (2013). "Numerical Analysis for the Stability of Over-Length Trench Wall Based on a Novel Pre-Supporting Excavation Method." *New Frontiers in Engineering Geology and the Environment*, 47, 259-262.

Zhuo, H. C., Yang, Y. Y., Zhang, Z. X., Pan, C. H., and Duan, C. F. (2014). "Stability of Long Trench in Soft Soils by Bentonite-Water Slurry." *Journal of Central South University*, 21(9), 3674-3681.

APPENDICES

Appendix A – The FLAC Code

```
;Geometry
config
grid 80,30
gen 450,300 450,393 690,393 690,300
model m
;trench
gen line 502,372.5 502,309
gen line 502,309 504,309
gen line 504,309 504,372.5
;soil layers
gen line 450,338 690,338
gen line 450,330 690,330
gen line 450,312 690,312
```

;embankment

gen line 450,372.5 506,372.5

gen line 506,372.5 510,375.5

gen line 510,375.5 552,389.5

gen line 552,389.5 560,390

gen line 560,390 563,390

gen line 563,390 573,389.5

gen line 573,389.5 619.48,372.5

gen line 619.48,372.5 681,350

gen line 681,350 690,350

gen line 506,372.5 536,372.5

gen line 536,372.5 555.5,359.5

gen line 555.5,359.5 570.5,359.5

gen line 570.5,359.5 590,372.5

gen line 590,372.5 619.48,372.5

gen line 590,372.5 619.48,372.5

mark i 21 j 26

mark i 42 j 30

mark i 35 j 30

mark i 42 j 20

ini x 506.21423 y 372.22467 i 20 j 24

ini x 511.5782 y 375.92838 i 21 j 26

ini x 572.3696 y 359.45334 i 42 j 20

ini x 618.857 y 372.60794 i 57 j 24

ini x 573.39136 y 361.24133 i 42 j 21

ini x 502.1274 y 337.35895 i 18 j 13

ini x 501.89258 y 372.49225 i 18 j 24

ini x 504.00494 y 372.54642 i 19 j 24

gen adjust

model null i 54 j 25

group 'null' i 54 j 25

group delete 'null'

model null i 55 j 25

group 'null' i 55 j 25

group delete 'null'

model null i 56 j 25

group 'null' i 56 j 25

group delete 'null'

model null i 57 j 25

group 'null' i 57 j 25

group delete 'null'

model null i 57 j 24

group 'null' i 57 j 24

group delete 'null'

model null i 20 j 25

group 'null' i 20 j 25

group delete 'null'

model null i 19 j 24

group 'null' i 19 j 24

group delete 'null'

model null i 19 j 25

group 'null' i 19 j 25

group delete 'null'

model null region 29 30

group 'null' region 29 30

group delete 'null'

model null i 20 j 25

group 'null' i 20 j 25

group delete 'null'

model null i 19 j 24

group 'null' i 19 j 24

group delete 'null'

model null i 19 j 25

group 'null' i 19 j 25

group delete 'null'

model null region 15 27

group 'null' region 15 27

group delete 'null'

model null region 14 27

group 'null' region 14 27

group delete 'null'

;Material

group 'User:Upper Sand' notnull j 11 12

group 'User:Lower Sand' notnull j 5 10

group 'User:Basal Clay' j 1 4

group 'User:Embankment' notnull i 20 41 j 24 29

group 'User:Embankment' notnull i 42 56 j 24 29

group 'User:Embankment' i 35 42 j 21 23

group 'User:Embankment' i 43 45 j 23

group 'User:Embankment' i 43 j 22

group 'User:Embankment' i 44 j 22

group 'User:Embankment' i 31 34 j 23

group 'User:Embankment' i 33 34 j 22

group 'User:Embankment' i 34 j 21

group 'User:Stratum 1A' notnull i 1 30 j 15 23

group 'User:Stratum 1A' i 31 32 j 22

group 'User:Stratum 1A' i 31 j 21

group 'User:Stratum 1A' i 32 j 21

group 'User:Stratum 1A' i 33 j 21

group 'User:Stratum 1A' notnull i 31 80 j 14 20

group 'User:Stratum 1A' notnull j 13 14

group 'User:Stratum 1A' notnull i 47 65 j 21 23

group 'User:Stratum 1A' i 46 j 23

group 'User:Stratum 1A' i 46 j 22

group 'User:Stratum 1A' i 45 j 22

group 'User:Stratum 1A' i 45 j 21

group 'User:Stratum 1A' i 46 j 21

group 'User:Stratum 1A' i 44 j 21

group 'User:Stratum 1A' i 43 j 21

group 'User:Embankment' i 36 41 j 20

model mohr notnull group 'User:Upper Sand'

prop density=4.04 bulk=3.48091E6 shear=7.459E5 cohesion=0.0 friction=32. dilation=0.0 tension=0.0 notnull group 'User:Upper Sand'

model mohr notnull group 'User:Lower Sand'

prop density=4.04 bulk=3.48091E6 shear=7.459E5 cohesion=0.0 friction=32. dilation=0.0 tension=0.0 notnull group 'User:Lower Sand'

model mohr notnull group 'User:Basal Clay'

prop density=4.04 bulk=3.48091E6 shear=7.459E5 cohesion=180.0 friction=20. dilation=0.0 tension=0.0 notnull group 'User:Basal Clay'

model mohr notnull group 'User:Embankment'

prop density=4.04 bulk=3.48091E6 shear=7.459E5 cohesion=180.0 friction=20. dilation=0.0 tension=0.0 notnull group 'User:Embankment'

model mohr notnull group 'User:Stratum 1A'

prop density=4.04 bulk=3.48091E6 shear=7.459E5 cohesion=180.0 friction=20. dilation=0.0 tension=0.0 notnull group 'User:Stratum 1A'

;Boundray

table 1 450.0 366.6 504.0 366.6 611.5 374.0 690.0 374.0

water density=1.939

water table=1

set gravity=32.17

fix x i 1 j 1 24

fix x i 81 j 1 17

fix y j 1

;slurry pressure

apply nstress 0 var 0.0 -6722.1 from 19,24 to 19,4

apply nstress 0 var 0.0 -6350 from 18,24 to 18,4

apply nstress -6350.0 from 18,4 to 19,4

apply nstress 0.0 var 0.0 -2246.4 from 56,25 to 81,17

prop density 4.274 notnull i 1 17 j 22 23

prop density 4.274 notnull i 19 30 j 23

prop density 4.274 notnull i 20 41 j 24 29

```
prop density 4.274 notnull i 42 53 j 24 29
prop density 4.274 notnull i 53 55 j 24 25
prop density 4.274 notnull i 55 56 j 24
;apply sstress 0.0 var 0.0 400.1 from 19,24 to 19,4
;FOSmode

**************************************************
new
;geometry
rest SlurryWall3D-2DMesh.sav

extrude block id 10 group embankment
extrude block id 20 group embankment
extrude block id 21 group embankment
extrude block id 22 group embankment
extrude block id 23 group embankment
extrude block id 24 group embankment
extrude block id 25 group embankment
extrude block id 26 group embankment
extrude block id 27 group stratum1
extrude block id 28 group stratum1
extrude block id 29 group stratum1
extrude block id 30 group stratum1
extrude block id 31 group stratum1
extrude block id 32 group stratum1
extrude block id 33 group stratum1
```

```
extrude block id 34 group stratum1
extrude block id 35 group stratum1
extrude block id 44 group stratum1
extrude set segment size 1 40
extrude set segment length 1 120
gen zone extrude

group uppersand range z 330 338
group lowersand range z 312 330
group basalclay range z 300 312

;material
model mohr
prop bulk 3.48e6 shear 7.46e5 c 180. fric 20. dens 4.04 range group embankment ;cohesive
prop bulk 3.48e6 shear 7.46e5 c 180. fric 20. dens 4.04 range group stratum1 ;cohesive
prop bulk 3.48e6 shear 7.46e5 c 0.00 fric 32. dens 4.04 range group uppersand ;cohesionless
prop bulk 3.48e6 shear 7.46e5 c 0.00 fric 32. dens 4.04 range group lowersand ;cohesionless
prop bulk 3.48e6 shear 7.46e5 c 180. fric 20. dens 4.04 range group basalclay ;cohesive

;boundary
fix x range x 449 451
fix x range x 689 691
fix y range y -1 1
fix y range y 119 121
fix z range z 299 301
```

;water

geometry set watersurface polygon id 1 pos (440,-1, 366.6) (440,121,366.6) (504, 121, 366.6) (504,-1, 366.6)

geometry set watersurface polygon id 2 pos (504, 121, 366.6) (504,-1, 366.6) (611.5,-1,374)(611.5,121,374)

geometry set watersurface polygon id 3 pos (611.5,-1,374)(611.5,121,374) (700,121,374)(700,-1,374)

range name moist geome watersurface count 0

prop dens 3.88 range moist

water set watersurface

water dens 1.938

set grav 32.2

water calc

apply nstress -23337.6 gra 0 0 62.4 range x 611 690 y 1 119 z 349 374

;define shallow layer

;geometry set shallow1 polygon id 1 pos (440,-1, 362.5) (440,121,362.5) (504, 121, 362.5) (504,-1, 362.5)

;geometry set shallow1 polygon id 2 pos (504, 121, 362.5) (504,-1, 362.5) (552.0,-1,379.5)(552.0,121,379.5)

;geometry set shallow1 polygon id 3 pos (552.0,-1,379.5)(552.0,121,379.5) (573.0,121,379.5)(573.0,-1,379.5)

;geometry set shallow1 polygon id 4 pos (573.0,121,379.5)(573.0,-1,379.5) (700.0,-1,340.0)(700.0,121,340.0)

;range name shallow geome shallow1 count 0

;prop bulk 3.48e6 shear 7.46e5 c 180. fric 22. dens 4.04 range shallow ;cohesive-shallow

;solve initial equilibrium

```
solve elas

ini xdisp=0 ydisp=0 zdisp=0


save ini.sav


**********************************************

rest ini.sav



;slurry wall

delete zone range x 502 504 y 0 60 z 309 372.5

apply nstress -37250 gra 0 0 100 range x 501.8 504.2 y 0 60 z 309 372.5


;solve

solve fos

**********************************************
```

Appendix B – FLAC^{3D} Results

Panel (1) (Y=5 ft)

Table B 1 All Numerical Results for Panel 1

Excavation A (Z=12.7 ft)

Note: 1slug = 32.174 lb

depth Z (ft)	σ_{xx} (slugsf)	σ_{xx} (ksf)	xx strain
0	0.0	0.0	2.08E-04
-12.7	2303.0	74.2	6.95E-04
-25.4	3441.0	110.8	2.65E-03

-38.1	4595.0	148.0	2.86E-03
-50.8	5842.0	188.1	3.49E-03
-63.5	7557.0	243.3	3.13E-03

depth Z (ft)	yy strain	τ_{xy} (slugsf)	τ_{xy} (ksf)
0	6.36E-04	62	1.9964
-12.7	6.25E-04	356	11.4632
-25.4	1.42E-04	495	15.939
-38.1	5.94E-05	777	25.0194
-50.8	3.23E-05	1035	33.327
-63.5	2.56E-05	940	30.268

depth Z (ft)	x disp (ft)	x disp (in)	Z settlement (ft)	Z settlement (in)
0	8.17E-03	9.80E-02	0.00762	0.09144
-12.7	1.04E-02	1.24E-01	0.00849	0.10188
-25.4	1.27E-02	1.52E-01	0.00643	0.07716
-38.1	1.53E-02	1.84E-01	0.0047	0.0564
-50.8	1.70E-02	2.03E-01	0.00243	0.02916
-63.5	1.87E-02	2.24E-01	0.000414	0.004968

Excavation B (Z=25.4 ft)

depth Z (ft)	σ_{xx} (slugsf)	σ_{xx} (ksf)	xx strain
0	0.0	0.0	4.75E-03
-12.7	1195.3	38.5	3.42E-03
-25.4	3612.0	116.3	1.28E-03
-38.1	4578.8	147.4	2.88E-03
-50.8	5845.9	188.2	3.52E-03
-63.5	7598.2	244.7	3.28E-03

depth Z (ft)	yy strain	τ_{xy} (slugsf)	τ_{xy} (ksf)
0	9.08E-04	89.99	2.897678
-12.7	2.45E-03	240.566	7.7462252
-25.4	1.02E-03	511.159	16.4593198
-38.1	2.55E-07	799.044	25.7292168
-50.8	1.66E-05	1062.14	34.200908
-63.5	1.29E-05	934.728	30.0982416

depth Z (ft)	x disp (ft)	x disp (in)	Z settlement (ft)	Z settlement (in)

0	9.17E-03	1.10E-01	0.00635	0.0762
-12.7	1.45E-02	1.74E-01	0.00511	0.06132
-25.4	1.26E-02	1.51E-01	0.00634	0.07608
-38.1	1.46E-02	1.75E-01	0.00463	0.05556
-50.8	1.69E-02	2.03E-01	0.00241	0.02892
-63.5	1.87E-02	2.24E-01	0.000272	0.003264

Excavation C (Z=38.1 ft)

depth Z (ft)	σ_{xx} (slugsf)	σ_{xx} (ksf)	xx strain
0	0.0	0.0	5.10E-04
-12.7	1186.3	38.2	1.67E-03
-25.4	2407.7	77.5	5.71E-03
-38.1	4586.2	147.7	3.19E-04
-50.8	5926.1	190.8	4.03E-03
-63.5	7680.1	247.3	3.50E-03

depth Z (ft)	yy strain	τ_{xy} (slugsf)	τ_{xy} (ksf)
0	1.08E-03	92.259	2.9707398
-12.7	3.11E-03	193.535	6.231827
-25.4	4.54E-03	369.72	11.904984
-38.1	2.08E-03	750.519	24.1667118
-50.8	3.86E-04	977.398	31.4722156
-63.5	1.92E-04	897.69	28.905618

depth Z (ft)	x disp (ft)	x disp (in)	Z settlement (ft)	Z settlement (in)
0	9.70E-03	1.16E-01	0.00587	0.07044
-12.7	1.53E-02	1.84E-01	0.00441	0.05292
-25.4	1.91E-02	2.29E-01	0.00255	0.0306
-38.1	1.57E-02	1.88E-01	0.00771	0.09252
-50.8	1.70E-02	2.04E-01	0.00324	0.03888
-63.5	1.85E-02	2.22E-01	0.000719	0.008628

Excavation D (Z=50.8 ft)

depth Z (ft)	σ_{xx} (slugsf)	σ_{xx} (ksf)	xx strain
0	0.0	0.0	4.76E-04
-12.7	1264.5	40.7	1.91E-03
-25.4	2457.3	79.1	4.99E-03
-38.1	3818.6	123.0	3.08E-03

-50.8	6108.3	196.7	2.92E-03
-63.5	7587.7	244.3	3.42E-03

depth Z (ft)	yy strain	τ_{xy} (slugsf)	τ_{xy} (ksf)
0	1.12E-03	95.058	3.0608676
-12.7	2.99E-03	184.309	5.9347498
-25.4	4.61E-03	363.213	11.6954586
-38.1	4.09E-03	860.003	27.6920966
-50.8	1.38E-03	1002.9	32.29338
-63.5	6.91E-05	917.444	29.5416968

depth Z (ft)	x disp (ft)	x disp (in)	Z settlement (ft)	Z settlement (in)
0	9.58E-03	1.15E-01	0.00561	0.06732
-12.7	1.56E-02	1.87E-01	0.00401	0.04812
-25.4	1.89E-02	2.27E-01	0.00197	0.02364
-38.1	1.81E-02	2.17E-01	0.00269	0.03228
-50.8	1.71E-02	2.05E-01	0.00289	0.03468
-63.5	1.87E-02	2.24E-01	0.000701	0.008412

Excavation E (Z=63.5 ft)

depth Z (ft)	σ_{xx} (slugsf)	σ_{xx} (ksf)	xx strain
0	0.0	0.0	5.22E-04
-12.7	1275.4	41.1	2.09E-03
-25.4	2585.4	83.2	4.69E-03
-38.1	3947.3	127.1	3.05E-03
-50.8	5200.8	167.5	1.48E-03
-63.5	7843.7	252.6	1.21E-03

depth Z (ft)	yy strain	τ_{xy} (slugsf)	τ_{xy} (ksf)
0	1.17E-03	98.982	3.1872204
-12.7	2.86E-03	183.691	5.9148502
-25.4	4.50E-03	383.983	12.3642526
-38.1	4.18E-03	874.788	28.1681736
-50.8	4.74E-03	1145.01	36.869322
-63.5	2.17E-03	825.879	26.5933038

depth Z (ft)	x disp (ft)	x disp (in)	Z settlement (ft)	Z settlement (in)
0	9.75E-03	1.17E-01	0.00528	0.06336

-12.7	1.49E-02	1.79E-01	0.00369	0.04428
-25.4	1.89E-02	2.27E-01	0.00178	0.02136
-38.1	1.84E-02	2.21E-01	0.00209	0.02508
-50.8	1.99E-02	2.39E-01	0.00107	0.01284
-63.5	1.93E-02	2.32E-01	0.00139	0.01668

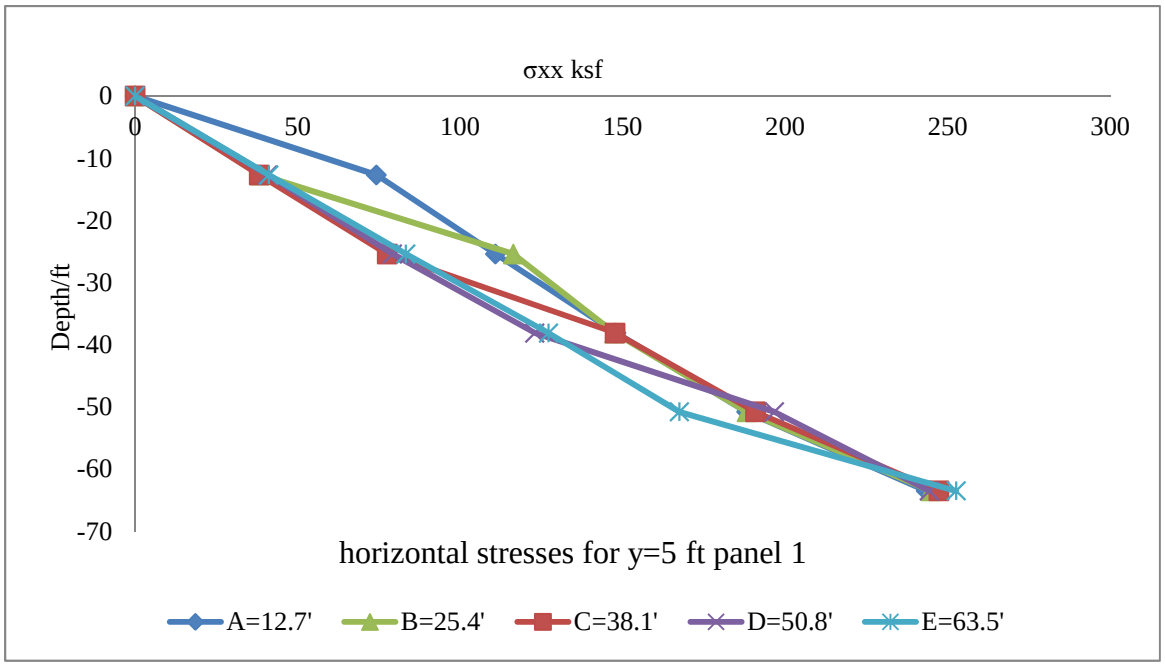

Figure B 1 Horizontal Stresses for Panel 1

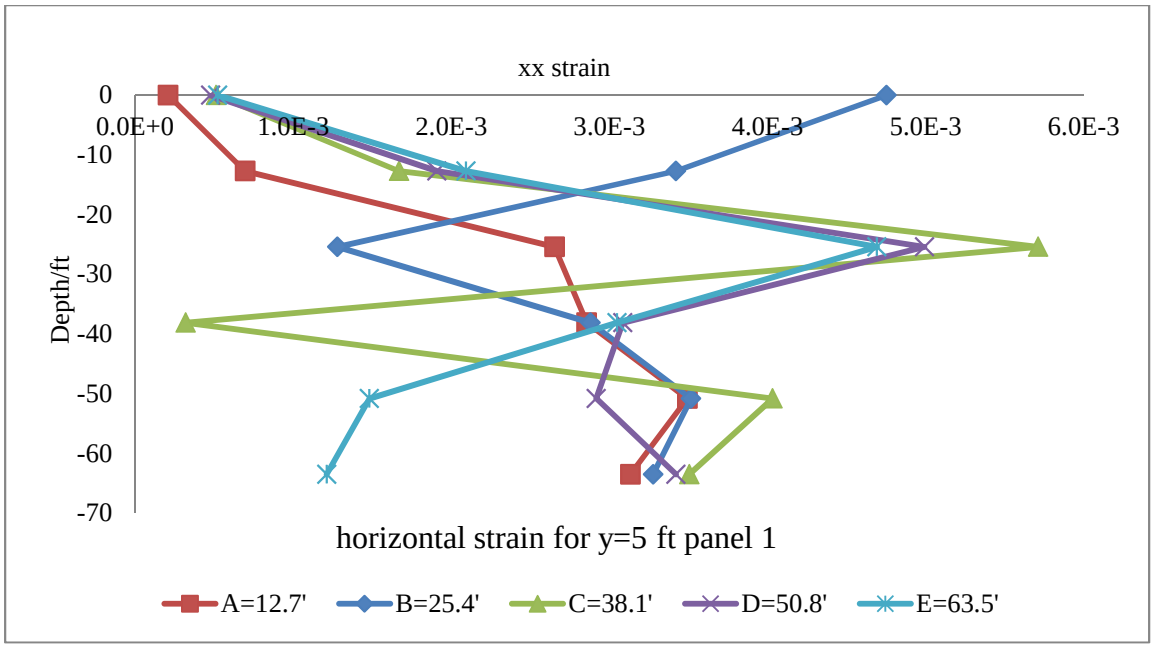

Figure B 2 Horizontal Strain in XX Direction for Panel 1

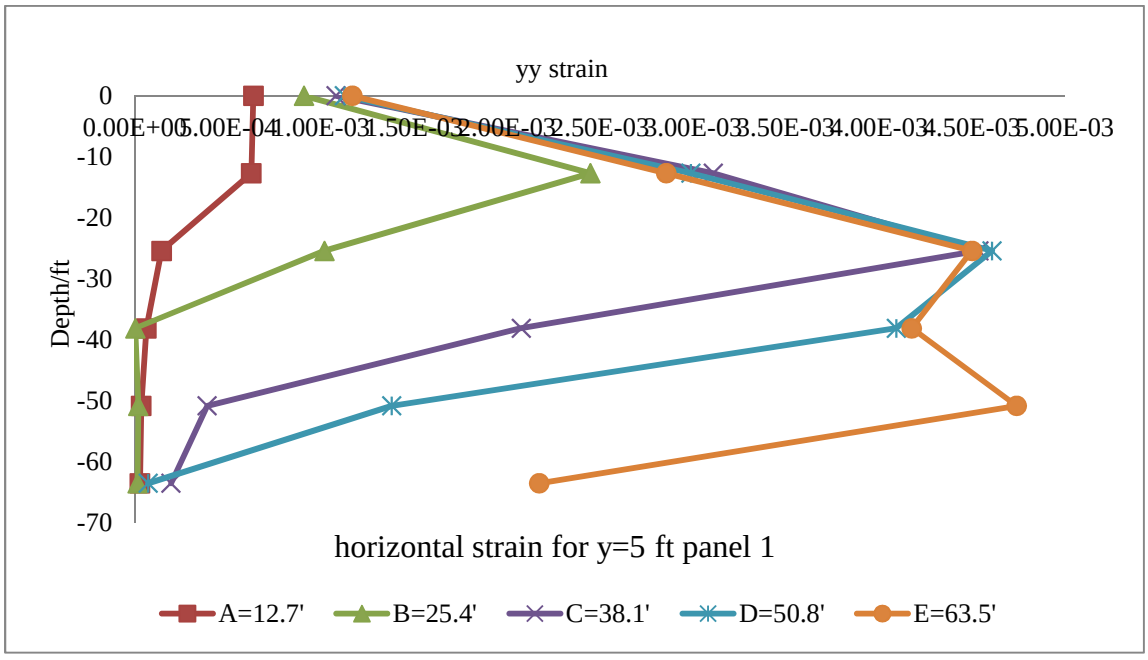

Figure B 3 Horizontal Strain in YY Direction for Panel 1

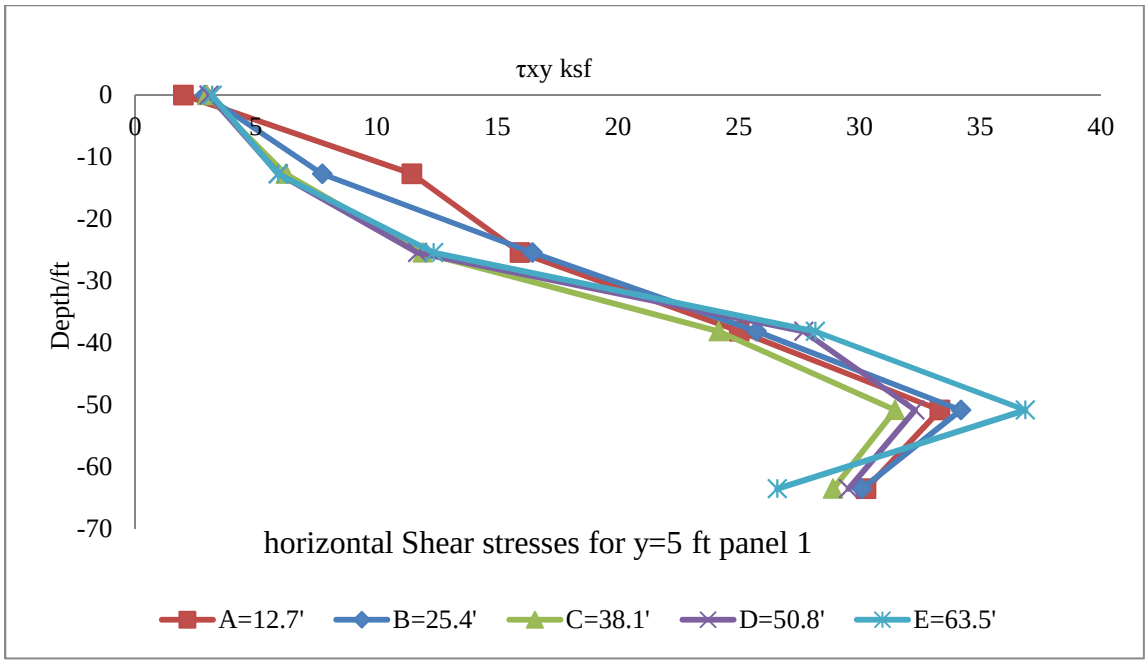

Figure B 4 Horizontal Shear Stresses for Panel 1

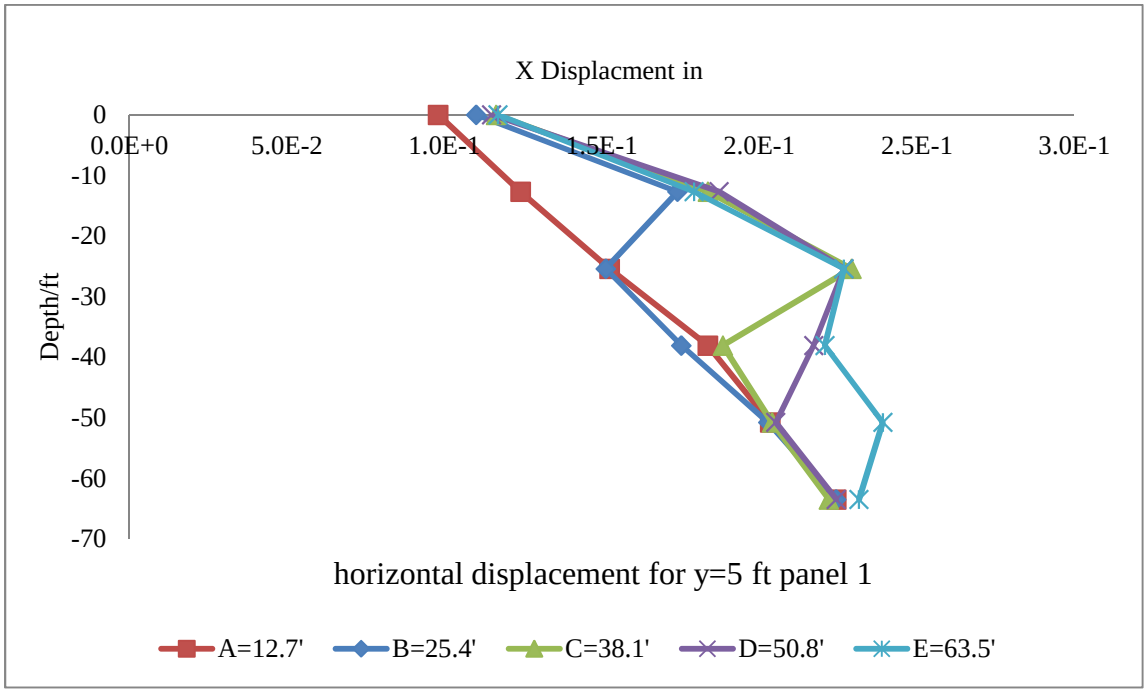

Figure B 5 Horizontal Displacement for Panel 1

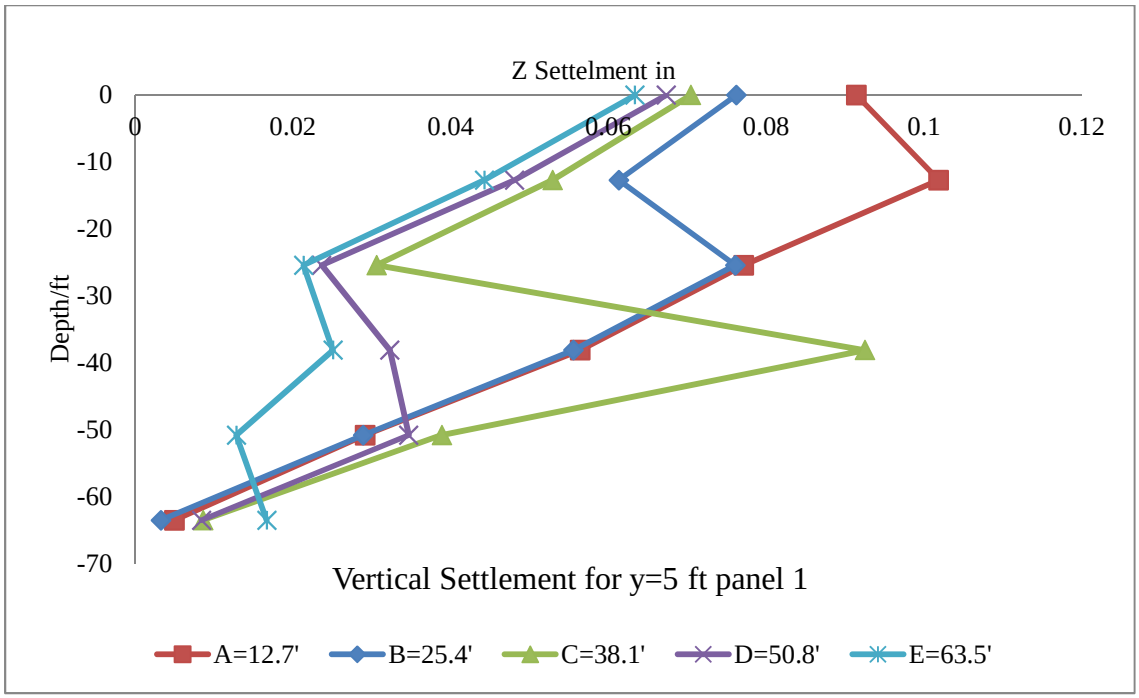

Figure B 6 Vertical Settlement for Panel 1

Panel (2) (Y=10 ft)

Table B 2 All Numerical Results for Panel 2

Excavation A (Z=12.7 ft)

depth Z (ft)	σ_{xx} (slugsf)	σ_{xx} (ksf)	xx strain
0	0.0	0.0	2.78E-05
-12.7	1938.8	62.4	3.57E-04
-25.4	3434.2	110.6	2.90E-03
-38.1	4604.0	148.2	2.90E-03
-50.8	5890.1	189.7	3.55E-03
-63.5	7600.1	244.7	3.34E-03

depth Z (ft)	yy strain	τ_{xy} (slugsf)	τ_{xy} (ksf)
0	1.41E-04	74.174	2.3884028
-12.7	2.55E-04	385.339	12.4079158
-25.4	1.30E-04	485.346	15.6281412
-38.1	8.86E-05	792.072	25.5047184

-50.8	5.20E-05	1037.52	33.408144
-63.5	4.17E-05	924.944	29.7831968

depth Z (ft)	x disp (ft)	x disp (in)	Z settlement (ft)	Z settlement (in)
0	1.19E-02	1.43E-01	0.00662	0.07944
-12.7	1.18E-02	1.42E-01	0.00833	0.09996
-25.4	1.25E-02	1.50E-01	0.00678	0.08136
-38.1	1.47E-02	1.76E-01	0.00493	0.05916
-50.8	1.71E-02	2.05E-01	0.00261	0.03132
-63.5	1.85E-02	2.22E-01	0.000506	0.006072

Excavation B (Z=25.4 ft)

depth Z (ft)	σ_{xx} (slugsf)	σ_{xx} (ksf)	xx strain
0	0.0	0.0	4.27E-05
-12.7	1298.5	41.8	1.49E-03
-25.4	3623.5	116.7	1.84E-03
-38.1	4693.2	151.1	3.01E-03
-50.8	5853.3	188.5	3.55E-03
-63.5	7623.9	245.5	3.30E-03

depth Z (ft)	yy strain	τ_{xy} (slugsf)	τ_{xy} (ksf)
0	3.59E-04	45.589	1.4679658
-12.7	3.47E-04	209.123	6.7337606
-25.4	3.33E-04	547.579	17.6320438
-38.1	3.34E-05	771.36	24.837792
-50.8	3.79E-05	1038.9	33.45258
-63.5	3.11E-05	936.131	30.1434182

depth Z (ft)	x disp (ft)	x disp (in)	Z settlement (ft)	Z settlement (in)
0	1.57E-02	1.88E-01	0.00386	0.04632
-12.7	1.94E-02	2.33E-01	0.00304	0.03648
-25.4	1.28E-02	1.53E-01	0.00681	0.08172
-38.1	1.47E-02	1.76E-01	0.00484	0.05808
-50.8	1.72E-02	2.06E-01	0.002495	0.02994
-63.5	1.84E-02	2.21E-01	0.000468	0.005616

Excavation C (Z=38.1 ft)

depth Z (ft)	σ_{xx} (slugsf)	σ_{xx} (ksf)	xx strain
0	0.0	0.0	1.19E-04
-12.7	1402.2	45.2	5.86E-04
-25.4	2523.6	81.3	2.99E-03
-38.1	4649.0	149.7	5.16E-04
-50.8	5876.0	189.2	4.30E-03
-63.5	7636.8	245.9	3.53E-03

depth Z (ft)	yy strain	τ_{xy} (slugsf)	τ_{xy} (ksf)
0	3.75E-04	49.977	1.6092594
-12.7	7.31E-04	165.363	5.3246886
-25.4	3.13E-04	448.831	14.4523582
-38.1	3.48E-04	806.475	25.968495
-50.8	4.85E-04	932.834	30.0372548
-63.5	2.74E-04	869.189	27.9878858

depth Z (ft)	x disp (ft)	x disp (in)	Z settlement (ft)	Z settlement (in)
0	1.67E-02	2.01E-01	0.00269	0.03228
-12.7	2.17E-02	2.60E-01	0.00188	0.02256
-25.4	2.54E-02	3.05E-01	0.000472	0.005664
-38.1	1.62E-02	1.94E-01	0.00938	0.11256
-50.8	1.72E-02	2.06E-01	0.00396	0.04752
-63.5	1.87E-02	2.24E-01	0.000941	0.011292

Excavation D (Z=50.8 ft)

depth Z (ft)	σ_{xx} (slugsf)	σ_{xx} (ksf)	xx strain
0	0.0	0.0	1.11E-04
-12.7	1339.0	43.1	6.12E-04
-25.4	2571.9	82.8	1.90E-03
-38.1	3823.4	123.1	7.47E-04
-50.8	6094.5	196.2	4.39E-03
-63.5	7631.5	245.7	3.52E-03

depth Z (ft)	yy strain	τ_{xy} (slugsf)	τ_{xy} (ksf)
0	4.27E-04	47.964	1.5444408
-12.7	8.86E-04	150.415	4.843363
-25.4	3.31E-04	442.073	14.2347506
-38.1	6.94E-04	875.778	28.2000516

-50.8	1.80E-04	1068.14	34.394108
-63.5	9.23E-05	905.729	29.1644738

depth Z (ft)	x disp (ft)	x disp (in)	Z settlement (ft)	Z settlement (in)
0	1.70E-02	2.04E-01	0.00242	0.02904
-12.7	2.15E-02	2.58E-01	0.00153	0.01836
-25.4	2.55E-02	3.06E-01	0.000269	0.003228
-38.1	2.12E-02	2.54E-01	0.00193	0.02316
-50.8	1.75E-02	2.10E-01	0.00326	0.03912
-63.5	1.88E-02	2.26E-01	0.000683	0.008196

Excavation E (Z=63.5 ft)

depth Z (ft)	σ_{xx} (slugsf)	σ_{xx} (ksf)	xx strain
0	0.0	0.0	1.11E-04
-12.7	1325.3	42.7	5.52E-04
-25.4	2612.6	84.1	1.63E-03
-38.1	3770.5	121.4	5.32E-04
-50.8	5086.4	163.8	9.67E-04
-63.5	7868.4	253.4	3.70E-03

depth Z (ft)	yy strain	τ_{xy} (slugsf)	τ_{xy} (ksf)
0	4.05E-04	56.773	1.8280906
-12.7	8.50E-04	158.665	5.109013
-25.4	4.78E-04	440.2	14.17444
-38.1	3.84E-04	866.182	27.8910604
-50.8	1.82E-04	1113.2	35.84504
-63.5	1.50E-05	870.952	28.0446544

depth Z (ft)	x disp (ft)	x disp (in)	Z settlement (ft)	Z settlement (in)
0	1.68E-02	2.02E-01	0.00238	0.02856
-12.7	2.19E-02	2.63E-01	0.001517	0.018204
-25.4	2.56E-02	3.07E-01	0.000186	0.002232
-38.1	2.21E-02	2.65E-01	0.00181	0.02172
-50.8	2.26E-02	2.71E-01	0.000953	0.011436
-63.5	2.04E-02	2.44E-01	0.00208	0.02496

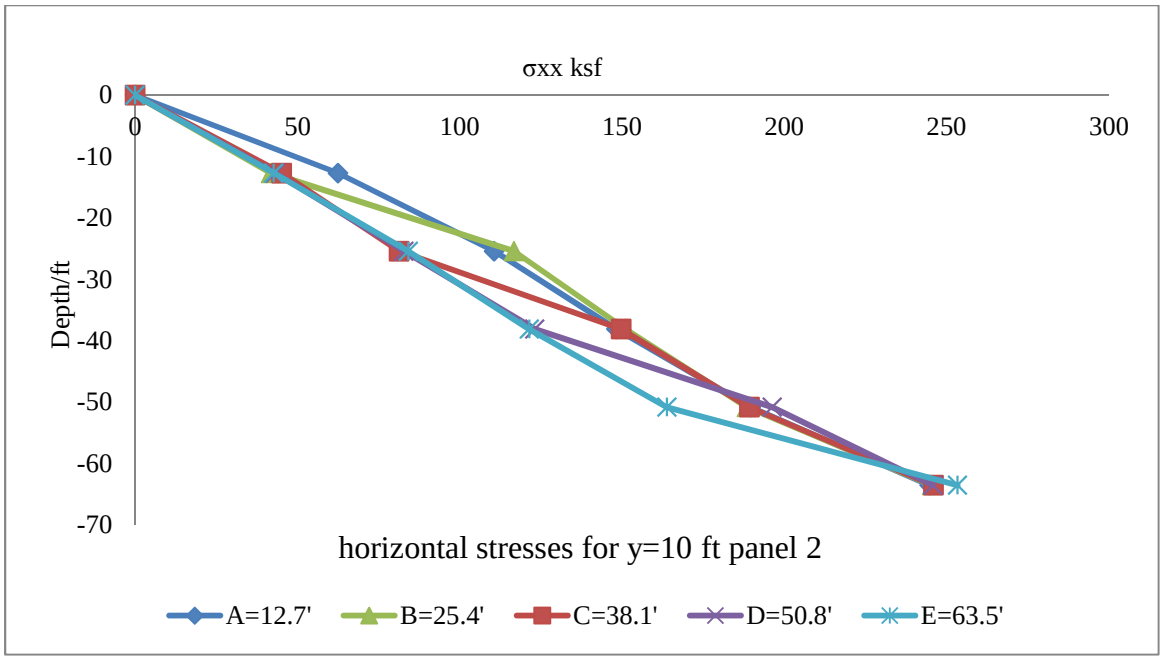

Figure B 7 Horizontal Stresses for Panel 2

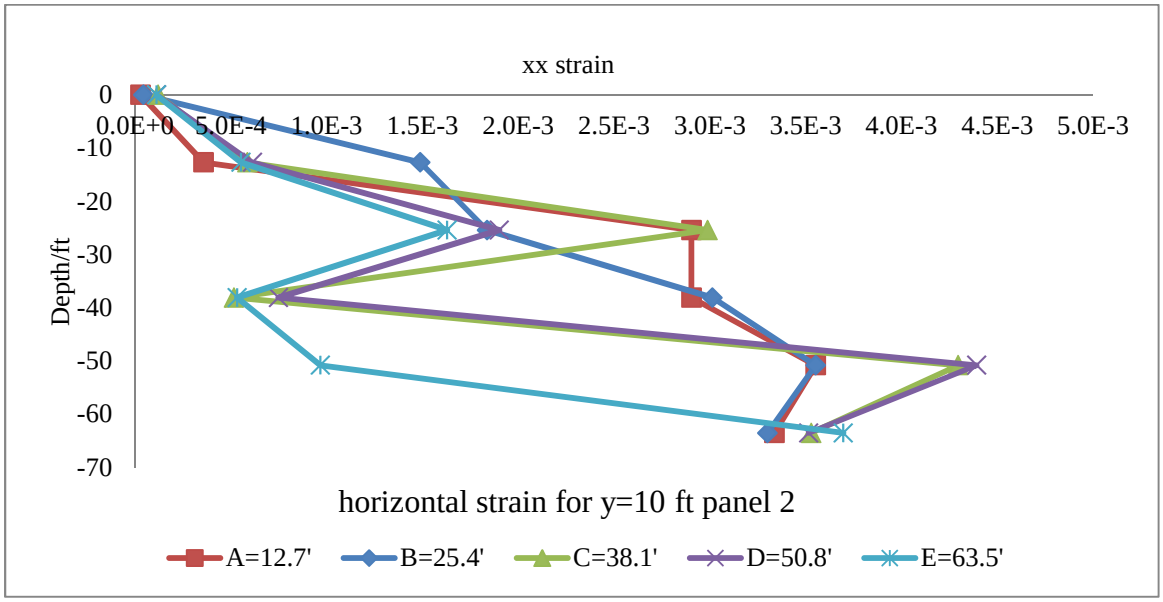

Figure B 8 Horizontal Strain in XX Direction for Panel 2

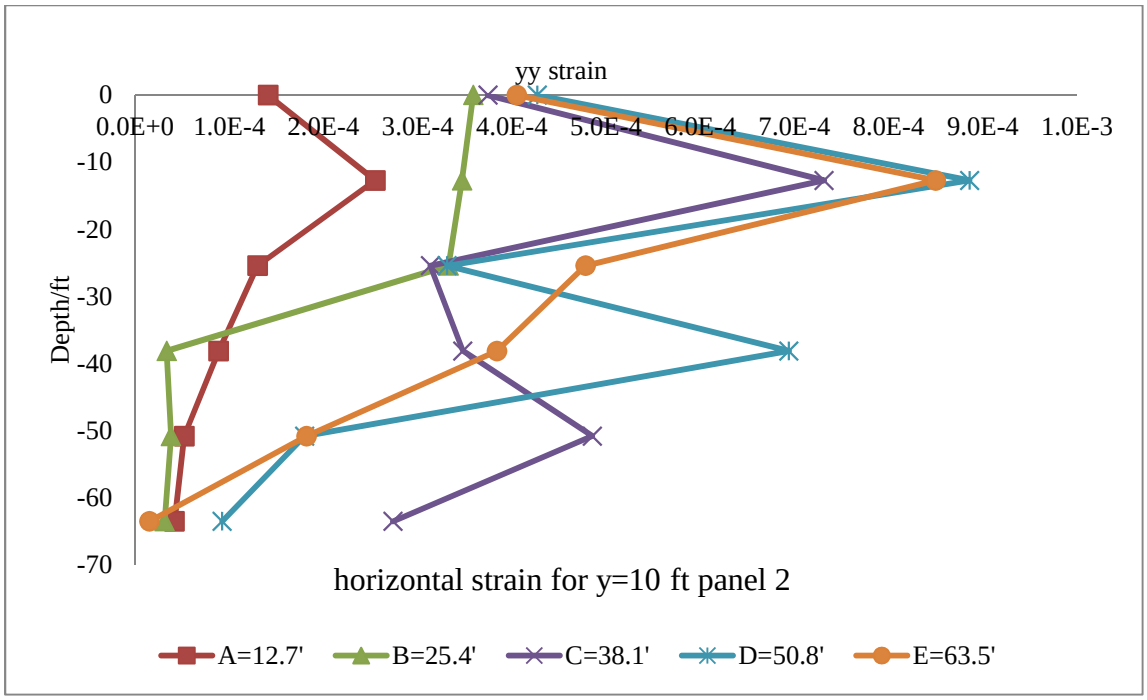

Figure B 9 Horizontal Strain in YY Direction for Panel 2

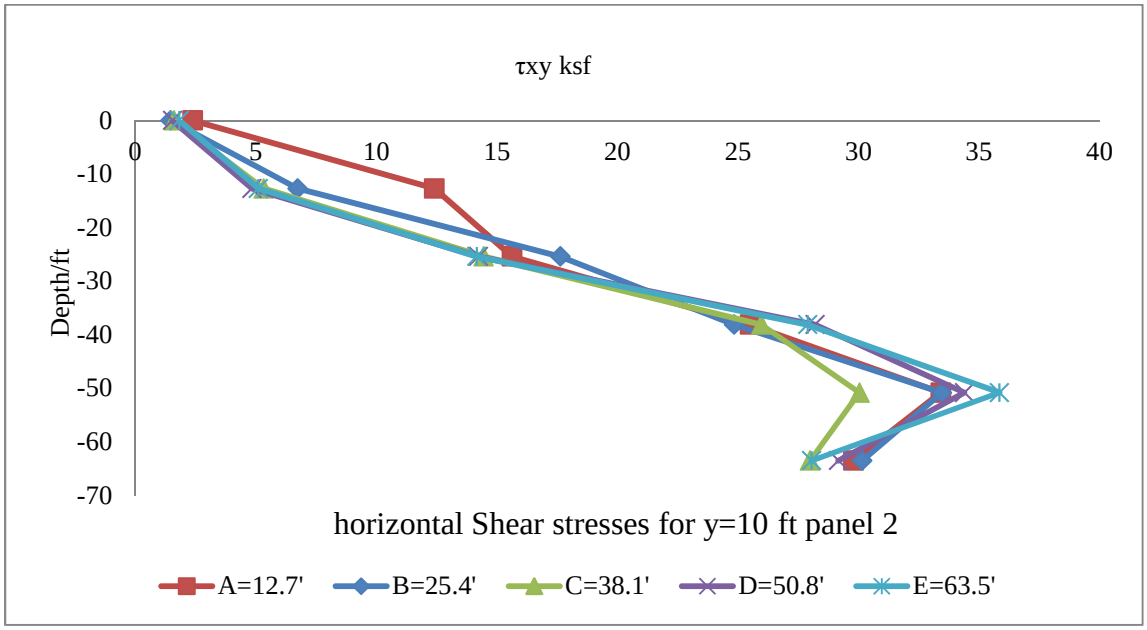

Figure B 10 Horizontal Shear Stresses for Panel 2

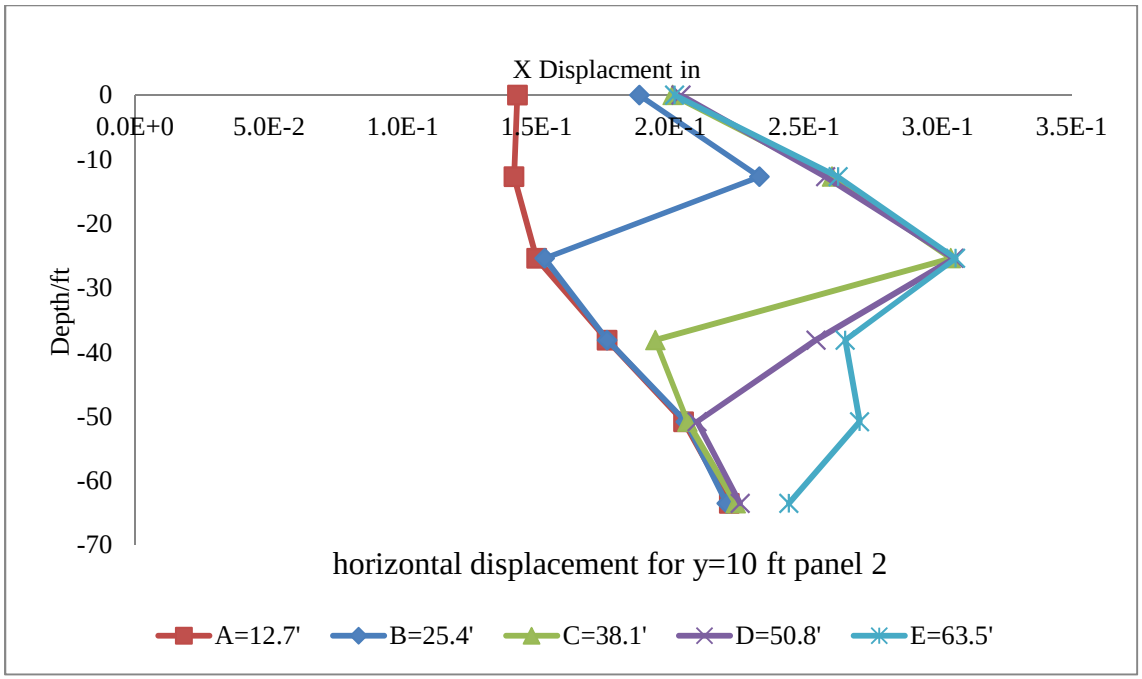

Figure B 11 Horizontal Displacement for Panel 2

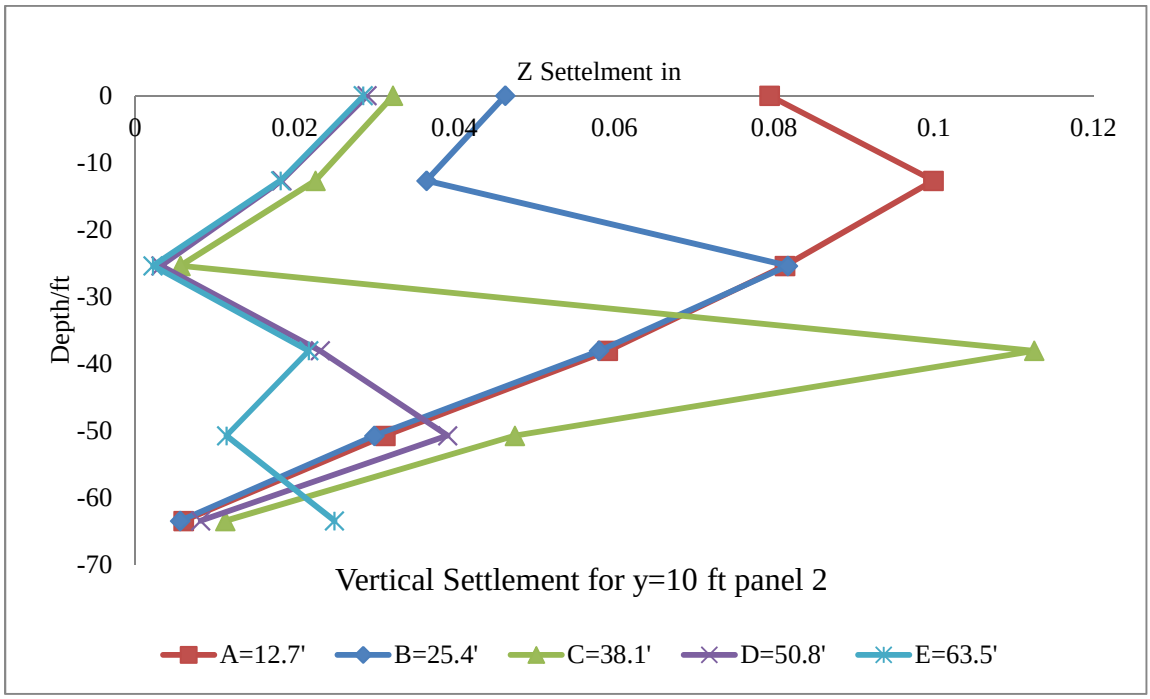

Figure B 12 Vertical Settlement for Panel 2

Panel (3) (Y=15 ft)

Table B 3 All Numerical Results for Panel 3

Excavation A (Z=12.7 ft)

depth Z (ft)	σ_{xx} (slugsf)	σ_{xx} (ksf)	xx strain
0	0.0	0.0	5.86E-06
-12.7	1975.3	63.6	1.52E-03
-25.4	3495.9	112.6	3.01E-03
-38.1	4608.7	148.4	2.99E-03
-50.8	5854.0	188.5	3.59E-03
-63.5	7673.1	247.1	3.34E-03

depth Z (ft)	yy strain	τ_{xy} (slugsf)	τ_{xy} (ksf)
0	8.55E-04	112.903	3.6354766
-12.7	6.51E-04	401.918	12.9417596
-25.4	4.59E-05	493.416	15.8879952
-38.1	1.17E-04	765.322	24.6433684
-50.8	8.49E-05	1033.74	33.286428
-63.5	6.95E-05	933.707	30.0653654

depth Z (ft)	x disp (ft)	x disp (in)	Z settlement (ft)	Z settlement (in)
0	2.31E-02	2.77E-01	0.003275	0.0393
-12.7	1.44E-02	1.73E-01	0.007967	0.095604
-25.4	1.26E-02	1.51E-01	0.007178	0.086136
-38.1	1.47E-02	1.76E-01	0.005054	0.060648
-50.8	1.71E-02	2.05E-01	0.002679	0.032148
-63.5	1.85E-02	2.22E-01	0.0005594	0.0067128

Excavation B (Z=25.4 ft)

depth Z (ft)	σ_{xx} (slugsf)	σ_{xx} (ksf)	xx strain
0	0.0	0.0	2.80E-04
-12.7	1304.2	42.0	5.72E-03
-25.4	3719.4	119.8	4.53E-04
-38.1	4631.5	149.1	3.09E-03
-50.8	5903.4	190.1	3.60E-03
-63.5	7624.6	245.5	3.38E-03

depth Z (ft)	yy strain	τ_{xy} (slugsf)	τ_{xy} (ksf)
0	1.67E-04	72.2102	2.32516844
-12.7	1.18E-03	294.619	9.4867318
-25.4	7.85E-04	567.897	18.2862834
-38.1	2.50E-05	783.373	25.2246106
-50.8	6.57E-05	1031.98	33.229756
-63.5	6.46E-05	930.739	29.9697958

depth Z (ft)	x disp (ft)	x disp (in)	Z settlement (ft)	Z settlement (in)
0	3.70E-02	4.43E-01	0.00478	0.05736
-12.7	3.75E-02	4.50E-01	0.004993	0.059916
-25.4	1.26E-02	1.51E-01	0.007112	0.085344
-38.1	1.47E-02	1.76E-01	0.005026	0.060312
-50.8	1.70E-02	2.04E-01	0.002661	0.031932
-63.5	1.85E-02	2.22E-01	0.0005415	0.006498

Excavation C (Z=38.1 ft)

depth Z (ft)	σ_{xx} (slugsf)	σ_{xx} (ksf)	xx strain
0	0.0	0.0	6.02E-04
-12.7	1346.3	43.4	8.60E-04
-25.4	2485.4	80.0	7.60E-03
-38.1	4873.7	156.9	2.85E-03
-50.8	5934.9	191.1	4.72E-03
-63.5	7673.3	247.1	3.83E-03

depth Z (ft)	yy strain	τ_{xy} (slugsf)	τ_{xy} (ksf)
0	8.35E-04	74.321	2.3931362
-12.7	2.23E-04	255.742	8.2348924
-25.4	1.14E-03	498.897	16.0644834
-38.1	1.04E-03	853.686	27.4886892
-50.8	3.87E-04	910.942	29.3323324
-63.5	4.10E-04	842.937	27.1425714

depth Z (ft)	x disp (ft)	x disp (in)	Z settlement (ft)	Z settlement (in)
0	4.29E-02	5.14E-01	0.0095	0.114
-12.7	4.67E-02	5.60E-01	0.0102	0.1224
-25.4	4.57E-02	5.48E-01	0.00971	0.11652
-38.1	1.63E-02	1.96E-01	0.00944	0.11328

-50.8	1.69E-02	2.03E-01	0.00492	0.05904
-63.5	1.87E-02	2.25E-01	0.00121	0.01452

Excavation D (Z=50.8 ft)

depth Z (ft)	σ_{xx} (slugsf)	σ_{xx} (ksf)	xx strain
0	0.0	0.0	6.16E-04
-12.7	1303.9	42.0	9.20E-04
-25.4	2532.1	81.5	4.39E-03
-38.1	3777.2	121.6	4.45E-03
-50.8	6320.5	203.5	5.30E-03
-63.5	7694.0	247.7	3.74E-03

depth Z (ft)	yy strain	τ_{xy} (slugsf)	τ_{xy} (ksf)
0	8.53E-04	71.7199	2.30938078
-12.7	5.79E-05	256.844	8.2703768
-25.4	9.27E-04	500.105	16.103381
-38.1	2.12E-03	965.052	31.0746744
-50.8	6.15E-04	1126.49	36.272978
-63.5	5.62E-05	904.045	29.110249

depth Z (ft)	x disp (ft)	x disp (in)	Z settlement (ft)	Z settlement (in)
0	4.31E-02	5.17E-01	0.01	0.12
-12.7	4.71E-02	5.65E-01	0.0108	0.1296
-25.4	4.66E-02	5.59E-01	0.0104	0.1248
-38.1	2.99E-02	3.59E-01	0.00217	0.02604
-50.8	1.80E-02	2.16E-01	0.00342	0.04104
-63.5	1.92E-02	2.30E-01	0.00075	0.009

Excavation E (Z=63.5 ft)

depth Z (ft)	σ_{xx} (slugsf)	σ_{xx} (ksf)	xx strain
0	0.0	0.0	5.19E-04
-12.7	1311.2	42.2	7.06E-04
-25.4	2557.1	82.3	3.90E-03
-38.1	3757.7	121.0	2.34E-03
-50.8	5068.3	163.2	8.34E-04
-63.5	8358.4	269.1	4.81E-03

depth Z (ft)	yy strain	τ_{xy} (slugsf)	τ_{xy} (ksf)
0	9.09E-04	75.231	2.4224382
-12.7	3.34E-05	267.776	8.6223872
-25.4	8.64E-04	498.798	16.0612956
-38.1	1.98E-03	927.939	29.8796358
-50.8	1.81E-03	1154.43	37.172646
-63.5	4.04E-04	887.877	28.5896394

depth Z (ft)	x disp (ft)	x disp (in)	Z settlement (ft)	Z settlement (in)
0	4.32E-02	5.18E-01	0.00999	0.11988
-12.7	4.73E-02	5.67E-01	0.0107	0.1284
-25.4	4.75E-02	5.70E-01	0.01053	0.12636
-38.1	3.23E-02	3.87E-01	0.003922	0.047064
-50.8	2.70E-02	3.24E-01	0.000738	0.008856
-63.5	2.17E-02	2.61E-01	0.001992	0.023904

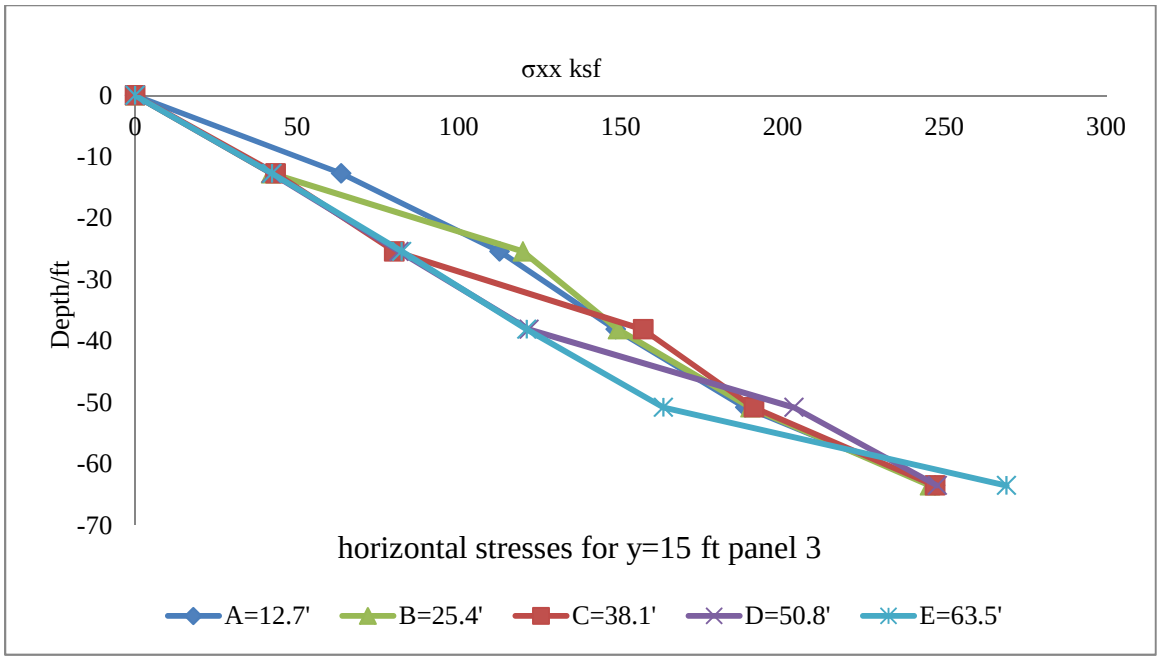

Figure B 13 Horizontal Stresses for Panel 3

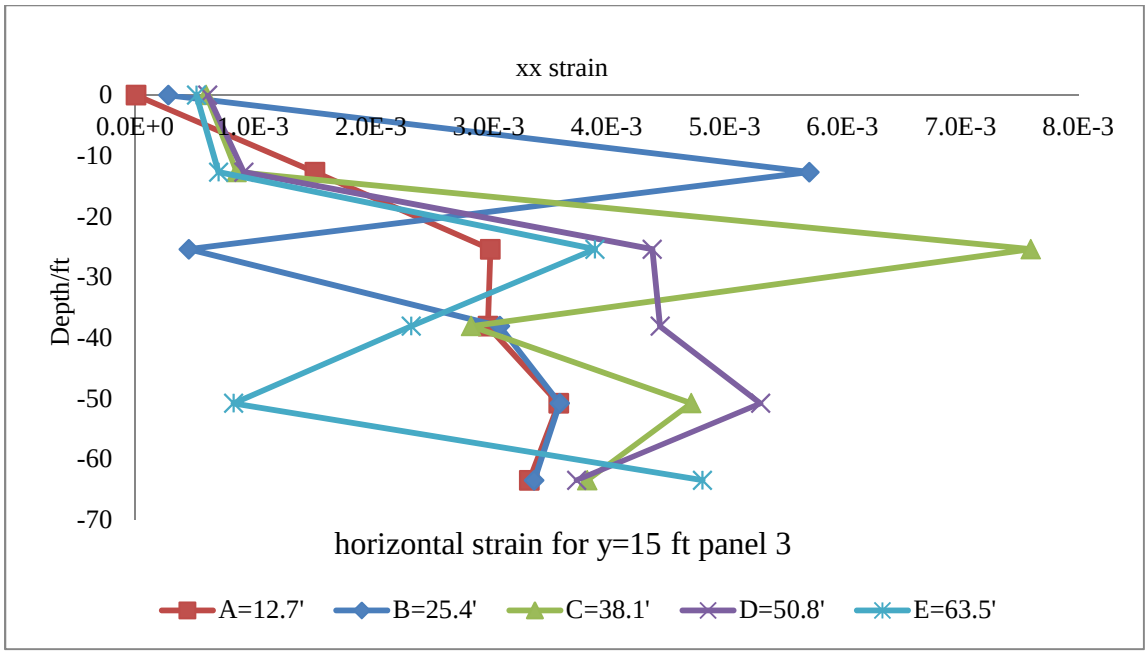

Figure B 14 Horizontal Strain in XX Direction for Panel 3

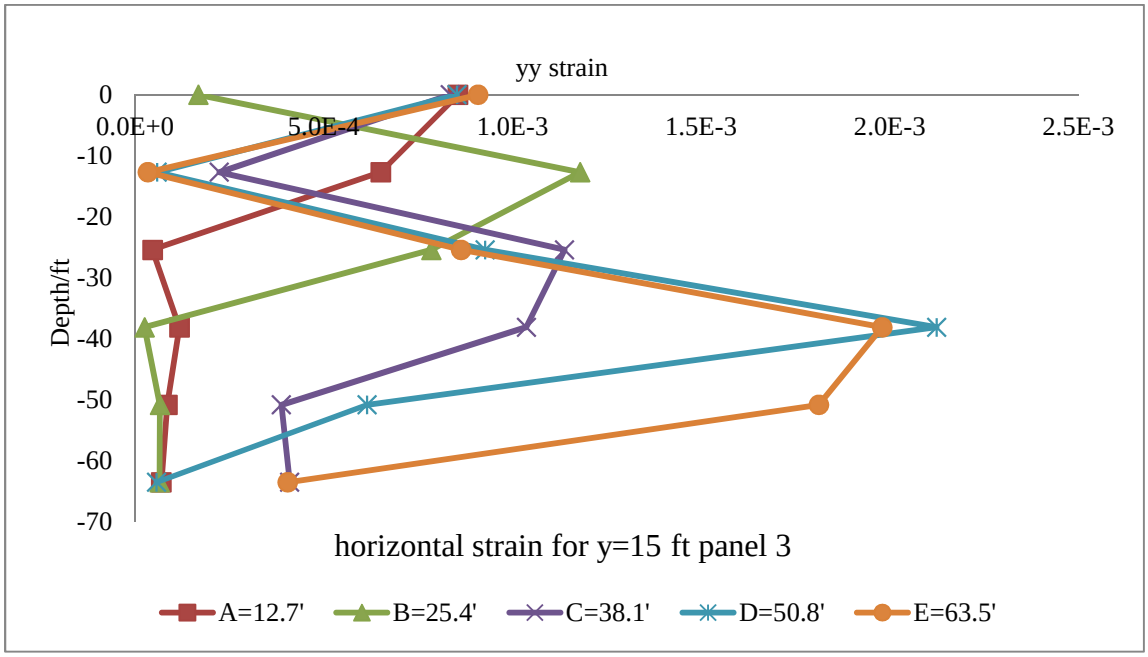

Figure B 15 Horizontal Strain in YY Direction for Panel 3

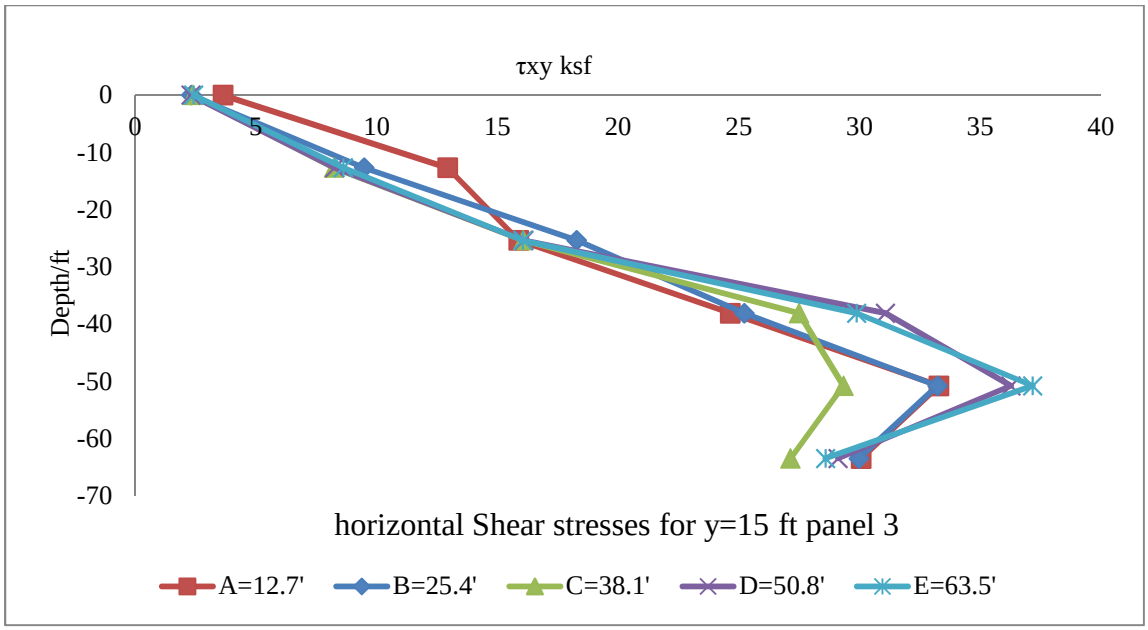

Figure B 16 Horizontal Shear Stresses for Panel 3

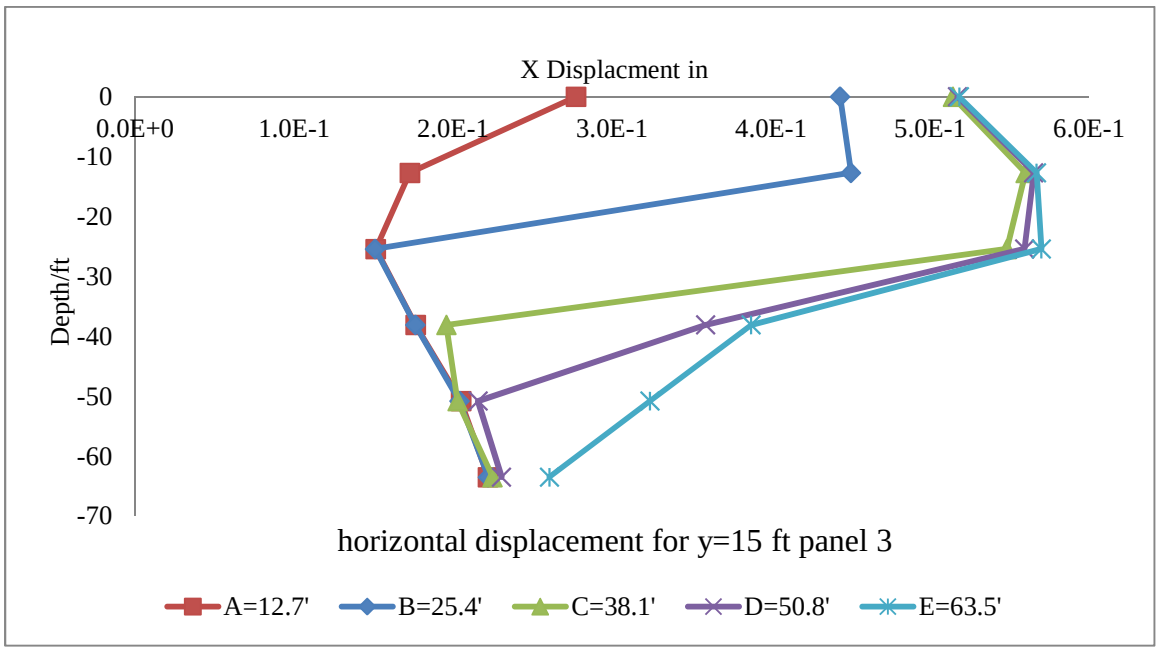

Figure B 17 Horizontal Displacement for Panel 3

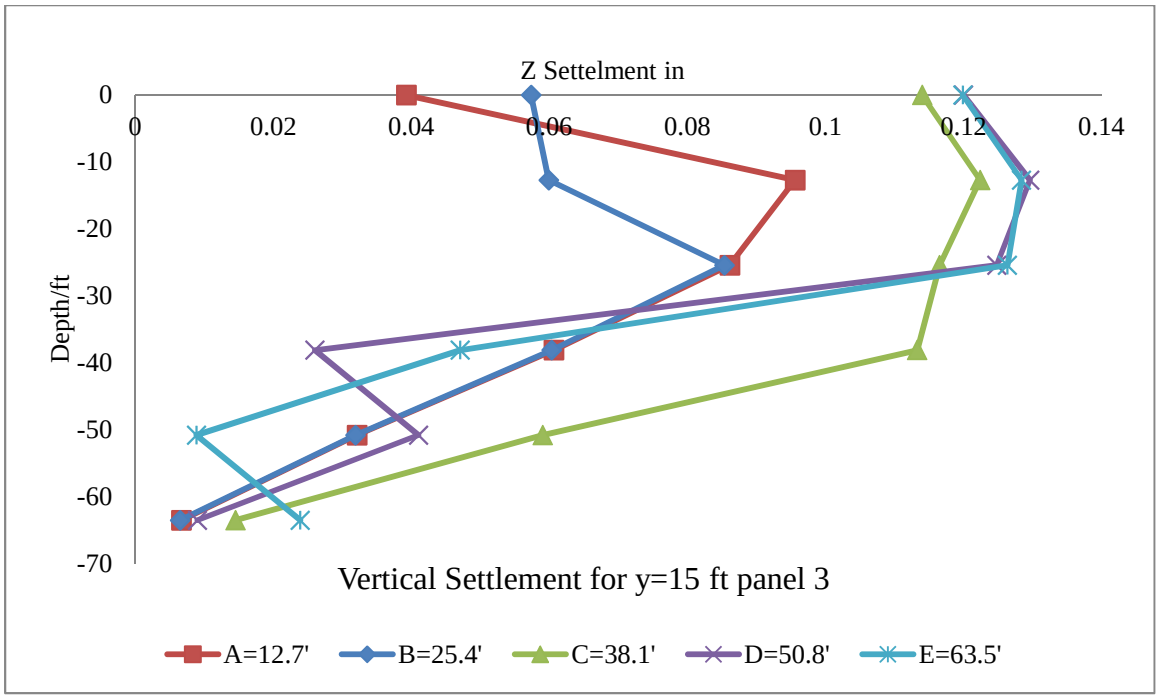

Figure B 18 Vertical Settlement for Panel 3

Panel (4) (Y=20 ft)

Table B 4 All Numerical Results for Panel 4

Excavation A (Z=12.7 ft)

depth Z (ft)	σ_{xx} (slugsf)	σ_{xx} (ksf)	xx strain
0	0.0	0.0	3.90E-04
-12.7	2025.2	65.2	2.49E-03
-25.4	3425.3	110.3	3.04E-03
-38.1	4596.4	148.0	2.99E-03
-50.8	5855.1	188.5	3.62E-03
-63.5	7576.2	244.0	3.36E-03

depth Z (ft)	yy strain	τ_{xy} (slugsf)	τ_{xy} (ksf)
0	1.20E-03	122.82	3.954804
-12.7	6.67E-04	420.422	13.5375884
-25.4	1.69E-05	494.425	15.920485
-38.1	1.12E-04	760.657	24.4931554

-50.8	9.77E-05	1027.89	33.098058
-63.5	8.44E-05	916.531	29.5122982

depth Z (ft)	x disp (ft)	x disp (in)	Z settlement (ft)	Z settlement (in)
0	3.32E-02	3.98E-01	0.00061	0.00732
-12.7	1.82E-02	2.18E-01	0.00792	0.09504
-25.4	1.25E-02	1.50E-01	0.007336	0.088032
-38.1	1.47E-02	1.76E-01	0.005284	0.063408
-50.8	1.69E-02	2.03E-01	0.00276	0.03312
-63.5	1.85E-02	2.22E-01	0.00064	0.00768

Excavation B (Z=25.4 ft)

depth Z (ft)	σ_{xx} (slugsf)	σ_{xx} (ksf)	xx strain
0	0.0	0.0	2.59E-04
-12.7	1278.7	41.2	1.43E-02
-25.4	3667.7	118.1	8.59E-03
-38.1	4644.0	149.5	3.07E-03
-50.8	5858.4	188.6	3.60E-03
-63.5	7570.6	243.8	3.36E-03

depth Z (ft)	yy strain	τ_{xy} (slugsf)	τ_{xy} (ksf)
0	6.38E-05	94.93	3.056746
-12.7	2.84E-03	340.075	10.950415
-25.4	9.78E-04	567.459	18.2721798
-38.1	2.81E-06	775.624	24.9750928
-50.8	8.85E-05	1027.2	33.07584
-63.5	9.91E-05	925.512	29.8014864

depth Z (ft)	x disp (ft)	x disp (in)	Z settlement (ft)	Z settlement (in)
0	8.43E-02	1.01E+00	0.0709	0.8508
-12.7	7.93E-02	9.52E-01	0.02637	0.31644
-25.4	1.21E-02	1.45E-01	0.00716	0.08592
-38.1	1.45E-02	1.74E-01	0.00515	0.0618
-50.8	1.69E-02	2.03E-01	0.002838	0.034056
-63.5	1.85E-02	2.22E-01	0.0006258	0.0075096

Excavation C (Z=38.1 ft)

depth Z (ft)	σ_{xx} (slugsf)	σ_{xx} (ksf)	xx strain
0	0.0	0.0	3.24E-02
-12.7	1340.8	43.2	7.27E-02
-25.4	2491.4	80.2	3.72E-01
-38.1	4558.9	146.8	1.01E-01
-50.8	5956.0	191.8	5.00E-03
-63.5	7585.7	244.3	4.12E-03

depth Z (ft)	yy strain	τ_{xy} (slugsf)	τ_{xy} (ksf)
0	3.11E-02	182.655	5.881491
-12.7	2.39E-02	360.865	11.619853
-25.4	2.69E-02	525.659	16.9262198
-38.1	3.45E-03	805.552	25.9387744
-50.8	4.51E-04	865.742	27.8768924
-63.5	6.10E-04	798.183	25.7014926

depth Z (ft)	x disp (ft)	x disp (in)	Z settlement (ft)	Z settlement (in)
0	1.11E+00	1.33E+01	0.6615	7.938
-12.7	9.48E-01	1.14E+01	0.6445	7.734
-25.4	5.77E-01	6.92E+00	0.4239	5.0868
-38.1	2.67E-02	3.20E-01	0.00295	0.0354
-50.8	1.61E-02	1.93E-01	0.00578	0.06936
-63.5	1.82E-02	2.19E-01	0.00175	0.021

Excavation D (Z=50.8 ft)

depth Z (ft)	σ_{xx} (slugsf)	σ_{xx} (ksf)	xx strain
0	0.0	0.0	1.62E-02
-12.7	1286.7	41.4	3.02E-02
-25.4	2517.3	81.1	1.46E-01
-38.1	3773.0	121.5	7.80E-02
-50.8	6421.9	206.8	4.30E-03
-63.5	7697.9	247.9	3.67E-03

depth Z (ft)	yy strain	τ_{xy} (slugsf)	τ_{xy} (ksf)
0	1.62E-02	181.816	5.8544752
-12.7	9.73E-03	356.223	11.4703806
-25.4	1.01E-02	521.554	16.7940388
-38.1	2.12E-03	939.989	30.2676458

-50.8	1.28E-04	1033.41	33.275802
-63.5	2.25E-04	905.177	29.1466994

depth Z (ft)	x disp (ft)	x disp (in)	Z settlement (ft)	Z settlement (in)
0	5.02E-01	6.02E+00	0.2915	3.498
-12.7	4.44E-01	5.33E+00	0.2851	3.4212
-25.4	3.02E-01	3.62E+00	0.2013	2.4156
-38.1	6.83E-02	8.19E-01	0.031	0.372
-50.8	1.74E-02	2.09E-01	0.00356	0.04272
-63.5	1.88E-02	2.25E-01	0.0008205	0.009846

Excavation E (Z=63.5 ft)

depth Z (ft)	σ_{xx} (slugsf)	σ_{xx} (ksf)	xx strain
0	0.0	0.0	1.50E-02
-12.7	1275.8	41.1	2.83E-02
-25.4	2513.9	80.9	1.41E-01
-38.1	3758.7	121.0	6.95E-02
-50.8	5059.8	162.9	1.58E-03
-63.5	8284.4	266.8	4.67E-03

depth Z (ft)	yy strain	τ_{xy} (slugsf)	τ_{xy} (ksf)
0	1.63E-02	187.48	6.036856
-12.7	9.05E-03	349.16	11.242952
-25.4	1.03E-02	525.022	16.9057084
-38.1	2.44E-03	938.299	30.2132278
-50.8	7.43E-04	1263.43	40.682446
-63.5	2.92E-04	885.994	28.5290068

depth Z (ft)	x disp (ft)	x disp (in)	Z settlement (ft)	Z settlement (in)
0	4.81E-01	5.78E+00	0.279	3.348
-12.7	4.29E-01	5.14E+00	0.27226	3.26712
-25.4	2.89E-01	3.47E+00	0.1867	2.2404
-38.1	7.11E-02	8.53E-01	0.030447	0.365364
-50.8	3.05E-02	3.66E-01	0.002838	0.034056
-63.5	2.18E-02	2.62E-01	0.001898	0.022776

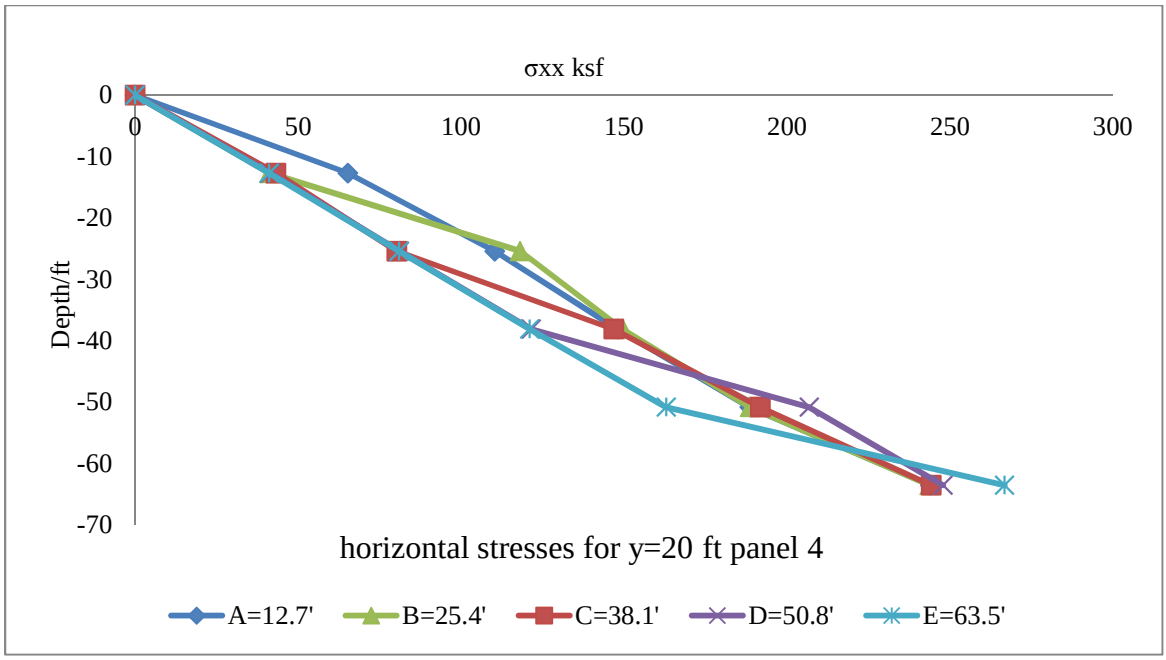

Figure B 19 Horizontal Stresses for Panel 4

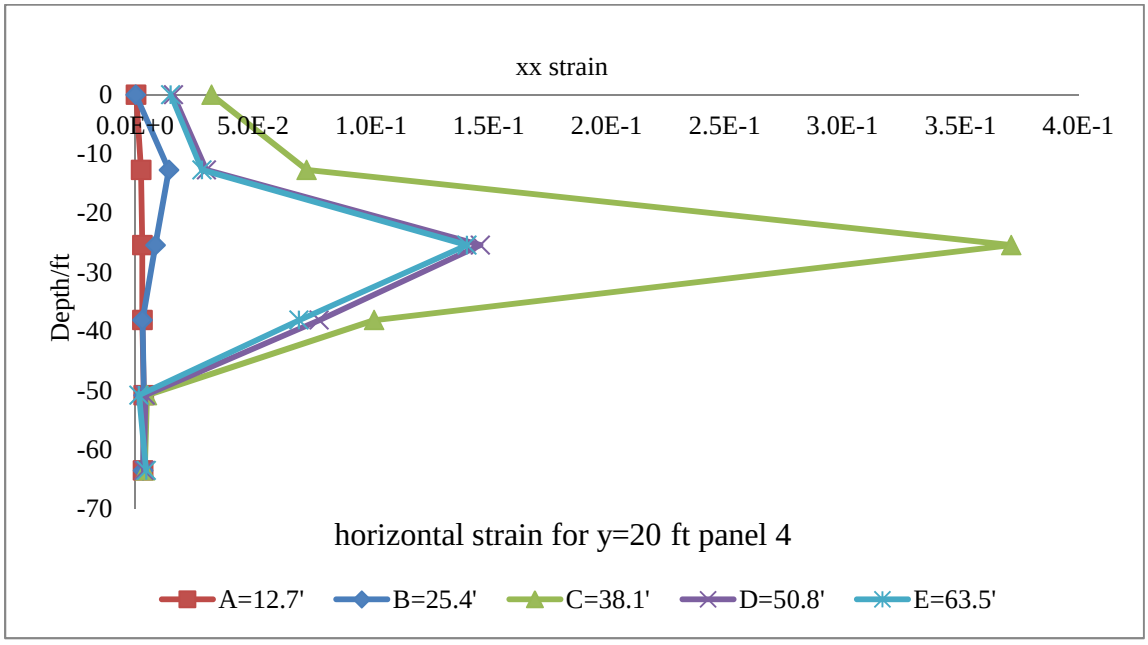

Figure B 20 Horizontal Strain in XX Direction for Panel 4

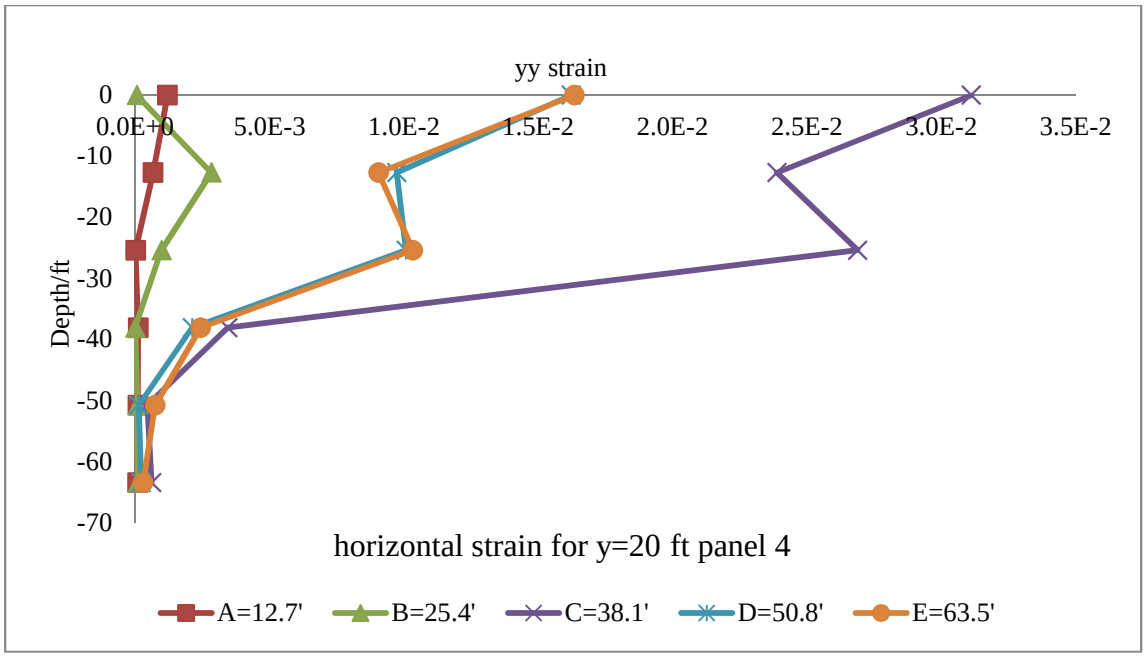

Figure B 21 Horizontal Strain in YY Direction for Panel 4

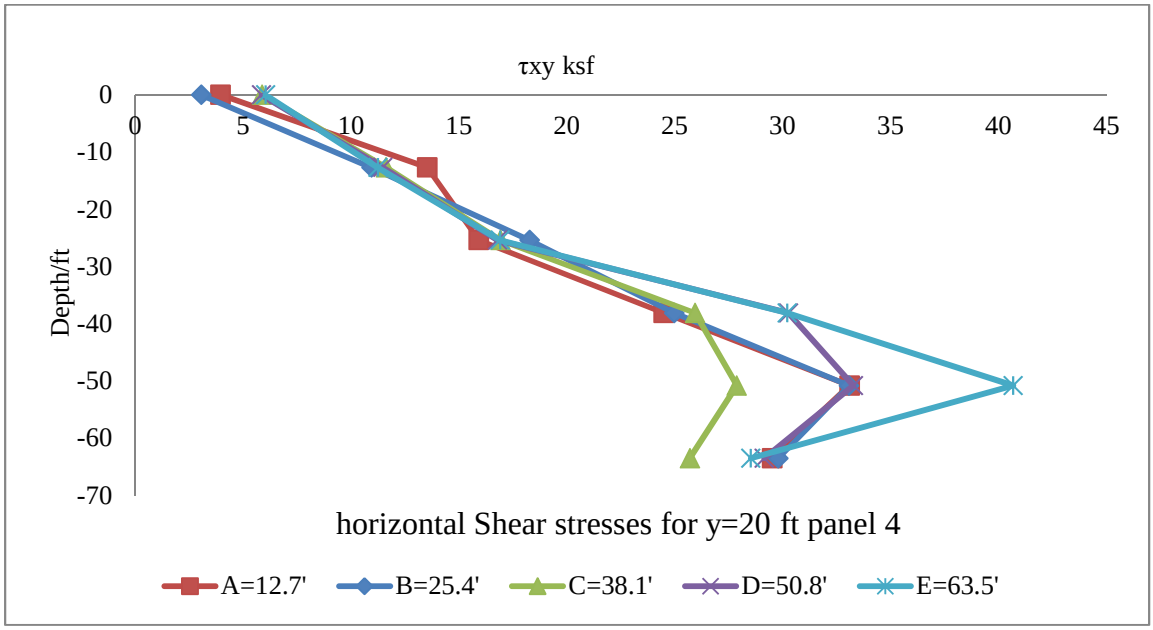

Figure B 22 Horizontal Shear Stresses for Panel 4

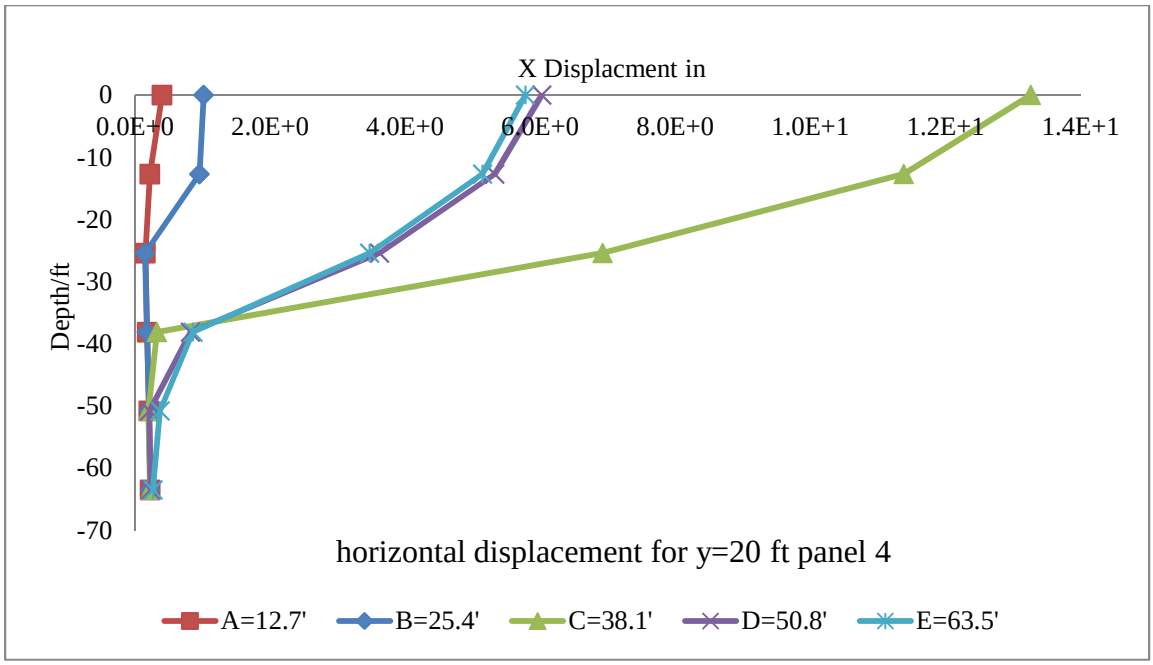

Figure B 23 Horizontal Displacement for Panel 4

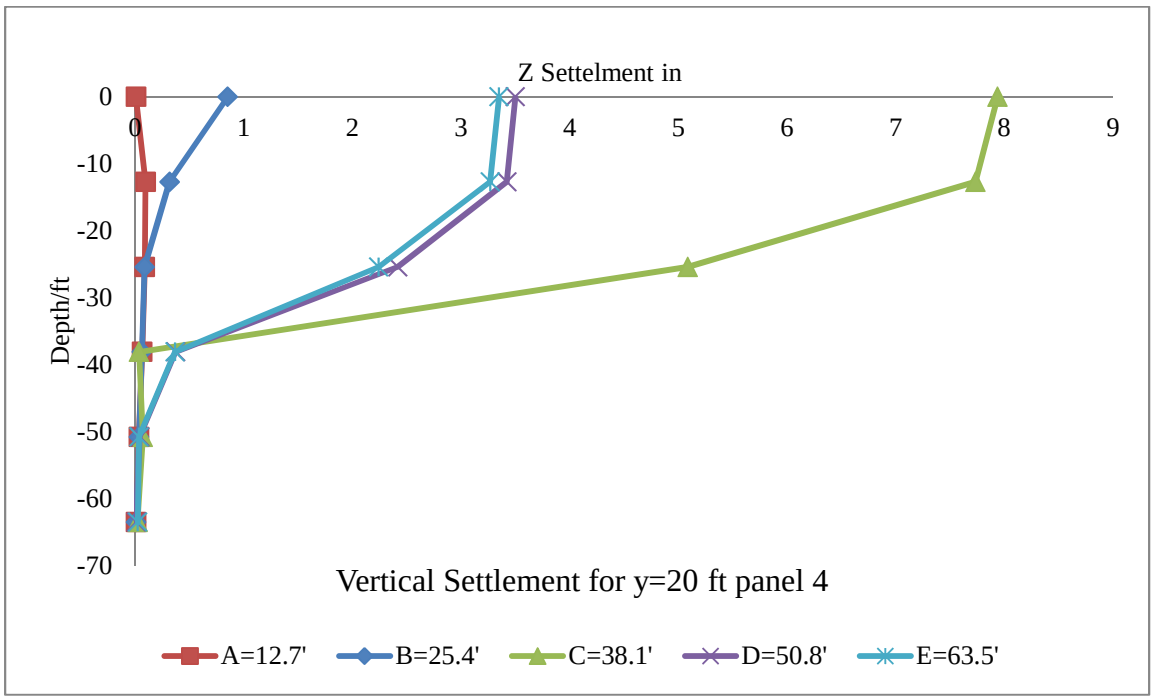

Figure B 24 Vertical Settlement for Panel 4

Panel (5) (Y=25 ft)

Table B 5 All Numerical Results for Panel 5

Excavation A (Z=12.7 ft)

depth Z (ft)	σ_{xx} (slugsf)	σ_{xx} (ksf)	xx strain
0	0.0	0.0	5.34E-04
-12.7	2013.9	64.8	4.68E-03
-25.4	3479.4	112.0	3.07E-03
-38.1	4605.6	148.3	3.05E-03
-50.8	6003.3	193.3	3.64E-03
-63.5	7625.7	245.5	3.42E-03

depth Z (ft)	yy strain	τ_{xy} (slugsf)	τ_{xy} (ksf)
0	1.44E-03	133.269	4.2912618
-12.7	8.49E-04	419.547	13.5094134
-25.4	5.90E-05	499.835	16.094687
-38.1	8.68E-05	761.534	24.5213948
-50.8	9.85E-05	1028.18	33.107396
-63.5	9.31E-05	905.346	29.1521412

depth Z (ft)	x disp (ft)	x disp (in)	Z settlement (ft)	Z settlement (in)
0	3.81E-02	4.57E-01	0.00073	0.00876
-12.7	2.03E-02	2.43E-01	0.006936	0.083232
-25.4	1.24E-02	1.49E-01	0.007307	0.087684
-38.1	1.48E-02	1.77E-01	0.00526	0.06312
-50.8	1.71E-02	2.05E-01	0.002867	0.034404
-63.5	1.87E-02	2.25E-01	0.0006392	0.0076704

Excavation B (Z=25.4 ft)

depth Z (ft)	σ_{xx} (slugsf)	σ_{xx} (ksf)	xx strain
0	0.0	0.0	4.09E-03
-12.7	1268.0	40.8	1.62E-01
-25.4	3640.6	117.2	9.48E-02
-38.1	4617.6	148.7	3.18E-03
-50.8	5887.8	189.6	3.69E-03
-63.5	7637.9	245.9	3.39E-03

depth Z (ft)	yy strain	τ_{xy} (slugsf)	τ_{xy} (ksf)
0	3.59E-03	126.866	4.0850852
-12.7	2.63E-02	343.569	11.0629218
-25.4	4.87E-03	582.712	18.7633264
-38.1	1.89E-04	803.042	25.8579524
-50.8	1.08E-04	1015.4	32.69588
-63.5	1.65E-04	909.102	29.2730844

depth Z (ft)	x disp (ft)	x disp (in)	Z settlement (ft)	Z settlement (in)
0	6.68E-01	8.02E+00	0.3383	4.0596
-12.7	5.50E-01	6.59E+00	0.3157	3.7884
-25.4	1.14E-02	1.37E-01	0.00743	0.08916
-38.1	1.40E-02	1.68E-01	0.005598	0.067176
-50.8	1.65E-02	1.98E-01	0.003149	0.037788
-63.5	1.83E-02	2.19E-01	0.0007346	0.0088152

Excavation C (Z=38.1 ft)

depth Z (ft)	σ_{xx} (slugsf)	σ_{xx} (ksf)	xx strain
0	0.0	0.0	2.13E-02
-12.7	1309.1	42.2	3.84E-02
-25.4	2512.2	80.9	4.00E-01
-38.1	4646.0	149.6	1.09E-01
-50.8	5934.6	191.1	5.18E-03
-63.5	7638.8	246.0	4.20E-03

depth Z (ft)	yy strain	τ_{xy} (slugsf)	τ_{xy} (ksf)
0	2.08E-02	163.208	5.2552976
-12.7	2.43E-02	337.312	10.8614464
-25.4	3.96E-02	526.318	16.9474396
-38.1	5.13E-03	844.376	27.1889072
-50.8	2.34E-04	869.866	28.0096852
-63.5	6.00E-04	800.284	25.7691448

depth Z (ft)	x disp (ft)	x disp (in)	Z settlement (ft)	Z settlement (in)
0	1.17E+00	1.40E+01	0.7019	8.4228
-12.7	1.07E+00	1.28E+01	0.6959	8.3508
-25.4	7.54E-01	9.05E+00	0.54357	6.52284
-38.1	3.55E-02	4.26E-01	0.0097	0.1164

-50.8	1.59E-02	1.91E-01	0.006159	0.073908
-63.5	1.80E-02	2.16E-01	0.0019927	0.0239124

Excavation D (Z=50.8 ft)

depth Z (ft)	σ_{xx} (slugsf)	σ_{xx} (ksf)	xx strain
0	0.0	0.0	2.10E-02
-12.7	1323.7	42.6	3.24E-02
-25.4	2545.1	82.0	2.63E-01
-38.1	3794.9	122.2	1.89E-01
-50.8	6529.6	210.3	3.42E-03
-63.5	7736.4	249.1	4.02E-03

depth Z (ft)	yy strain	τ_{xy} (slugsf)	τ_{xy} (ksf)
0	2.07E-02	159.488	5.1355136
-12.7	1.63E-02	332.427	10.7041494
-25.4	2.95E-02	530.058	17.0678676
-38.1	6.92E-03	990.541	31.8954202
-50.8	1.20E-03	1060.66	34.153252
-63.5	1.04E-04	916.73	29.518706

depth Z (ft)	x disp (ft)	x disp (in)	Z settlement (ft)	Z settlement (in)
0	9.16E-01	1.10E+01	0.5538	6.6456
-12.7	8.45E-01	1.01E+01	0.5499	6.5988
-25.4	6.14E-01	7.36E+00	0.4239	5.0868
-38.1	1.20E-01	1.44E+00	0.0762	0.9144
-50.8	1.72E-02	2.07E-01	0.0039325	0.04719
-63.5	1.87E-02	2.24E-01	0.00107	0.01284

Excavation E (Z=63.5 ft)

depth Z (ft)	σ_{xx} (slugsf)	σ_{xx} (ksf)	xx strain
0	0.0	0.0	1.95E-02
-12.7	1317.1	42.4	2.65E-02
-25.4	2518.8	81.1	2.67E-01
-38.1	3751.5	120.8	1.66E-01
-50.8	5105.1	164.4	4.66E-03
-63.5	8317.2	267.8	4.00E-03

depth Z (ft)	yy strain	τ_{xy} (slugsf)	τ_{xy} (ksf)
0	2.15E-02	166.946	5.3756612
-12.7	1.73E-02	334.14	10.759308
-25.4	2.66E-02	529.461	17.0486442
-38.1	6.68E-03	980.743	31.5799246
-50.8	4.76E-03	1276.71	41.110062
-63.5	9.83E-04	939.761	30.2603042

depth Z (ft)	x disp (ft)	x disp (in)	Z settlement (ft)	Z settlement (in)
0	9.10E-01	1.09E+01	0.55033	6.60396
-12.7	8.37E-01	1.00E+01	0.5464	6.5568
-25.4	6.16E-01	7.39E+00	0.4163	4.9956
-38.1	1.22E-01	1.47E+00	0.08785	1.0542
-50.8	3.56E-02	4.27E-01	0.006428	0.077136
-63.5	2.27E-02	2.72E-01	0.001999	0.023988

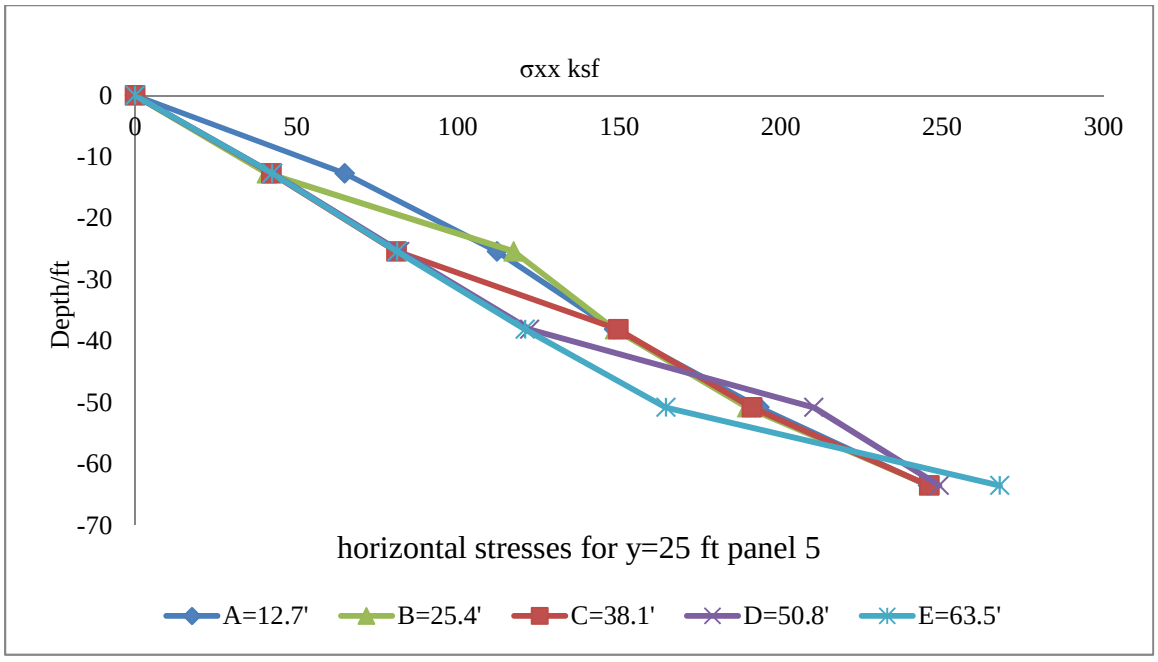

Figure B 25 Horizontal Stresses for Panel 5

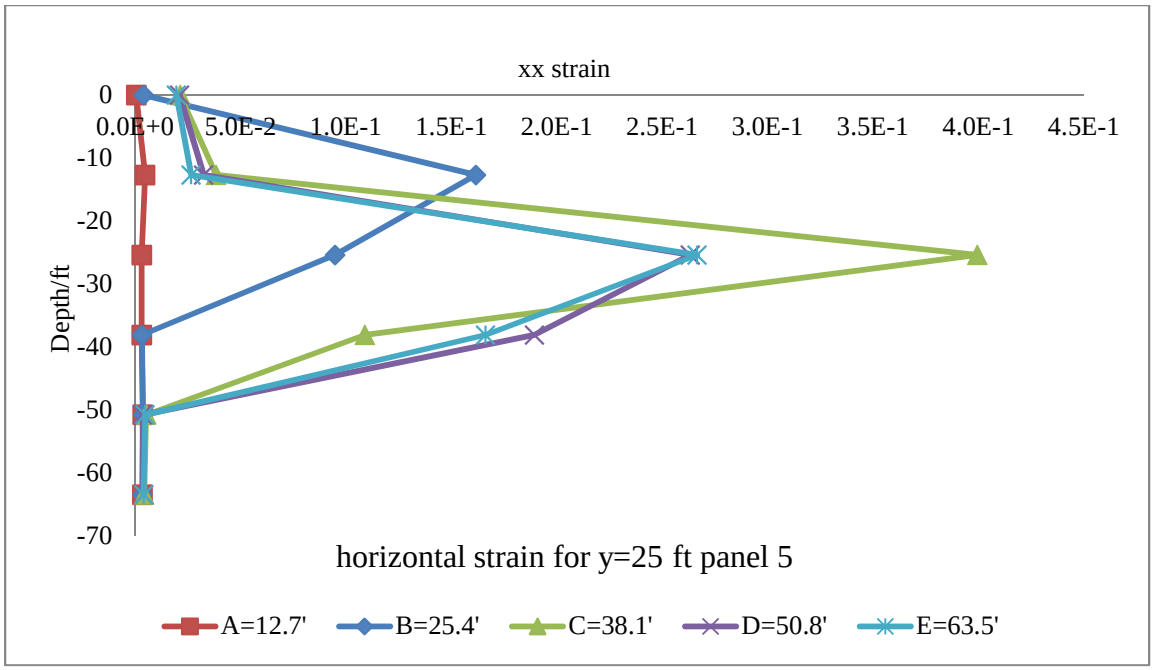

Figure B 26 Horizontal Strain in XX Direction for Panel 5

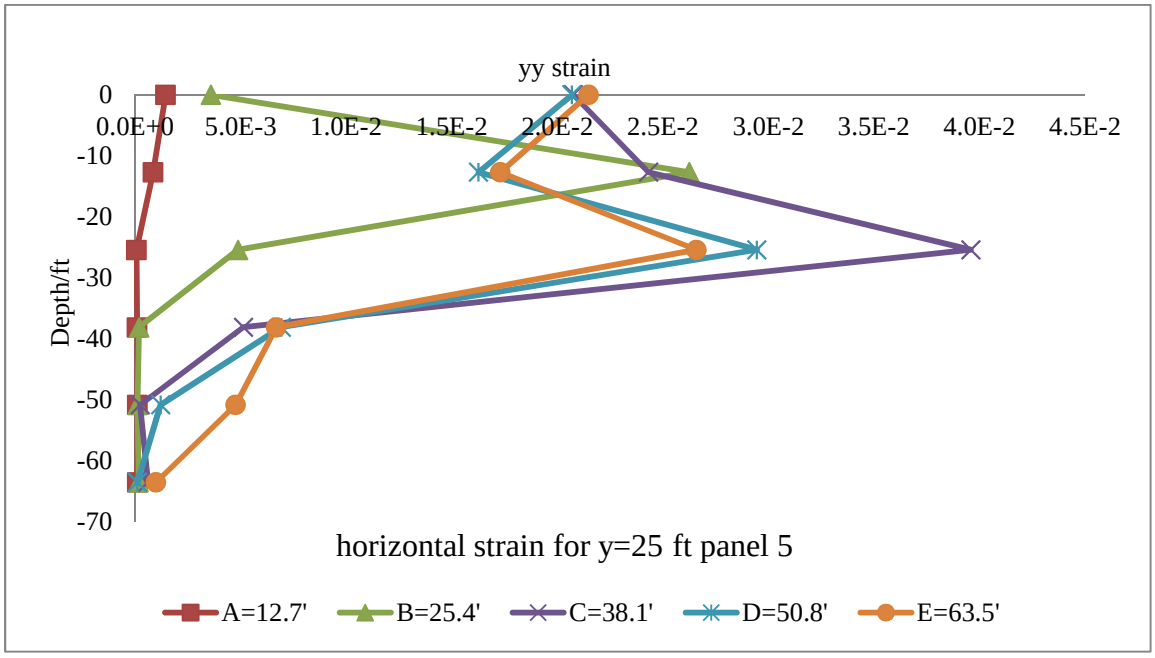

Figure B 27 Horizontal Strain in YY Direction for Panel 5

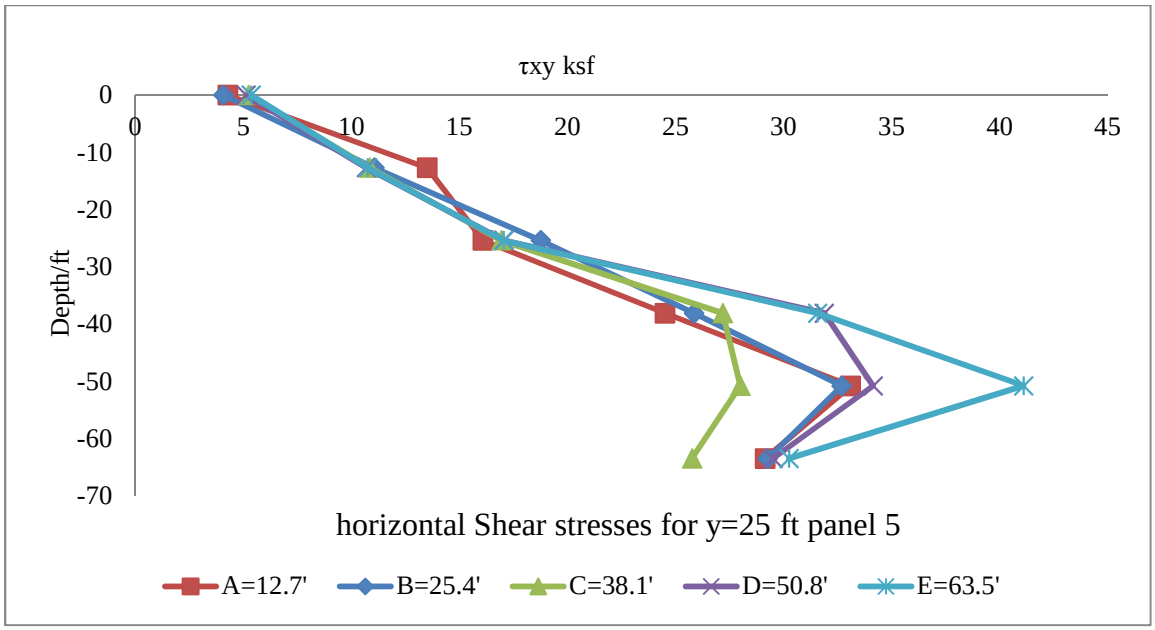

Figure B 28 Horizontal Shear Stresses for Panel 5

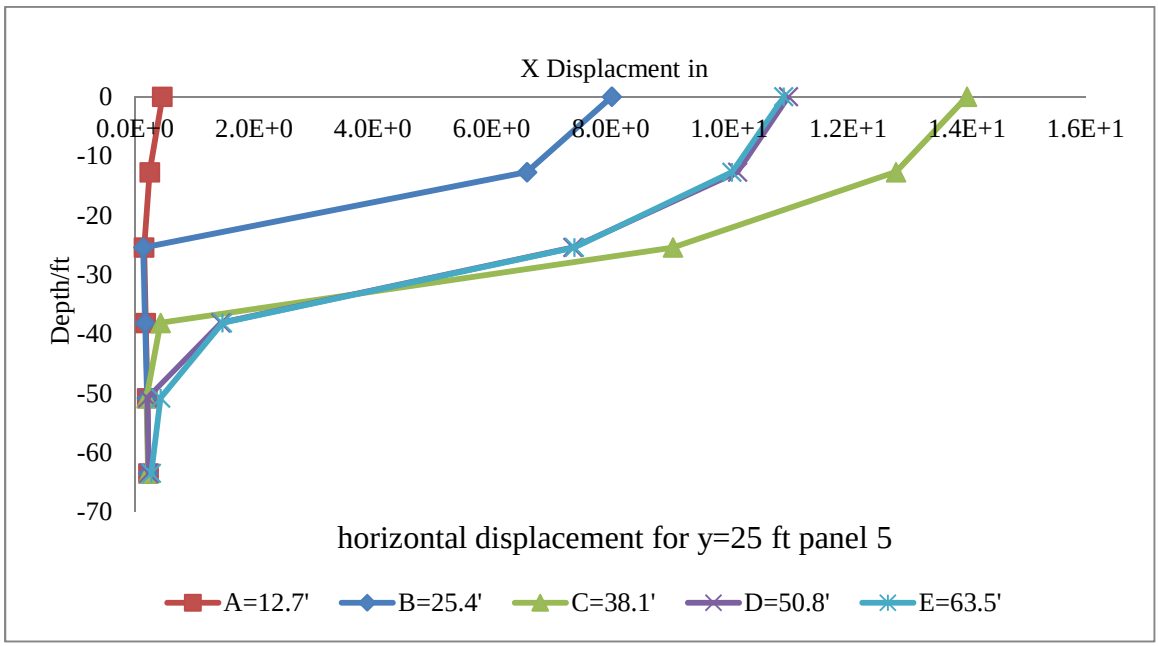

Figure B 29 Horizontal Displacement for Panel 5

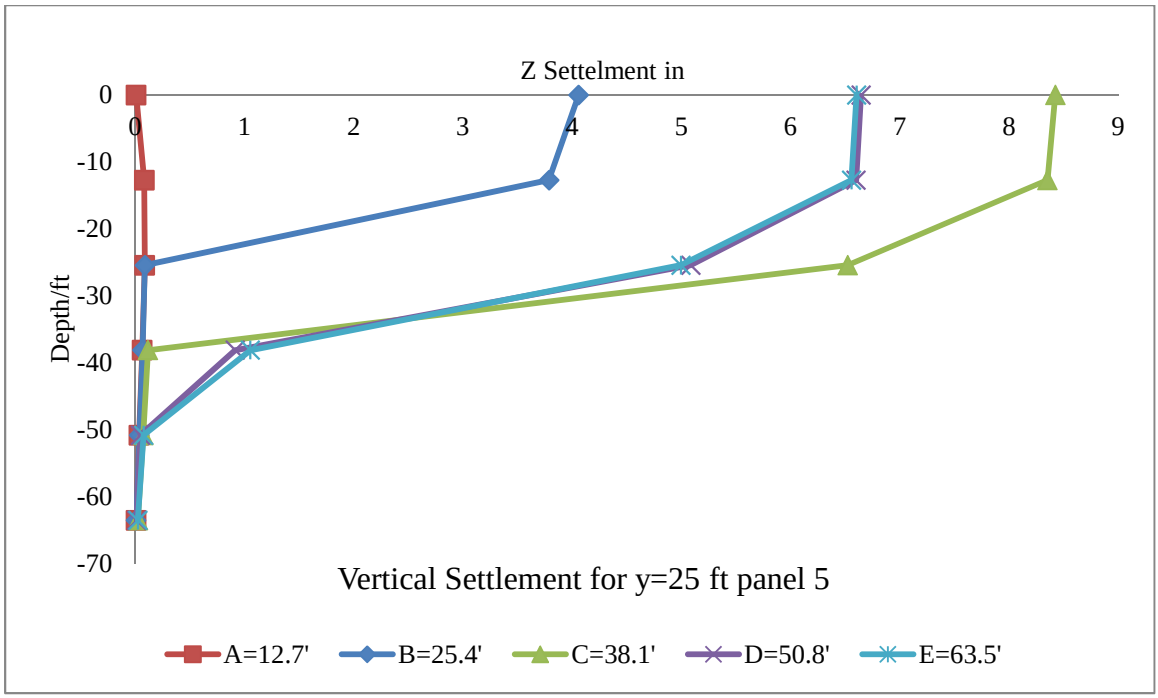

Figure B 30 Vertical Settlement for Panel 5

Panel (6) (Y=30 ft)

Table B 6 All Numerical Results for Panel 6

Excavation A (Z=12.7 ft)

depth Z (ft)	σ_{xx} (slugsf)	σ_{xx} (ksf)	xx strain
0	0.0	0.0	7.07E-04
-12.7	2027.0	65.3	6.00E-03
-25.4	3494.8	112.5	3.06E-03
-38.1	4584.9	147.6	3.03E-03
-50.8	5889.5	189.6	3.66E-03
-63.5	7610.8	245.1	3.39E-03

depth Z (ft)	yy strain	τ_{xy} (slugsf)	τ_{xy} (ksf)
0	1.54E-03	129.296	4.1633312
-12.7	7.92E-04	429.181	13.8196282
-25.4	9.43E-05	503.56	16.214632
-38.1	6.21E-05	756.544	24.3607168

-50.8	9.81E-05	1022.21	32.915162
-63.5	1.02E-04	929.62	29.933764

depth Z (ft)	x disp (ft)	x disp (in)	Z settlement (ft)	Z settlement (in)
0	4.68E-02	5.61E-01	0.00304	0.03648
-12.7	2.09E-02	2.50E-01	0.0069	0.0828
-25.4	1.27E-02	1.52E-01	0.007277	0.087324
-38.1	1.49E-02	1.79E-01	0.0054116	0.0649392
-50.8	1.73E-02	2.08E-01	0.002846	0.034152
-63.5	1.86E-02	2.23E-01	0.00063133	0.00757605

Excavation B (Z=25.4 ft)

depth Z (ft)	σ_{xx} (slugsf)	σ_{xx} (ksf)	xx strain
0	0.0	0.0	1.35E-03
-12.7	1314.3	42.3	1.98E-01
-25.4	3705.7	119.3	1.54E-01
-38.1	4599.0	148.1	3.11E-03
-50.8	5883.9	189.5	3.62E-03
-63.5	7624.8	245.5	3.39E-03

depth Z (ft)	yy strain	τ_{xy} (slugsf)	τ_{xy} (ksf)
0	1.04E-02	144.034	4.6378948
-12.7	1.86E-02	325.622	10.4850284
-25.4	2.42E-03	598.053	19.2573066
-38.1	3.16E-04	797.579	25.6820438
-50.8	6.20E-05	1030.56	33.184032
-63.5	1.57E-04	930.995	29.978039

depth Z (ft)	x disp (ft)	x disp (in)	Z settlement (ft)	Z settlement (in)
0	8.96E-01	1.07E+01	0.4315	5.178
-12.7	8.01E-01	9.62E+00	0.41725	5.007
-25.4	1.14E-02	1.37E-01	0.007017	0.084204
-38.1	1.37E-02	1.65E-01	0.005506	0.066072
-50.8	1.62E-02	1.95E-01	0.00315447	0.03785364
-63.5	1.79E-02	2.15E-01	0.0007996	0.0095952

Excavation C (Z=38.1 ft)

depth Z (ft)	σ_{xx} (slugsf)	σ_{xx} (ksf)	xx strain
0	0.0	0.0	3.46E-03
-12.7	1279.2	41.2	9.91E-03
-25.4	2507.4	80.7	2.40E-01
-38.1	4621.8	148.8	8.80E-02
-50.8	5793.8	186.6	4.60E-03
-63.5	7443.9	239.7	3.95E-03

depth Z (ft)	yy strain	τ_{xy} (slugsf)	τ_{xy} (ksf)
0	2.12E-03	134.84	4.341848
-12.7	1.06E-02	329.378	10.6059716
-25.4	2.47E-02	569.564	18.3399608
-38.1	2.58E-03	918.573	29.5780506
-50.8	9.65E-05	927.74	29.873228
-63.5	5.23E-04	894.368	28.7986496

depth Z (ft)	x disp (ft)	x disp (in)	Z settlement (ft)	Z settlement (in)
0	7.26E-01	8.72E+00	0.42696	5.12352
-12.7	6.99E-01	8.39E+00	0.42458	5.09496
-25.4	5.45E-01	6.54E+00	0.354	4.248
-38.1	1.86E-02	2.23E-01	0.004439	0.053268
-50.8	1.40E-02	1.68E-01	0.005781	0.069372
-63.5	1.58E-02	1.90E-01	0.00204	0.02448

Excavation D (Z=50.8 ft)

depth Z (ft)	σ_{xx} (slugsf)	σ_{xx} (ksf)	xx strain
0	0.0	0.0	4.78E-03
-12.7	1310.4	42.2	1.25E-02
-25.4	2523.6	81.3	1.77E-01
-38.1	3772.7	121.5	1.53E-01
-50.8	6551.9	211.0	3.03E-03
-63.5	7535.0	242.6	3.63E-03

depth Z (ft)	yy strain	τ_{xy} (slugsf)	τ_{xy} (ksf)
0	3.12E-03	150.691	4.8522502
-12.7	8.82E-03	342.041	11.0137202
-25.4	1.91E-02	571.465	18.401173
-38.1	6.94E-03	1084.61	34.924442

-50.8	1.08E-03	1154.47	37.173934
-63.5	5.25E-05	1005.08	32.363576

depth Z (ft)	x disp (ft)	x disp (in)	Z settlement (ft)	Z settlement (in)
0	6.93E-01	8.32E+00	0.414147	4.969764
-12.7	6.67E-01	8.01E+00	0.41283	4.95396
-25.4	5.18E-01	6.21E+00	0.35628	4.27536
-38.1	1.15E-01	1.38E+00	0.07991	0.95892
-50.8	1.50E-02	1.80E-01	0.003129	0.037548
-63.5	1.65E-02	1.98E-01	0.001101	0.013212

Excavation E (Z=63.5 ft)

depth Z (ft)	σ_{xx} (slugsf)	σ_{xx} (ksf)	xx strain
0	0.0	0.0	5.53E-03
-12.7	1318.1	42.4	1.13E-02
-25.4	2550.3	82.1	2.17E-01
-38.1	3737.4	120.3	1.62E-01
-50.8	5097.6	164.1	9.67E-03
-63.5	8062.5	259.6	4.19E-03

depth Z (ft)	yy strain	τ_{xy} (slugsf)	τ_{xy} (ksf)
0	3.88E-03	165.544	5.3305168
-12.7	9.68E-03	336.043	10.8205846
-25.4	2.40E-02	565.855	18.220531
-38.1	7.68E-03	1087.77	35.026194
-50.8	4.67E-03	1422	45.7884
-63.5	1.01E-03	1048.39	33.758158

depth Z (ft)	x disp (ft)	x disp (in)	Z settlement (ft)	Z settlement (in)
0	8.00E-01	9.60E+00	0.48126	5.77512
-12.7	7.71E-01	9.26E+00	0.4812	5.7744
-25.4	6.08E-01	7.29E+00	0.40859	4.90308
-38.1	1.47E-01	1.77E+00	0.0920217	1.1042604
-50.8	3.52E-02	4.22E-01	0.008007	0.096084
-63.5	2.13E-02	2.56E-01	0.0015174	0.0182088

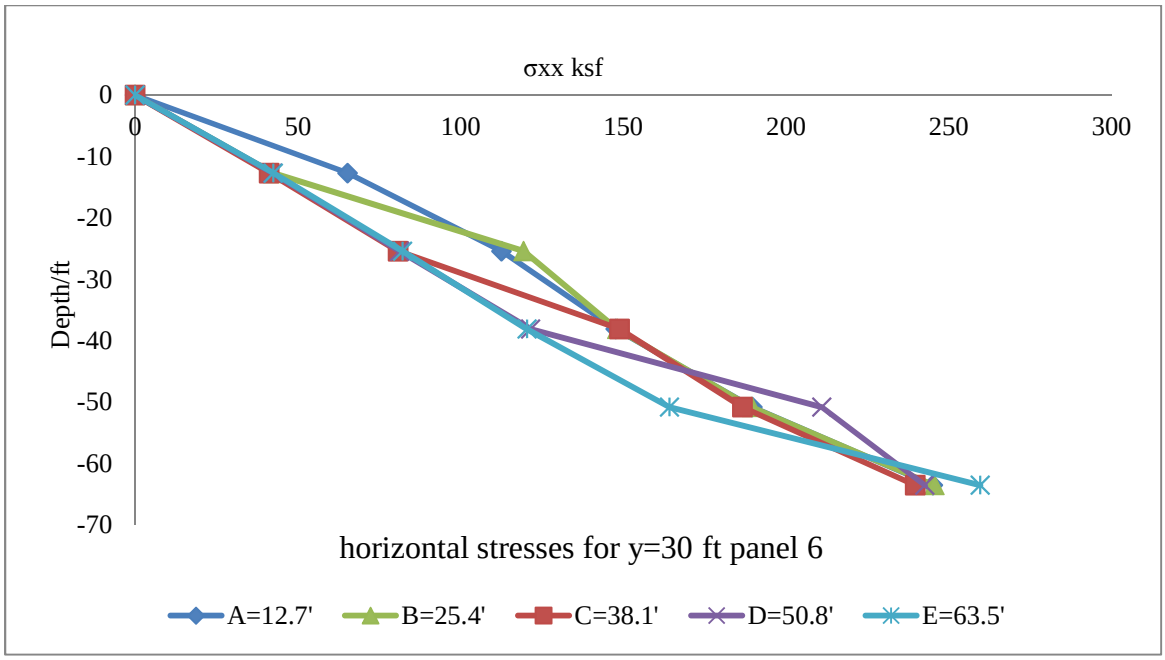

Figure B 31 Horizontal Stresses for Panel 6

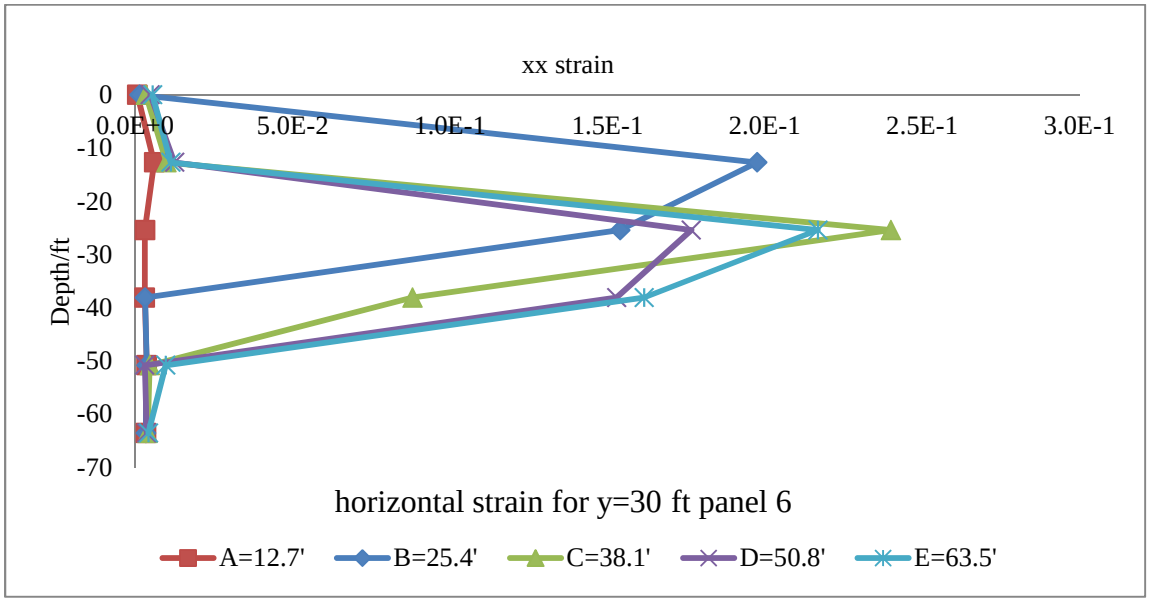

Figure B 32 Horizontal Strain in XX Direction for Panel 6

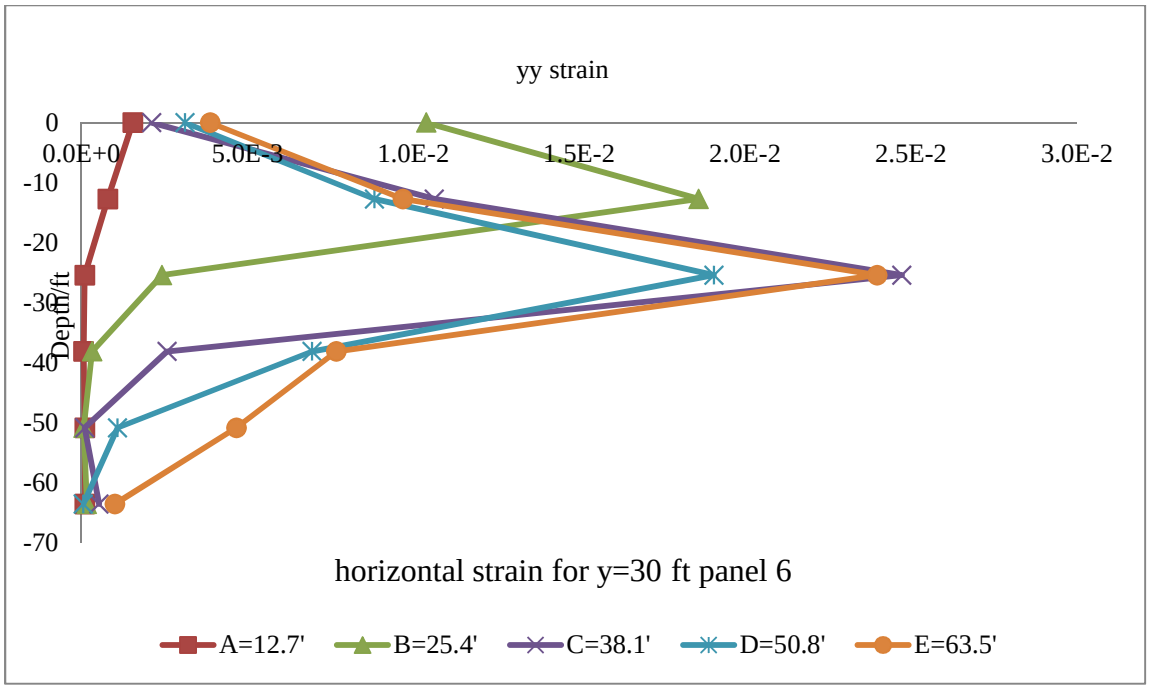

Figure B 33 Horizontal Strain in YY Direction for Panel 6

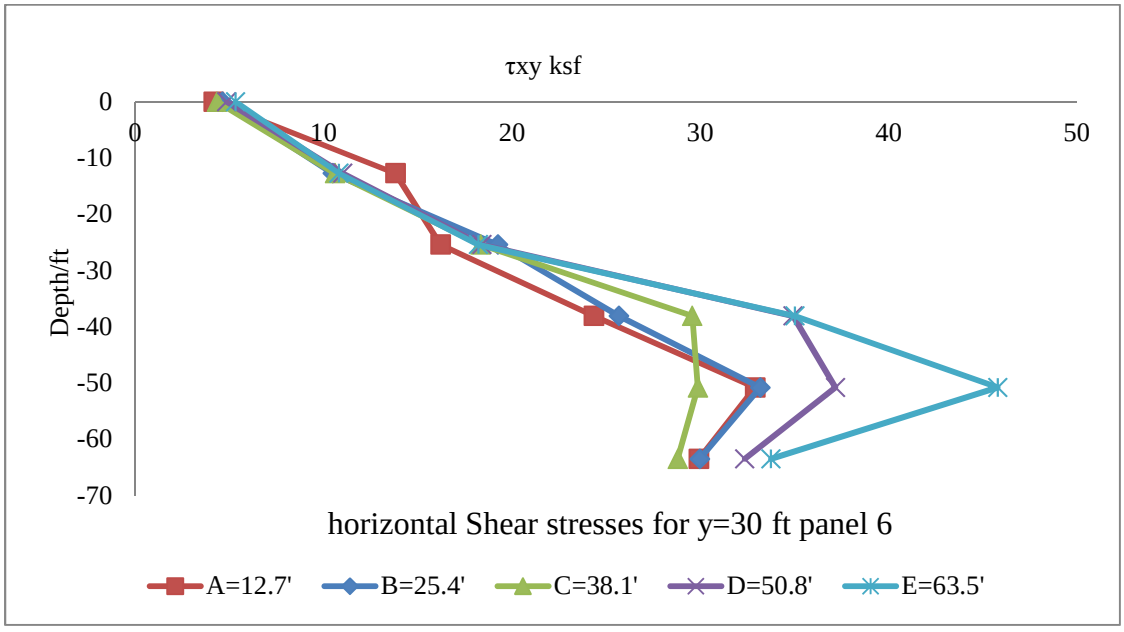

Figure B 34 Horizontal Shear Stresses for Panel 6

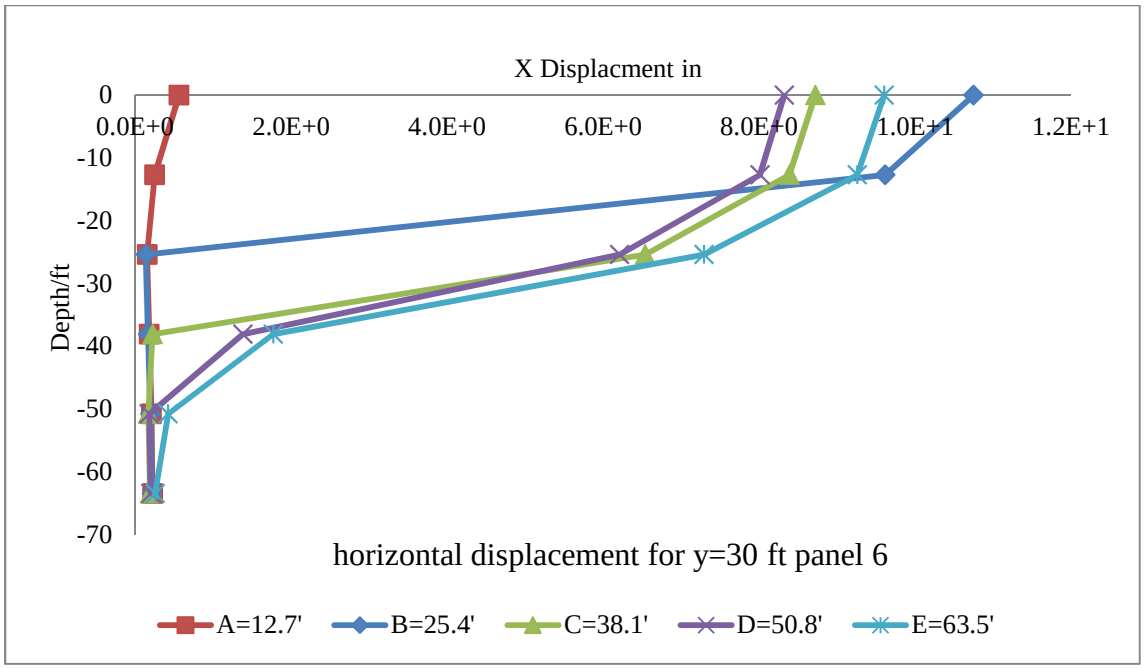

Figure B 35 Horizontal Displacement for Panel 6

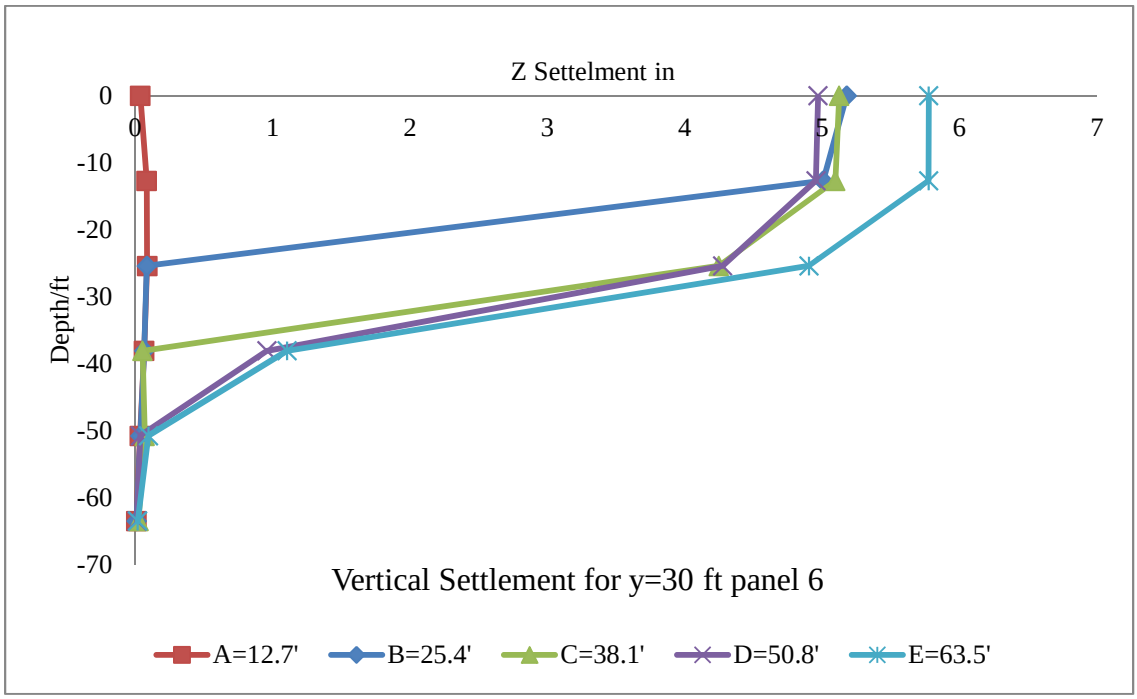

Figure B 36 Vertical Settlement for Panel 6

Panel (7) (Y=35 ft)

Table B 7 All Numerical Results for Panel 7

Excavation A (Z=12.7 ft)

depth Z (ft)	σ_{xx} (slugsf)	σ_{xx} (ksf)	xx strain
0	0.0	0.0	8.55E-04
-12.7	2037.6	65.6	8.82E-03
-25.4	3514.8	113.2	3.08E-03
-38.1	4603.1	148.2	3.04E-03
-50.8	5888.1	189.6	3.67E-03
-63.5	7610.6	245.1	3.43E-03

depth Z (ft)	yy strain	τ_{xy} (slugsf)	τ_{xy} (ksf)
0	1.51E-03	124.405	4.005841
-12.7	7.49E-04	428.137	13.7860114
-25.4	8.72E-05	512.402	16.4993444
-38.1	4.89E-05	788.936	25.4037392
-50.8	9.27E-05	1029.16	33.138952
-63.5	1.03E-04	916.37	29.507114

depth Z (ft)	x disp (ft)	x disp (in)	Z settlement (ft)	Z settlement (in)
0	5.95E-02	7.14E-01	0.00619	0.07428
-12.7	2.80E-02	3.36E-01	0.005253	0.063036
-25.4	1.27E-02	1.53E-01	0.007348	0.088176
-38.1	1.49E-02	1.79E-01	0.005368	0.064416
-50.8	1.72E-02	2.06E-01	0.0029165	0.034998
-63.5	1.87E-02	2.25E-01	0.0006783	0.0081396

Excavation B (Z=25.4 ft)

depth Z (ft)	σ_{xx} (slugsf)	σ_{xx} (ksf)	xx strain
0	0.0	0.0	3.65E-03
-12.7	1340.2	43.2	1.02E-01
-25.4	3767.5	121.3	8.93E-02
-38.1	4596.6	148.0	2.90E-03
-50.8	5809.8	187.1	3.39E-03
-63.5	7569.9	243.8	3.32E-03

depth Z (ft)	yy strain	τ_{xy} (slugsf)	τ_{xy} (ksf)
0	8.06E-03	144.034	4.6378948
-12.7	1.06E-02	331.31	10.668182
-25.4	1.74E-03	606.734	19.5368348
-38.1	2.31E-04	803.246	25.8645212
-50.8	4.42E-05	1031.01	33.198522
-63.5	1.44E-04	962.085	30.979137

depth Z (ft)	x disp (ft)	x disp (in)	Z settlement (ft)	Z settlement (in)
0	5.55E-01	6.66E+00	0.247782	2.973384
-12.7	5.19E-01	6.23E+00	0.24582	2.94984
-25.4	1.10E-02	1.32E-01	0.00674627	0.08095524
-38.1	1.32E-02	1.59E-01	0.00510299	0.06123588
-50.8	1.58E-02	1.89E-01	0.00294899	0.03538788
-63.5	1.73E-02	2.07E-01	0.00083119	0.00997428

Excavation C (Z=38.1 ft)

depth Z (ft)	σ_{xx} (slugsf)	σ_{xx} (ksf)	xx strain
0	0.0	0.0	3.44E-04
-12.7	1325.6	42.7	6.49E-03
-25.4	2484.1	80.0	2.77E-01
-38.1	4733.3	152.4	1.09E-01
-50.8	5698.6	183.5	4.03E-03
-63.5	7356.0	236.9	3.64E-03

depth Z (ft)	yy strain	τ_{xy} (slugsf)	τ_{xy} (ksf)
0	2.02E-03	152.185	4.900357
-12.7	1.06E-02	323.524	10.4174728
-25.4	2.63E-02	593.647	19.1154334
-38.1	2.86E-03	938.456	30.2182832
-50.8	7.25E-05	970.222	31.2411484
-63.5	4.61E-04	961.867	30.9721174

depth Z (ft)	x disp (ft)	x disp (in)	Z settlement (ft)	Z settlement (in)
0	8.53E-01	1.02E+01	0.496	5.952
-12.7	8.24E-01	9.89E+00	0.4949	5.9388
-25.4	6.68E-01	8.01E+00	0.42186	5.06232
-38.1	3.68E-02	4.42E-01	0.00253925	0.030471

-50.8	1.25E-02	1.50E-01	0.0053233	0.0638796
-63.5	1.41E-02	1.69E-01	0.00199035	0.0238842

Excavation D (Z=50.8 ft)

depth Z (ft)	σ_{xx} (slugsf)	σ_{xx} (ksf)	xx strain
0	0.0	0.0	1.52E-03
-12.7	1367.7	44.0	5.34E-03
-25.4	2538.2	81.7	2.24E-01
-38.1	3769.4	121.4	2.16E-01
-50.8	6298.7	202.8	5.18E-04
-63.5	7327.8	236.0	3.07E-03

depth Z (ft)	yy strain	τ_{xy} (slugsf)	τ_{xy} (ksf)
0	3.92E-04	120.775	3.888955
-12.7	9.60E-03	315.322	10.1533684
-25.4	2.13E-02	609.926	19.6396172
-38.1	6.52E-03	1189	38.2858
-50.8	7.97E-04	1218.82	39.246004
-63.5	1.11E-04	1089.27	35.074494

depth Z (ft)	x disp (ft)	x disp (in)	Z settlement (ft)	Z settlement (in)
0	8.64E-01	1.04E+01	0.513245	6.15894
-12.7	8.37E-01	1.00E+01	0.513536	6.162432
-25.4	6.64E-01	7.97E+00	0.455628	5.467536
-38.1	1.37E-01	1.64E+00	0.102916	1.234992
-50.8	1.36E-02	1.64E-01	0.0023127	0.0277524
-63.5	1.44E-02	1.72E-01	0.00092665	0.0111198

Excavation E (Z=63.5 ft)

depth Z (ft)	σ_{xx} (slugsf)	σ_{xx} (ksf)	xx strain
0	0.0	0.0	2.00E-03
-12.7	1281.4	41.3	5.27E-03
-25.4	2531.3	81.5	2.60E-01
-38.1	3759.8	121.1	2.44E-01
-50.8	5049.1	162.6	1.70E-02
-63.5	8267.5	266.2	3.75E-03

depth Z (ft)	yy strain	τ_{xy} (slugsf)	τ_{xy} (ksf)
0	4.41E-04	123.116	3.9643352
-12.7	1.05E-02	330.327	10.6365294
-25.4	2.59E-02	591.971	19.0614662
-38.1	7.64E-03	1189.86	38.313492
-50.8	3.10E-03	1528.75	49.22575
-63.5	3.66E-04	1172.27	37.747094

depth Z (ft)	x disp (ft)	x disp (in)	Z settlement (ft)	Z settlement (in)
0	1.02E+00	1.22E+01	0.61	7.32
-12.7	9.90E-01	1.19E+01	0.6081	7.2972
-25.4	8.11E-01	9.73E+00	0.53636	6.43632
-38.1	2.03E-01	2.44E+00	0.12534	1.50408
-50.8	3.43E-02	4.12E-01	0.0106	0.1272
-63.5	1.86E-02	2.23E-01	0.001291	0.015492

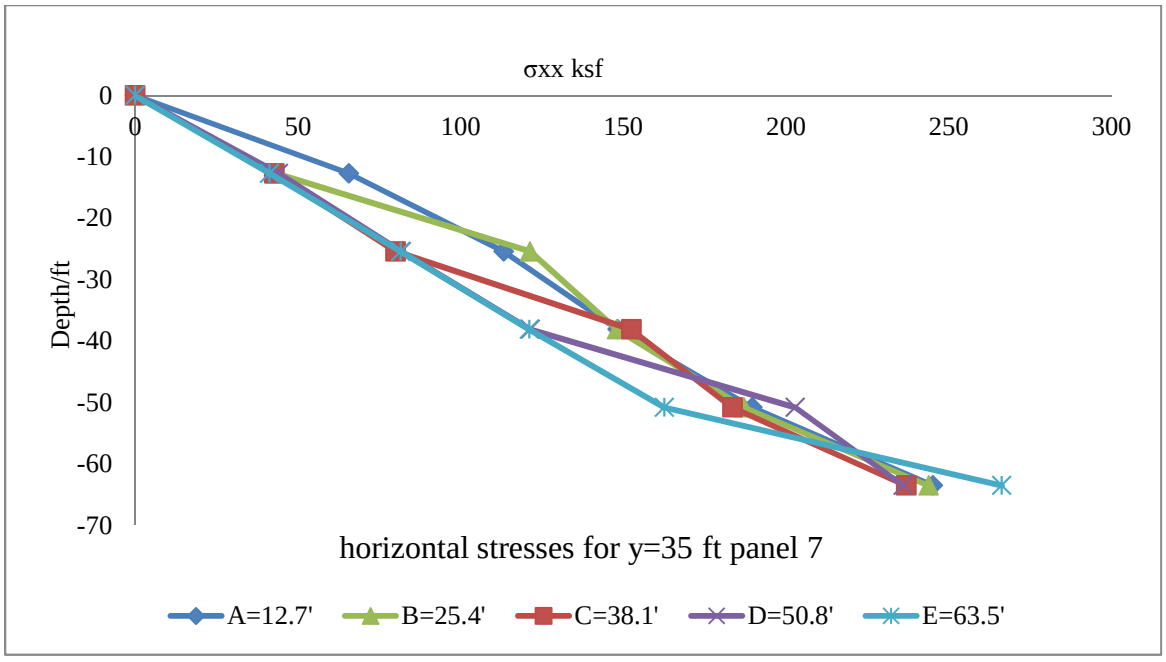

Figure B 37 Horizontal Stresses for Panel 7

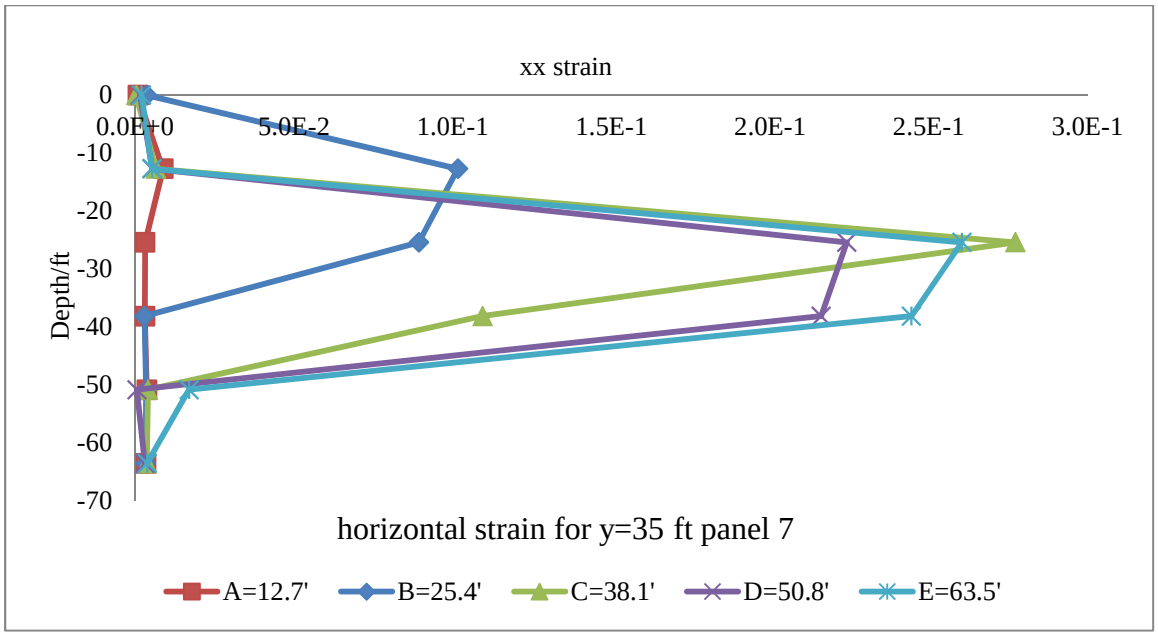

Figure B 38 Horizontal Strain in XX Direction for Panel 7

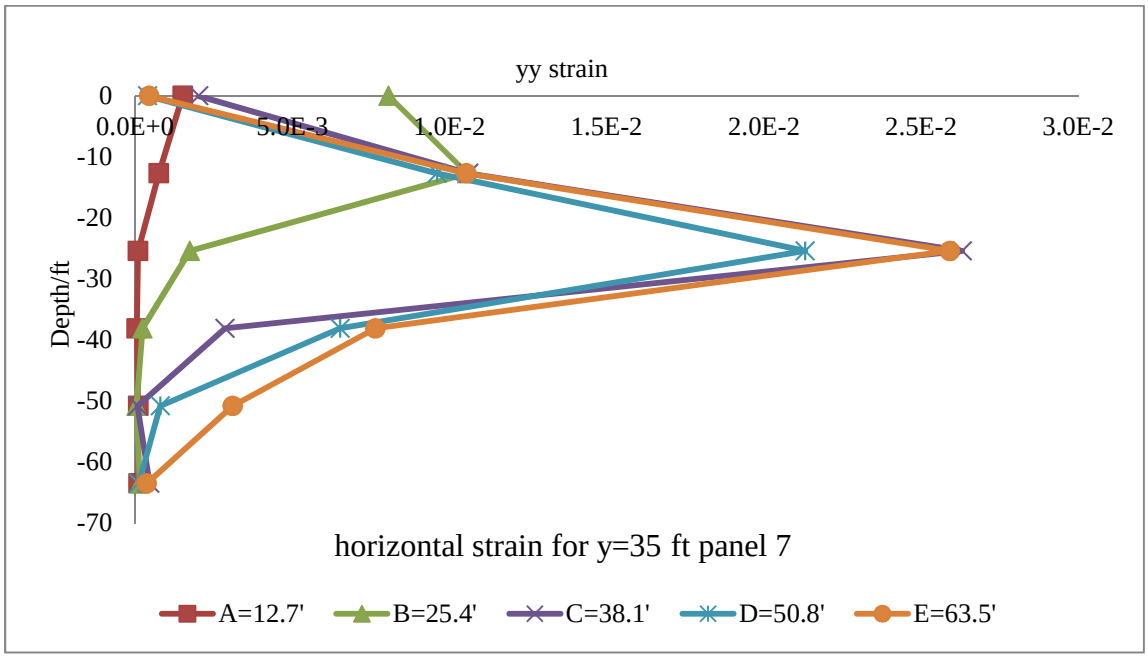

Figure B 39 Horizontal Strain in YY Direction for Panel 7

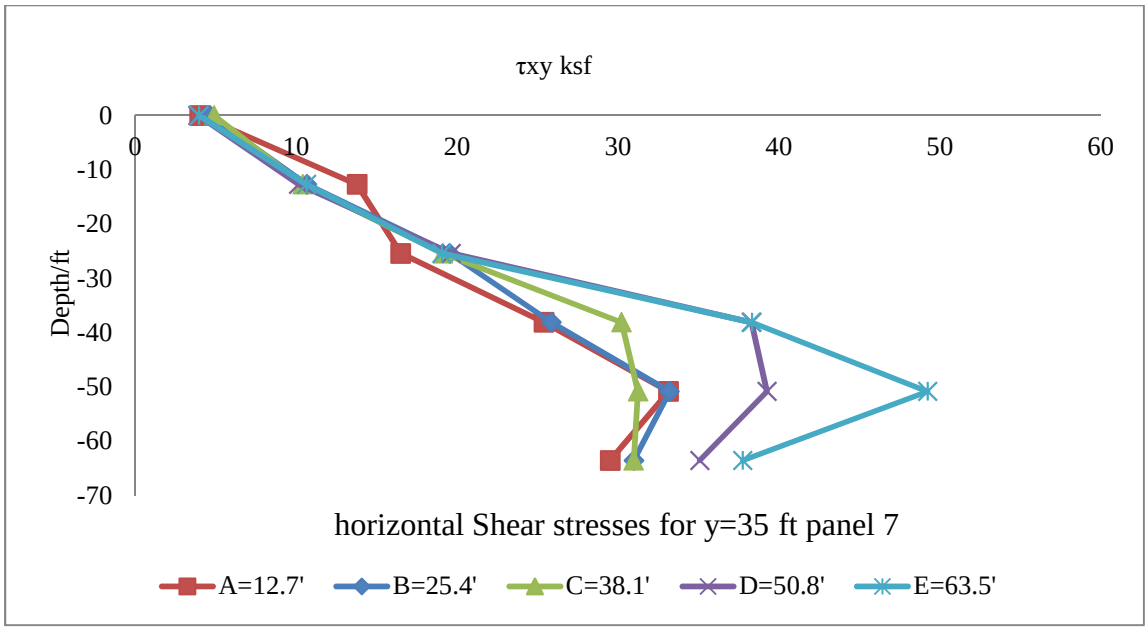

Figure B 40 Horizontal Shear Stresses for Panel 7

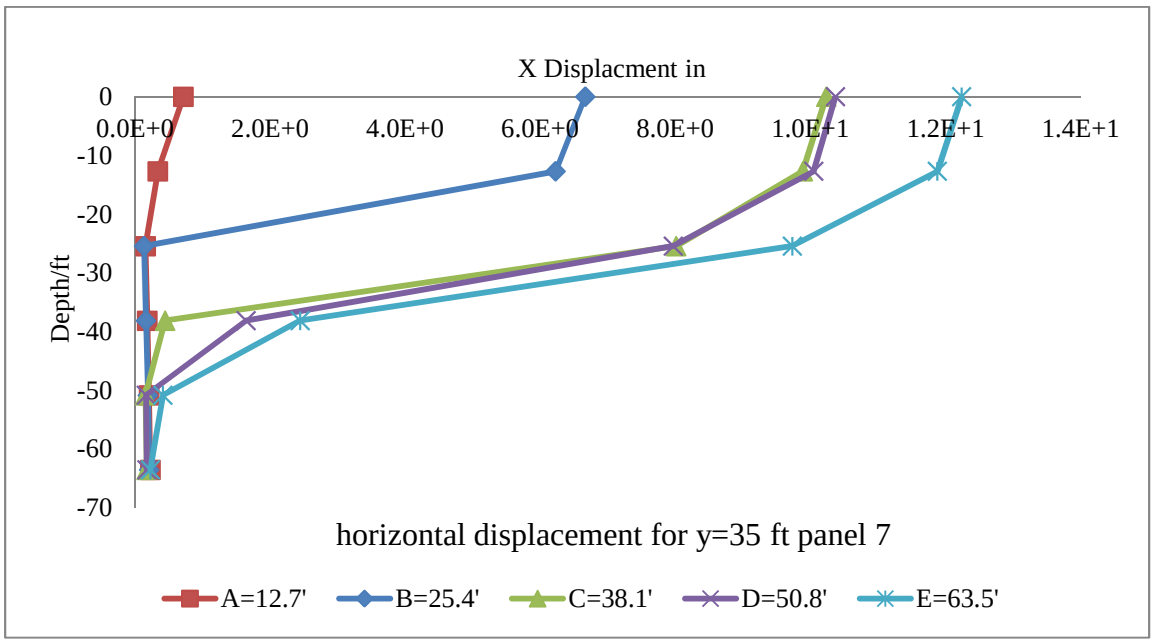

Figure B 41 Horizontal Displacement for Panel 7

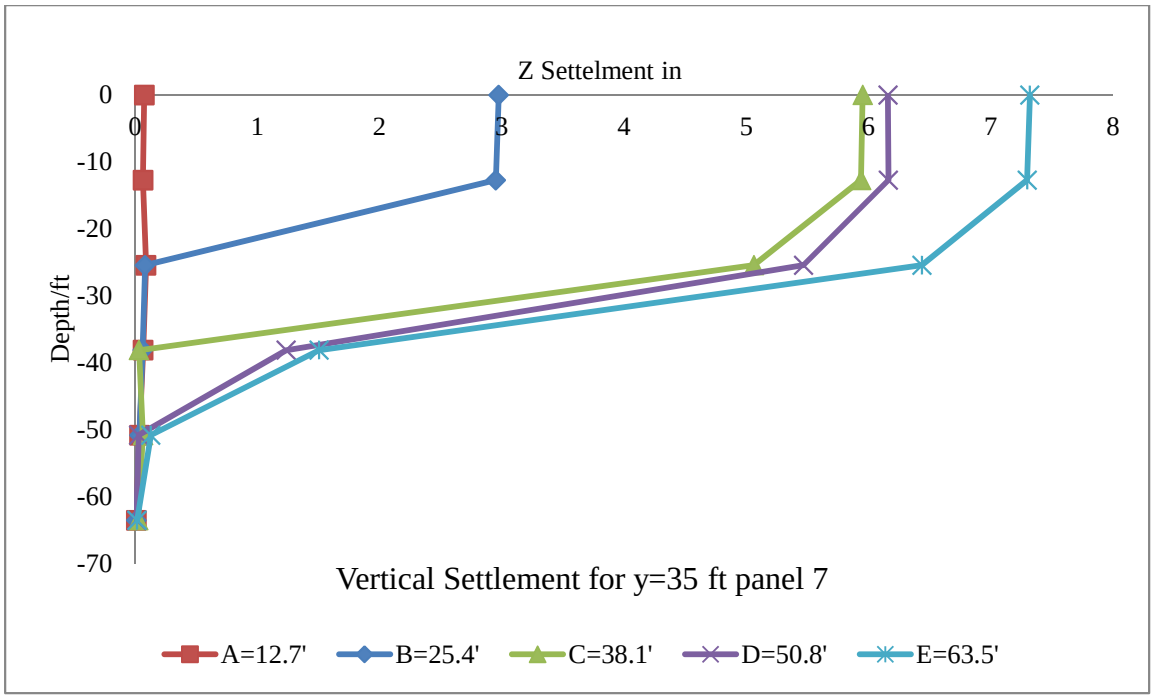

Figure B 42 Vertical Settlement for Panel 7

Panel (8) (Y=40 ft)

Table B 8 All Numerical Results for Panel 8

Excavation A (Z=12.7 ft)

depth Z (ft)	σ_{xx} (slugsf)	σ_{xx} (ksf)	xx strain
0	0.0	0.0	1.65E-03
-12.7	2120.7	68.3	9.14E-03
-25.4	3547.6	114.2	3.05E-03
-38.1	4604.2	148.3	3.06E-03
-50.8	5854.8	188.5	3.67E-03
-63.5	7609.1	245.0	3.45E-03

depth Z (ft)	yy strain	τ_{xy} (slugsf)	τ_{xy} (ksf)
0	1.78E-03	121.006	3.8963932
-12.7	8.11E-04	424.936	13.6829392
-25.4	1.39E-04	522.861	16.8361242
-38.1	1.33E-05	789.386	25.4182292

-50.8	8.41E-05	1029.08	33.136376
-63.5	1.03E-04	912.464	29.3813408

depth Z (ft)	x disp (ft)	x disp (in)	Z settlement (ft)	Z settlement (in)
0	7.47E-02	8.96E-01	0.01057	0.12684
-12.7	2.86E-02	3.44E-01	0.004199	0.050388
-25.4	1.28E-02	1.54E-01	0.007395	0.08874
-38.1	1.51E-02	1.81E-01	0.005375	0.0645
-50.8	1.72E-02	2.07E-01	0.0029237	0.0350844
-63.5	1.88E-02	2.25E-01	0.00066596	0.00799152

Excavation B (Z=25.4 ft)

depth Z (ft)	σ_{xx} (slugsf)	σ_{xx} (ksf)	xx strain
0	0.0	0.0	6.79E-03
-12.7	1275.4	41.1	1.55E-01
-25.4	3721.9	119.8	1.20E-01
-38.1	4599.9	148.1	2.82E-03
-50.8	5790.0	186.4	3.29E-03
-63.5	7530.7	242.5	3.26E-03

depth Z (ft)	yy strain	τ_{xy} (slugsf)	τ_{xy} (ksf)
0	1.30E-02	146.142	4.7057724
-12.7	1.23E-02	332.874	10.7185428
-25.4	1.91E-03	622.086	20.0311692
-38.1	2.99E-04	831.259	26.7665398
-50.8	2.88E-06	1045.42	33.662524
-63.5	1.32E-04	960.024	30.9127728

depth Z (ft)	x disp (ft)	x disp (in)	Z settlement (ft)	Z settlement (in)
0	7.24E-01	8.68E+00	0.32446	3.89352
-12.7	6.66E-01	7.99E+00	0.32125	3.855
-25.4	2.39E-02	2.86E-01	0.00651	0.07812
-38.1	1.28E-02	1.54E-01	0.005	0.06
-50.8	1.50E-02	1.80E-01	0.002995	0.03594
-63.5	1.68E-02	2.01E-01	0.00086499	0.01037988

Excavation C (Z=38.1 ft)

depth Z (ft)	σ_{xx} (slugsf)	σ_{xx} (ksf)	xx strain
0	0.0	0.0	3.72E-04
-12.7	1267.0	40.8	1.95E-03
-25.4	2526.8	81.4	1.99E-01
-38.1	4746.8	152.8	7.65E-02
-50.8	5757.5	185.4	3.83E-03
-63.5	7254.9	233.6	3.54E-03

depth Z (ft)	yy strain	τ_{xy} (slugsf)	τ_{xy} (ksf)
0	3.35E-03	156.675	5.044935
-12.7	7.90E-03	314.402	10.1237444
-25.4	1.87E-02	603.722	19.4398484
-38.1	2.43E-03	1001.43	32.246046
-50.8	6.23E-05	993.5	31.9907
-63.5	3.62E-04	996.856	32.0987632

depth Z (ft)	x disp (ft)	x disp (in)	Z settlement (ft)	Z settlement (in)
0	6.34E-01	7.61E+00	0.36061	4.32732
-12.7	6.18E-01	7.42E+00	0.360208	4.322496
-25.4	5.08E-01	6.10E+00	0.323016	3.876192
-38.1	1.14E-02	1.37E-01	0.0008449	0.0101388
-50.8	1.19E-02	1.43E-01	0.0050518	0.0606216
-63.5	1.34E-02	1.61E-01	0.002018	0.024216

Excavation D (Z=50.8 ft)

depth Z (ft)	σ_{xx} (slugsf)	σ_{xx} (ksf)	xx strain
0	0.0	0.0	3.80E-04
-12.7	1290.2	41.5	3.28E-03
-25.4	2839.4	91.4	1.95E-01
-38.1	3780.5	121.7	2.07E-01
-50.8	6400.1	206.1	7.20E-04
-63.5	7343.7	236.5	3.02E-03

depth Z (ft)	yy strain	τ_{xy} (slugsf)	τ_{xy} (ksf)
0	2.52E-03	159.115	5.123503
-12.7	9.00E-03	322.086	10.3711692
-25.4	1.83E-02	616.177	19.8408994
-38.1	7.16E-03	1212.36	39.037992

-50.8	1.15E-03	1275.77	41.079794
-63.5	1.21E-04	1135.07	36.549254

depth Z (ft)	x disp (ft)	x disp (in)	Z settlement (ft)	Z settlement (in)
0	8.00E-01	9.60E+00	0.47086	5.65032
-12.7	7.79E-01	9.35E+00	0.470413	5.644956
-25.4	6.43E-01	7.72E+00	0.432927	5.195124
-38.1	1.44E-01	1.73E+00	0.103403	1.240836
-50.8	1.34E-02	1.60E-01	0.00181062	0.02172744
-63.5	1.40E-02	1.68E-01	0.00085076	0.01020915

Excavation E (Z=63.5 ft)

depth Z (ft)	σ_{xx} (slugsf)	σ_{xx} (ksf)	xx strain
0	0.0	0.0	2.09E-04
-12.7	1325.7	42.7	1.51E-03
-25.4	2535.8	81.7	1.07E-01
-38.1	3753.4	120.9	8.06E-02
-50.8	5030.1	162.0	1.09E-02
-63.5	8212.3	264.4	4.00E-03

depth Z (ft)	yy strain	τ_{xy} (slugsf)	τ_{xy} (ksf)
0	1.18E-03	151.789	4.8876058
-12.7	5.53E-03	307.031	9.8863982
-25.4	1.02E-02	623.812	20.0867464
-38.1	5.61E-03	1212	39.0264
-50.8	3.80E-03	1608.49	51.793378
-63.5	1.02E-03	1222.38	39.360636

depth Z (ft)	x disp (ft)	x disp (in)	Z settlement (ft)	Z settlement (in)
0	4.85E-01	5.82E+00	0.278174	3.338088
-12.7	4.82E-01	5.78E+00	0.278585	3.34302
-25.4	4.08E-01	4.90E+00	0.253679	3.044148
-38.1	1.20E-01	1.44E+00	0.0739161	0.8869932
-50.8	3.39E-02	4.07E-01	0.0099064	0.1188768
-63.5	1.90E-02	2.27E-01	0.00087029	0.01044355

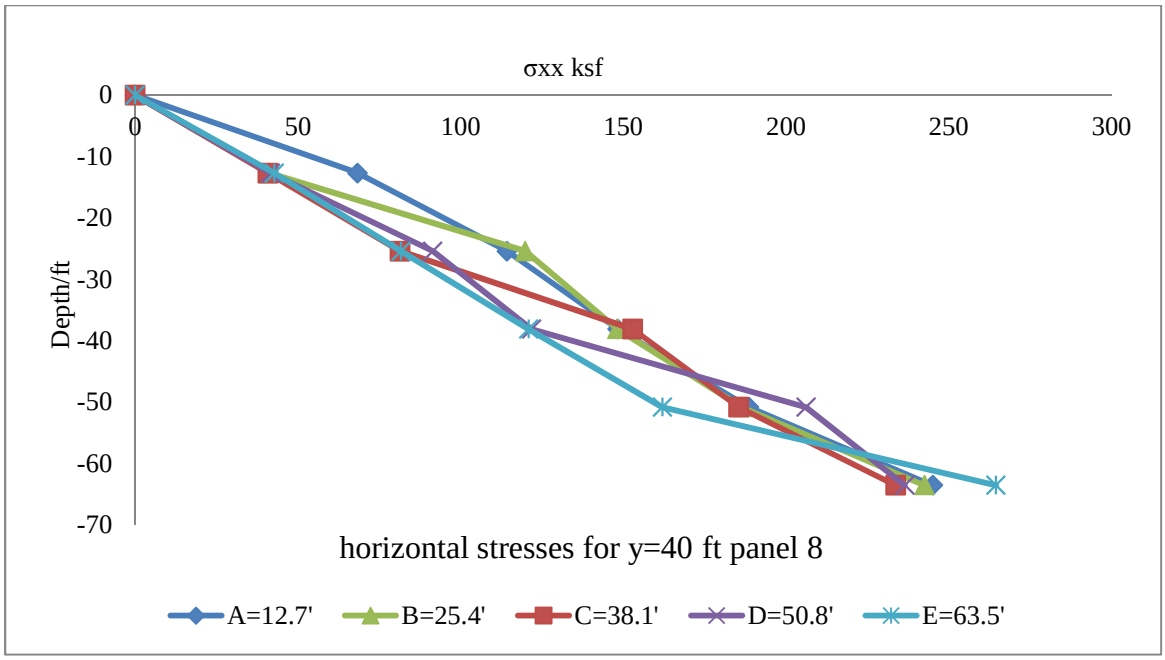

Figure B 43 Horizontal Stresses for Panel 8

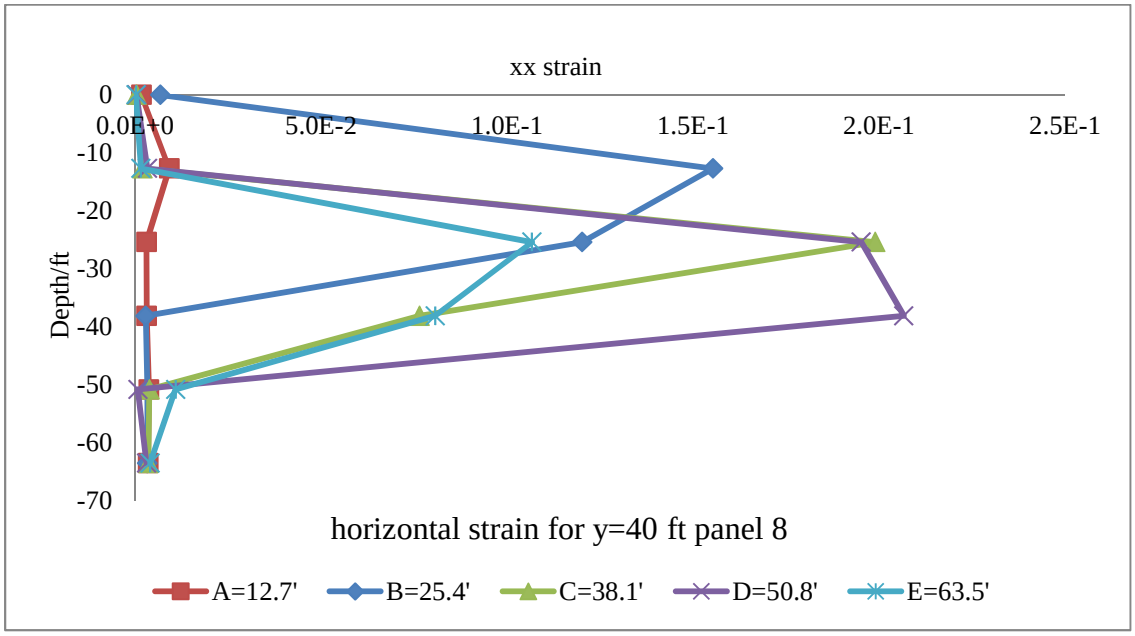

Figure B 44 Horizontal Strain in XX Direction for Panel 8

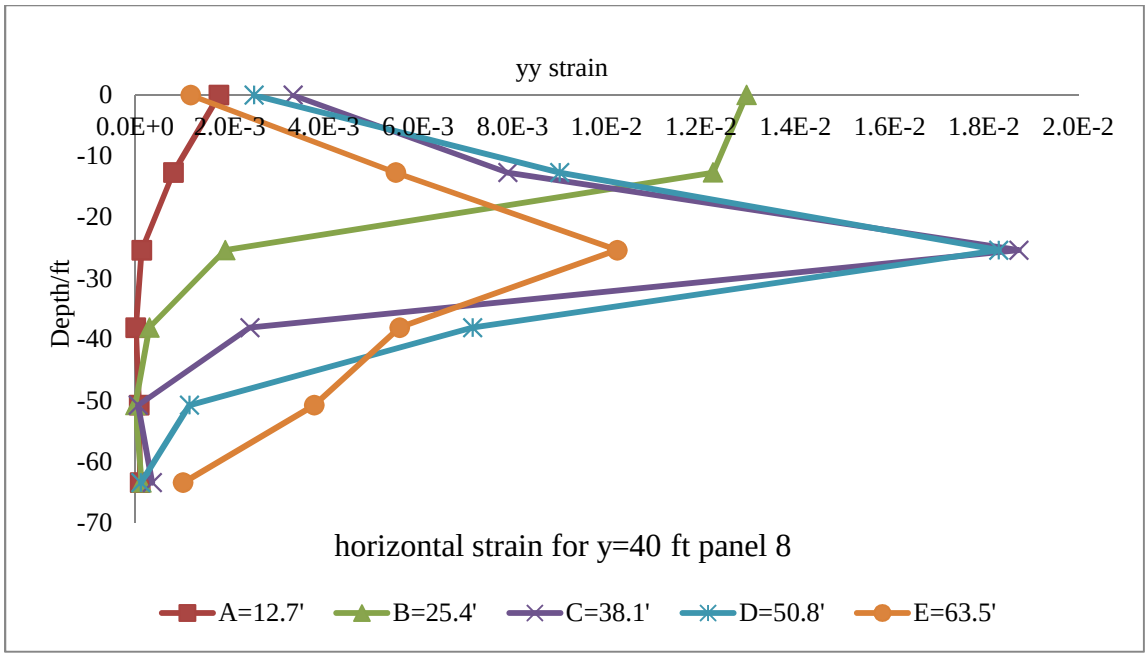

Figure B 45 Horizontal Strain in YY Direction for Panel 8

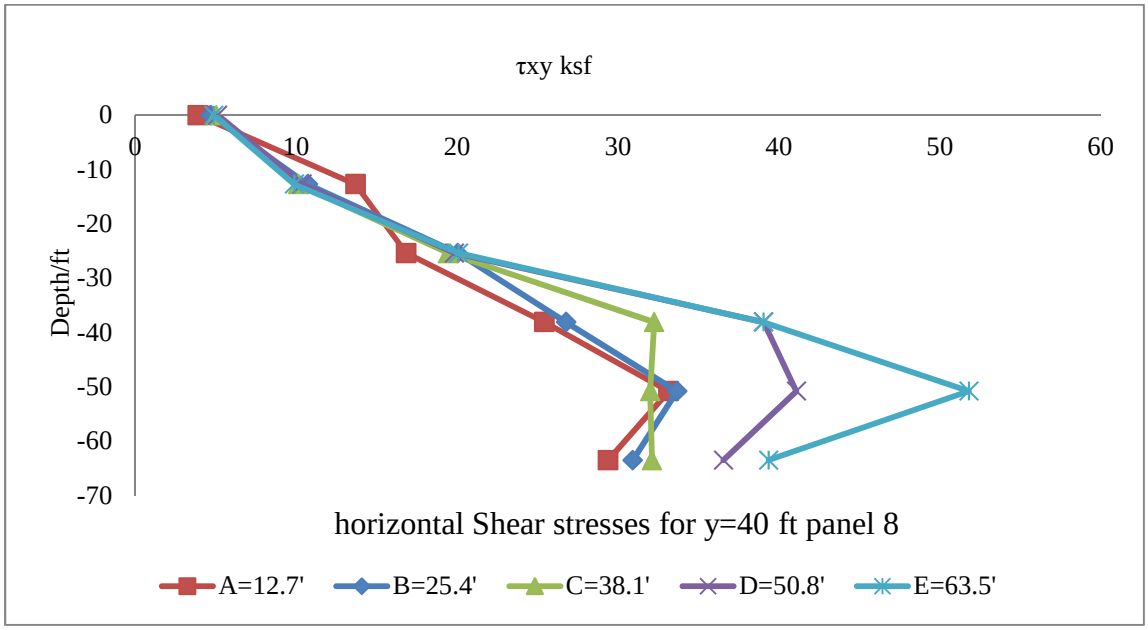

Figure B 46 Horizontal Shear Stresses for Panel 8

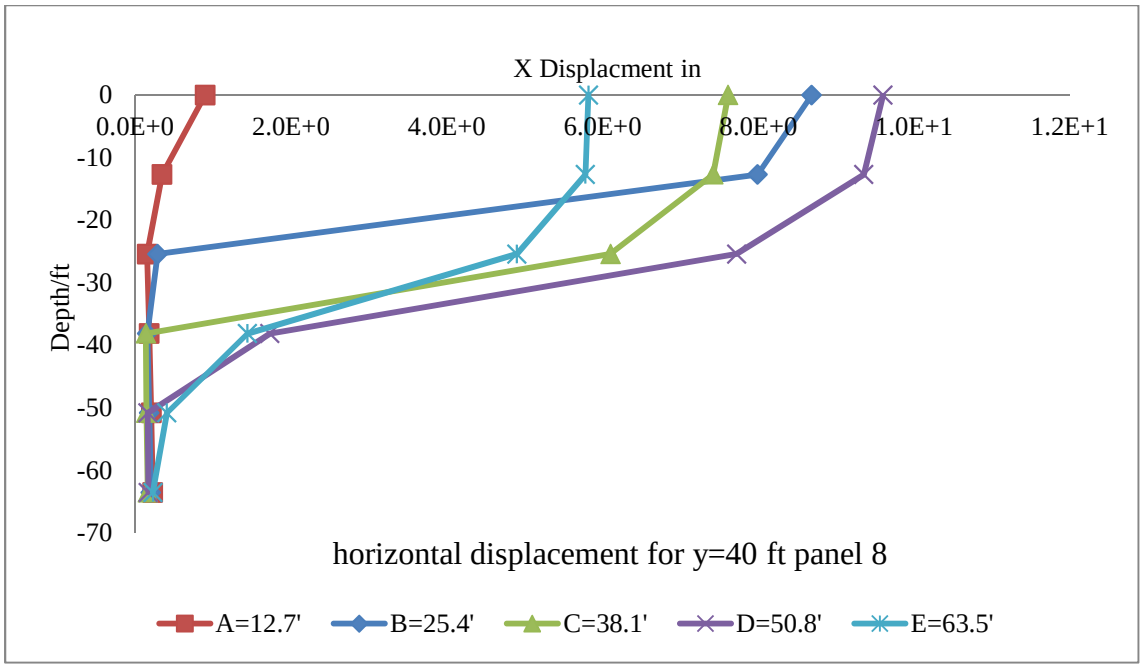

Figure B 47 Horizontal Displacement for Panel 8

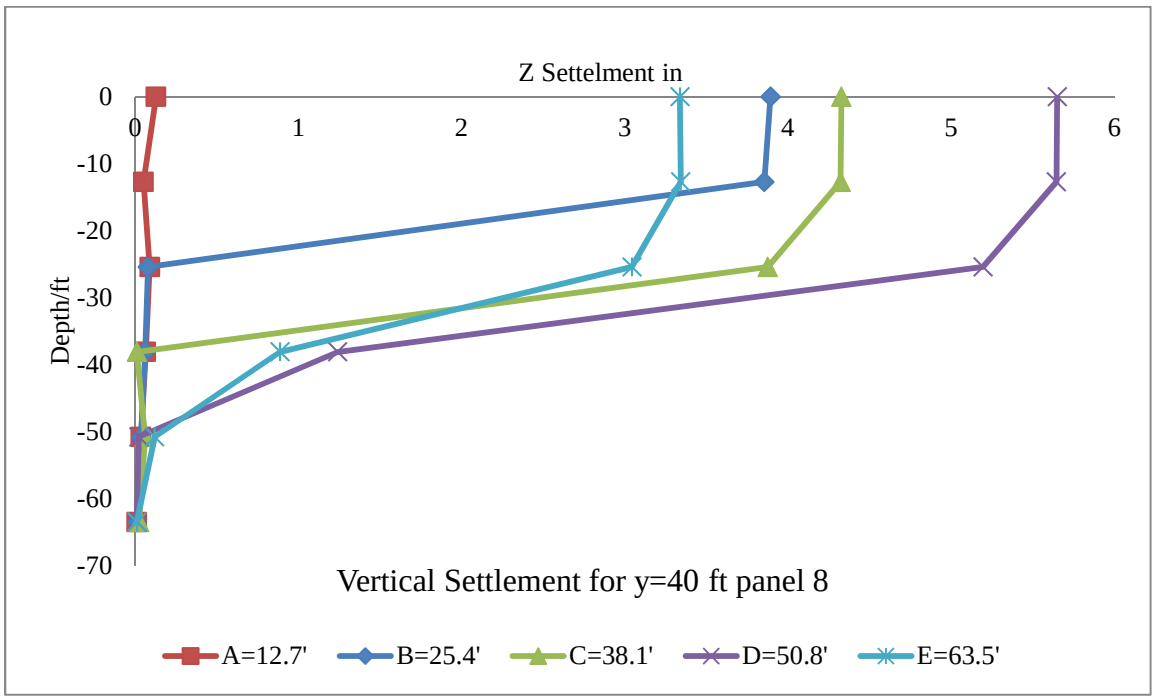

Figure B 48 Vertical Settlement for Panel 8

Panel (9) (Y=45 ft)

Table B 9 All Numerical Results for Panel 9

Excavation A (Z=12.7 ft)

depth Z (ft)	σ_{xx} (slugsf)	σ_{xx} (ksf)	xx strain
0	0.0	0.0	1.92E-03
-12.7	2174.7	70.0	1.23E-02
-25.4	3533.6	113.8	3.10E-03
-38.1	4604.9	148.3	3.07E-03
-50.8	5879.7	189.3	3.66E-03
-63.5	7630.1	245.7	3.43E-03

depth Z (ft)	yy strain	τ_{xy} (slugsf)	τ_{xy} (ksf)
0	1.68E-03	119.157	3.8368554
-12.7	7.84E-04	432.49	13.926178
-25.4	1.30E-04	523.559	16.8585998
-38.1	3.13E-06	780.094	25.1190268
-50.8	7.18E-05	1020.06	32.845932
-63.5	9.72E-05	905.797	29.1666634

depth Z (ft)	x disp (ft)	x disp (in)	Z settlement (ft)	Z settlement (in)
0	8.05E-02	9.66E-01	0.0122698	0.1472376
-12.7	3.44E-02	4.13E-01	0.00448067	0.05376804
-25.4	1.28E-02	1.53E-01	0.00733287	0.08799444
-38.1	1.49E-02	1.79E-01	0.0053869	0.0646428
-50.8	1.72E-02	2.06E-01	0.00298373	0.03580476
-63.5	1.87E-02	2.24E-01	0.00065125	0.00781509

Excavation B (Z=25.4 ft)

depth Z (ft)	σ_{xx} (slugsf)	σ_{xx} (ksf)	xx strain
0	0.0	0.0	5.69E-03
-12.7	1335.1	43.0	1.15E-01
-25.4	3745.9	120.6	1.06E-01
-38.1	4565.8	147.0	2.64E-03
-50.8	5709.3	183.8	3.05E-03
-63.5	7488.3	241.1	3.15E-03

depth Z (ft)	yy strain	τ_{xy} (slugsf)	τ_{xy} (ksf)
0	1.12E-02	154.693	4.9811146
-12.7	1.09E-02	335.136	10.7913792
-25.4	1.52E-03	642.364	20.6841208
-38.1	2.95E-04	839.035	27.016927
-50.8	3.92E-05	1077.78	34.704516
-63.5	9.21E-05	999.306	32.1776532

depth Z (ft)	x disp (ft)	x disp (in)	Z settlement (ft)	Z settlement (in)
0	6.88E-01	8.26E+00	0.301337	3.616044
-12.7	6.31E-01	7.58E+00	0.297662	3.571944
-25.4	1.06E-02	1.27E-01	0.0060981	0.0731772
-38.1	1.22E-02	1.47E-01	0.0045689	0.0548268
-50.8	1.22E-02	1.46E-01	0.00279052	0.03348624
-63.5	1.58E-02	1.90E-01	0.00082176	0.00986116

Excavation C (Z=38.1 ft)

depth Z (ft)	σ_{xx} (slugsf)	σ_{xx} (ksf)	xx strain
0	0.0	0.0	4.32E-04
-12.7	1293.9	41.7	1.10E-03
-25.4	2516.8	81.0	1.54E-01
-38.1	4749.4	152.9	4.87E-02
-50.8	5685.0	183.1	3.42E-03
-63.5	7171.1	230.9	3.24E-03

depth Z (ft)	yy strain	τ_{xy} (slugsf)	τ_{xy} (ksf)
0	4.12E-03	161.589	5.2031658
-12.7	7.06E-03	335.558	10.8049676
-25.4	1.26E-02	629.054	20.2555388
-38.1	2.14E-03	1055.48	33.986456
-50.8	1.12E-04	1032	33.2304
-63.5	2.43E-04	1058.05	34.06921

depth Z (ft)	x disp (ft)	x disp (in)	Z settlement (ft)	Z settlement (in)
0	5.13E-01	6.16E+00	0.283911	3.406932
-12.7	5.03E-01	6.03E+00	0.284079	3.408948
-25.4	4.22E-01	5.06E+00	0.250935	3.01122
-38.1	1.71E-02	2.05E-01	0.0031682	0.0380184

-50.8	1.11E-02	1.33E-01	0.00454855	0.0545826
-63.5	1.23E-02	1.48E-01	0.00173722	0.02084664

Excavation D (Z=50.8 ft)

depth Z (ft)	σ_{xx} (slugsf)	σ_{xx} (ksf)	xx strain
0	0.0	0.0	3.41E-04
-12.7	1256.4	40.5	1.08E-03
-25.4	2561.8	82.5	1.79E-01
-38.1	3740.3	120.4	2.01E-01
-50.8	6312.2	203.3	3.37E-04
-63.5	7307.3	235.3	2.62E-03

depth Z (ft)	yy strain	τ_{xy} (slugsf)	τ_{xy} (ksf)
0	4.65E-03	166.563	5.3633286
-12.7	8.13E-03	346.564	11.1593608
-25.4	1.60E-02	635.261	20.4554042
-38.1	6.60E-03	1289.79	41.531238
-50.8	1.13E-03	1346.97	43.372434
-63.5	2.39E-04	1205.08	38.803576

depth Z (ft)	x disp (ft)	x disp (in)	Z settlement (ft)	Z settlement (in)
0	7.68E-01	9.21E+00	0.44379	5.32548
-12.7	7.50E-01	9.00E+00	0.444152	5.329824
-25.4	6.36E-01	7.63E+00	0.4070777	4.8849324
-38.1	1.45E-01	1.74E+00	0.106892	1.282704
-50.8	1.28E-02	1.53E-01	0.00088631	0.01063576
-63.5	1.31E-02	1.57E-01	0.00058884	0.00706608

Excavation E (Z=63.5 ft)

depth Z (ft)	σ_{xx} (slugsf)	σ_{xx} (ksf)	xx strain
0	0.0	0.0	1.40E-04
-12.7	1330.5	42.8	1.18E-04
-25.4	2539.0	81.8	1.11E-01
-38.1	3770.7	121.4	1.26E-01
-50.8	5041.9	162.3	1.41E-02
-63.5	8214.6	264.5	3.87E-03

depth Z (ft)	yy strain	τ_{xy} (slugsf)	τ_{xy} (ksf)
0	2.81E-03	158.588	5.1065336
-12.7	5.76E-03	333.132	10.7268504
-25.4	1.05E-02	637.715	20.534423
-38.1	5.33E-03	1263.98	40.700156
-50.8	3.77E-03	1684.62	54.244764
-63.5	1.15E-03	1295.89	41.727658

depth Z (ft)	x disp (ft)	x disp (in)	Z settlement (ft)	Z settlement (in)
0	5.43E-01	6.52E+00	0.308798	3.705576
-12.7	5.39E-01	6.47E+00	0.309316	3.711792
-25.4	4.61E-01	5.53E+00	0.275906	3.310872
-38.1	1.38E-01	1.65E+00	0.0929204	1.1150448
-50.8	3.55E-02	4.26E-01	0.0127499	0.1529988
-63.5	1.79E-02	2.15E-01	0.00023813	0.00285756

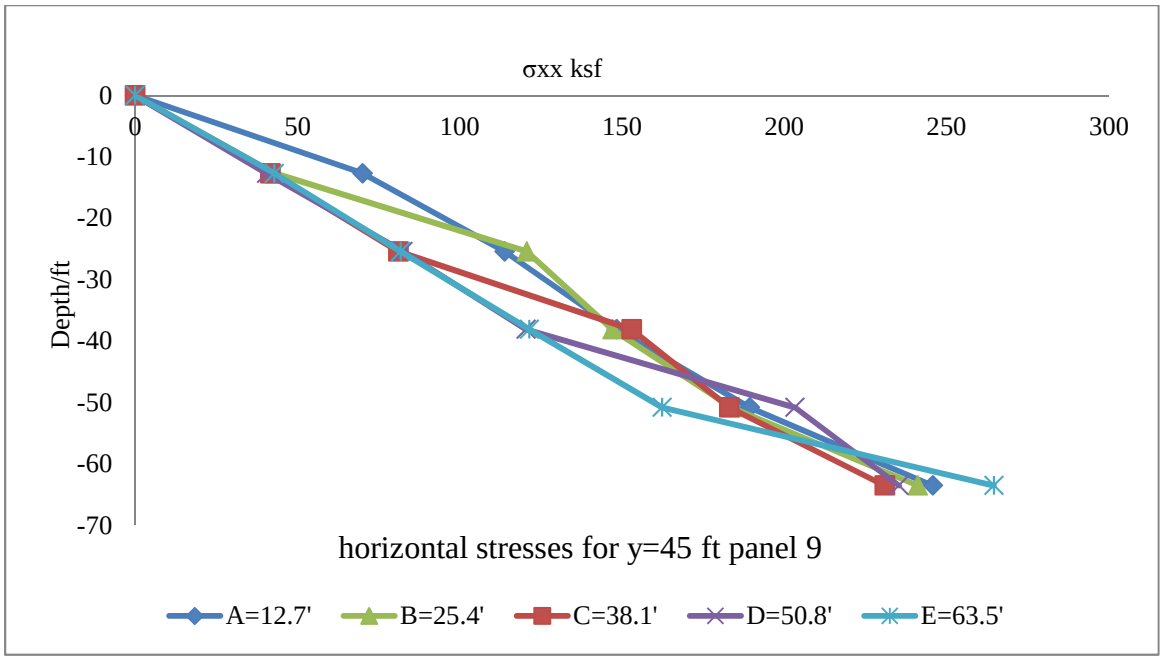

Figure B 49 Horizontal Stresses for Panel 9

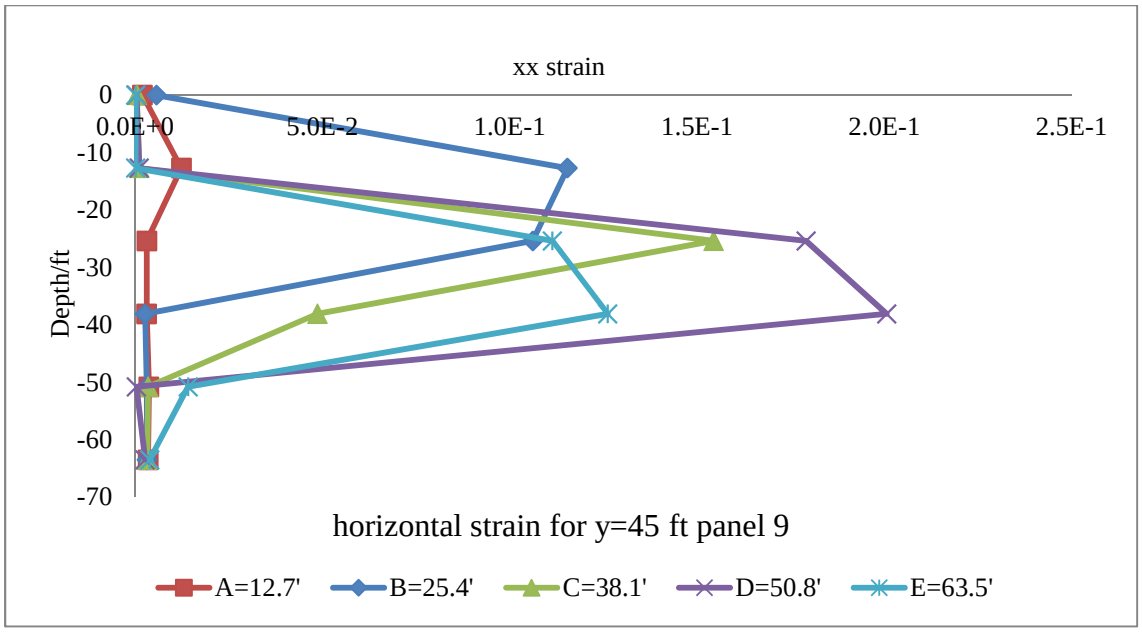

Figure B 50 Horizontal Strain in XX Direction for Panel 9

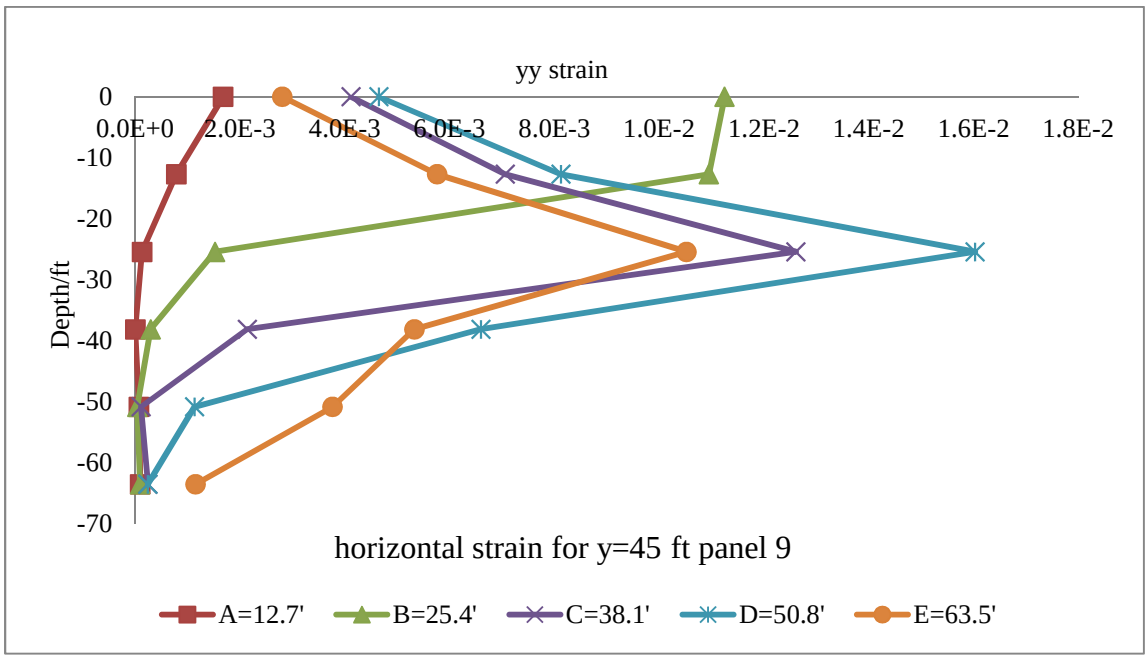

Figure B 51 Horizontal Strain in YY Direction for Panel 9

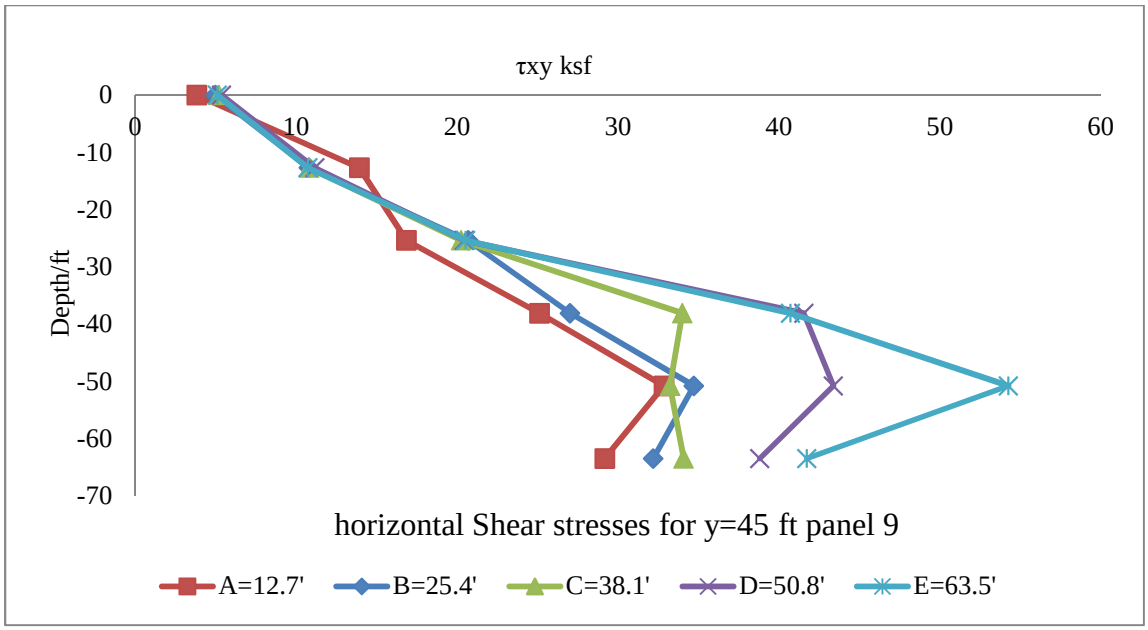

Figure B 52 Horizontal Shear Stresses for Panel 9

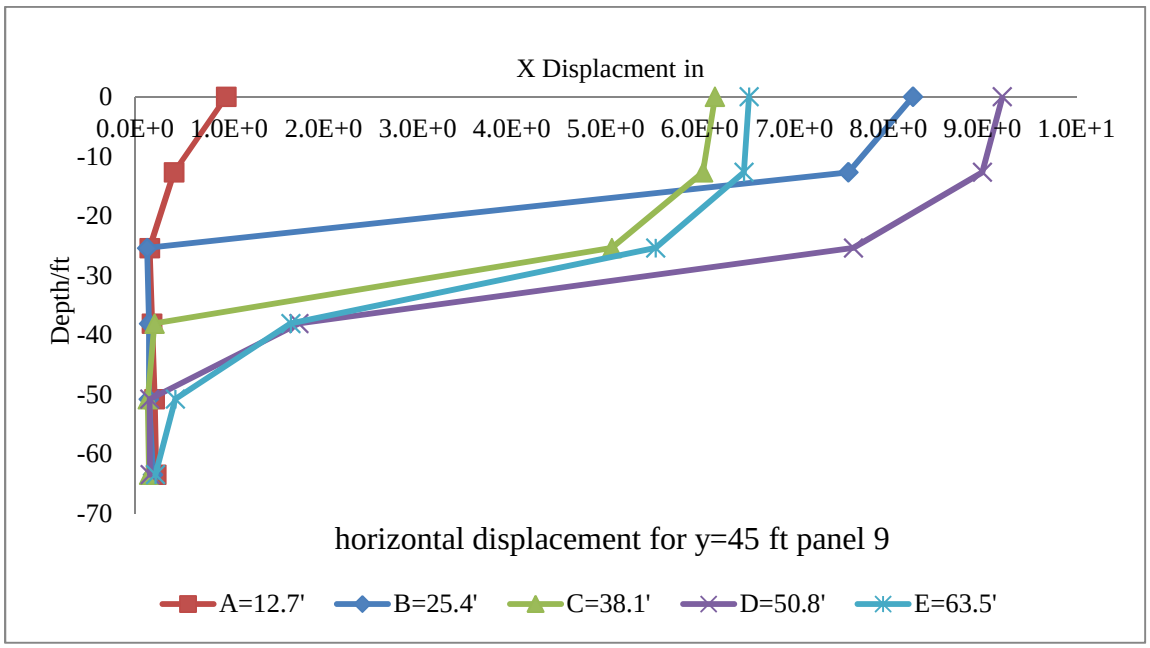

Figure B 53 Horizontal Displacement for Panel 9

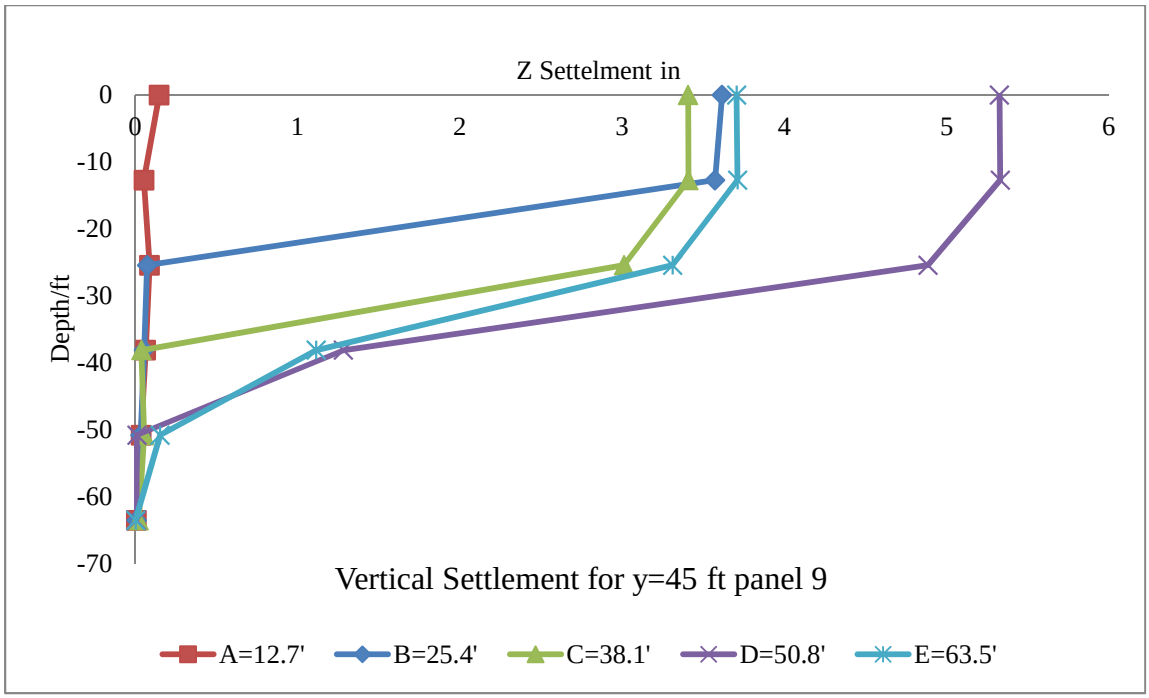

Figure B 54 Vertical Settlement for Panel 9

Panel (10) (Y=50 ft)

Table B 10 All Numerical Results for Panel 10

Excavation A (Z=12.7 ft)

depth Z (ft)	σ_{xx} (slugsf)	σ_{xx} (ksf)	xx strain
0	0.0	0.0	4.31E-03
-12.7	1945.8	62.7	2.13E-02
-25.4	3536.3	113.9	3.09E-03
-38.1	4582.9	147.6	3.05E-03
-50.8	5839.9	188.0	3.67E-03
-63.5	7618.8	245.3	3.41E-03

depth Z (ft)	yy strain	τ_{xy} (slugsf)	τ_{xy} (ksf)
0	1.93E-03	116.504	3.7514288
-12.7	8.26E-04	440.195	14.174279
-25.4	1.18E-04	524.478	16.8881916
-38.1	9.83E-06	785.826	25.3035972

-50.8	5.84E-05	1038.13	33.427786
-63.5	8.90E-05	916.738	29.5189636

depth Z (ft)	x disp (ft)	x disp (in)	Z settlement (ft)	Z settlement (in)
0	1.21E-01	1.46E+00	0.02474	0.29688
-12.7	5.16E-02	6.20E-01	0.00159334	0.01912008
-25.4	1.30E-02	1.56E-01	0.00719534	0.08634408
-38.1	1.50E-02	1.80E-01	0.00528722	0.06344664
-50.8	1.72E-02	2.07E-01	0.00291519	0.03498228
-63.5	1.88E-02	2.26E-01	0.00066993	0.00803925

Excavation B (Z=25.4 ft)

depth Z (ft)	σ_{xx} (slugsf)	σ_{xx} (ksf)	xx strain
0	0.0	0.0	3.99E-03
-12.7	1281.8	41.3	1.42E-01
-25.4	3797.3	122.3	1.15E-01
-38.1	4538.0	146.1	2.49E-03
-50.8	5443.8	175.3	2.85E-03
-63.5	7449.9	239.9	3.01E-03

depth Z (ft)	yy strain	τ_{xy} (slugsf)	τ_{xy} (ksf)
0	1.09E-02	157.481	5.0708882
-12.7	9.57E-03	335.051	10.7886422
-25.4	1.12E-03	654.689	21.0809858
-38.1	2.37E-04	848.911	27.3349342
-50.8	5.02E-05	1083.47	34.887734
-63.5	6.75E-05	1044.83	33.643526

depth Z (ft)	x disp (ft)	x disp (in)	Z settlement (ft)	Z settlement (in)
0	7.32E-01	8.78E+00	0.31677	3.80124
-12.7	6.69E-01	8.03E+00	0.311974	3.743688
-25.4	3.46E-03	4.16E-02	0.00556288	0.06675456
-38.1	1.20E-02	1.44E-01	0.00417187	0.05006244
-50.8	1.38E-02	1.66E-01	0.00258881	0.03106572
-63.5	1.53E-02	1.84E-01	0.00082102	0.0098523

Excavation C (Z=38.1 ft)

depth Z (ft)	σ_{xx} (slugsf)	σ_{xx} (ksf)	xx strain
0	0.0	0.0	8.09E-04
-12.7	1336.6	43.0	7.70E-04
-25.4	2505.7	80.7	2.05E-01
-38.1	4687.2	150.9	8.08E-02
-50.8	5603.3	180.4	3.16E-03
-63.5	7185.8	231.4	2.96E-03

depth Z (ft)	yy strain	τ_{xy} (slugsf)	τ_{xy} (ksf)
0	6.28E-03	171.477	5.5215594
-12.7	8.05E-03	349.445	11.252129
-25.4	1.43E-02	645.048	20.7705456
-38.1	2.00E-03	1082.93	34.870346
-50.8	1.10E-04	1042.33	33.563026
-63.5	1.94E-04	1099.52	35.404544

depth Z (ft)	x disp (ft)	x disp (in)	Z settlement (ft)	Z settlement (in)
0	6.69E-01	8.02E+00	0.368731	4.424772
-12.7	6.49E-01	7.79E+00	0.367452	4.409424
-25.4	5.10E-01	6.13E+00	0.313019	3.756228
-38.1	1.73E-02	2.08E-01	0.00198291	0.02379492
-50.8	1.04E-02	1.24E-01	0.00415251	0.04983012
-63.5	1.17E-02	1.40E-01	0.00164794	0.01977528

Excavation D (Z=50.8 ft)

depth Z (ft)	σ_{xx} (slugsf)	σ_{xx} (ksf)	xx strain
0	0.0	0.0	1.47E-04
-12.7	1283.5	41.3	1.83E-03
-25.4	2561.2	82.5	1.29E-01
-38.1	3751.6	120.8	1.57E-01
-50.8	6246.9	201.2	3.29E-04
-63.5	7240.3	233.1	2.17E-03

depth Z (ft)	yy strain	τ_{xy} (slugsf)	τ_{xy} (ksf)
0	3.75E-03	175.115	5.638703
-12.7	6.29E-03	337.907	10.8806054
-25.4	9.63E-03	649.238	20.9054636
-38.1	4.44E-03	1328.98	42.793156

-50.8	8.20E-04	1375.6	44.29432
-63.5	1.32E-04	1243.09	40.027498

depth Z (ft)	x disp (ft)	x disp (in)	Z settlement (ft)	Z settlement (in)
0	5.97E-01	7.16E+00	0.336169	4.034028
-12.7	5.86E-01	7.03E+00	0.336037	4.032444
-25.4	4.90E-01	5.88E+00	0.30418	3.65016
-38.1	1.15E-01	1.38E+00	0.08305	0.9966
-50.8	1.21E-02	1.45E-01	0.00028651	0.00343821
-63.5	1.23E-02	1.48E-01	0.00039722	0.00476674

Excavation E (Z=63.5 ft)

depth Z (ft)	σ_{xx} (slugsf)	σ_{xx} (ksf)	xx strain
0	0.0	0.0	5.96E-04
-12.7	1231.3	39.6	1.63E-03
-25.4	2513.1	80.9	2.08E-01
-38.1	3738.4	120.4	2.42E-01
-50.8	5056.3	162.8	2.88E-02
-63.5	8186.8	263.6	2.26E-03

depth Z (ft)	yy strain	τ_{xy} (slugsf)	τ_{xy} (ksf)
0	6.61E-03	179.549	5.7814778
-12.7	1.05E-02	345.661	11.1302842
-25.4	1.57E-02	657.102	21.1586844
-38.1	5.94E-03	1316.2	42.38164
-50.8	3.36E-03	1748.96	56.316512
-63.5	8.32E-04	1407.95	45.33599

depth Z (ft)	x disp (ft)	x disp (in)	Z settlement (ft)	Z settlement (in)
0	9.97E-01	1.20E+01	0.573225	6.8787
-12.7	9.75E-01	1.17E+01	0.571825	6.8619
-25.4	8.30E-01	9.96E+00	0.526199	6.314388
-38.1	2.35E-01	2.82E+00	0.161643	1.939716
-50.8	4.06E-02	4.88E-01	0.0179191	0.2150292
-63.5	1.69E-02	2.03E-01	0.00018541	0.00222494

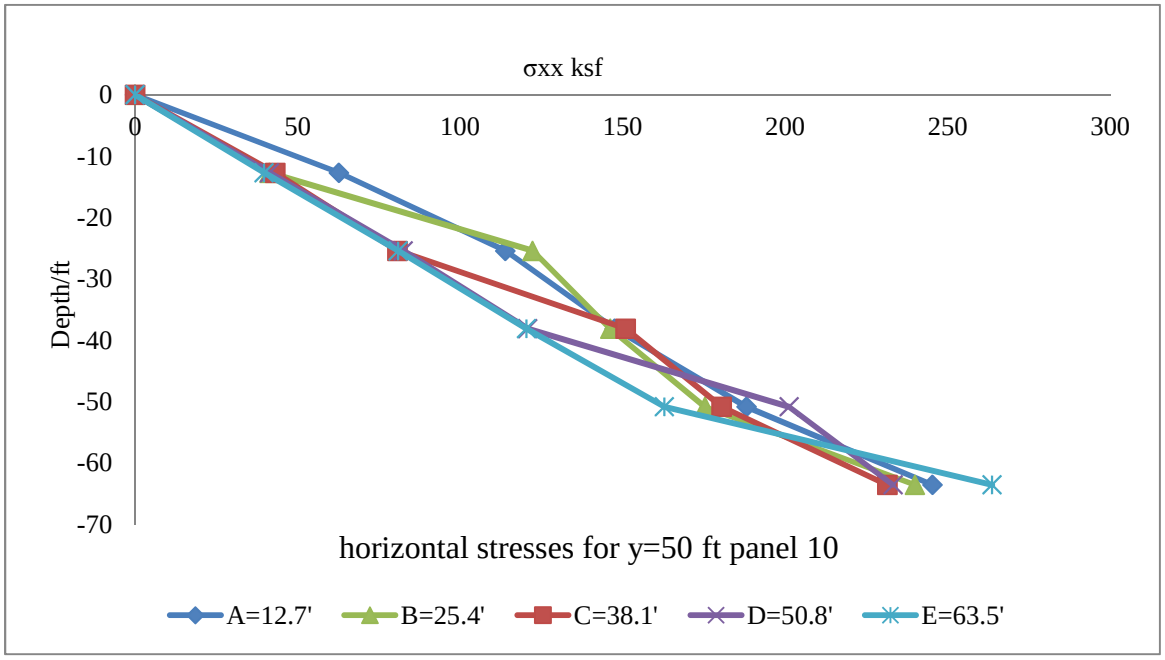

Figure B 55 Horizontal Stresses for Panel 10

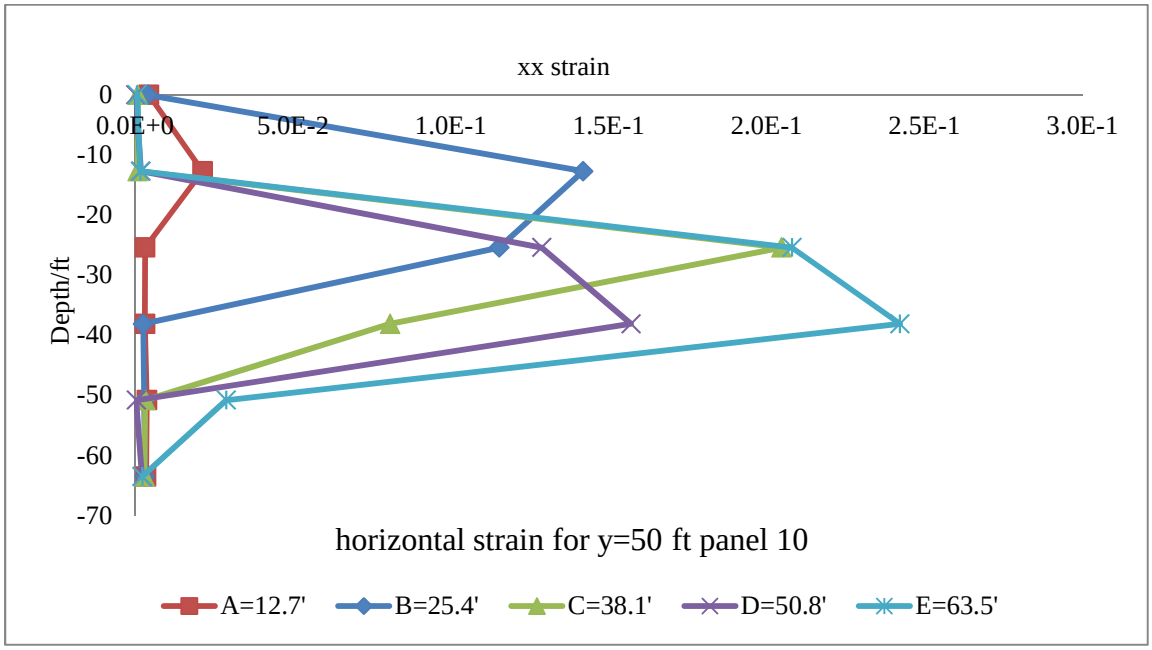

Figure B 56 Horizontal Strain in XX Direction for Panel 10

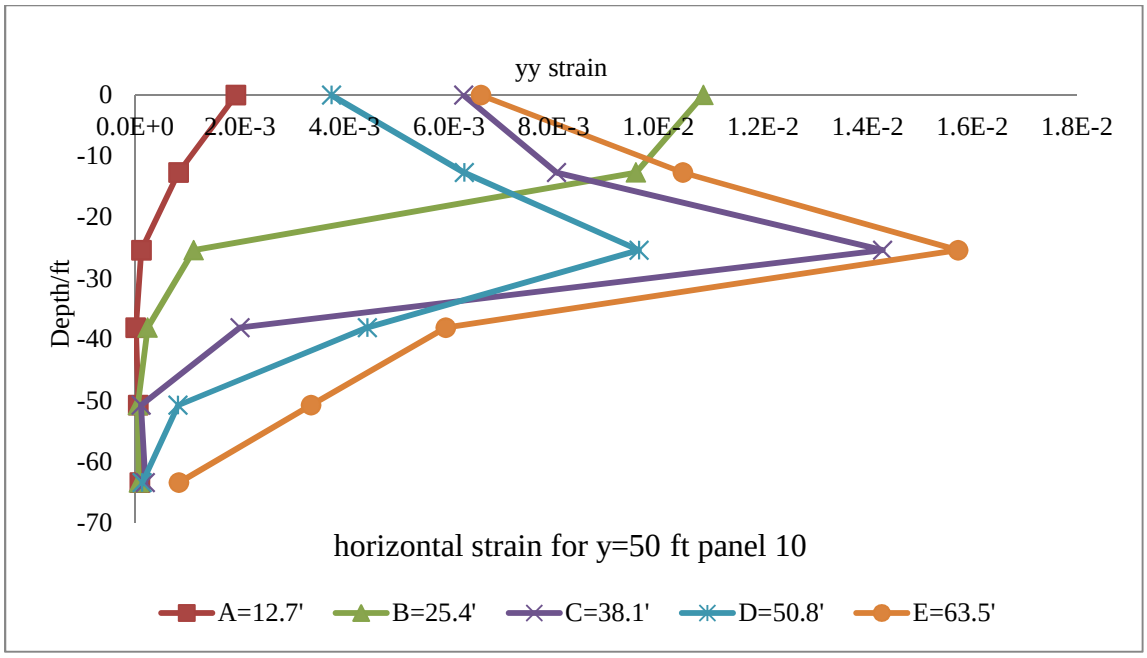

Figure B 57 Horizontal Strain in YY Direction for Panel 10

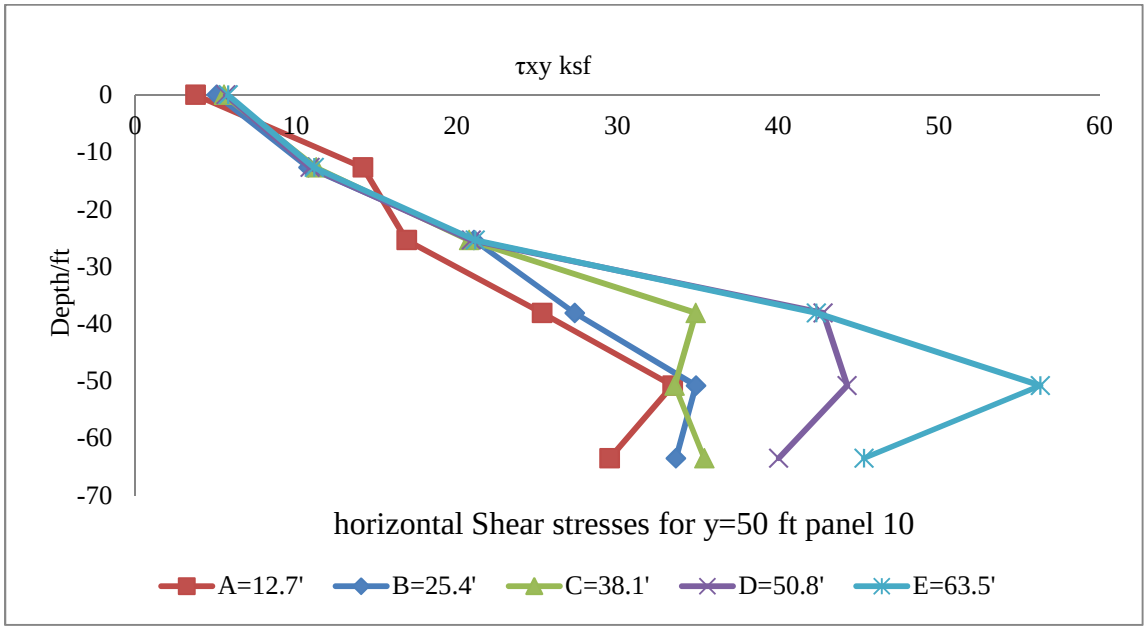

Figure B 58 Horizontal Shear Stresses for Panel 10

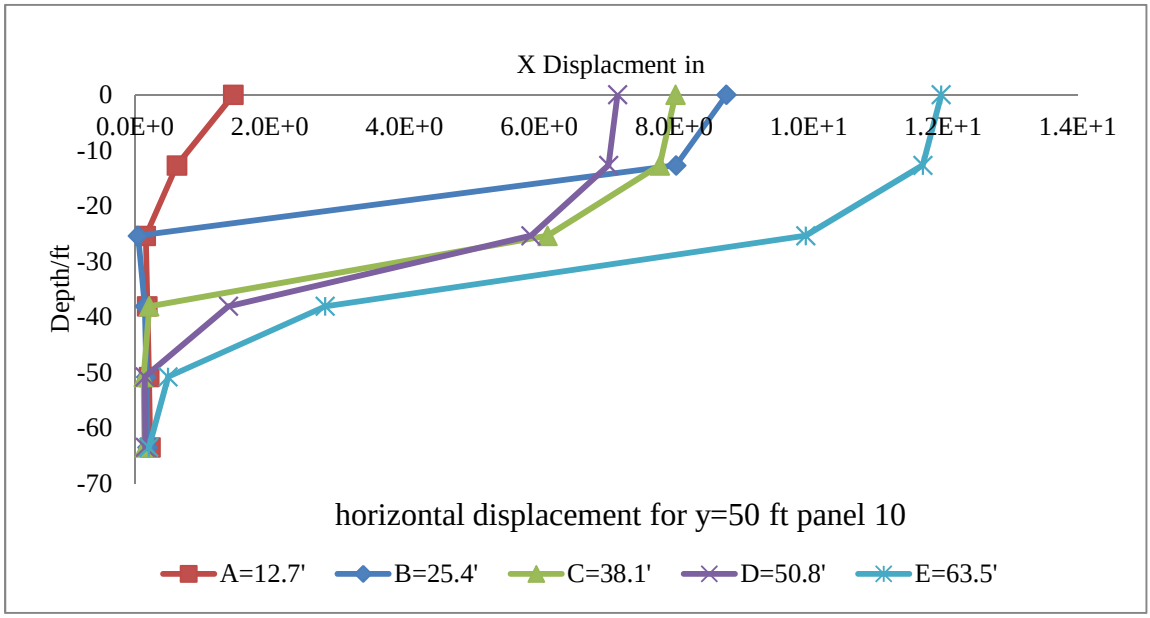

Figure B 59 Horizontal Displacement for Panel 10

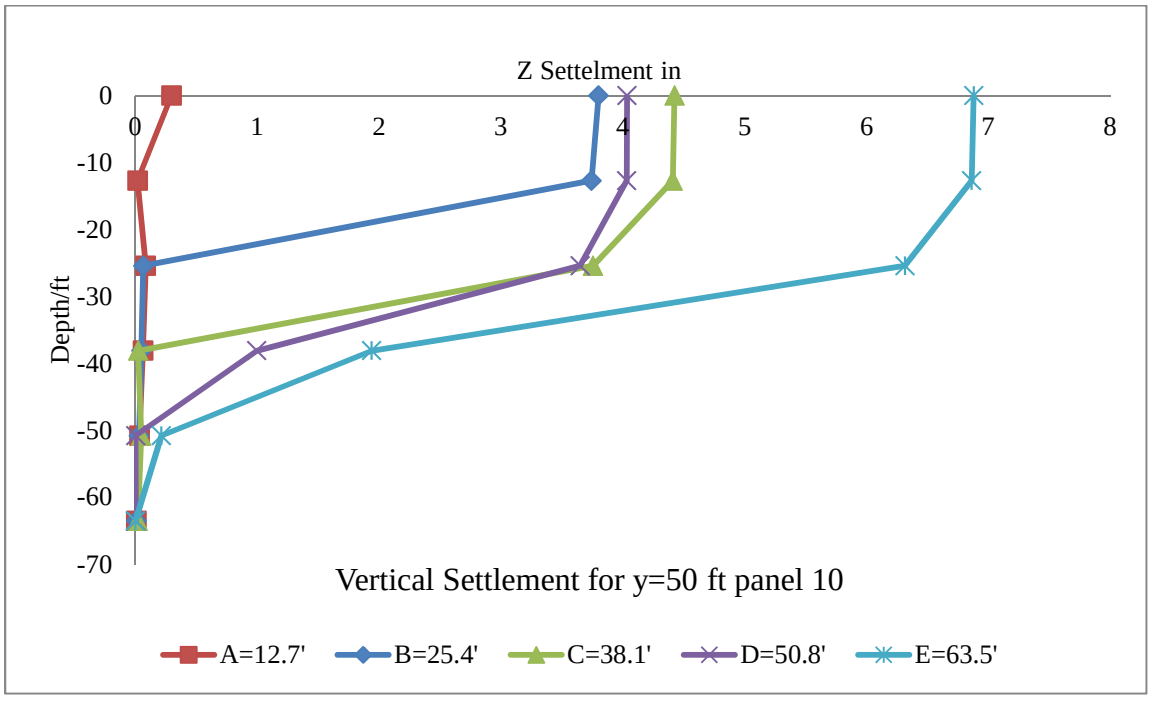

Figure B 60 Vertical Settlement for Panel 10

Panel (11) (Y=55 ft)

Table B 11 All Numerical Results for Panel 11

Excavation A (Z=12.7 ft)

depth Z (ft)	σ_{xx} (slugsf)	σ_{xx} (ksf)	xx strain
0	0.0	0.0	8.40E-03
-12.7	1961.2	63.1	2.87E-02
-25.4	3541.5	114.0	3.14E-03
-38.1	4595.2	148.0	3.07E-03
-50.8	5843.0	188.1	3.66E-03
-63.5	7657.3	246.6	3.43E-03

depth Z (ft)	yy strain	τ_{xy} (slugsf)	τ_{xy} (ksf)
0	2.25E-03	105.974	3.4123628
-12.7	8.35E-04	432.507	13.9267254
-25.4	1.41E-04	527.998	17.0015356
-38.1	3.45E-05	790.859	25.4656598
-50.8	4.46E-05	1039.32	33.466104
-63.5	8.14E-05	927.759	29.8738398

depth Z (ft)	x disp (ft)	x disp (in)	Z settlement (ft)	Z settlement (in)
0	1.55E-01	1.85E+00	0.035778	0.429336
-12.7	4.98E-02	5.98E-01	0.00175459	0.02105508
-25.4	1.30E-02	1.55E-01	0.00730493	0.08765916
-38.1	1.50E-02	1.81E-01	0.00536825	0.064419
-50.8	1.73E-02	2.08E-01	0.002919	0.035028
-63.5	1.89E-02	2.26E-01	0.00066162	0.00793946

Excavation B (Z=25.4 ft)

depth Z (ft)	σ_{xx} (slugsf)	σ_{xx} (ksf)	xx strain
0	0.0	0.0	4.78E-03
-12.7	1309.9	42.2	1.75E-01
-25.4	3790.4	122.1	1.43E-01
-38.1	4536.5	146.1	2.43E-03
-50.8	5717.3	184.1	2.78E-03
-63.5	7392.2	238.0	2.96E-03

depth Z (ft)	yy strain	τ_{xy} (slugsf)	τ_{xy} (ksf)
0	1.30E-02	161.197	5.1905434
-12.7	1.17E-02	326.598	10.5164556
-25.4	1.08E-03	662.007	21.3166254
-38.1	2.78E-04	873.881	28.1389682
-50.8	9.49E-05	1090.4	35.11088
-63.5	3.12E-05	1052.56	33.892432

depth Z (ft)	x disp (ft)	x disp (in)	Z settlement (ft)	Z settlement (in)
0	9.02E-01	1.08E+01	0.390796	4.689552
-12.7	8.20E-01	9.85E+00	0.388262	4.659144
-25.4	1.05E-02	1.26E-01	0.00540986	0.06491832
-38.1	1.18E-02	1.41E-01	0.00402779	0.04833348
-50.8	1.35E-02	1.62E-01	0.00249296	0.02991552
-63.5	1.50E-02	1.79E-01	0.00082278	0.00987340

Excavation C (Z=38.1 ft)

depth Z (ft)	σ_{xx} (slugsf)	σ_{xx} (ksf)	xx strain
0	0.0	0.0	7.50E-04
-12.7	1279.7	41.2	1.12E-03
-25.4	2526.5	81.4	1.33E-01
-38.1	4609.1	148.4	6.22E-02
-50.8	5596.5	180.2	3.09E-03
-63.5	7096.2	228.5	2.91E-03

depth Z (ft)	yy strain	τ_{xy} (slugsf)	τ_{xy} (ksf)
0	4.04E-03	174.217	5.6097874
-12.7	6.41E-03	348.043	11.2069846
-25.4	9.61E-03	652.11	20.997942
-38.1	1.56E-03	1098.39	35.368158
-50.8	1.76E-04	1062.02	34.197044
-63.5	1.15E-04	1125.32	36.235304

depth Z (ft)	x disp (ft)	x disp (in)	Z settlement (ft)	Z settlement (in)
0	4.69E-01	5.63E+00	0.253468	3.041616
-12.7	4.58E-01	5.49E+00	0.252962	3.035544
-25.4	3.75E-01	4.50E+00	0.225267	2.703204
-38.1	1.81E-02	2.17E-01	0.00485154	0.05821848

-50.8	1.04E-02	1.24E-01	0.00402909	0.04834908
-63.5	1.14E-02	1.37E-01	0.00162676	0.01952112

Excavation D (Z=50.8 ft)

depth Z (ft)	σ_{xx} (slugsf)	σ_{xx} (ksf)	xx strain
0	0.0	0.0	5.67E-04
-12.7	1281.1	41.3	4.54E-04
-25.4	2555.7	82.3	1.04E-01
-38.1	3777.4	121.6	1.33E-01
-50.8	6207.1	199.9	6.86E-05
-63.5	7215.5	232.3	2.11E-03

depth Z (ft)	yy strain	τ_{xy} (slugsf)	τ_{xy} (ksf)
0	3.59E-03	172.903	5.5674766
-12.7	5.61E-03	353.504	11.3828288
-25.4	8.08E-03	661.429	21.2980138
-38.1	4.33E-03	1329.88	42.822136
-50.8	1.00E-03	1418.78	45.684716
-63.5	2.94E-04	1275.05	41.05661

depth Z (ft)	x disp (ft)	x disp (in)	Z settlement (ft)	Z settlement (in)
0	5.14E-01	6.17E+00	0.285974	3.431688
-12.7	5.05E-01	6.07E+00	0.285899	3.430788
-25.4	4.32E-01	5.18E+00	0.2669	3.2028
-38.1	1.06E-01	1.27E+00	0.0683364	0.8200368
-50.8	1.21E-02	1.45E-01	1.23E-05	0.00014746
-63.5	1.22E-02	1.46E-01	0.00028215	0.00338588

Excavation E (Z=63.5 ft)

depth Z (ft)	σ_{xx} (slugsf)	σ_{xx} (ksf)	xx strain
0	0.0	0.0	2.78E-04
-12.7	1260.9	40.6	4.33E-04
-25.4	2479.8	79.8	1.55E-01
-38.1	3762.5	121.2	1.87E-01
-50.8	5020.6	161.7	2.47E-02
-63.5	8088.0	260.4	1.18E-03

depth Z (ft)	yy strain	τ_{xy} (slugsf)	τ_{xy} (ksf)
0	4.82E-03	183.524	5.9094728
-12.7	8.16E-03	363.312	11.6986464
-25.4	1.19E-02	660.299	21.2616278
-38.1	5.72E-03	1298.32	41.805904
-50.8	3.66E-03	1782.08	57.382976
-63.5	1.29E-03	1402.93	45.174346

depth Z (ft)	x disp (ft)	x disp (in)	Z settlement (ft)	Z settlement (in)
0	7.59E-01	9.11E+00	0.429751	5.157012
-12.7	7.45E-01	8.94E+00	0.42864	5.14368
-25.4	6.35E-01	7.62E+00	0.407249	4.886988
-38.1	1.84E-01	2.21E+00	0.134883	1.618596
-50.8	4.02E-02	4.83E-01	0.0179955	0.215946
-63.5	1.71E-02	2.05E-01	0.000597587	0.007171044

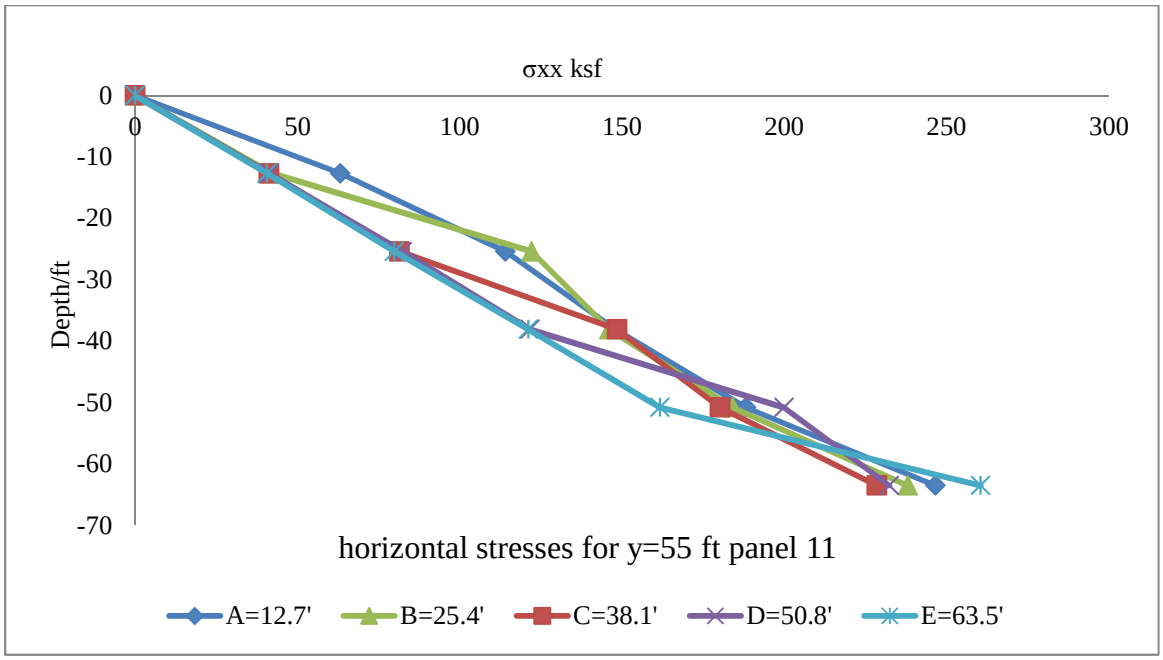

Figure B 61 Horizontal Stresses for Panel 11

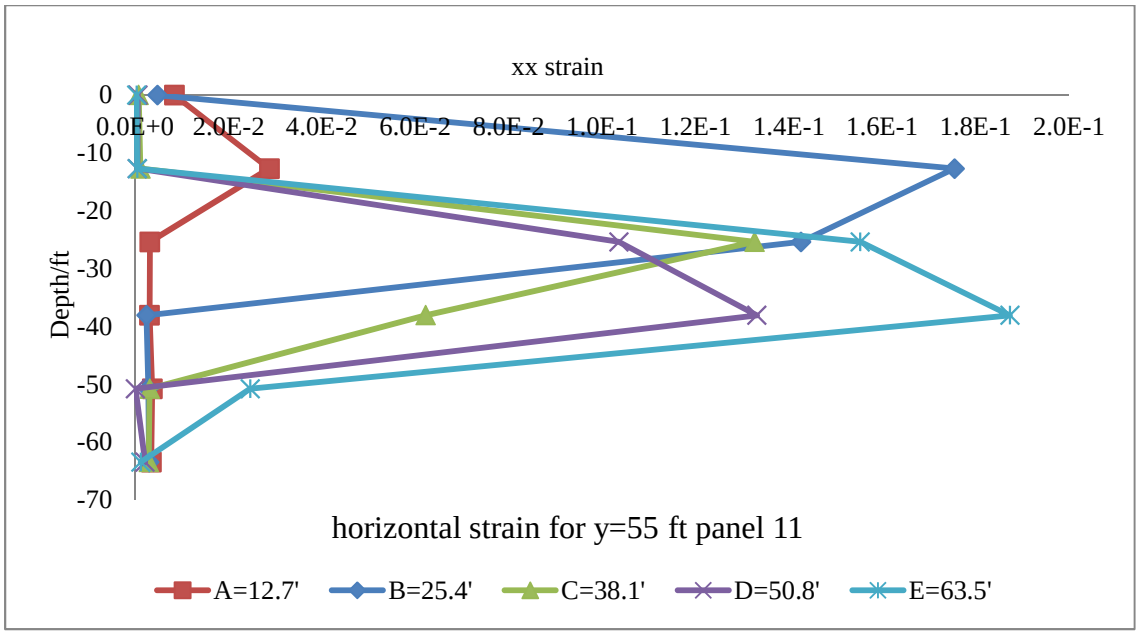

Figure B 62 Horizontal Strain in XX Direction for Panel 11

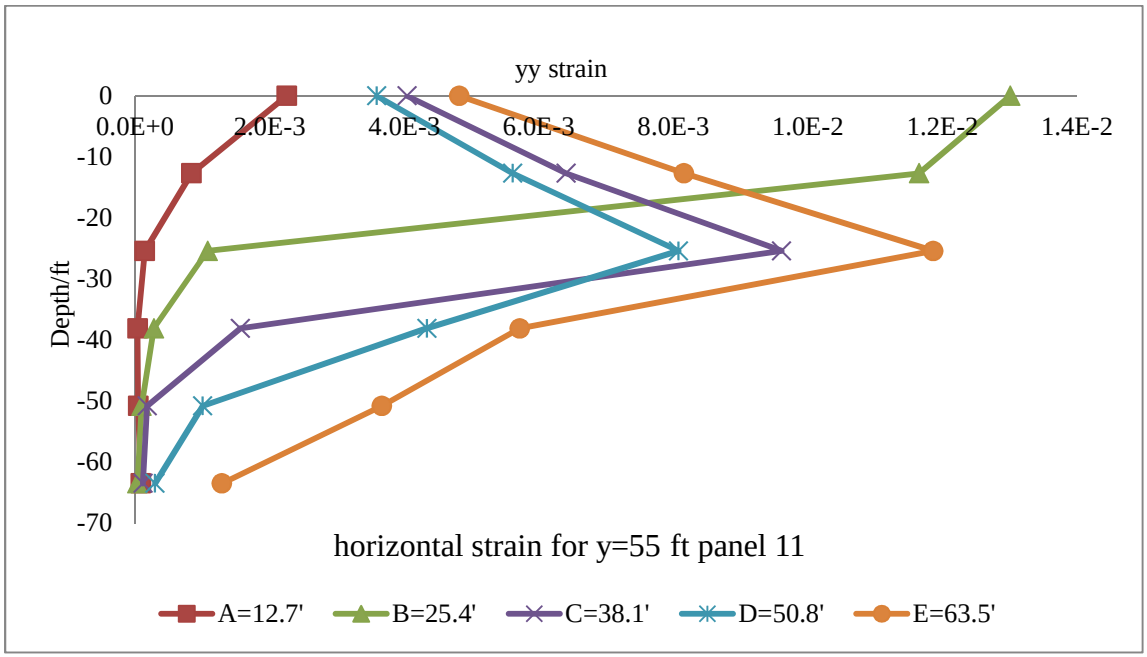

Figure B 63 Horizontal Strain in YY Direction for Panel 11

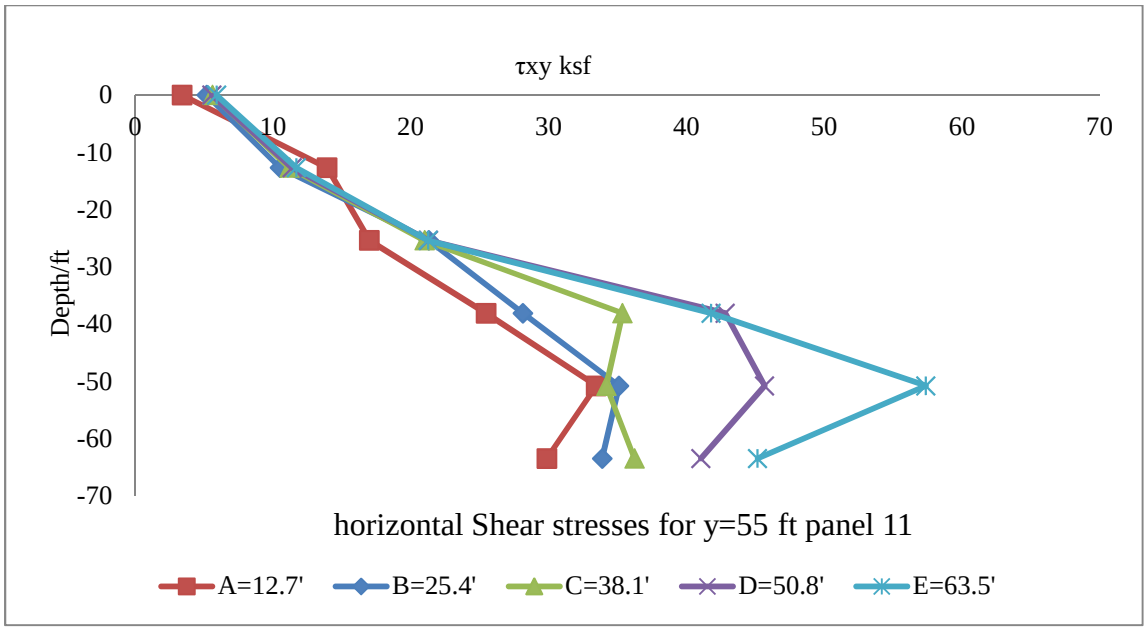

Figure B 64 Horizontal Shear Stresses for Panel 11

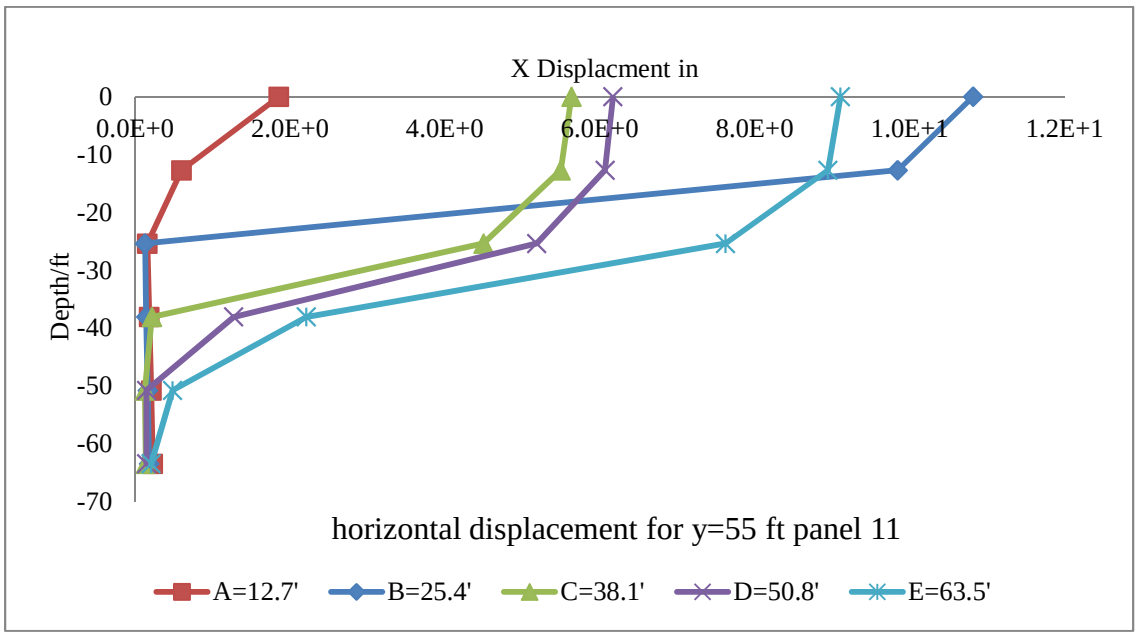

Figure B 65 Horizontal Displacement for Panel 11

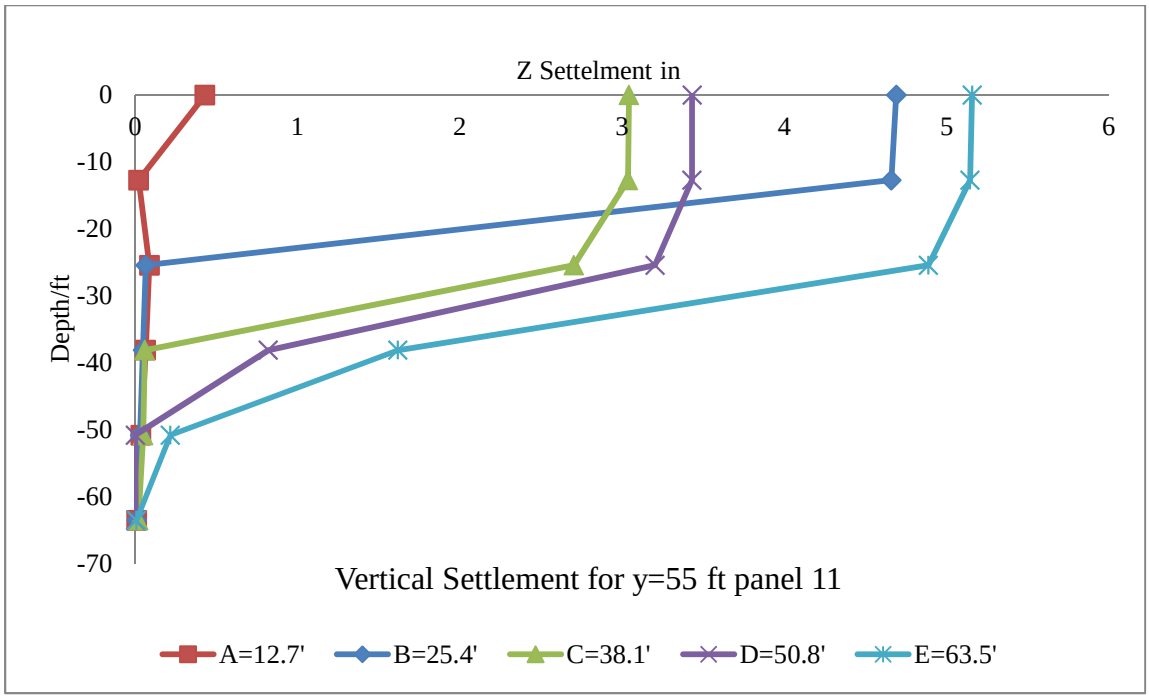

Figure B 66 Vertical Settlement for Panel 11

Panel (12) (Y=60 ft)

Table B 12 All Numerical Results for Panel 12

Excavation A (Z=12.7 ft)

depth Z (ft)	σ_{xx} (slugsf)	σ_{xx} (ksf)	xx strain
0	0.0	0.0	1.41E-02
-12.7	2110.2	67.9	5.33E-02
-25.4	3550.8	114.3	3.17E-03
-38.1	4593.0	147.9	3.02E-03
-50.8	5859.2	188.7	3.66E-03
-63.5	7581.5	244.1	3.40E-03

depth Z (ft)	yy strain	τ_{xy} (slugsf)	τ_{xy} (ksf)
0	3.05E-03	106.202	3.4197044
-12.7	8.91E-04	437.557	14.0893354
-25.4	1.40E-04	528.493	17.0174746
-38.1	4.95E-05	796.638	25.6517436

-50.8	2.57E-05	1038.67	33.445174
-63.5	6.59E-05	928.096	29.8846912

depth Z (ft)	x disp (ft)	x disp (in)	Z settlement (ft)	Z settlement (in)
0	2.68E-01	3.21E+00	0.0712007	0.8544084
-12.7	8.46E-02	1.01E+00	0.00756992	0.09083904
-25.4	1.30E-02	1.57E-01	0.00702783	0.08433396
-38.1	1.51E-02	1.82E-01	0.005342	0.064104
-50.8	1.74E-02	2.09E-01	0.00287985	0.0345582
-63.5	1.88E-02	2.26E-01	0.00067034	0.00804412

Excavation B (Z=25.4 ft)

depth Z (ft)	σ_{xx} (slugsf)	σ_{xx} (ksf)	xx strain
0	0.0	0.0	2.68E-03
-12.7	1276.6	41.1	9.88E-02
-25.4	3790.6	122.1	8.37E-02
-38.1	4507.8	145.2	2.33E-03
-50.8	5653.9	182.1	2.64E-03
-63.5	7357.3	236.9	2.88E-03

depth Z (ft)	yy strain	τ_{xy} (slugsf)	τ_{xy} (ksf)
0	6.69E-03	147.377	4.7455394
-12.7	6.61E-03	345.23	11.116406
-25.4	9.84E-04	670.261	21.5824042
-38.1	2.23E-04	868.881	27.9779682
-50.8	8.06E-05	1098.71	35.378462
-63.5	7.43E-06	1078.19	34.717718

depth Z (ft)	x disp (ft)	x disp (in)	Z settlement (ft)	Z settlement (in)
0	5.45E-01	6.54E+00	0.230883	2.770596
-12.7	4.94E-01	5.93E+00	0.223407	2.680884
-25.4	5.18E-03	6.21E-02	0.00501379	0.06016548
-38.1	1.15E-02	1.38E-01	0.00381144	0.04573728
-50.8	1.32E-02	1.58E-01	0.00239492	0.02873904
-63.5	1.44E-02	1.73E-01	0.00081258	0.00975099

Excavation C (Z=38.1 ft)

depth Z (ft)	σ_{xx} (slugsf)	σ_{xx} (ksf)	xx strain
0	0.0	0.0	5.70E-04
-12.7	1313.6	42.3	3.32E-03
-25.4	2575.7	82.9	2.20E-01
-38.1	4740.3	152.6	1.07E-01
-50.8	5614.4	180.8	2.95E-03
-63.5	7120.2	229.3	2.74E-03

depth Z (ft)	yy strain	τ_{xy} (slugsf)	τ_{xy} (ksf)
0	6.96E-03	177.395	5.712119
-12.7	9.61E-03	350.472	11.2851984
-25.4	1.33E-02	676.204	21.7737688
-38.1	1.96E-03	1116.9	35.96418
-50.8	2.45E-04	1081.38	34.820436
-63.5	1.85E-05	1161.74	37.408028

depth Z (ft)	x disp (ft)	x disp (in)	Z settlement (ft)	Z settlement (in)
0	7.38E-01	8.86E+00	0.40179	4.82148
-12.7	7.13E-01	8.56E+00	0.400553	4.806636
-25.4	5.84E-01	7.01E+00	0.357672	4.292064
-38.1	1.80E-02	2.16E-01	0.00834908	0.10018896
-50.8	1.02E-02	1.22E-01	0.00372263	0.04467156
-63.5	1.11E-02	1.33E-01	0.00146918	0.01763016

Excavation D (Z=50.8 ft)

depth Z (ft)	σ_{xx} (slugsf)	σ_{xx} (ksf)	xx strain
0	0.0	0.0	5.77E-04
-12.7	1272.6	41.0	1.75E-03
-25.4	2544.8	81.9	1.83E-01
-38.1	3763.6	121.2	2.21E-01
-50.8	6343.8	204.3	1.75E-03
-63.5	7124.3	229.4	1.90E-03

depth Z (ft)	yy strain	τ_{xy} (slugsf)	τ_{xy} (ksf)
0	6.42E-03	169.413	5.4550986
-12.7	9.18E-03	355.297	11.4405634
-25.4	1.24E-02	665.697	21.4354434
-38.1	4.94E-03	1378.63	44.391886

-50.8	1.04E-03	1447.64	46.614008
-63.5	4.17E-04	1323.75	42.62475

depth Z (ft)	x disp (ft)	x disp (in)	Z settlement (ft)	Z settlement (in)
0	8.49E-01	1.02E+01	0.476728	5.720736
-12.7	8.24E-01	9.89E+00	0.477324	5.727888
-25.4	6.99E-01	8.39E+00	0.441756	5.301072
-38.1	1.50E-01	1.80E+00	0.106218	1.274616
-50.8	1.19E-02	1.43E-01	0.00050053	0.00600636
-63.5	1.20E-02	1.44E-01	3.94E-05	0.000473328

Excavation E (Z=63.5 ft)

depth Z (ft)	σ_{xx} (slugsf)	σ_{xx} (ksf)	xx strain
0	0.0	0.0	1.84E-04
-12.7	1296.1	41.7	5.86E-04
-25.4	2545.1	82.0	1.44E-01
-38.1	3728.9	120.1	1.76E-01
-50.8	5032.5	162.0	2.70E-02
-63.5	8303.6	267.4	1.36E-03

depth Z (ft)	yy strain	τ_{xy} (slugsf)	τ_{xy} (ksf)
0	4.97E-03	174.24	5.610528
-12.7	7.92E-03	323.8	10.42636
-25.4	9.33E-03	666.014	21.4456508
-38.1	4.84E-03	1374.08	44.245376
-50.8	3.36E-03	1825.85	58.79237
-63.5	1.23E-03	1462.81	47.102482

depth Z (ft)	x disp (ft)	x disp (in)	Z settlement (ft)	Z settlement (in)
0	7.44E-01	8.92E+00	0.416445	4.99734
-12.7	7.30E-01	8.76E+00	0.416446	4.997352
-25.4	6.32E-01	7.59E+00	0.388537	4.662444
-38.1	1.92E-01	2.30E+00	0.14551	1.74612
-50.8	4.33E-02	5.20E-01	0.0215782	0.2589384
-63.5	1.77E-02	2.12E-01	0.00067377	0.00808525

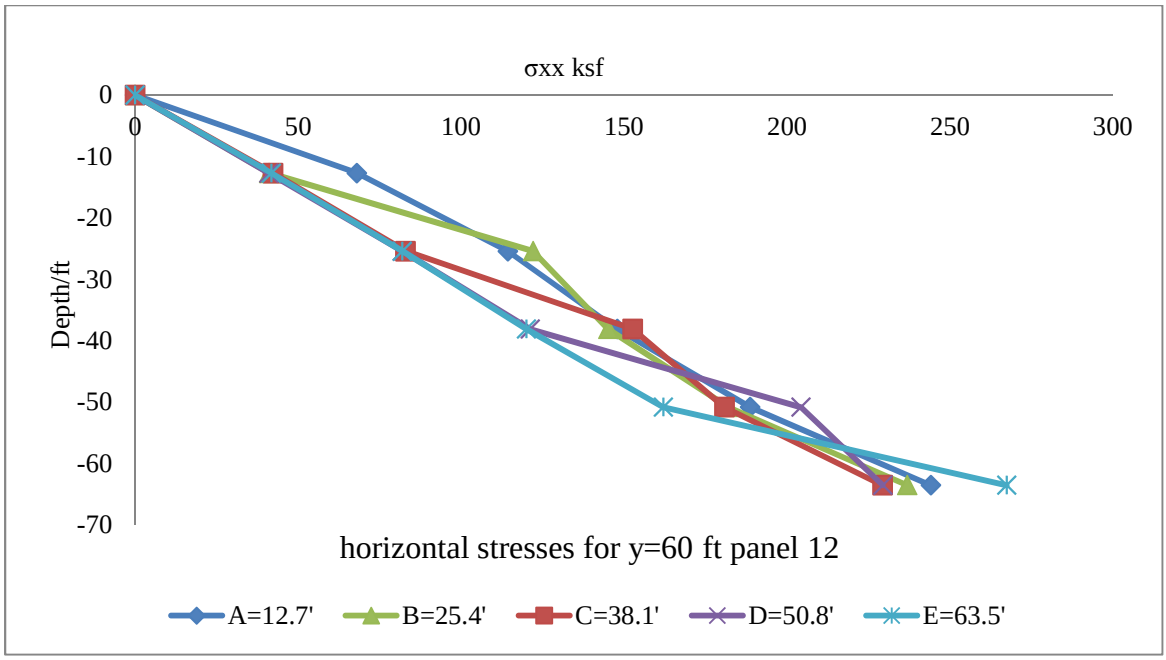

Figure B 67 Horizontal Stresses for Panel 12

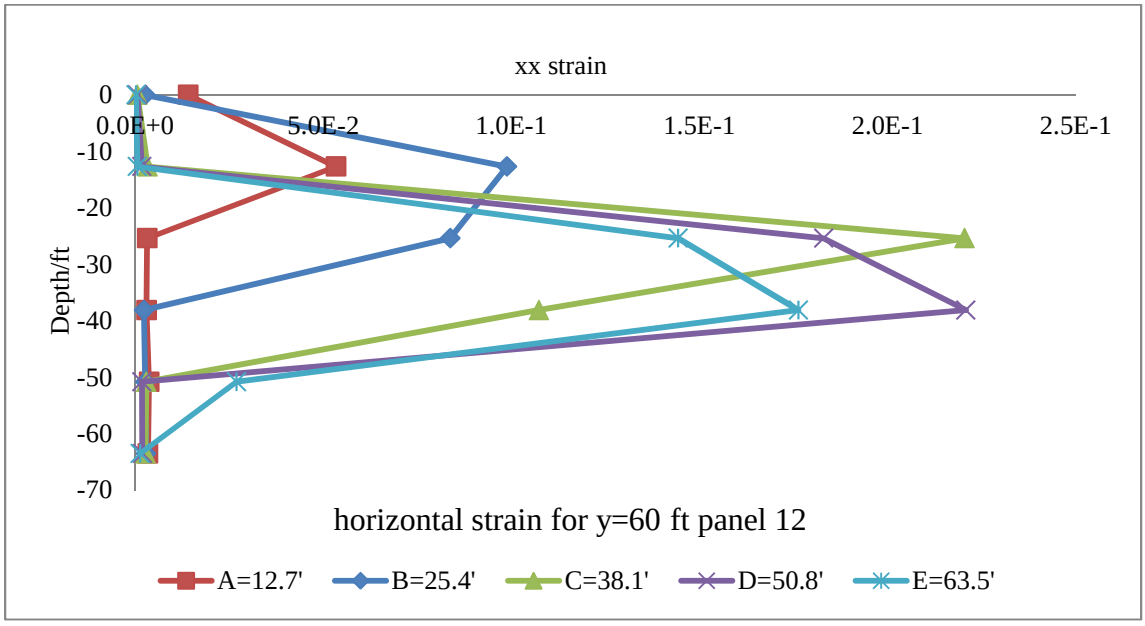

Figure B 68 Horizontal Strain in XX Direction for Panel 12

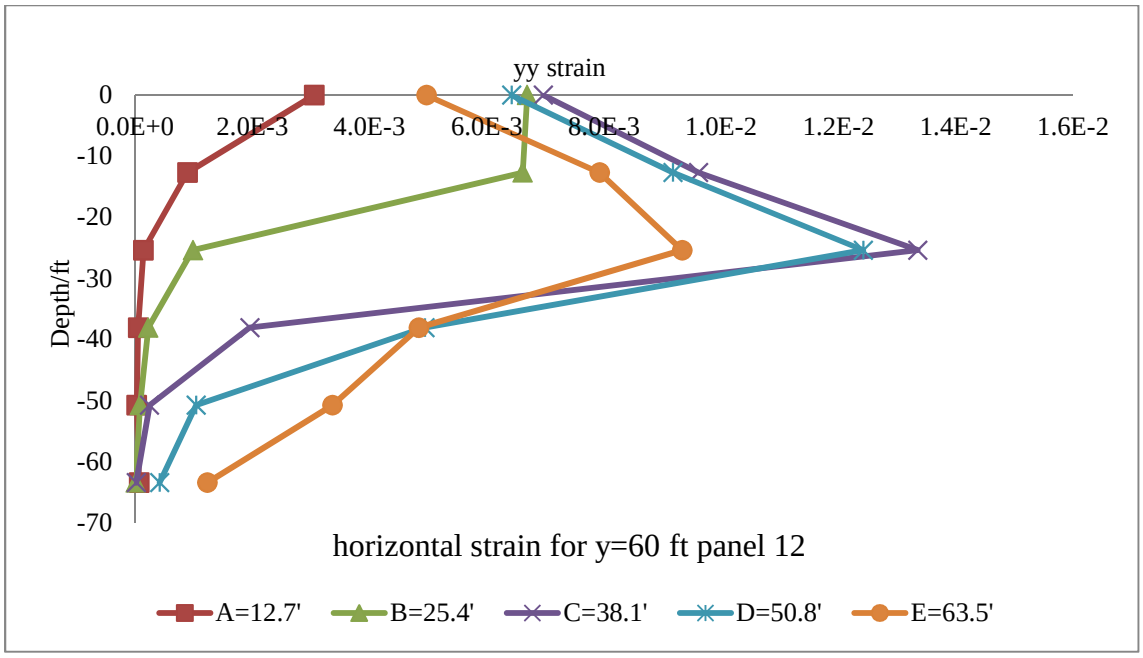

Figure B 69 Horizontal Strain in YY Direction for Panel 12

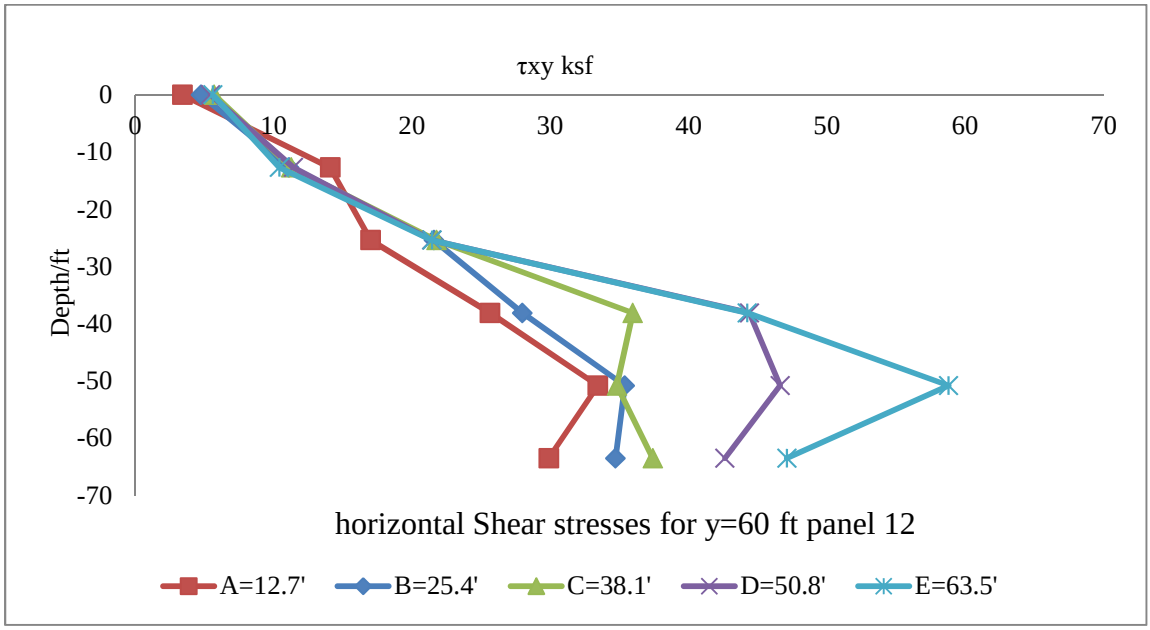

Figure B 70 Horizontal Shear Stresses for Panel 12

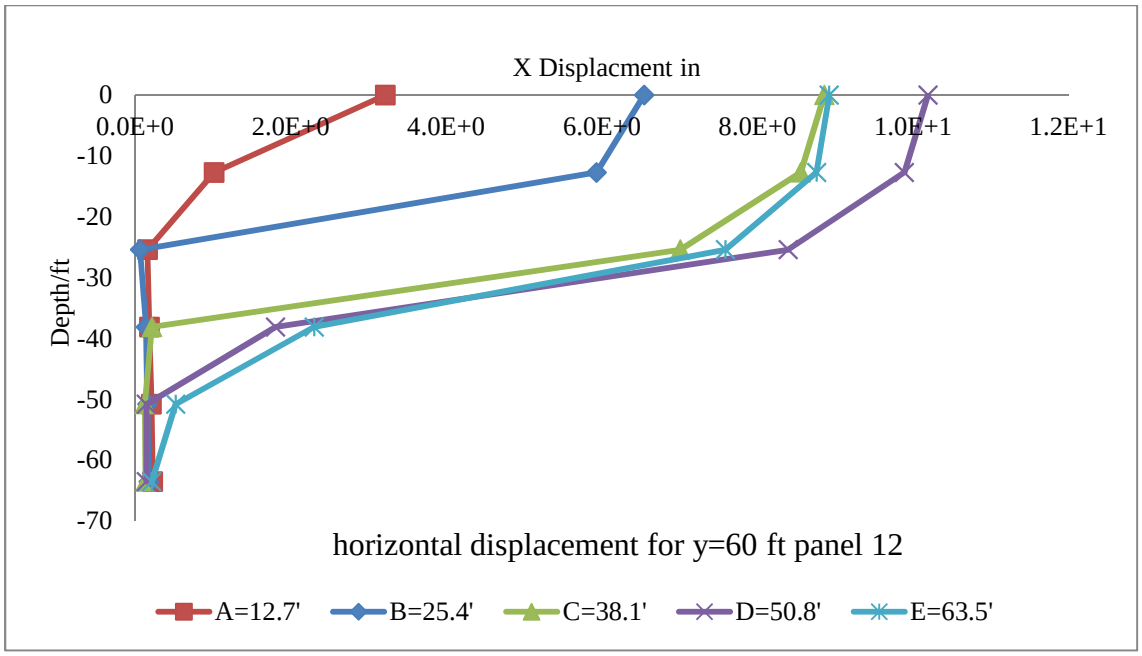

Figure B 71 Horizontal Displacement for Panel 12

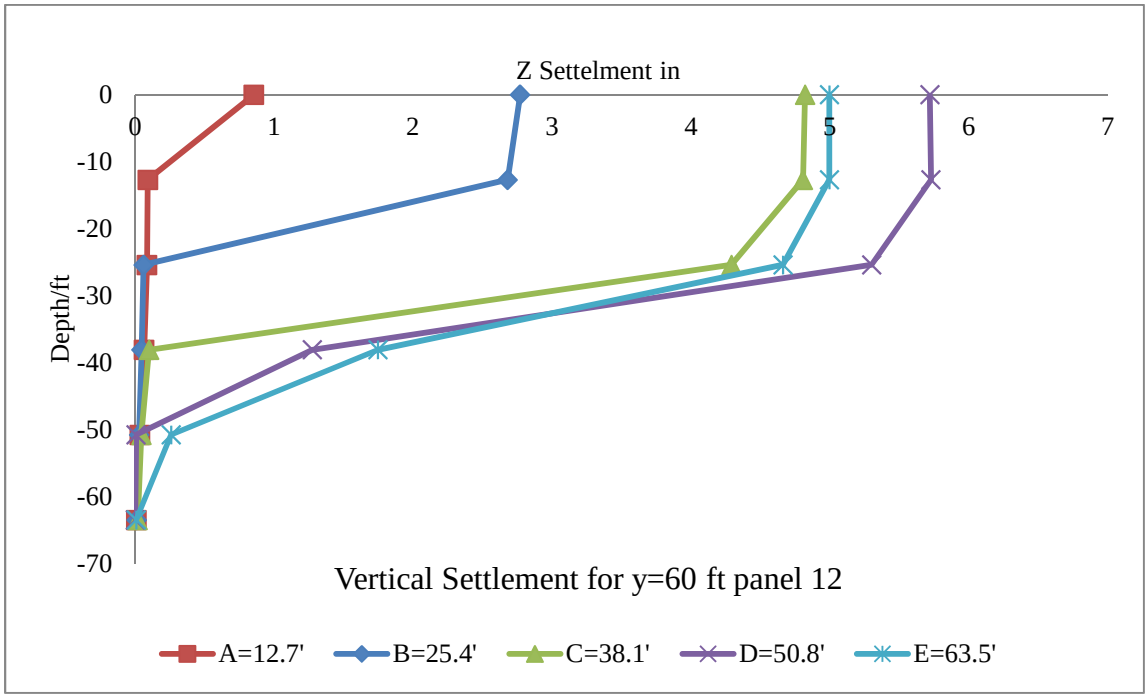

Figure B 72 Vertical Settlement for Panel 12

VITA

OMAR ALI M. MOUDABEL

Candidate for the Degree of

Doctor of Philosophy

Dissertation: A PRACTICAL NUMERICAL ANALYSIS OF A THREE-DIMENSIONAL TRENCH SLURRY WALL DURING CONSTRUCTION USING FLAC3D

Major Field: Civil Engineering

Biographical:

Education:

Completed the requirements for the Doctor of Philosophy in your major at Oklahoma State University, Stillwater, Oklahoma in May, 2019.

Completed the requirements for the Master of Science in your major at Oklahoma State University, Stillwater, Oklahoma in May, 2013.

Completed the requirements for the Bachelor of Science in your major at Tripoli University, Tripoli, Libya in 1997.

Experience:

Project Engineer at GMRA Construction Company
Project Engineer at BESIX Construction Company
Construction Site Manager at Biwater Construction Company
Construction Site Manager at EM-HIDROMANTAZA Construction Company
Consultant Engineer at National Union Consultants
Intern at Kleinfelder Geotechnical Company, Tulsa office
Intern at Oklahoma State University, Stillwater OK

Professional Memberships:

American Society of Civil Engineers (ASCE)
Geo-Institute (G-I) of ASCE
The Honor Society of Phi Kappa Phi